500699

School of Electrical and Computer Engineering

Estimation of Electrochemical Noise Impedance and Corrosion Rates from Electrochemical Noise Measurements

Alexander M. Lowe

This thesis is presented as part of the requirements for
the award of the Degree of Doctor of Philosophy
of the Curtin University of Technology

January 2002

ACKNOWLEDGMENTS

I am in debt to: Dr. Halit Eren for his outstanding supervision, encouragement and feedback provided throughout the project; Dr. Yong-Jun Tan for introducing me to electrochemical noise, and educating me in its analysis; Mr. Brian Kinsella of the West Australian Corrosion Research Group for providing laboratory space and equipment and valuable technical advice; Dr. Stuart Bailey also of the West Australian Corrosion Research Group for his assistance, advice and feedback with preparation of published works; and my dear parents for all their support.

ABSTRACT

Electrochemical noise refers to the spontaneous fluctuations in potential and current that can be observed on a corroding metal. The use of electrochemical noise for obtaining information on the corrosion process generates much interest in research fields. One important application is the measurement of corrosion rate. This can be achieved using the electrochemical noise of an pair of electrically coupled corroding metals to obtain an estimate of electrochemical impedance — an abstract quantity that reflects various aspects of the corrosion process.

There are a number of problems associated with estimation of impedance information from the electrochemical noise data, particularly regarding data pretreatment, accuracy and precision. In addition, the present methods are incomplete: current literature does not offer information regarding the phase of the impedance; and assumptions regarding symmetry of an electrode pair cannot be tested without additional measurements.

The thesis addresses the above mentioned problems. Specifically,

- analysis of the impedance estimation process is given to determine how precision can be affected by various factors;
- a novel signal processing technique is described that is shown to yield a local optimum precision;
- the application of the proposed signal processing to time varying systems is demonstrated by use of a time varying, frequency dependent impedance estimate;
- a technique for recovering phase information, given certain conditions, is suggested so that Nyquist impedance diagrams can be constructed; and
- a technique for testing the symmetry of a coupled pair of corroding metals is described.

An integral part of electrochemical noise analysis is the software used for numerical computation. The Matlab package from MathWorks inc. provides an extensible platform for electrochemical noise analysis. Matlab code is provided in Appendix A to implement much of the theory discussed in the thesis.

Impedance analysis and many other electrochemical corrosion monitoring techniques are primarily used for uniform corrosion, where the corrosion patterns occur uniformly over the exposed surface. In order to map localised corrosion, where the corrosion is typically concentrated within a small area, a wire beam electrode can be used. A wire beam electrode is a surface that is divided into a matrix of mini-electrodes so that the corrosion rate at different points can be monitored. However, manual connection of each mini-electrode to the measurement device can

prove cumbersome. The final chapter of this thesis describes the design and testing of specialised multiplexing hardware to automate the process.

In general, the thesis shows that by careful conditioning of the electrochemical noise prior to analysis, many of the problems with the technique of impedance estimation from the electrochemical noise data can be overcome. It is shown that the electrochemical noise impedance estimation can be extended to encompass a time varying, frequency dependent quantity for studying dynamic systems; that phase information can be recovered from electrochemical noise for the purpose of constructing Nyquist impedance diagrams; and that asymmetric electrodes can be detected without requiring additional measurements.

Contents

List of Figures

Chapter 1

Introduction

ISO standard 8044 [1] defines corrosion as the chemical reaction between a metal and its environment, which leads to a change of the characteristics of the metal and which can lead to substantial impairments of the function of the metal. Corrosion frequently occurs in presence of, *eg*, conductive fluids, atmospheric moisture and/or high temperatures. Examples are rusting of iron, pitting of stainless steels, crevice corrosion, selective dissolution (*eg* of zinc in brass) and stress corrosion cracking. Corrosion is also frequently encountered in the presence of gases such as CO_2 [2]. Corrosion has been estimated to cost approximately 2.5 to 3.5 % of gross national product in industrialised countries [3]. In Australia, costs have been estimated to exceed one billion dollars annually [4].

In order to control corrosion, research into better materials and better corrosion prevention techniques is ongoing. As part of such research, techniques for accurate and reliable corrosion monitoring are necessary.

Corrosion monitoring can be complex since industrial process operations provide a wide variety of dynamic environments and service conditions. No single method can necessarily work or provide optimum results in all applications.

One of the most fundamental quantities of corrosion monitoring is the rate of corrosion. It is given in terms of the average depth of penetration of corrosion per unit time and is often quoted in millimetres per year.

The rate of corrosion can be directly measured by observing its effects. For example the change in mass of a specimen (coupon) can be measured by periodically weighing it, or the thickness of a wall can be monitored using ultrasonics [5]. However, for relatively low rates of corrosion, such techniques can require a long time before sufficient corrosion can be observed.

One class of techniques that is well suited to low rates of corrosion in conductive solutions is based on the *electrochemical impedance* of a corroding metal [6] [7] [8]. The electrochemical impedance is a linear approximation of the potential-current relationship that is observed when the corroding metal (referred to as the *electrode*)

is *polarised* by an external source. Polarisation refers to the application of a potential so that a net current is passed between the metal and its environment (or *vice versa*).

By analogy with electric circuits, examining the components of the electrochemical impedance allows useful information to be inferred about the corrosion process. In particular, by the Stern-Geary relationship [9] [10] [11], the rate of corrosion can be inferred from a component of the impedance known as the *polarisation resistance.*

Conventionally, the electrochemical impedance is measured by polarisation with small sinusoidal potentials at varying frequencies so that the net current response can be observed [8], [7]. However, there has been much interest in deriving impedance information from the spontaneous fluctuations in potential and current that can be observed on a pair of electrically coupled corroding specimens. These fluctuations are respectively referred to as electrochemical potential noise (EPN) and electrochemical current noise (ECN), or collectively as electrochemical noise (EN). Dawson [12] provides a comprehensive review of EN theory and technology. EN is generally random in nature and is of relatively low frequency.

The statistical relationship between the EPN and ECN signals can be used to infer impedance information, as first suggested by Eden *et al* in 1986 [13] and Gabrielli *et al* in 1993 [14]. The approach of Eden *et al* is to observe the ECN between two electrically coupled corroding electrodes while simultaneously monitoring the EPN at the point of coupling with respect to a third "reference" electrode. This measurement will be referred to as an EPN/ECN measurement. The approach of Gabrielli *et al* is to separately log the EPN and ECN from a single corroding electrode, using a potentiostat (a device for polarising electrodes). This thesis is concerned with analysis of data obtained from the EPN/ECN measurement of Eden *et al.*

The EPN/ECN technique for impedance estimation offers some advantage over polarisation techniques because the equipment is often less complicated and less expensive. Also, in some applications, the external signals associated with the polarisation techniques can affect the system under investigation.

The EN techniques are not without their problems, however. Inherent limitations of the EN technique are that:

- Impedance information cannot always include phase information, although this thesis shows how to partially overcome this limitation as is discussed later;
- Analysis is limited to a much lower range of frequencies in comparison with AC polarisation techniques, due mainly to the dominance of instrumentation noise at higher frequencies;
- The required signal processing adds to the complexity of analysis.

But even with these limitations, is is possible to extract useful information from the EPN/ECN data as long as certain issues are addressed. The issues addressed in the thesis are listed below:

Trend removal and other signal conditioning. It has been found that low frequency drifts in the EN measurements can significantly affect the results of analysis. In order to obtain more reliable results, some form of trend removal is often applied, where the low frequency drift is estimated and then removed. Linear trend removal (LTR) [15] uses linear regression to achieve this. The main criticism of LTR is that the drift does not necessarily follow a linear model. The moving average removal (MAR) [16] is a technique that is able to cope with non-linear drifts, however there have some questions raised over its use [17], [15]. Other types of trend removal that have been applied include spline fitting, point-to-point subtraction and various forms of conventional high pass filters (both analogue and digital). Many of these methods are defined by one or more parameters: *eg* the cut-off frequency of a high pass filter, or the averaging time of an MAR filter. The precise effect that these trend removal methods have on the EN analysis has not been widely investigated. It remains unclear as to what is the best approach to trend removal and signal conditioning in general.

Implicit frequency dependency. The most basic parameter of EN impedance analysis, the *noise resistance* [13], has been linked with the polarisation resistance of the electrode [18], [12]. If equivalence between the polarisation and noise resistances can be shown, then the noise resistance can be used for corrosion rate estimation purposes. The theory given in [19] shows, however, that the noise resistance is implicitly a frequency dependent quantity. It is actually an average value of impedance magnitude over the bandwidth of the EN and is only equal to the polarisation resistance under specific conditions. The experimental data given in [20] tends to verify these theoretical observations. The *spectral noise impedance*, as defined in references [21] and [19], is an alternative to the noise resistance that is explicitly frequency dependent. It allows the impedance magnitude of the electrode to be appraised across a band of frequencies so that a likely value for polarisation resistance can be extracted from it. Unlike the noise resistance, however, the spectral noise impedance is difficult to apply to dynamic systems by continuous computation over a sliding window, *a la* the continuous "fast" noise resistance [16]. Thus if EN impedance techniques are to be applied to dynamic systems, a solution to the noise resistance's implicit frequency dependency problem needs to be found.

Minimum duration of measurement. The continuous "fast" noise resistance [16] shows how the noise resistance can be used to track a dynamic system. In essence, the noise resistance is computed over a sliding window of some width. The shorter the width of the sliding window, the better the time resolution of

the measurement. However, there has been some concern regarding how short the window can be made before unreliable results are achieved [17]. The effect that the measurement duration and the bandwidth of the EN signals have on the precision and accuracy of the final estimate require investigation before the approach can be applied with confidence.

Detection of asymmetric electrodes. One of the assumptions of the EN impedance technique is that a pair of "nominally identical" electrodes are required [13], [22]. If the electrode pair is asymmetric, *ie* if they are not nominally identical, then erroneous results can be obtained. While it is possible to assess symmetry by separate measurements on each electrode using non-EN techniques, doing so defeats the purpose of using the EN techniques. A method of analysing the EN to detect an asymmetric electrode pair that doesn't require any additional measurements will enhance the utility and reliability of the EN technique.

Spectral Noise Impedance is real valued. The spectral noise impedance is a quantity that is thought to represent the electrochemical impedance of the underlying electrodes. However, an impedance is a complex valued function of frequency. It is typically depicted graphically by a polar plot of magnitude versus phase, known as a Nyquist diagram. Since the spectral noise impedance is entirely real valued, half the information, the phase component is missing. This makes identifying the precise model of the components of the impedance more difficult. The ability to compute the phase information from the EPN/ECN data will enhance the utility of the EN technique.

After the introductory and background chapters, the thesis is composed of three parts:

1. Chapter 4 investigates how the noise resistance can best be estimated from EPN/ECN data. The effect of the bandwidth of the EN signals and the duration of the measurement is quantified with respect to precision of the noise resistance. Pre-processing of the EN signals to optimise the estimate and to control (and even to exploit) the frequency dependency is examined. The performance of the moving average removal [16] is discussed. A new method of signal conditioning based on a whitening filter [23] is proposed.

2. Chapter 5 deals with three novel EPN/ECN analysis techniques that can be applied to extract more information from the measurement: the *time varying spectral noise impedance*; the *complex noise impedance*; and the EN *cross correlation.*

   Time Varying Spectral Noise Impedance is a combination of the continuous "fast" noise resistance [16] and the spectral noise impedance [21]

[24] [25] [19]. It makes use of the signal pre-processing techniques described in chapter 4 to obtain the noise resistance as a function of time and frequency. The time varying spectral noise impedance shows how the equivalent impedance of the corrosion system varies during the course of an experiment. Such information can be used to make a more informed decision about how best to calculate the noise resistance at different points of the measurement. It is useful for dynamic systems, such as the one analysed in Section 5.2, where the system's properties change during the course of an experiment.

Complex Noise Impedance: The spectral noise impedance is a technique that estimates the magnitude of the electrode equivalent impedance. Unfortunately, the spectral noise impedance does not convey any information regarding the phase of the equivalent impedance. Without the phase information, the precise model of the impedance under study cannot be inferred with the same degree of confidence as other impedance measurement techniques such as AC polarisation and the approach of Gabrielli *et al* [14]. Given an electrode pair with some degree of asymmetry (*ie*, an electrode pair with impedances and/or EN power spectral densities that differ to some degree), the complex noise impedance can extract phase information from the EN signals. Used in conjunction with the spectral noise impedance, Nyquist impedance diagrams can be constructed entirely from an EPN/ECN measurement from an asymmetric electrode pair.

Coefficient of Correlation: The theory relating the noise resistance to the polarisation resistance assumes that the pair of working electrodes has equal impedances. Also, to be able to extract phase information with the complex noise impedance, some degree of electrode asymmetry is required, as will be described in Section 5.2. It is therefore useful to know whether or not the electrode pair is symmetric. The cross correlation between the EPN and ECN data is proposed as a means to assess the symmetry of an electrode pair entirely from the EPN/ECN measurement. This alleviates the need to assess symmetry by non-EN techniques, which would otherwise defeat the purpose of using EN.

3. Chapter 6 describes an auto-switch that is used for automatic configuration of a *wire beam electrode* (WBE) [26] [27] [28]. The majority of conventional corrosion monitoring techniques, electrochemical impedance included, assume that corrosion occurs uniformly over the exposed surface. The WBE is a technique of corrosion measurement where a surface is split into a matrix of mini-electrodes. It is assumed that corrosion occurs uniformly on each mini-

electrode, even though the corrosion may occur non-uniformly across the entire surface. The rate of corrosion on each mini-electrode is measured, typically using EN techniques, and a surface map is produced depicting the rate of corrosion over the exposed surface. The WBE technique requires that the mini-electrodes be connected to the measurement device in arbitrary combinations. Manually performing these connections is unpractical. Thus a device has been constructed to perform the task automatically. Chapter 6 describes in detail the design and construction of the auto-switch device.

Chapter 7 provides summary and conclusions of the thesis.

At various points throughout the thesis, results of data analysis and simulation are presented. These are performed in Matlab using a set of routines developed by the author. The software is available with accompanying documentation under the General Public License from http://chemistry.curtin.edu.au/staff/alowe/en [29]. See also Appendix A, which contains the documentation and source of selected functions. The routine used for a particular analysis or simulation will be indicated at the appropriate place in the thesis.

Chapter 2

Background: Corrosion and Electrochemical Noise

Corrosion occurs in many forms and environments and the methods of monitoring corrosion are correspondingly varied. No single monitoring technique can provide a general solution for all corrosion problems. The thesis is concerned with the simultaneous potential/current noise (EPN/ECN) measurement as a technique for estimating corrosion rate.

This chapter provides background to corrosion and corrosion monitoring technology with emphasis on electrochemical impedance spectroscopy (EIS) and electrochemical noise (EN). In Section 2.1, corrosion is introduced and the characteristic forms and the methods of monitoring corrosion are discussed. Section 2.2 explains the theory of EIS as a method for corrosion rate measurement. Section 2.3 provides general background on EN and its applications.

A subsequent chapter (Chapter 3) focuses on the background theory and practice relating to impedance measurement by EPN/ECN data and introduces the required mathematical tools.

2.1 Corrosion

ISO standard 8044 [1] defines corrosion as the chemical reaction between a metal and its environment, which leads to a change of the characteristics of the metal and which can lead to substantial impairments of the function of the metal. It is an industry cancer with direct costs estimated to at 2.5 to 3.5 % of the gross nation product in industrialised countries [3]. In Australia, costs have been estimated to exceed one billion dollars annually [4].

The most typically known form of corrosion is the rusting of iron and ordinary steel. Examples include perforation by rusting of silencers and exhaust systems of cars, of car bodies and of various kinds of structural steel work. Rusting and

corrosion are often considered synonymous. However, a more general definition is given by the Corrosion Education Manual of the European Federation of Corrosion:

> Corrosion: attack on a material by reaction with the environment with a consequent deterioration of properties. When no reference is made to the material it is normally understood that a metal is involved, and that the valency of the metal is increased; an exception is the dissolution of a metal in a liquid metal or in a fused salt. The term corrosion may refer either to the process or to the damage caused.

Corrosion predominantly relates to metal, however the definition allows any material to be included: *eg* failure of coatings (such as plastic or paint) due to chemical reaction; oxidation of carbon-carbon composites in high temperatures; and stress corrosion cracking of plastic tubing in potable water [30]. The thesis is concerned with corrosion of metals.

Two general classes of corrosion exist: *uniform* and *localised* corrosion.

Uniform corrosion takes place evenly across the entire exposed surface. The damage caused by this type of corrosion is usually predictable and can be quantified by the *corrosion rate* – typically in millimetres per year.

The different types of localised corrosion are concentrated to small areas of the exposed surface. Although the net rates of corrosion are typically quite low, localised corrosion is particularly insidious because concentrated attack often results in deep penetration of the material and its mechanical strength can become impaired. Because of the low net rates of corrosion, the corrosion rate generally makes an inadequate measure for monitoring localised corrosion.

The *electrochemical* theory is most generally accepted as an explanation of corrosion [31]: The metal and its environment form an electrochemical cell. Charge is transferred between the metal and the environment in two distinct, and possibly physically separate, half reactions — the oxidation half reaction and the reduction half reaction. The result is a net dissolution of the metal into its environment.

Section 2.1.1 outlines the electrochemical theory of corrosion. Section 2.1.2 gives a brief overview of some of the common forms of corrosion. Corrosion monitoring methods are reviewed in Section 2.1.3.

2.1.1 Driving Forces of Corrosion Reactions [31]

If a metal, M, is placed in a solution that contains its own ions, M^{n+}, the dynamic equilibrium:

$$M^{n+} + ne^- \Longleftrightarrow M \tag{2.1}$$

will be established. This causes an electrical potential difference between the metal and the solution. When equilibrium has been reached this potential is given by the

Nernst equation:

$$E = E_0 + \frac{RT}{nF} \ln[\mathrm{M}^{n+}] \tag{2.2}$$

where E is the potential of the metal, E_0 is called the standard potential, R is the gas constant (8.314 J.mole^{-1}.K^{-1}), T is temperature (degrees Kelvin), F is Faraday's constant (9.648×10^4 Coulombs/mole) and $[\mathrm{M}^{n+}]$ denotes the concentration of the ionic species at equilibrium.

When the metals are placed in order of increasing E_0, the *electrochemical series* of the metals is obtained. The zero point of this series is chosen as the standard potential of the hydrogen electrode. When two electrodes with different equilibrium potentials are connected with a conducting wire a current will flow in such a direction that the potential difference tends to decrease. At one of the electrodes, (2.1) proceeds in the forward direction (*reduction*) and the electrode is referred to as the *cathode*. At the other electrode, referred to as the *anode*, (2.1) proceeds in the reverse direction and *oxidation* takes place.

The above is applicable to all redox reactions of the general type:

$$a\mathrm{Ox} + n\mathrm{e}^- \Longleftrightarrow b\mathrm{Red} \tag{2.3}$$

where Ox is the oxidant and Red is the reductant. The potential is given by the corresponding Nernst equation:

$$E = E_0 + \frac{RT}{nF} \ln \frac{[\mathrm{Ox}]^a}{[\mathrm{Red}]^b} \tag{2.4}$$

where [Ox] and [Red] denote the concentration (or partial pressure in the case of a gas) of the oxidant and the reductant respectively.

Two important examples that are often found in practical cases of corrosion are

the hydrogen evolution reaction:

$$2\mathrm{H}^+ + 2\mathrm{e}^- \Longleftrightarrow \mathrm{H}_2 \tag{2.5}$$

with $E = 0.0 + \frac{RT}{2F} \ln \frac{[\mathrm{H}^+]^2}{p_{\mathrm{H}_2}}$ where p_{H_2} is the partial pressure of the H_2 gas; and

the oxygen reduction reaction:

$$\mathrm{O}_2 + 2\mathrm{H}_2\mathrm{O} + 4\mathrm{e}^- \Longleftrightarrow 4\mathrm{OH}^- \tag{2.6}$$

with a potential of $E = 0.401 + \frac{RT}{4F} \ln \frac{p_{\mathrm{O}_2}}{[\mathrm{OH}^-]^4}$

A metal will tend to corrode if it is placed in an environment in which the oxidised form of the redox couple (Ox) has an equilibrium potential higher than that of the metal. For example any metal with an equilibrium potential below 0 V will tend to dissolve in solutions containing high concentrations of H^+ ions (*ie* acid solutions).

In some instances metal ions can precipitate to form solid compounds, which can completely cover the metal so that further reaction of the metal is inhibited. This is called *passivation*. Aluminium is an example that exhibits passivation under many environmental conditions.

2.1.2 Forms of Electrochemical Corrosion [31]

Corrosion assessment can be complex since industrial process operations provide a wide variety of dynamic environments and service conditions. Such diverse environments can lead to many possible forms of corrosion.

Gellings [31] provides an overview of some of the important characteristic forms of electrochemical corrosion:

- Rusting and atmospheric corrosion of iron and steel.
- Pitting corrosion.
- Crevice corrosion and deposit attack.
- Selective dissolution.
- Inter-crystalline corrosion.
- Stress corrosion cracking and corrosion fatigue.
- Erosion and cavitation corrosion; impingement attack.

This section briefly summarises them.

Rusting and Atmospheric Corrosion of Iron and Steel

Rust refers to compounds of the general composition $FeO(OH).nH_2O$ containing Fe^{3+}. It is formed when iron and steels are exposed to approximately neutral solutions or to the atmosphere.

After Gellings [31]:

> In the anodic reaction, iron dissolves as Fe^{2+} ions, while simultaneously hydroxyl-ions are formed at the cathode. In the solution where these ions meet, the solubility product of $Fe(OH)_2$ will be exceeded so that this compound precipitates. Subsequently it is rapidly oxidised by the oxygen present in the solution at some distance from the metal surface.
>
> The cathodic and anodic areas move over the surface with time causing reasonably uniform corrosion. When the iron is continuously submerged the rust layer slows down the oxygen supply and thus the corrosion rate. In atmospheric corrosion the rate determining factor in the corrosion process is still the oxygen supply.

Pitting Corrosion

Pitting is a highly localised form of corrosion. While the majority of the exposed surface can remain largely free of corrosion, narrow pits are formed. These pits can penetrate deeply into the metal and impair its mechanical strength and cause failure.

In active metals that would otherwise corrode uniformly, pitting can be caused by local wetting or damaged spots in mill scale or a protective coating. The corrosion products accumulate moisture and other corrosively aggressive substances, which accelerates attack.

Pitting is often observed on *passive metals.* A passive metal is one that naturally possess a protective layer, called a passive layer. Examples are stainless steel and aluminium. The presence of chlorides is often associated with pitting of passive metals.

A pit is initiated when there is a local break down in the passive film. It can be caused by mechanical damage, heterogeneity, local cold-working of the metal, deposits of dirt, or differences in composition of the environment.

The potential difference between the freshly exposed metal and the remaining passive film can be up to 0.5 to 1 Volt. Depending on the environmental circumstances, the freshly exposed metal might then *repassivate* — *ie* the passive layer might reform. Such behaviour is referred to as *metastable pitting.* Alternatively, the local chloride concentration might increase due to its role in the charge transport in the solution, or the pH in the pit can decrease due to hydrolysis of the dissolved metal ions. Both these changes can make repassivation impossible and the affected area continues to corrode, thus forming a pit. This behaviour is referred to as *stable pitting.*

Figure 2.1 shows an example of pitting on aluminium [30].

> The localised pitting corrosion was produced in aluminium floats on a storage tank roof. The exposure conditions involved hydrocarbon fluids following an initial hydro-test. The pitting occurred in the absence of chlorides at a near neutral pH where aluminium would be expected to exhibit good resistance to corrosion. Sulfur corrosion products were found in the pits and sulfate reducing bacteria were suspected resulting from prolonged exposure to hydro-test water. [30]

Crevice Corrosion and Deposit Attack

Local differences in solution composition can cause potential differences on an exposed metal surface. Differential aeration is an example, where there is a non-uniform oxygen concentration. Such a scenario is especially prone to occur in narrow crevices such as in screw threads.

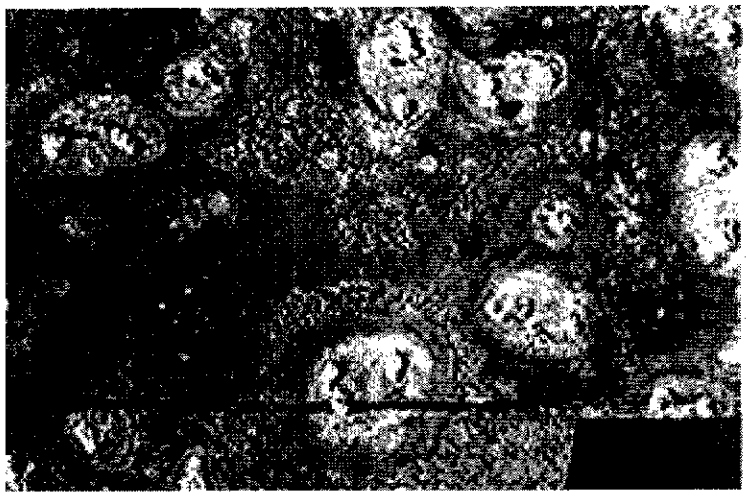

Figure 2.1: Pitting in aluminium [30].

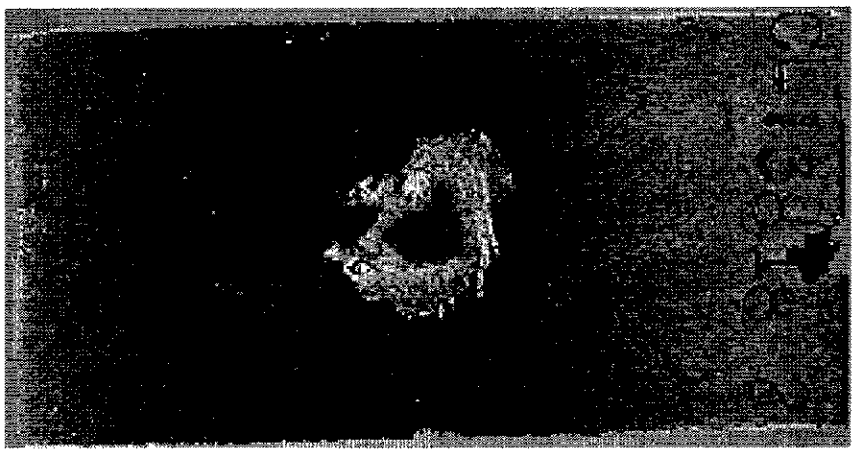

Figure 2.2: Crevice corrosion of stainless steel [30]

This differential aeration can cause the same type of process as with pitting corrosion to occur, where the local chloride concentration increases and the pH decreases. The result is corrosion that is localised to the crevice or the deposit.

Figure 2.2 shows an example of crevice corrosion on stainless steel [30].

> On this stainless steel test coupon from an ASTM G48 Method B ferric chloride test, the crevice was a non-metallic block. Note that the test coupon was not attacked by corrosion except in the middle of the coupon where it was in contact with the block and on the edges were a rubber band used to hold the block in place also came in contact with the metal surface. [30]

Selective Dissolution

Alloys are composed of more than one type of metal. In some alloys, the less noble component can dissolve, leaving the more noble component as a porous residue. The most common example is the *dezincification* of brass, where the zinc seems to be dissolved out of the brass. (The real mechanism includes a simultaneous dissolution of copper and zinc with subsequent precipitation of copper.) Layer type dezincification occurs uniformly over the entire surface. Plug type dezincification has also been observed where conical pits filled with a porous copper residue are formed.

Inter-Crystalline Corrosion

Metals are composed of a large number of small in size and randomly oriented grains. Inter-crystalline, or inter-granular corrosion, occurs when the adhesion between grains is compromised. The total rate of corrosion is usually very low, but the loss of adhesion between grains results in disintegration of the metal. It is most often observed on austenitic stainless steels. Intercrystalline (intergrannular) corrosion of stainless steel is a type of selective corrosion of chromium depleted near-grain boundary zones.

Stress Corrosion Cracking and Corrosion Fatigue

Stress corrosion cracking is the result of a combination of tensile stresses and corrosion. The cracks can be either trans-crystalline or inter-crystalline, but in both cases they are approximately perpendicular to the tensile stress. Most alloys are susceptible to stress corrosion cracking in very specific environments. Some examples are: copper alloys in humid atmospheres containing ammonia or sulfur dioxide (inter-crystalline), mild and low alloy steels in nitrates and concentrated alkalis (inter-crystalline) and in steam contaminated with chlorides (trans- and inter-crystalline), and aluminium alloys in sea water (inter-crystalline).

Figure 2.3 shows an example of stress corrosion cracking of stainless steel [30].

> The example shown indicates many intersecting, branched cracks with a trans-granular propagation mode. These are typical of stress corrosion cracking (SCC) in austenitic stainless steel. In this case, however, the alloy was reported to be resistant to SCC in the NaCl brine service environment. The location of cracking was limited to a region covered by an elastomeric sleeve. Under the sleeve, evidence of severe general and pitting corrosion were found and evidence of sulfur-containing corrosion products. Analysis of the elastomer indicate that it was not the correct grade and chemical degradation had occurred in service to produce organic acids and sulfur compounds. This local environment resulted in

Figure 2.3: Stress corrosion cracking of stainless steel [30].

enhanced localised susceptibility of the material to pitting corrosion and SCC. [30]

Erosion and Cavitation Corrosion; Impingement Attack

Erosion corrosion occurs when erosion from a fast streaming liquid causes corrosion attack that is much larger than would otherwise be expected from either the erosion or the corrosion separately. It can be observed where strong turbulence occurs such as at sharp bends, constructions, inlets of narrow tubes, pump impellers, *etc.* The erosive action of the turbulence destroys any protective layer, which causes direct contact between the active metal and the liquid.

2.1.3 Methods for Corrosion Monitoring [5]

The majority of this section is a summary of the article by Kane [5] on the subject of corrosion monitoring methods.

Corrosion monitoring has many purposes that can include one or more of the following:

- Diagnoses of corrosion problems.
- Monitoring of corrosion control methods (*eg* inhibition, pH control, *etc*).
- Advanced warning of system upsets leading to corrosion damage.
- Determination of inspection and/or maintenance schedules.

- Estimation of use service life of equipment.

Corrosion assessment can be complex since industrial process operations provide a wide variety of dynamic environments and service conditions. No single method will necessarily work or provide optimum results in all applications. In some cases, multiple technologies may be needed in combination to provide accurate and reliable corrosion monitoring information that can be used with confidence to make engineering decisions.

Classification of Techniques

Kane [5] classifies techniques for corrosion monitoring in two ways:

1. Intrusive or non-intrusive.
2. Direct or indirect.

An intrusive technique requires entry into the process stream. Corrosion coupons, electric resistance (ER) and linear polarisation resistance (LPR) probes and on-line pH or water analysis are intrusive since they require access to the inside of the equipment to be monitored. Examples of non-intrusive techniques are external hydrogen flux probes in H_2S containing environments and analysis of water samples through an existing valve.

Indirect corrosion monitoring techniques measure an outcome of the corrosion process. Techniques such as ultrasonic testing and radiography can be used to determine the remaining wall thickness of a pipe, vessel or other equipment affected by corrosion.

A direct technique measures the direct result of corrosion. Electrochemical methods, such as the EN analysis studied in the thesis, are examples. The three most common corrosion monitoring methods — including EN analysis, the technique studied in the thesis — are examples of direct methods:

- Corrosion coupons.
- Electric Resistance (ER).
- Linear polarisation resistance (LPR) and other electrochemical methods.

Corrosion Coupons

A corrosion coupon is a representative specimen of metal that is placed in the corrosive environment to be studied. After a set period of exposure the specimen is removed for inspection. An average rate of corrosion can be determined by a *mass loss* measurement. The coupon is weighed and then placed in the process to corrode. After a given amount of time, it is removed and the corrosion products are chemically

cleaned from the surface, whereupon it is reweighed. The change in mass indicates the rate of corrosion. An underlying assumption is that the corrosion observed on the coupon is representative of the corrosion attack to the plant.

Coupons provide the most reliable physical evidence possible. They yield information on average mass lost to corrosion and the extent and distribution of localised corrosion. They can also provide information on the nature of corrosion through analysis of their corrosion products. The biggest drawbacks that coupons have are that they usually require significant time in terms of labour and they only provide time averaged data that cannot be used for on-line corrosion monitoring.

Procedures for in-plant corrosion coupon testing are given in ASTM G84 [32]. This standard gives methods for placement, installation and exposure of in-plant corrosion coupons. ASTM G1 [33] gives useful guidelines for preparation, cleaning and weighing of corrosion coupons.

In addition to mass loss measurements, visual inspection of coupons after exposure is important to assess the degree to which uniform or localised corrosion is present. ASTM G46 [34] gives procedures for analysis of localised corrosion.

Electric Resistance Monitoring

The Electrical Resistance (ER) probe is comprised of a sensing element that is a loop of material made from a wire or strip. It is used to conduct an electrical signal. When exposed to a corrosive environment, the cross-section of the loop is reduced which increases the resistance of the sensing element thus producing a change in the output of the ER probe. Relevant information on this technique can be found in ASTM G96 [35] for in-plant corrosion monitoring.

The main benefit of the ER technique is that it can be utilised in continuous on-line process monitoring. Multiple probes can be used to access various locations in the process stream. Telemetry can be used to send this information back to a central location so that corrosion rates and the effects of process changes can be identified. Probes of varying materials and sensitivities are commonly available. One of the best aspects of the ER technique is that it does not require a continuous electrolyte current path to make measurements. Therefore, ER probes work in multi-phase environments that contain liquid hydrocarbons and they can be utilised to monitor corrosion in non-aqueous and even gaseous processes.

The limitations of ER probes are that they provide representative data for general corrosion only. They do not have the ability to detect localised attack accurately. ER probes, while available in varying sensitivity, typically require several days to determine a reliable corrosion rate trend. In some cases, namely where H_2S is present, the technique can be prone to error due to the presence of conductive sulfide corrosion products on the sensing element.

Electrochemical Methods

EN analysis, the subject of the thesis, is an electrochemical method.

Electrochemical corrosion monitoring is based on the premise that corrosion is an electrochemical process that can be monitored through the measurement of the potential and current relationship that characterises the corrosion process. The technique depends strongly on the ability to measure current flow through an electrolytic solution. It has limitations in many multi-phase (*eg* gas/oil/water) systems and cannot be used in non-aqueous and gaseous environments.

The main benefits of electrochemical methods are that they can provide fast, dynamic information. Therefore, they can identify rapid changes in process corrosivity.

The electrochemical methods of particular relevance to this thesis, are Linear Polarisation Resistance; Electrochemical Impedance Spectroscopy; Electrochemical Noise; and the wire beam electrode.

Linear Polarisation Resistance (LPR): The most popular electrochemical technique utilised for corrosion monitoring is the LPR technique, as described in ASTM G59 [36]. It utilises a measurement of the slope of the potential versus current plot approximately ± 10 mV about the corrosion potential to define a parameter called the *polarisation resistance*. For non-diffusion limited corrosion, the corrosion rate is inversely proportional to the polarisation resistance. [9]

Electrochemical Impedance Spectroscopy (EIS): EIS utilises an AC signal to perturb a corroding specimen so that its equivalent impedance can be observed. In a mechanistic sense, EIS monitors the electric response of the metal/environment interface to the applied AC signal over a frequency spectrum usually in the range of 10 kHz down to 50 mHz. At low frequencies, the EIS measurement is equivalent to an LPR measurement, but the higher frequencies can provide additional information.

The benefit of EIS over LPR is that it allows separation of the various components of the system impedance, *eg*, separation of the solution resistance from the polarisation resistance. EIS can be utilised to examine coated or inhibited materials more effectively than the LPR techniques. EIS data can be used to determine the properties of the surface layers such as pore resistance and film capacitance. Other areas of application for EIS is in the evaluation of corrosion of steel in concrete structures and in the evaluation of cathodic protection since both applications require significant compensation for resistive losses. The main limitations of EIS is that the analysis of the data is complex and its interpretation is not fully developed for all applications. It requires application of a theoretical equivalent circuit to analyse and interpret the data.

The theory of EIS is examined in more detail in Section 2.2.

Electrochemical Noise (EN): EN monitoring records the naturally occurring fluctuations in corrosion potential and current. As with EIS, the technical basis for this technique is still being developed. Qualitatively, EN data has been utilised to identify localised corrosion and to differentiate conditions where general and localised corrosion can occur. The technique is also being explored for estimation of corrosion rates by use of parameters such as the electrochemical noise resistance and spectral noise impedance. EN requires monitoring of very small signal fluctuations that may be prone to extraneous sources of signal noise. EN analysis is the subject of the thesis. EN is reviewed in more detail in Section 2.3. Theory relating to impedance estimation by EN is reviewed in 3

Wire beam electrode (WBE): Standard analyses of electrochemical data usually assume the measured corrosion rate is the result of general corrosion. In actuality, many cases are observed where less than 10 % of the surface of the specimen is actually corroding. This is the case with pitting or other forms of localised corrosion. The *wire beam electrode* (WBE) technique [26] [27] [37] is an experimental system that makes use of a matrix of mini-electrodes in an attempt to obtain a surface distribution map of corrosion characteristics by electrochemical methods. The wire beam electrode is discussed in more detail in Section 2.3.3.

2.2 Electrochemical Impedance Spectroscopy Theory [6]

An important method of corrosion monitoring is the study of the equivalent impedance of an electrochemical cell, known as electrochemical impedance spectroscopy (EIS). By fitting the observed impedance to a model, information regarding the physical properties of the cell can be inferred. The application of EIS to the study of electrochemical corrosion [7] is of particular interest to this thesis.

This section briefly summarises some of the EIS theory from Gamry Instruments' EIS documentation [6]. Also see Bard and Faulkner [8] for further explanation.

In Section 2.2.1, the concept of electrochemical impedance is explained. In Section 2.2.2, visualisation of impedances using Nyquist and Bode diagrams is introduced. Section 2.2.3 discusses the elements that typically make up the electrochemical impedance. Common equivalent circuit models are discussed in Section 2.2.4.

2.2.1 Impedance of an Electrochemical Cell

When a metal (the electrode) is placed in an electrolytic solution, in the steady state condition its potential with respect to the bulk solution approaches a certain value referred to as the corrosion potential, E_{corr}. If the electrode is disturbed by

an external potential source a net current is produced. For small potential disturbances about the corrosion potential, the magnitude of net current is approximately proportional to the magnitude of the potential disturbance. If the disturbance takes a sinusoidal shape,

$$v(t) = V_0 \cos(\omega t), \tag{2.7}$$

then there is a phase shift between the impressed potential and the current response. The current response is then given by

$$i(t) = I_0 \cos(\omega t - \phi), \tag{2.8}$$

where $v(t)$ is the impressed potential with respect to E_{corr};
$i(t)$ is the current response;
V_0 is the magnitude of the impressed potential;
I_0 is the magnitude of the current response;
ϕ is the phase difference between the potential and current;
t is the time; and
ω is the frequency of the sinusoid in radians per second.

The potential and current *phasors* (rotating vectors) are defined as

$$\vec{V} = V_0 \exp(\mathrm{j}\,\omega t) \tag{2.9}$$

$$\vec{I} = I_0 \exp[\mathrm{j}(\omega t - \phi)] \tag{2.10}$$

where $\mathrm{j}^2 = -1$ and $\vec{X}$ is used to denote a phasor. From Euler's relation,

$$\exp(\mathrm{j}x) = \cos(x) + \mathrm{j}\sin(x) \tag{2.11}$$

where x is any real number, it follows that

$$v(t) = \mathrm{Re}\left\{\vec{V}\right\} \tag{2.12}$$

$$i(t) = \mathrm{Re}\left\{\vec{I}\right\} \tag{2.13}$$

where $\mathrm{Re}\{z\}$ denotes the real part of z.

The relationship between $v(t)$ and $i(t)$ can be described by the *equivalent impedance* of the electrode — the ratio of the two phasors, $\vec{V}$ and $\vec{I}$:

$$Z = \frac{\vec{V}}{\vec{I}} = \frac{V_0}{I_0}\exp(\mathrm{j}\phi). \tag{2.14}$$

Because the phase difference between $\vec{V}$ and $\vec{I}$ remains constant, Z does not rotate and so is not denoted as $\vec{Z}$.

In general, it is found that I_0 and ϕ are dependent on the frequency of the impressed sinusoid, ω. Thus the impedance of the electrochemical cell is often

expressed as

$$Z(\omega) = Z_0(\omega) \exp\left[\mathrm{j}\,\phi(\omega)\right] \tag{2.15}$$

where $Z_0(\omega) = \frac{V_0}{I_0}$ (the magnitude of the impedance) is the constant of proportionality between the potential and current magnitudes and $\phi(\omega)$ (the phase of the impedance) is the phase difference between the potential and current sinusoids at a frequency of ω.

$Z(\omega)$ is useful because it can be applied in a similar manner to Ohm's law that describes the potential/current relationship associated with a resistor. It establishes a small-signal linear model for the current response of an electrode to an impressed sinusoidal potential (and *vice versa*):

$$\vec{V} = \vec{I}\,Z \tag{2.16}$$

so that

$$v(t) = \mathrm{Re}\left\{\vec{I}\,Z\right\} \tag{2.17}$$

$$i(t) = \mathrm{Re}\left\{\vec{V}\,Z^{-1}\right\} \tag{2.18}$$

For large signals, proportionality between potential and current magnitudes does not generally exist. In that case the presence of non-linearity introduces harmonic distortion into the current response so that (2.7) does not imply (2.8) and the concept of impedance becomes meaningless.

The principle of superposition for linear systems allows the concept of impedance to be extended to non-sinusoidal signals too. In that case the signal is viewed as a weighted sum of sinusoidal components, determined by the Fourier series/transform of the signal. The response of the system is then given by the weighted sum of the response to the individual sinusoidal components.

2.2.2 Nyquist and Bode Representations of the Impedance

The impedance of an electrochemical cell is a frequency dependent, complex valued quantity. Being complex valued, it has both a magnitude and a phase which makes graphical representation more difficult. Walter [38] provides a review of impedance plotting methods for use in corrosion performance analysis.

There are two common methods for graphical representation of a complex impedance. The Nyquist diagram is a polar plot of impedance magnitude versus phase (or equivalently a Cartesian plot of real part versus imaginary part). The Bode diagram plots the magnitude versus frequency on one pair of axes and the phase versus frequency on the other pair.

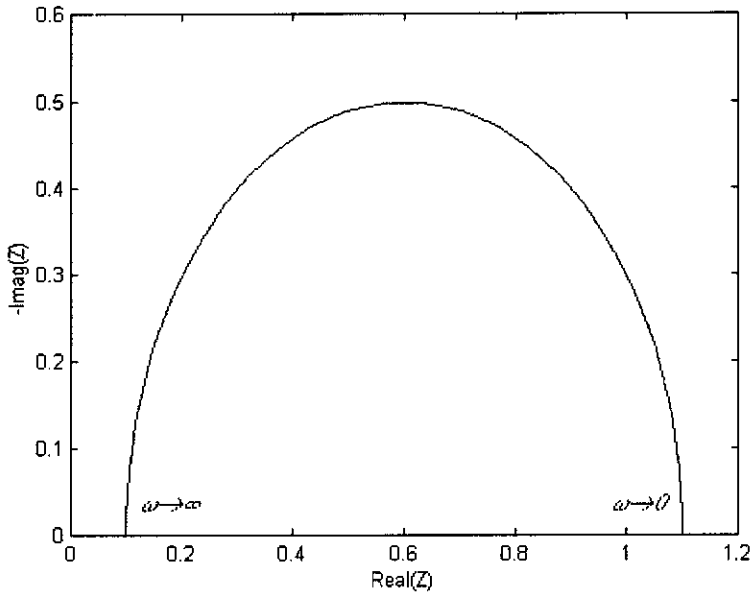

Figure 2.4: Example Nyquist Diagram

As an example, suppose an impedance is given by

$$Z(\omega) = R_{\mathrm{s}} + \frac{R_{\mathrm{p}}}{1 + \mathrm{j}\,\omega C R_{\mathrm{p}}}, \tag{2.19}$$

which describes Randle's cell (see Figure 2.7 on page 27).

The Nyquist diagram of (2.19) is shown in Figure 2.4 for $R = 1$ and $R_{\mathrm{s}} = 0.1$. Note that the capacitance, C, has no effect on the Nyquist Diagram.

From Figure 2.4, the topology of the impedance under study can be inferred, as can the values of the two resistors. However, the value of the capacitor cannot be found from Figure 2.4 as all frequency information is lost.

Figure 2.5 shows the Bode diagram of (2.19) with $R = 1$, $R_{\mathrm{s}} = 0.1$ and $C = 1$.

The shapes of the magnitude and phase plots in Figure 2.5 can also be used to infer the topology of the impedance. The values for R and R_{s} can be found by observing the high and low frequency impedance magnitudes. The time constant of the impedance, and hence the capacitance, can be found from the frequency at which the impedance is 3 dB smaller than $R + R_{\mathrm{s}}$.

2.2.3 Elements of Electrochemical Impedance [6]

Each of the elements of the electrochemical impedance is related to the physical properties of the cell. It is the purpose of electrochemical impedance spectroscopy to identify these elements so that the physical properties can be inferred. This section will describe each of the common components:

- Solution Resistance;

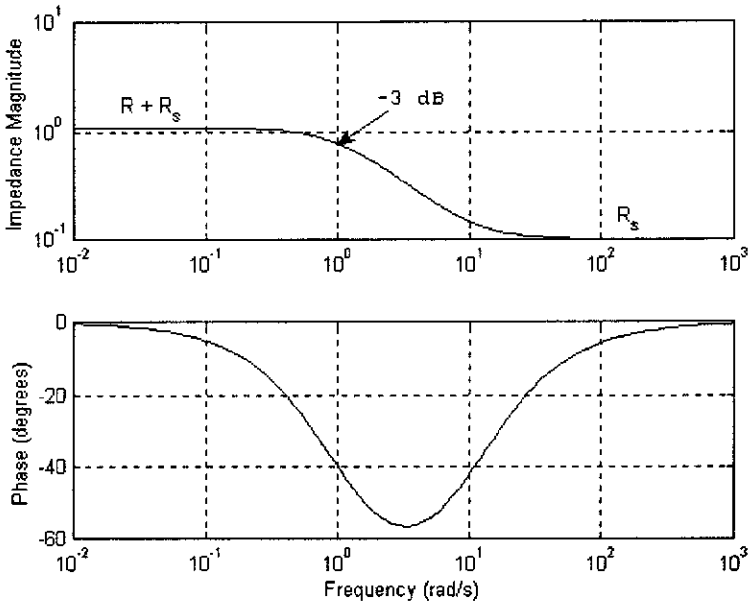

Figure 2.5: Example Bode Diagram

- Double Layer Capacitance;
- Polarisation Resistance;
- Charge Transfer Resistance;
- Diffusion Impedance; and
- Coating Capacitance.

Solution Resistance

The resistance of an ionic solution depends on the ionic concentration, type of ions, temperature, and the geometry of the area in which current is carried. In a bounded volume of cross sectional area A and length l carrying a uniform current the resistance is defined as:

$$R = \frac{\rho l}{A} \tag{2.20}$$

where ρ is the resistivity of the solution.

Standard chemical handbooks list resistivities for specific solutions — *eg* different concentrations of NaCl solutions at different temperatures. For other solutions, resistivity can be calculated from specific ion conductances.

Unfortunately, most electrochemical cells do not have uniform current distribution through a definite electrolyte area. The major problem in calculating solution resistance concerns determination of the current flow path and the geometry of the electrolyte that carries the current.

Double Layer Capacitance

An electrical double layer exists at the interface between an electrode and its surrounding electrolyte. This double layer is formed as ions from the solution are attached to the electrode surface. Charges in the electrode are separated from the charges of these ions. The separation is very small, of the order of few angstroms.

Charges separated by an insulator form a capacitor. On a bare metal immersed in an electrolyte, there will be approximately 30 μF of capacitance for every cm^2 of electrode area. [6]

The value of the double layer capacitance depends on many variables including electrode potential, temperature, ionic concentrations, type of ions, oxide layers, polish of the electrode surface, adsorption of impurities, *etc.*

Polarisation Resistance

Whenever the potential of an electrode is shifted away from its value at open circuit, it is referred to as polarising the electrode. When an electrode is polarised, it can cause current to flow via electrochemical reactions that occur at the electrode surface. The amount of current is controlled by the kinetics of the reactions and the diffusion of reactants both towards and away from the electrode.

In cells where an electrode undergoes uniform corrosion, the open circuit potential is controlled by two different electrochemical reactions. The open circuit potential stabilises at the potential where the cathodic and anodic currents are equal. It is referred to as a mixed potential. The magnitude of the current for either of the reactions is known as the corrosion current. The corrosion current is the rate of the corrosion reaction in coulombs per second.

When there are two simple, kinetically controlled reactions occurring, the potential of the cell is related to the current by the Butler-Volmer Equation:

$$i = I_0 \exp\left[\frac{E - E_0}{\beta_A}\right] - I_0 \exp\left[-\frac{E - E_0}{\beta_C}\right] \tag{2.21}$$

where I_0 is the corrosion current; E is the potential of the electrode; E_0 is the open circuit potential of the electrode; and β_A and β_C are known as the anodic and cathodic Tafel constants.

The corrosion current can be estimated by fitting the Butler-Volmer equation to the experimentally observed potential-current curve. In corrosion applications, the linear polarisation resistance (LPR) method is commonly used to determine the corrosion current as it requires only small (approximately ± 10 mV) perturbations to the electrode.

The LPR technique is to infer the corrosion current by measuring the gradient of the potential-current curve about the free corrosion potential (*ie* the equivalent impedance at low frequency) and to equate it with the gradient of the Butler-Volmer

equation. Doing so results in the Stern-Geary equation [9]:

$$\frac{\Delta V}{\Delta I} = R_{\mathrm{p}} = \frac{\beta_{\mathrm{A}}\beta_{\mathrm{C}}}{2.3(\beta_{\mathrm{A}} + \beta_{\mathrm{C}})I_0} \tag{2.22}$$

where $\frac{\Delta V}{\Delta I}$ is the observed gradient of the potential-current curve about the free corrosion potential and is defined as the *polarisation resistance*, R_{p}. β_{A}, β_{C} and I_0 are as defined in (2.21).

Given the polarisation resistance and if the Tafel constants, β_{A} and β_{C}, are known, (2.22) can be used to infer the corrosion current, I_0. Typical β_{A} and β_{C} values for mild steel are 100 to 120 mV per decade of current. Thus the polarisation resistance can often be regarded as representative of the rate of corrosion, I_0. By (2.22), the larger R_{p} is, the lower the rate of corrosion. The smaller R_{p} is, the larger the rate of corrosion.

Charge Transfer Resistance

A resistance similar to the polarisation resistance is formed by a single kinetically controlled electrochemical reaction. In this case, there is no mixed potential, but rather a single reaction at equilibrium.

Consider a metal substrate in contact with an electrolyte. The metal molecules can electrolytically dissolve into the electrolyte according to:

$$\mathrm{M} \Longleftrightarrow \mathrm{M}^{n+} + ne^{-} \tag{2.23}$$

In the forward reaction, electrons enter the metal and metal ions diffuse into the electrolyte so that charge is transferred. This charge transfer reaction proceeds at a certain rate. The rate depends on the type of reaction, the temperature, the concentration of the reaction products and the potential.

The general relation between the potential and the current is [6]:

$$i = i_0 \left[\frac{C}{C_0^*} \exp\left(\frac{\alpha n F \eta}{RT}\right) - \frac{C_{\mathrm{R}}}{C_{\mathrm{R}}^*} \exp\left(-\frac{(1-\alpha) n F \eta}{RT}\right) \right] \tag{2.24}$$

where i_0 is the exchange current density;
C_0 is the concentration of oxidant at the electrode surface;
C_0^* is the concentration of oxidant in the bulk solution;
C_R is the concentration of the reductant at the electrode surface;
C_R^* is the concentration of the reductant in the bulk solution;
F is Faraday's constant;
T is the temperature (degrees Kelvin);
R is the gas constant;
α is the reaction order;
n is the number of electrode involved; and
η is the over-potential.

The over-potential measures the degree of polarisation. It is the electrode potential minus the equilibrium potential for the reaction.

When the concentration in the bulk solution is the same as at the electrode surface, $C_0 = C_0^*$ and $C_R = C_R^*$. This simplifies (2.24) to

$$i = i_0 \left[\exp\left(\frac{\alpha n F \eta}{RT}\right) - \exp\left(-\frac{(1-\alpha) n F \eta}{RT}\right) \right] \tag{2.25}$$

Equation (2.25) is known as the Butler-Volmer equation. It is applicable when the polarisation is not dependent on diffusion of species to or from the electrode.

When the electrochemical system is at equilibrium, the gradient of η with respect to i about the equilibrium potential, (the *charge transfer resistance*), is given by

$$R_{ct} = \frac{RT}{nFi_0} \tag{2.26}$$

From (2.26), the exchange current density can be calculated when R_{ct} is known.

Diffusion

Diffusion can result in an apparent impedance known as the Warburg impedance. This impedance depends on the frequency of the potential perturbation. At high frequencies the Warburg impedance is small since diffusing reactants don't have to move very far between metal and bulk solution. At low frequencies the reactants have to diffuse farther, thereby increasing the Warburg impedance.

The equation for the "infinite" Warburg impedance is:

$$Z(\omega) = \sigma \omega^{-0.5}(1 - \mathrm{j}) \tag{2.27}$$

and is characterised by a constant phase of 45°.

In (2.27), σ is the Warburg coefficient defined as

$$\sigma = \frac{RT}{n^2F^2A\sqrt{2}}\left(\frac{1}{C_0^*\sqrt{D_0}} + \frac{1}{C_R^*\sqrt{D_R}}\right) \tag{2.28}$$

where ω is the frequency in radians per second;
D_0 is the diffusion coefficient of the oxidant;
D_R is the diffusion coefficient of the reductant;
A is the surface area of the electrode;
n is the number of electrode transferred; and
C^* is the bulk concentration of the diffusing species (moles.cm^{-3})

This form of the Warburg impedance is only valid if the diffusion layer has an infinite thickness. Quite often this is not the case. If the diffusion layer is bounded, the impedance at lower frequencies no longer obeys (2.27) [6]. Instead,

$$Z_0(\omega) = \sigma\omega^{0-.5}\tanh\left(\delta\sqrt{\frac{j\omega}{D}}\right) \tag{2.29}$$

where δ is the Nernst diffusion layer thickness; and D is an average value of the diffusion coefficients of the diffusing species.

Equation (2.29) is called the "finite" Warburg impedance. For high frequencies where $\omega \to \infty$, or for an infinite thickness of the diffusion layer where $\delta \to \infty$, (2.29) simplifies to the infinite Warburg impedance [equation 2.27].

Coating Capacitance

A capacitor is formed when two conducting plates are separated by a non-conducting media, called the dielectric. The value of the capacitance depends on the size of the plates, the distance between the plates and the properties of the dielectric. The capacitance is given by

$$C = \varepsilon_0\varepsilon_r\frac{A}{d} \tag{2.30}$$

where ε_0 is the electrical permittivity of free space;
ε_r is the relative electrical permittivity of the dielectric;
A is surface area of the conducting plate; and
d is the distance between the two plates.

An organic coating typically has a relative permittivity of 4 to 8, whereas water at 20 °C has a relative permittivity of 80.1. The capacitance of a coated substrate changes significantly as it absorbs water. If the capacitance is measured, this absorption process can be detected. [6]

Figure 2.6: Equivalent impedance for a purely capacitive coating. [6]

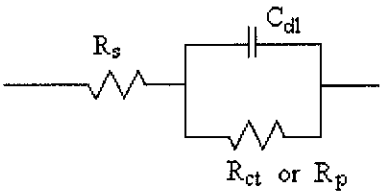

Figure 2.7: Randle's cell. [6]

2.2.4 Equivalent Impedance Topologies

The elements of electrochemical impedance discussed above often occur in different serial/parallel combinations according to the types of processes occurring. This section describes some of the common models.

Purely capacitive coating

A metal covered with an undamaged coating typically has a very high impedance. It's equivalent impedance is shown in Figure 2.6.

The resistance is primarily due to the electrolyte while the capacitance is due to the coating.

Randle's Cell

Randle's cell is one of the simplest and most common models of electrochemical impedance. It includes a solution resistance (R_s) a double layer capacitor (C_{dl}) and a charge transfer (R_{ct}) or polarisation resistance (R_p). Figure 2.7 depicts Randle's cell.

In addition to being a useful model in its own right, Randle's cell is often the starting point for more complex models such as the model for mixed kinetic and diffusion and for coated metal.

Mixed Kinetic and Diffusion Control

When the diffusion of species to and from the electrode surface is at least partially a rate limiting step, the Warburg impedance (W) is added in series with the charge transfer resistance in Randle's cell, as depicted in Figure 2.8.

The Warburg impedance cannot be modelled by a simple capacitance or inductance or resistance and so is assigned a symbol of its own in Figure 2.8.

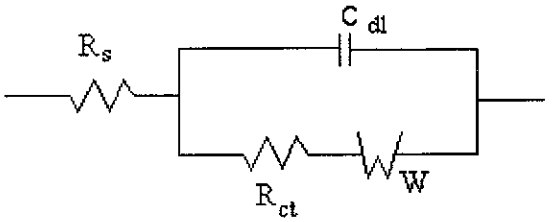

Figure 2.8: Equivalent impedance for mixed control. [6]

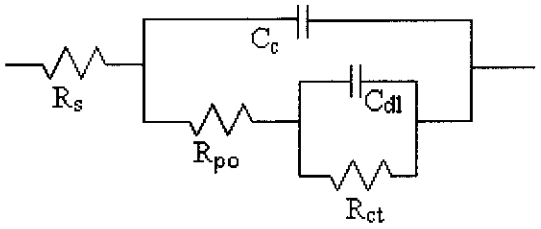

Figure 2.9: Equivalent impedance of a coated metal. [6]

Coated Metal

The impedance behaviour of a purely capacitive coating has been discussed above. Most coatings degrade with time, resulting in more complex behaviour. After a certain amount of time, water penetrates into the coating and forms a new liquid/metal interface under the coating. Corrosion phenomena can occur at this new interface.

The impedance of coated metals has been widely studied. The interpretation of impedance data from failed coatings can be very complicated. Only the simple equivalent circuit shown in Figure 2.9 is discussed here.

Even this simple model has been the cause of some controversy in the literature. Most researchers agree that this model can be used to evaluate the quality of a coating. However, they do not agree on the physical processes that the equivalent circuit elements represent. The following discussion is therefore only one of several interpretations of this model.

The capacitance of the intact coating is represented by C_c. Its value is much smaller than a typical double layer capacitance. R_{po} (pore resistance) is the resistance of ion conducting paths that develop in the coating.

On the metal side of the pore, it is presumed that an area of the coating has delaminated and a pocket filled with an electrolyte solution has formed. This electrolyte solution can be very different from the bulk solution outside of the coating. The interface between this pocket of solution and the bare metal is modelled as a double layer capacity in parallel with a kinetically controlled charge transfer reaction.

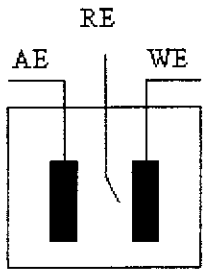

Figure 2.10: Configuration for EN Measurements under Potentiostatic or Galvanostatic Control. [40]

2.3 Electrochemical Noise

Electrochemical noise (EN) refers to the spontaneous fluctuations in potential (electrochemical potential noise, EPN) that can be observed on a corroding electrode or the spontaneous fluctuations in current (electrochemical current noise, ECN) when the electrode is polarised by an external source. It was first proposed by Iverson [39] that "investigation of these [EPN] fluctuations appears to offer much promise for the detection and study of the corrosion process."

Eden [40] describes two basic configurations for performing EN measurements using a three-electrode system:

Figure 2.10 shows a system that can be used for *potentiostatic* or *galvanostatic* control. Under potentiostatic control, the potential of the working electrode (WE, the corroding electrode under study) with respect to the reference electrode (RE) is held at a constant level by polarising the WE via the auxiliary electrode (AE). For galvanostatic control, the current flowing between AE and WE is held at a constant level. This type of arrangement is often used for laboratory studies, particularly for accelerated testing of material susceptibility to a variety of failure mechanisms within defined potential regions [40].

Figure 2.11 shows a configuration used for EN measurements at the free corrosion potential. The naturally occurring ECN and EPN can be monitored simultaneously. Typically, WE1 and WE2 are electrically coupled via a zero resistance ammeter (see Section 2.3.4) so that the current EN flowing between them can be logged. Simultaneously, the potential at the point of coupling with respect to RE is logged. This type of arrangement is useful for the study of the evolution of naturally occurring corrosion processes. It is widely used in plant monitoring/surveillance situations. In applications where a reference electrode might be unpractical, the reference electrode is often replaced with another working electrode [40].

It is the analysis of this simultaneous EPN/ECN measurement that is the subject of the thesis.

An example EPN/ECN measurement is shown in Figure 2.12. It was obtained

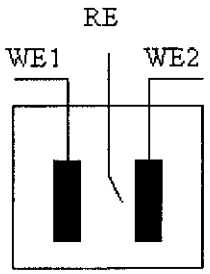

Figure 2.11: Configuration for EPN and ECN measurement between two working electrodes. [40]

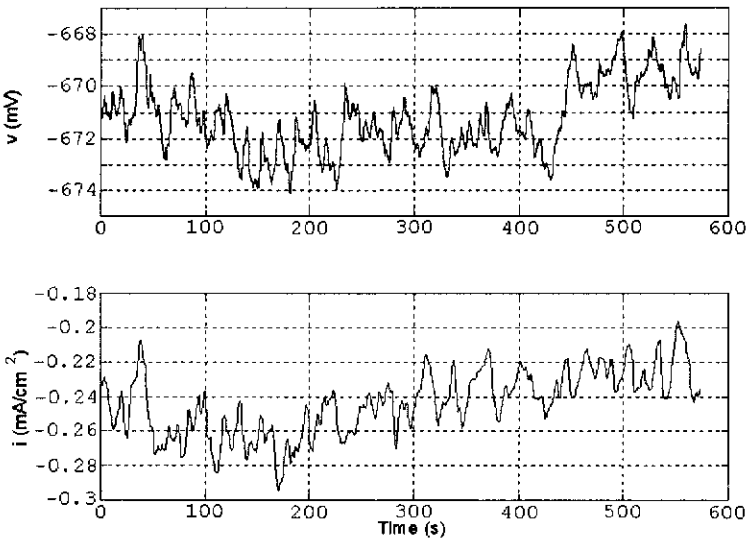

Figure 2.12: Example potential and current EN

from a corrosion system consisting of a coupled pair of mild steel electrodes immersed in 3 % NaCl solution at 70 °C. Of particular note is the large DC component in the potential measurement and the large time scale.

The EN literature is comprehensively reviewed by Gabrielli, Keddam and coworkers between 1990 and 1992 [41] [42] [43] and by Dawson's keynote address to a symposium on EN measurements in 1996 [12]. Tan, Kinsella and Bailey [44] published a review focusing on the unsolved problems in EN analysis theory in 1997.

Section 2.3.1 list the types of systems where EN has been observed. Section 2.3.2 reviews the literature dealing with the models and theoretical sources of EN. Section 2.3.3 explains the use of a wire beam electrode with EN measurements. The so called Zero Resistance Ammeter (ZRA), used for EN measurements, is described in Section 2.3.4. See Appendix C for details of tests on the author's ZRA. Section 2.3.5 discusses the applications of EN.

2.3.1 Systems Exhibiting EN

EN has been observed on a wide range of systems covering a wide range of corrosion mechanisms:

- Uniform corrosion of iron and iron alloys in various saline solutions have been extensively studied. [45] [46] [47] [48]
- Hardon, Lambert and page [49] studied the EN from salt contaminated, steel reinforced concrete.
- CO_2 corrosion and organic inhibitor films have been studied by Tan, Kinsella and Bailey. [50] [51] [16]
- Coated steel systems have been found to yield EN. [21] [52]
- There has been much interest in the behaviour and analysis of EN resulting from localised corrosion processes involving $NaNO_2$ inhibited iron [53] and stainless steels in general. [54] [55] [56] [57] [58] [59] [60] [61] [62]
- EN has been observed on metals such as aluminium, magnesium and zinc. [39] [63] [64]
- The pitting of aluminium and copper has been seen to yield unique EN phenomena. [65] [66] [54] [67] [68] [69]
- Gabrielli, Huet and Keddam [14] examined the EN arising from the potassium ferri-ferro-cyanide reaction on platinum.
- The EN from mechanical forms of corrosion such as stress corrosion cracking and erosion-corrosion has interested several researchers. [70] [71] [72] [73] [74]

With such a variety of systems exhibiting EN phenomena, the sources and models of EN can be expected to be just as varied.

2.3.2 EN Sources and Models

In the review by Gabrielli *et al* [42] EN phenomena are regarded as a result of the random nature of corrosion reactions.

> From the micro-structural point of view, metals are generally polycrystalline materials, consisting of grains of different forms and orientation, on the boundaries of which various chemical elements are concentrated. In addition cracks, inclusions ... occur within metals. These micro-structural features cause metals to be susceptible to random variations in physical properties and, consequently, in their corrosion behaviour. Likewise, local variations in flow conditions, temperature, pH, etc ...

> are some of the environmental parameters to be considered. Thus the inherent randomness of the corrosion system may be viewed from the high degree of complexity of the metal-protection-environment combination that can produce significant variations in : (1) the active corrosion driving-forces, (2) the resistance to corrosion and, consequently, (3) the local corrosion rate even though the nominal metal-protection-environment parameters appear uniform.

Hladky and Dawson [75] explain the source of EN as being classified into three categories:

> Charge carrier effects contribute noise whose spectral density, the amount of noise present in a given bandwidth, is essentially constant over a wide range of frequencies and is of a low amplitude. This category covers noise originating from thermal agitation of charge carriers, noise caused by charge being transferred in discrete amounts and by other such phenomena.
>
> A second source of noise relates to surface processes occurring on the electrodes and specifically to their [heterogeneity]. These give rise to fluctuations at frequencies of approximately 1 Hz and below. The observed spectral density of these fluctuations in general varies with frequency and the amplitude can be much higher than that caused by charge carrier effects.
>
> At very low frequencies environmental changes, such as variations of the physical and chemical parameters of the observed system, result in slow fluctuations of the electrode potential or current. These often have the appearance of drift of the electrode potential and can sometimes be accounted for by existing theories of electrode thermodynamics and kinetics.

By observation of discrete transient EN phenomenon simultaneously with the physical evolution of hydrogen gas bubbles when iron is exposed to acidic medium, hydrogen gas evolution has been conclusively shown to be a source of potential EN. [43]

Legat [76] studies the effect of electrolyte movement on the EN measurement. A significant change in the EN characteristics are observed with laminar flow. The study confirms that:

> ... the main source for this change is transformation of corrosion processes: in a still solution, the corrosion process tends to be localised, whereas during strong movement of the electrolyte, this tendency is oriented toward uniform corrosion ...

> ... it was established that the direct effect of the electrolyte movement on measured EN (modulation of signals caused by spatio-temporal flow disturbances) is small.

With a variety of different possible mechanisms for generation of EN, the problem of modelling EN has been an on going one:

Blanc *et al* [77] propose a model of EN generated by electrochemical reactions including the effects of diffusion:

> The elementary fluctuations are supposed to be the particle fluxes which are Poisson white noise. This model is successfully used to describe the experimental stochastic behaviour of the two cases of non-equilibrium, electrochemical interfaces: the noise generated by anodic dissolution of iron in acidic medium and that by diffusion of a reacting species in the bulk of the electrolyte.

A unified approach to the problem of modelling electrochemical fluctuations is presented by Seralathan and Rangarajan [78] [79]. Dawson [12] summarises their work:

> The Rangarajan models consider electrochemical noise a process involving faradaic shot noise; their methodology provides a fundamental treatment of [previous studies] ... It involves, first, consideration of primary noise sources, which are fundamental, but invariably uncorrelated (the Langevin approach), and second, assessment of macroscopic phenomena that provide the secondary source of noise. The treatment includes equations for conversion of the current into power spectra. The [macrovariables] include partial faradaic currents, electron transfer, and chemical kinetics, but these are described as discrete Poisson processes. The formalisation was not extended to corrosion studies such as pit nucleation and growth; it is nevertheless an approach that could be used to formalise corrosion processes.

Gabrielli, Huet and Keddam [80] [14] model the stochastic behaviour of the electrochemical interface when diffusion limited reactions occur on the electrode surface. Comparison is made with experimental measurements with good correlation.

Cottis [81] models EN as a superposition of bursts associated with the discrete unlocking of chains or "ledges" of atoms of random length from the metal surface.

Huet *et al* [82] uses the electrochemical permeation technique and a model for hydrogen diffusion in a metal to explain observed fluctuations in potential and absorbed hydrogen concentration. It is found that at cathodic potentials the fluctuations can be explained by evolution of large hydrogen gas bubbles but that the model is inadequate near the corrosion potential.

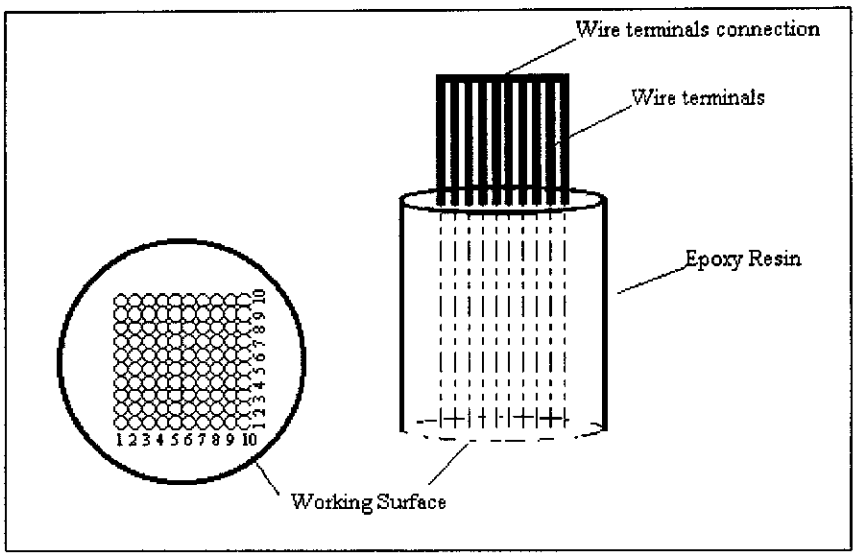

Figure 2.13: A 10x10 Wire Beam Electrode Matrix

Bertocci *et al* [83] compare the time domain features of the EN with its PSD and demonstrate the use of the PSD for estimating various EN parameters. To do so, they used an empirical model of EN that is composed of superimposed transient spikes.

2.3.3 The Wire Beam Electrode

The wire beam electrode (WBE) [26] [27] is a tool for monitoring uniform and localised metal corrosion rates and corrosion patterns. The WBE is constructed from many closely bound, electrically insulated metal wires, which divide a large electrode area into many small individual parts or mini-electrodes, as depicted in Figure 2.13. The entire surface is termed the sensor or WBE while the individual wires are termed mini-electrodes, or just wires. The electrochemical corrosion processes occurring on local areas of the sensor can be monitored using these mini-electrodes in conjunction with suitable corrosion monitoring techniques (*eg* electrochemical noise analysis).

A large amount of electrochemical data are acquired from each wire and from each pair of neighbouring wires. This requires the measurement of EPN and ECN signals from selected electrode pairs, as well as the measurement of the corrosion potential of each electrode individually. The measurement of galvanic currents between each individual electrode and the remainder of the whole electrode system also gives useful information. These measurements enable maps of corrosion rate distribution, corrosion potential distribution and galvanic current distribution to be constructed. [28]

The WBE electrode has been used to study protective oil coatings [84] [85] the crevice corrosion of copper [86] and organic coatings [87].

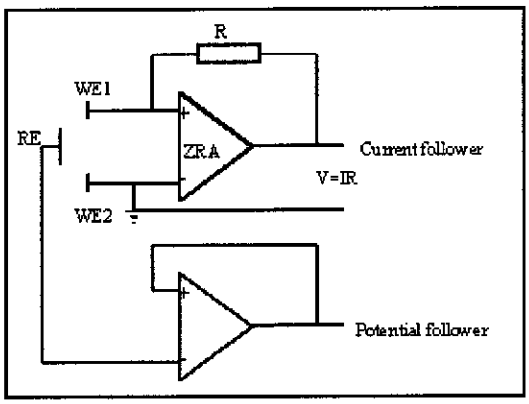

Figure 2.14: Schematic of a Zero Resistance Ammeter. [40]

Because of the large number of mini-electrodes that form the sensor, specially designed multiplexing hardware is required. Chapter 6 discusses the novel construction of such hardware and associated software. The work described in Chapter 6 is also published in reference [88].

2.3.4 The Zero Resistance Ammeter

An integral part of EN measurements is the zero resistance ammeter (ZRA). Using solid state electronics, it achieves a current measurement with very low resistance and a potential measurement with very high impedance. Figure 2.14 shows the schematic of a ZRA connected to two working electrodes and the reference electrode of Figure 2.11.

According to Eden [40]

> The ZRA acts to maintain the potentials of the two working electrodes at the same potential (with modern devices the potential difference can be maintained within a microvolt). The current required to maintain the two working electrodes at the same potential flows through the feedback resistor R, and the voltage output of the ZRA is related to the current flowing through the system by $V = IR$. The potential buffer is often used to ensure that there is no current drain on the reference electrode.

2.3.5 Applications of EN

EN has found application for

- corrosion rate estimation;
- classification of corrosion type; and
- study of corrosion phenomena.

This section reviews the literature relating to these applications.

Rate Estimation

Initially, the variance of EPN was proposed as an indicator of rate of corrosion. Hardon *et al* [49] provides copious experimental data to demonstrate correlation between the variance of EPN and the corrosion current. But the data also demonstrates a large degree of scatter, which shows that the technique is not particularly reliable.

Legat and Zevnik [45] demonstrate strong correlation between current EN power and the corrosion current in mild and stainless steel systems employing various water solutions.

Gabrielli *et al* [14] demonstrate impedance measurements using EPN and ECN obtained under galvanostatic and potentiostatic conditions respectively, which allows rate information to be inferred by EIS theory. (Figure 2.10, page 29)

However, it is the noise resistance technique proposed by Eden *et al* [13] that has drawn the most attention. The noise resistance is obtained from a simultaneous EPN/ECN measurement using a system with two coupled working electrodes (Figure 2.11, page 30). It is defined as the ratio of EPN standard deviation and ECN standard deviation.

The background to noise resistance and the related *spectral noise impedance* are examined in more detail in Section 3.1.

Classification and Detection of Localised Corrosion

The analysis of EN to classify the type of corrosion has attracted a significant amount of interest over the past 20 years. The idea is to identify a unique "signature" feature of the EN that identifies a particular mode of corrosion, especially for distinguishing between general corrosion, pitting corrosion and crevice corrosion.

Hladky and Dawson [89] investigate a aluminium/magnesium alloy, copper and mild steel immersed in aerated synthetic sea water. They conclude:

> there is a correlation between the nature of the corrosion attack and the low frequency fluctuations of the electrode potential. The [power spectral density of] electrochemical noise ... is of a constant amplitude over a range of very low frequencies and decreases in amplitude at frequencies above this range. The slope of the high frequency roll-off bears a relation to the nature of the corrosion attack ... A sharp peak at a single frequency indicates crevice attack.

Searson and Dawson [90] corroborate with Hladky and Dawson, finding a slope of -20 dB/decade for pitting attack and -40 dB/decade for uniform corrosion.

However, other researches have not been able to confirm these findings in all cases:

Mansfeld and Xiao [91] found that a roll-off of -20 dB/decade in EN power spectrum is not necessarily the characteristic of localised corrosion. Legat and Zevnik [45] concluded that it is the difference between EPN and ECN power-spectral densities, not the roll-off in the EN power spectrum that is related to the type of corrosion. Gusmano *et al* [92] did not completely confirm the findings of Hladky and Dawson either. In general, they did not find any clear correlation between EN power spectrum slopes, test parameters and corrosion behaviour.

There have been alternative proposed means of detecting and classifying localised corrosion, mostly with good results in their specific application:

Smith and Francis [69] were able to distinguish between pitting caused by copper tubing contaminated by a deleterious film and uncontaminated tubing. The analysis used was the standard deviation and the coefficient of variation of the EN.

Kelly *et al* [59] investigates the corrosion of 410 stainless steel in a variety of solutions covering widely different corrosivity. They find that in solutions where pitting occurs, the open circuit potential of the electrode is more sensitive to the pitting process than the *pitting index* (defined as the ratio of standard deviation of ECN to the root mean square of the ECN).

Pride, Scully, and Hudson [66] compare methods of analysing ECN and EPN associated with metastable pitting and the transition from metastable to stable pitting. They find statistics involving the radius of the pits more useful than the pitting index and noise resistance. They find that spectral analysis provides qualitative information on pit susceptibility but they were unable to accurately define the transition to stable pitting.

Roberge [63] proposes the use of a Stochastic Process Detector for analysis of EN and suggests that certain features thus extracted are indicative of localised corrosion in AA 7075-T6 aluminium alloy.

Legat and co-workers [48] [93] apply chaotic analysis to EN measured on localised and general corrosion systems. The general corrosion rate is found to have no influence on the fractal dimensions of the EN. They conclude that localised corrosion is generated by a deterministic chaotic process (*ie* a process where infinitesimally small, and thus unmeasurable, events can have significant and deterministic effect on the whole), whereas uniform corrosion is a random process.

The use of an artificial neural network is explored by Barton, Tuck and Wells [60] to classify the type of localised corrosion. 96 % of their test data was accurately detected and classified with no mis-classifications.

Dai [94] uses the discrete wavelet transform to extract a feature vector (histogram of the wavelet coefficients) from the EN. The feature vector is shown to be capable of quantitatively discriminating between (i) baseline corrosion (ii) pitting (iii) crevicing

and (iv) mixed pitting and crevicing.

MacDonald, Liu and Manahan [46] investigate the EN obtained from carbon and stainless steels in high sub-critical and supercritical aqueous environments. They conclude that, for their measurements, the magnitude of the EN responds sensibly to changes in the chemical and physical properties of the fluid and the pattern of the EN contains information on the nature of the corrosion processes that occur, including general corrosion, pitting attack, and stress corrosion cracking.

Alawadhi and Cottis [95] suggest that the cross-spectral density at low frequencies might be used to compute the quantity of charge in transient pulses and thus is indicative of localised corrosion.

The Study of Localised Corrosion

In addition to the detection and classification of localised corrosion EN has been used to study specific aspects of localised corrosion. The techniques are mainly rooted in analysis of transient spikes in EN that can be observed when a passive film breaks down. Parameters such the shape, peak value, quantity of charge, rate of occurrence, and various frequency domain characteristics of the transients have all been used to infer parameters for various models describing the process.

For example, pitting corrosion is studied in references [58], [57], [96], [97], [53], and [65]; crevice corrosion in references [62] and [67]. References [70], [71], [72] and [73] study stress corrosion cracking.

2.4 Conclusion

This chapter has reviewed various aspects of corrosion and corrosion monitoring technology. Although the techniques of corrosion monitoring are as diverse as the form and environments in which corrosion occurs, particular emphasis has been placed on EIS and the phenomenon of EN, as they relate to the thesis.

Chapter 3 reviews in detail how EN can be used for impedance estimation.

Chapter 3

Background: Electrochemical Noise Impedance Analysis

The traditional methods of electrochemical impedance measurement involve polarising the electrodes with sinusoids of varying frequencies so that the current response can be observed [8]. In some systems this polarisation, even if small in magnitude, might affect the corrosion process. By using EN for impedance measurement, the need for externally polarising the electrodes can be eliminated. An additional benefit is that the costs of the associated instrumentation can be reduced because no polarisation capability is required. Some disadvantages include a limited frequency range and inceased complexity of analysis.

Section 3.1 provides the background to impedance measurement using simultaneously obtained EPN/ECN. Sections 3.2 and 3.3 cover the mathematical tools required for impedance analysis with EN.

3.1 Impedance Measurement by Electrochemical Noise

This section explains how EN can be used to measure the impedance of a coupled electrode pair without specialised polarising equipment such as a potentiostat. Once the impedance is measured, analysis can proceed as per conventional EIS, described in Section 2.2.

The history of impedance measurement by EN is given in Section 3.1.1. The theory is covered in Section 3.1.2. Trend removal and asymmetric electrodes are discussed in Sections 3.1.3 and 3.1.4 and the unsolved problems with impedance measurement by EN are described in Section 3.1.5.

3.1.1 History

The electrochemical noise resistance was first described by Eden *et al* [13] for measuring the corrosion current of a corroding element in an electrochemical cell. The noise

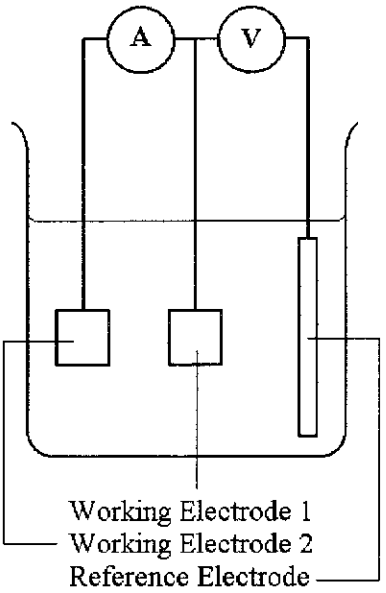

Figure 3.1: Noise resistance/impedance measurement setup

resistance measurement consists of a pair of nominally identical working electrodes electrically coupled by an ammeter. In addition to the current flowing between the two electrodes, the potential at the point of coupling is logged with respect to a reference electrode. In this way, a simultaneous EPN and ECN measurement is obtained from the cell. The *noise resistance* is defined as the ratio of the standard deviations of the EPN and ECN data. Figure 3.1 depicts the measurement set up and Figure 2.12 (page 30) shows an example EPN/ECN measurement.

Eden *et al* originally stated, with supporting theory, that the noise resistance is inversely proportional to the corrosion current. But it was subsequently found that the noise resistance is often comparable to the polarisation resistance [52] [50] [98]. If the noise resistance can indeed be used to measure the polarisation resistance, then by the Stern-Geary equation [9] [10] the noise resistance provides a means of rate estimation. However, despite theory concluding that the noise resistance and the polarisation resistance are equal [18] [99] [100] [101] [102] equality has not always been observed in practice [21] [59] [25].

The work of Bertocci *et al* [19] [47], based on the equivalent circuit of the noise resistance measurement, explains one reason for discrepancy between practice and the previous theory. They find that "the noise resistance, R_n, is equal to the polarisation resistance, R_p, if the impedance of the electrodes is R_p in the frequency bandwidth investigated."

Mansfeld and coworkers [103] [20] compare the noise resistance with polarisation resistance from a variety of polymer coated steel systems exposed to seawater. They suggest that the noise resistance is a "frequency dependent" quantity (*ie* dependent

on the frequency characteristics of the EN) and conclude that: "noise resistance is equal to the polarisation resistance, R_p, only for frequency-independent spectral noise [*ie* electrode impedance] plots."

In order to cope with the frequency dependency, Mansfeld and co-workers introduced the *spectral noise impedance* [21], defined as the ratio of the potential and current Fourier transforms. (Bertocci *et al* [19] define a similar quantity, but as the square root of the ratio of the power spectral densities instead.) In a study on polymer coated steel samples in sea water, Mansfeld, Lee, and Zhang [103] find that there is excellent agreement between the spectral noise impedance and the impedance as obtained by AC polarisation techniques.

In order to cope with dynamic systems, where the impedance of the cell varies with time, Tan, Bailey and Kinsella [50] propose a "fast" noise resistance calculation. It involves continuously computing the noise resistance over a sliding window so that it is a function of time. The technique is applied to study the formation and destruction of inhibitor films, where the properties of a protective coating change with time [16] [51]. However, there have been some questions raised as to how short the width of the sliding window can be made before erroneous results are obtained [17].

3.1.2 Theory

The noise resistance is defined by Eden *et al* [13] as

$$R_n = \frac{\sigma_v}{\sigma_i} \tag{3.1}$$

where σ_n^2 and σ_i^2 are the variances of the EPN and ECN respectively.

To emphasise the continuous noise resistance of Tan, Bailey and Kinsella [50] a time dependent "continuous" noise resistance can be denoted as

$$R_n(t) = \frac{\sigma_v(t)}{\sigma_i(t)}. \tag{3.2}$$

Tan *et al* estimate this continuous noise resistance by employing a sliding window:

$$\hat{R}_n(t) = \sqrt{\frac{\int_{t-T}^{t+T} v^2(\tau)\mathrm{d}\tau}{\int_{t-T}^{t+T} i^2(\tau)\mathrm{d}\tau}} \tag{3.3}$$

where $v(t)$ and $i(t)$ are the respective EPN and ECN after trend removal (see Section 3.1.3) and T defines the width of the sliding window. It is noted that the publications of Tan *et al* use a discrete time notation whereas (3.3) is a continuous time notation.

Xiao and Mansfeld [21] introduce the spectral noise impedance, originally as a function of the Fourier transforms of EPN and ECN signals. Bertocci *et al* [19]

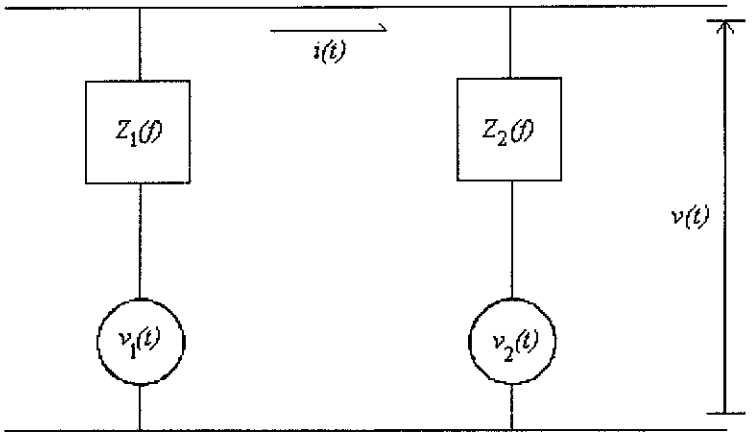

Figure 3.2: Thevenin model of noise resistance measurement

define it in terms of the power spectral densities (PSD, see Section 3.2.4):

$$R_{\mathrm{sn}}(f) = \sqrt{\frac{S_{\mathrm{v}}(f)}{S_{\mathrm{i}}(f)}} \tag{3.4}$$

where $S_{\mathrm{v}}(f)$ and $S_{\mathrm{i}}(f)$ are the PSDs of the EPN and ECN respectively.

The work of Bertocci *et al* [19] [47] models the electrochemical cell with a small signal equivalent circuit as in Figure 3.2. Figure 3.2 is the *Thevenin equivalent circuit* model and, for simplicity, the solution resistance is incorporated into $Z_1(f)$ and $Z_2(f)$.

In Figure 3.2, $v_1(t)$ and $v_2(t)$ are the Thevenin equivalent sources of EN originating from each of the two working electrodes and $Z_1(f)$ and $Z_2(f)$ are the equivalent impedances of each electrode/solution interface about the potential of operation (plus solution resistance).

It is noted that the $Z_1(f)$ and $Z_2(f)$ in Figure 3.2 are the (frequency dependent) gradients of the potential/current polarisation curves about the combined corrosion potential after the electrodes are coupled. If the two electrodes' individual free corrosion potentials differ excessively, they will polarise each other when they are coupled and the $Z_1(f)$ and $Z_2(f)$ gradients might differ from the gradients about the respective free corrosion potentials.

Based on the equivalent circuit, the PSD of the EN measurements, $v(t)$ and $i(t)$ are found to be

$$S_{\mathrm{v}}(f) = \left|\frac{Z_2(f)}{Z_1(f)+Z_2(f)}\right|^2 S_{\mathrm{v1}}(f) + \left|\frac{Z_1(f)}{Z_1(f)+Z_2(f)}\right|^2 S_{\mathrm{v2}}(f) \tag{3.5}$$

and

$$S_{\mathrm{i}}(f) = \frac{S_{\mathrm{v1}}(f)+S_{\mathrm{v2}}(f)}{|Z_1(f)+Z_2(f)|^2} \tag{3.6}$$

where $S_{v1}(f)$ and $S_{v2}(f)$ are the PSDs of $v_1(t)$ and $v_2(t)$ respectively.

Dividing (3.5) by (3.6) gives the square of the spectral noise impedance:

$$R_{sn}^2 = \frac{|Z_2(f)|^2 S_{v1}(f) + |Z_1(f)|^2 S_{v2}(f)}{S_{v1}(f) + S_{v2}(f)}. \tag{3.7}$$

When $Z_1(f) = Z_2(f) = Z(f)$, (3.7) reduces to

$$R_{sn}(f) = |Z(f)| \tag{3.8}$$

so that the spectral noise impedance is equal to the magnitude of the equivalent impedance regardless of the behaviour of the EN sources, $S_{v1}(f)$ and $S_{v2}(f)$.

Thus, according to the theory, when the two electrodes have identical impedances, conventional EIS theory can be applied to $R_{sn}(f)$ including inference of the polarisation resistance [with the exception that $R_{sn}(f)$ lacks all information regarding the phase of the impedance].

The relation between the R_n and $R_{sn}(f)$ is also examined by Bertocci *et al.* In terms of the PSDs of the measurement, $R_n$the noise resistance is given by

$$R_n = \frac{\sigma_v}{\sigma_i} = \sqrt{\frac{\int S_v(f)\mathrm{d}f}{\int S_i(f)\mathrm{d}f}} \tag{3.9}$$

Without further information on the shape of the source PSDs, $S_{v1}(f)$ and $S_{v2}(f)$, the integrals in (3.9) cannot be computed and no further expression for R_n can be deduced.

However, with the spectral noise impedance defined as in (3.4), the noise resistance can be expressed as

$$R_n = \sqrt{\frac{\int_{f_{min}}^{f_{max}} S_i(f) R_{sn}^2(f)\mathrm{d}f}{\int_{f_{min}}^{f_{max}} S_i(f)\mathrm{d}f}} \tag{3.10}$$

where f_{min} and f_{max} cover the effective bandwidth of $v(t)$ and $i(t)$.

Equation (3.10) shows that when $R_{sn}(f)$ is frequency independent in the range $[f_{min}, f_{max}]$ (with a value of R_{sn0}) then R_n is equal to R_{sn0}, regardless of the shape of $S_i(f)$. If f_{min} and f_{max} can be restricted to a range where R_{sn0} takes on some interesting value (*eg* the polarisation resistance or the solution resistance), then R_n can be used to determine that value.

This "frequency selectivity" will be used in Chapters 4 and 5 to estimate impedance within specific bands of frequencies.

3.1.3 Trend Removal

The measured EN is regarded as consisting of random fluctuations about some mean value. For the case of EPN, that mean value is the corrosion potential [50]. It is often observed that the corrosion potential tends to drift during the course of a measurement and it has been shown that this drift can greatly influence the results obtained from an analysis of the EN [104] [105] [106] [15]. The phenomenon is referred to as *DC trend* and the process of removing it is called *trend removal.*

In terms of stochastic processes, trend removal is the attempt to transform a non-stationary process into a stationary one. Shanmugan and Breipohl [107] and Bendat [108] discuss trend removal in general.

The two most prominent methods of trend removal that have been applied to EN are:

Linear Trend Removal (LTR) [15] [90] [62] where the trend is assumed to approximate a linear expression and linear regression is used to estimate it; and

Moving Average Removal (MAR) [50] where the trend is estimated using a moving average of some length.

There remains some controversy regarding how DC trend in EN analysis should be dealt with. Tan *et al* [44] note that "DC trend may follow any pattern and is normally not linear, nor in fact can it be fitted by a simple polynomial."

Figure 3.3 illustrates this point, where an example EPN signal with an exponentially shaped trend is seen. Tan *et al* propose MAR as a suitable solution. However, Mansfeld *et al* [15] have found that the moving average removal "did not remove a straight line ... but instead removed a straight line with superimposed small potential or current steps which changed the original [EN] in an erroneous manner" and they recommend that the moving average removal method not be applied in practice.

The MAR is examined in Section 4.3.5 and compared experimentally with other techniques in Section 4.4, where it is concluded that MAR is a useful technique.

Figure 3.4 shows the signal of Figure 3.3 after LTR and Figure 3.5 shows the result after MAR. It is duly noted that in the case of the example, in order to minimise edge effects, MAR has been applied to the signal after first applying LTR. In any case, a "residual" trend is evident in Figure 3.4, whereas there is no apparent trend in the signal of Figure 3.5.

Other methods of trend removal that have been applied are differencing [107], analogue high-pass filters prior to sampling (*eg* references [109] [47] and [39]) and various forms of digital high-pass or band-pass filters subsequent to sampling.

Section 4.3 of the thesis explores trend removal and its relation to impedance estimation in detail.

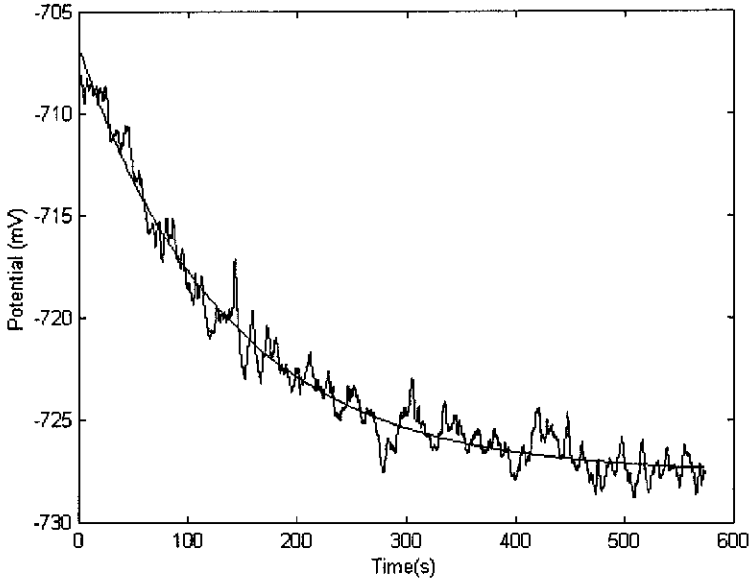

Figure 3.3: Potential EN with an exponential trend

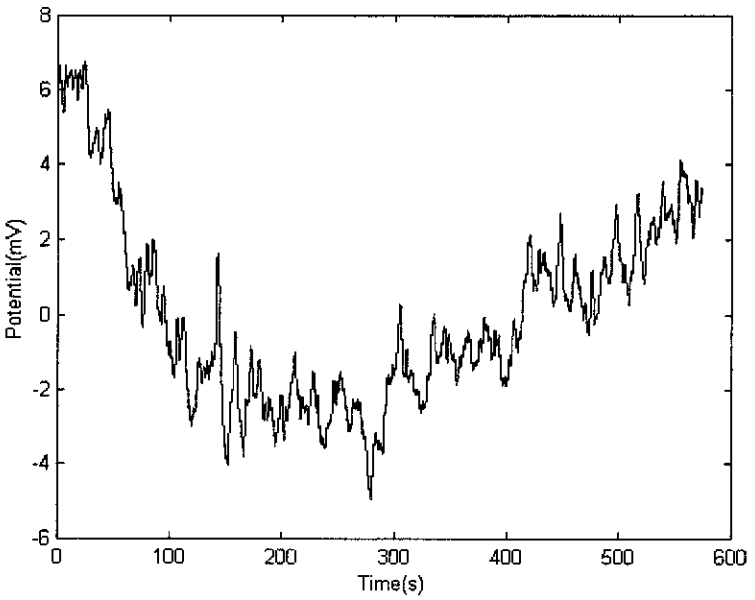

Figure 3.4: Signal of Figure 3.3 After Linear Trend Removal

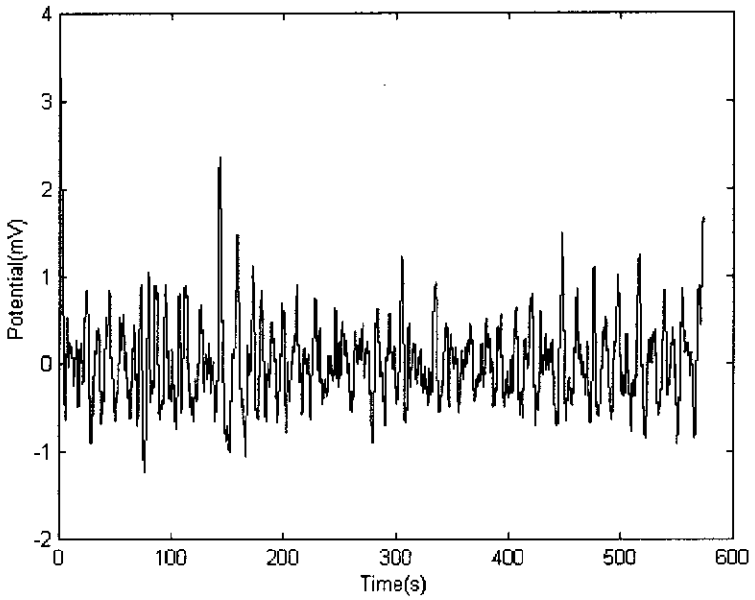

Figure 3.5: Signal of Figure 3.4 after further trend removal by Moving Average Removal

3.1.4 Asymmetric Electrodes

In the original paper describing the noise resistance, Eden *et al* [13] made it clear that "nominally identical" electrodes were assumed so that neither electrode applies any significant polarising potential to the other. The theory given by Bertocci *et al* [19] demonstrates that the electrodes require equal impedances if the spectral noise impedance is to be equal to the magnitude of the impedance.

A natural question to ask, however, is: how might the noise resistance and spectral noise impedance be interpreted when the electrodes are not nominally identical, *ie* when they are asymmetric?

Mansfeld *et al* [22] investigates the asymmetry caused by damage to the protective coating of coated steel electrodes. They find that there is only significant change in the noise resistance and spectral noise impedance when both electrodes are damaged and explain this finding by noting that the impedance of the two electrodes appear in series in a noise resistance measurement.

In the theoretical analysis of spectral noise impedance provided by Bertocci *et al* [19], the effect of differing electrode impedance and source EN PSDs are examined in relation the equivalent circuit model. They find that for electrodes with identical impedances, as already stated by (3.8), the spectral noise impedance is equal to the electrode equivalent impedance. For electrodes with different impedances, three typical scenarios are mentioned that follow from (3.7) when $Z_2(f) \gg Z_1(f)$:

1. The potential EN of the electrode with low impedance is larger than that of the high impedance electrode: $S_{v1}(f) \gg S_{v2}(f)$. This corre-

sponds to out-of-equilibrium situations where the EN is generated by localised corrosion (pitting, crevice, cracking, *etc.*). Then

$$R_{\mathrm{sn}}(f) = |Z_2(f)|\,. \tag{3.11}$$

2. The EN of the two electrodes is about the same: $S_{\mathrm{v1}}(f) \approx S_{\mathrm{v2}}(f)$. Then

$$R_{\mathrm{sn}}(f) = \frac{|Z_2(f)|}{\sqrt{2}}. \tag{3.12}$$

3. The potential EN of the electrode with high impedance is larger than that of the low impedance electrode: $S_{\mathrm{v2}}(f) \gg S_{\mathrm{v1}}(f)$, *eg*, at equilibrium where the EN is mainly thermal. Then

$$R^2_{\mathrm{sn}}(f) = |Z_1(f)|^2 + |Z_2(f)|^2 \frac{S_{\mathrm{v1}}(f)}{S_{\mathrm{v2}}(f)}. \tag{3.13}$$

These results tend to agree with the observations made by Mansfeld *et al* [22].

Bautista and Huet [109] extend the equivalent circuit theory of Bertocci *et al* to examine asymmetric electrodes in more detail. For asymmetric electrodes with known impedances, their work demonstrates how to calculate the ECN generated. They also show how corrosion occurring only on one electrode can be distinguished from corrosion occurring on both.

A measurement technique, called electrochemical emission spectroscopy (EES) that is related to the noise resistance measurement is proposed by Chen and Bogaerts [110]. One of the electrodes is replaced with a high impedance micro-cathode that is used for current sensing purposes. By proper analysis of the EPN and ECN obtained from this highly asymmetric system Chen and Bogaerts demonstrate that it is possible to "measure the general corrosion rate in real time and detect onset and repassivation of a localised corrosion site."

3.1.5 Unsolved Problems

As demonstrated by (3.10), the noise resistance, R_n, is implicitly a frequency dependent quantity. The frequency at which it manifests itself is largely determined by the PSD of the EN. The analyst has very little control over the PSD of the raw EN and, consequently, over the frequency at which R_n manifests. The alternative is to use the spectral noise impedance, $R_{\mathrm{sn}}(f)$, which is explicitly a function of frequency and the analyst can easily observe any interesting range of frequencies. But by doing so, the ability to monitor a dynamic system, *al la* the continuous noise resistance calculation of Tan *et al*, is largely conceded. To study a dynamic system, the analyst may wish to persist with analysis in the time domain by using $R_{\mathrm{n}}(t)$.

In that case there are a number of unsolved problems and other questions relating

to the noise resistance that need to be addressed:

- How can the implicit frequency dependency of the noise resistance be handled? How short can the sliding window in (3.3) be made? What is the precise effect of moving average removal on R_n [and even $R_{sn}(f)$ for that matter]? Can the time dependent $R_n(t)$ and the frequency dependent $R_{sn}(f)$ be combined to obtain a time-frequency dependent $R_n(t, f)$?

- The noise resistance is a statistical property of the EN and can only be estimated from a finite observation of EN. How do the observation time [*ie* length, T, of the sliding window in (3.3)] and the bandwidth of the EN affect the estimate of noise resistance? How can the EN signals be conditioned to optimised the estimate? If the estimate of noise resistance is poor, fair comparison cannot be made between the noise resistance and impedance measurements using AC or linear polarisation techniques in order to validate the EN technique.

- To validate the use of R_n [and $R_{sn}(f)$ too], knowledge of the symmetry of the pair of working electrodes is required. One way to assess symmetry is by separate impedance (by traditional AC polarisation techniques) and EPN measurement on each individual electrode. The separate impedance measurement defeats the purpose of using EN in the first place. How can symmetry be assessed purely from the EN measurement?

- Relating to impedance measurement by $R_{sn}(f)$, one outstanding problem is the construction of Nyquist impedance diagrams. $R_{sn}(f)$ is a real valued quantity. While the theory shows that $R_{sn}(f) = |Z(f)|$, the phase of $Z(f)$ is missing. This makes identifying an appropriate model for EIS analysis more difficult.

The above mentioned questions are all addressed by the thesis.

3.2 Random Variables, Estimation Theory and Random Processes

Much of the analysis of EN presented in this thesis is statistical in nature. The EN is regarded as a random process and statistical properties are computed from it to retrieve useful information. There are various concepts of random variables, estimation theory and stochastic processes the reader should be familiar with in order to fully appreciate the theory of noise resistance and the problems associated with it.

Texts by Papoulis [111], Honerkamp [112], and Shanmugan and Breipohl [107] provide good reference on the subject.

Section 3.2.1 introduces random variables. The expectation and other statistics of random variables are described in Section 3.2.2. Estimation theory is briefly

outlined in Section 3.2.3 and the concept of random variables is extended to random signals in Section 3.2.4

3.2.1 Random Variables

A random variable is a function that assigns a real number to every outcome of a random experiment. A simple example of a random variable is the number assignments of the faces of a die. In the case of EN, the EPN or ECN is sampled and the numerical value obtained is a random variable.

While the value of a random variable cannot be known with certainty before it is observed, its general behaviour is described by a distribution function. A distribution function shows what values the random variable is likely to take. For example, in the case of a fair six-faced die, the distribution function reflects that outcomes of 1, 2, 3, 4, 5 or 6 are all equally likely and that there can be no other outcomes.

Formally, the distribution function, $F_{\mathrm{x}}(\alpha)$, of a random variable x is defined as the probability that $x \leq \alpha$, where α is any real number.

Some of the properties of distribution functions are listed below:

- Because $F_{\mathrm{x}}(\alpha)$ is a probability and a probability is a number between 0 and 1, it follows that $0 \leq F_{\mathrm{x}}(\alpha) \leq 1$.
- Because it is impossible for any real number to be less than $-\infty$, the probability that $x \leq -\infty$ is zero. *ie* $F_{\mathrm{x}}(-\infty) = 0$.
- Because all real numbers have to be less than ∞, the probability that $x \leq \infty$ is 1. *ie* $F_{\mathrm{x}}(\infty) = 1$.
- $F_{\mathrm{x}}(\alpha)$ is a non-decreasing function of α. Hence if $\alpha \leq \beta$ then $F_{\mathrm{x}}(\alpha) \leq F_{\mathrm{x}}(\beta)$.
- For any $\alpha \leq \beta$, the probability that x lies between α and β is equal to $F_{\mathrm{x}}(\beta) - F_{\mathrm{x}}(\alpha)$.

In many cases it is easier to work with the derivative of the distribution function rather than with the distribution function itself. The probability density function is defined as

$$p_{\mathrm{x}}(\alpha) = \frac{\mathrm{d}F_{\mathrm{x}}(\alpha)}{\mathrm{d}\alpha} \tag{3.14}$$

Some of the properties of distribution functions are listed below:

- $p_{\mathrm{x}}(\alpha)$ is positive for all α, *ie* $p_{\mathrm{x}}(\alpha) \geq 0$.
- The probability that x lies between a and b is equal to $\int_a^b p_{\mathrm{x}}(\alpha)\mathrm{d}\alpha$, *ie* the area under $p_{\mathrm{x}}(\alpha)$ between a and b.
- $\int_{-\infty}^{\infty} p_{\mathrm{x}}(\alpha)\mathrm{d}\alpha = 1$, *ie* the total area under $p_{\mathrm{x}}(\alpha)$ is exactly equal to unity.

For continuous random variables, given a small number, Δ, the value of $p_x(\alpha)\Delta$ is approximately equal to the probability that x is within $\frac{\Delta}{2}$ either side of α. Thus $p_x(\alpha)$ can be thought of as a "density" of the probability that $x = \alpha$.

Many useful mathematical forms to describe probability density functions exist. Some common examples are:

Uniform:

$$p_x(\alpha) = \begin{cases} \frac{1}{2b} & -b < \alpha \leq b \\ 0 & \text{elsewhere} \end{cases}$$

Exponential:

$$p_x(\alpha) = \begin{cases} \frac{1}{b}\exp\left(-\frac{\alpha}{b}\right) & \alpha \geq 0 \\ 0 & \alpha < 0 \end{cases}$$

Gaussian:

$$p_x(\alpha) = \frac{1}{\sqrt{2\pi\sigma_x^2}}\exp\left(-\frac{\alpha^2}{2\sigma_x^2}\right)$$

Rayleigh:

$$p_x(\alpha) = \begin{cases} \frac{\alpha}{\sigma_x^2}\exp\left(-\frac{\alpha^2}{2\sigma_x^2}\right) & \alpha \geq 0 \\ 0 & \alpha < 0 \end{cases}$$

Chi-squared:

$$p_x(\alpha) = \begin{cases} \frac{\left(\frac{\alpha}{2}\right)^{\frac{n}{2}-1}\exp\left(-\frac{\alpha}{2}\right)}{2\Gamma\left(\frac{n}{2}\right)} & \alpha \geq 0 \\ 0 & \alpha < 0 \end{cases}$$

A uniform distribution is probably the simplest to understand. It occurs when a random variable is equally likely to take any value within a given range. For example, the error committed when rounding a random variable to the nearest unit is often uniformly distributed.

The Gaussian distribution is important because it arises in so many situations. One of the main reasons for its ubiquitous nature is the *central limit theorem.*

The central limit theorem states that for N independent random variables, the distribution of their sum tends to a Gaussian distribution as N tends to infinity regardless of the distribution of the constituent variables. Thus if many independent random effects are simultaneously operating on a system, the central limit theorem allows the collective effect to be represented as a Gaussian random variable.

The chi-squared distribution with n degrees of freedom arises when the square of n independent identically distributed Gaussian random variables are summed.

By the central limit theorem, the chi-squared distribution itself tends to a Gaussian distribution as n becomes large.

3.2.2 Expectation and Statistics of a Random Variable

Inherent to the concept of random variables is expectation. If the random variable, x, is repeatedly observed an infinite number of times, what will the average value of the observations be? That value is the expectation of the random variable and is denoted as $\mathrm{E}[x]$.

Using expectations, various statistics of the random variable can be defined. The n^{th} order statistic of x is defined as $\mathrm{E}[x^n]$. The zeroth order statistic, $\mathrm{E}[x^0]$ is always equal to unity. The first order statistic, $\mathrm{E}[x]$ is defined as the mean and the variance is defined as $\mathrm{E}[x^2] - \mathrm{E}^2[x]$. Higher order statistics ($n > 2$) are used to define parameters such as skew and kurtosis. However, all that is required to completely specify a Gaussian distribution are the first and second order statistics or, equivalently, the mean and the variance.

The *fundamental theorem of expectation* allows the expectation of a random variable (and perhaps more importantly, any function of the random variable) to be computed from its density function. Given a random variable, x, with a probability density function of $p_{\mathrm{x}}(\alpha)$ and an arbitrary function, $f(x)$, then the fundamental theorem of expectation asserts that

$$\mathrm{E}\left[f(x)\right] = \int_{-\infty}^{\infty} f(x) p_{\mathrm{x}}(\alpha) \mathrm{d}\alpha \tag{3.15}$$

3.2.3 Estimation Theory

Distinction needs to be made between a statistical property of a random variable (*eg* the mean or the variance) and an estimate of the statistical property. The statistical property is a precise and abstract quantity, while the estimated values, obtained from a finite number of samples of the random variable, are subject to random variation. A repeated estimate from a separate set of samples of the same random variable will generally give a different result. An estimated value is a random variable itself with a probability density function of its own and there will necessarily be some error associated with the estimate.

Estimation theory deals with how to best make an estimate of a statistical property from a finite set of observations. Questions such as how much confidence can be placed on an estimate arise and how much the estimate is likely to deviate from the true value.

The most frequently used estimators of statistical properties are averages over the data. Given N samples, $x_1, x_2, \ldots, x_N$, of a random variable, x, an estimate of

the mean of x is usually computed as

$$\hat{\mu}_{\mathrm{x}} = \frac{1}{N} \sum_{n=1}^{N} x_{\mathrm{n}} \tag{3.16}$$

where μ_{x} is the mean of x and the caret ($\hat{}$) denotes an estimate.

But other estimators are also possible. Say $x_{\max}$ and $x_{\min}$ are the largest and the smallest sample values that happened to occur among the N samples. The estimate of the mean might be taken as

$$\hat{\mu}_{\mathrm{x}} = \frac{x_{\max} + x_{\min}}{2} \tag{3.17}$$

There are circumstances in which the mean of x is better estimated by (3.17) than by (3.16). Equation (3.16) is a linear estimator and is "best" when the random variable has a Gaussian distribution. Equation (3.17) gives a "better" result when the samples are known to come from a uniformly distributed random variable. There are a number of factors to be considered when appraising the quality of an estimator.

Bias: A biased estimator tends to either over- or under-estimate the value of the statistical property. It is desirable for the estimator to be unbiased, *ie* for the expectation of the estimate to be equal to the statistical property.

Mean-square error: The mean square error of an estimator is the expectation of the square of the error. A poor estimate has a large mean-square error.

Consistency: If an estimator is unbiased and has a variance that tends to zero with increasing sample size, it is said to be consistent.

Efficiency: The efficiency of an unbiased estimate is measured by its variance. If repeated estimates have widely differing results, then the estimate has a large variance and is said to be inefficient.

Robustness: An estimator is robust if it maintains reasonable efficiency and lack of bias even when the assumption about the random variable's distribution is incorrect — *eg* assuming a random variable is Gaussian when in fact it is uniformly distributed. Generally speaking, linear estimators are more robust than non-linear estimators are.

In the case of a random variable with a uniform probability density function, (3.17) is a more efficient estimator of the mean than (3.16). Both estimators are unbiased and consistent. However, if the density function of the random variable departs from uniform, the efficiency of (3.17) deteriorates and it might even become biased while the efficiency of (3.16) is likely to remain unchanged.

The concept of efficiency provides a criterion for choosing between two competing estimators, but it does not give any assurance that the better of the two is any good.

How can one be sure, for example, that there is not another estimator whose variance (or mean-square error) is smaller than the two considered?

The *Cramér-Rao lower bound* specifies the best possible efficiency that any estimator can achieve. It is generally attributed to the work of Cramér [113] and Rao [114]. If an estimator is found that has an efficiency equal to the Cramér-Rao lower bound (called a minimum variance estimator), then one can be certain that no other estimator exists with a better efficiency. Unfortunately, a minimum variance estimator does not always exist.

An important class of estimators is the maximum likelihood estimators (MLE). With MLE, the estimate is taken to be the statistical property that maximises the likelihood of the observed data. For example, suppose a sequence of N samples, $x_1, x_2, \ldots, x_N$, is obtained from a random variable, x, that is known to be zero mean and Gaussian distributed, but with an unknown variance of σ_{x}^2. The MLE of σ_{x}^2 is the value of σ_{x}^2 that maximises the probability of the observed sequence, $x_1, x_2, \ldots, x_N$ occurring. In this case, the MLE of $sigma_{\mathrm{x}}^2$ is given by

$$\hat{\sigma}_{\mathrm{x}}^2 = \frac{1}{N} \sum_{n=1}^{N} x_{\mathrm{n}}^2. \tag{3.18}$$

The estimate given by (3.18) has the additional benefit that it is a robust estimate of variance. If the distribution from which the samples are taken deviates from the assumed Gaussian distribution, (3.18) still provides a good estimate of variance.

MLEs possess a number of desirable properties (invariance, consistency, efficiency and asymptotic normality) that make it a popular method of estimation. One of the most important properties is efficiency. If an estimator exists that has a mean-square error equal to the Cramér-Rao minimum bound, then the MLE is that estimator. The invariance property asserts that if Z is the MLE of z, then $f(Z)$ is the MLE of $f(z)$, where f is any arbitrary function.

One of the disadvantages of the MLE is that they can become significantly biased when small sample sizes are used. For example, (3.18) tends to overestimate σ_{x}^2 by a factor of $\frac{N}{N-1}$. In order to obtain an unbiased estimate, one may instead choose to use

$$\hat{\sigma}_{\mathrm{x}}^2 = \frac{1}{N-1} \sum_{n=1}^{N} x_{\mathrm{n}}^2. \tag{3.19}$$

However, though it is unbiased, (3.19) is not the MLE of σ_{x}^2.

3.2.4 Random Processes

Rather than producing a random variable, a random process has a random signal associated with it. Whereas a random variable can take on any real value, a random process yields a unique signal from an *ensemble* of possible signals.

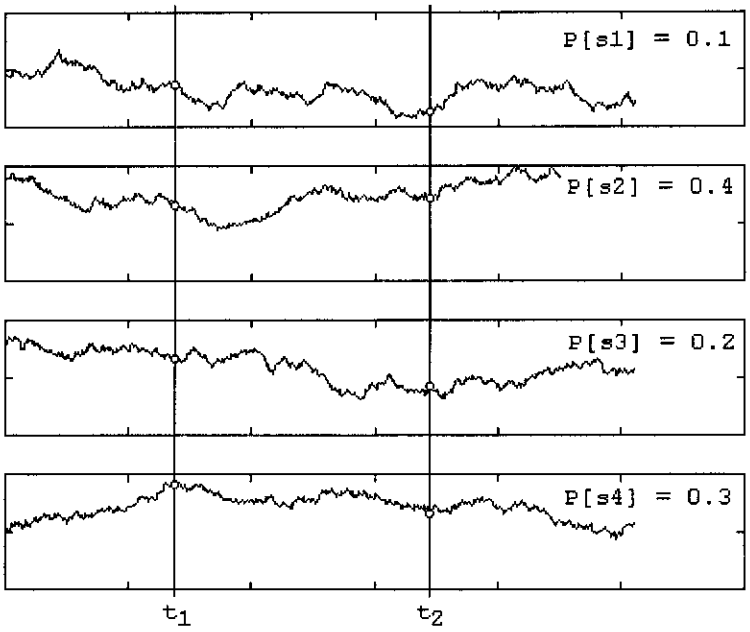

Figure 3.6: An ensemble of four random signals

Figure 3.6 shows an ensemble that consists of four signals with varying probabilities of occurrence. For any observation, only one of the four signals occurs. A repetition of the experiment associated with this ensemble might yield a different one of the four signals. The random factor is that it cannot be known with certainty exactly which signal will occur prior to the observation. But it is known that it will be one, and only one, of them and what the probability of occurrence of each signal is.

As illustrated in Figure 3.6, if the ensemble of signals is sampled at some time instant, t_1, a random variable is obtained that can take on four discrete values. Sampling at time t_2 yields a different random variable with four different discrete values.

The ensemble does not have to be limited to a finite number of signals. In most practical situations, the ensemble consists of an infinite number of unique signals and the probability of any specific signal occurring becomes infinitesimally small.

The *auto-correlation* is a function that specifies much about a Gaussian random process. It is defined as the expectation of the product of samples taken at arbitrary times of t_1 and t_2:

$$R_{xx}(t_1, t_2) = \mathrm{E}[x(t_1)x(t_2)] \tag{3.20}$$

When dealing with a random process, quantities such as the mean and the variance across the ensemble at any instant in time generally become dependent on the time that the signal is sampled. But when a random process has time invariant first and second order statistics, *ie* if $\mathrm{E}[x(t)]$ is independent of t and $\mathrm{E}[x(t_1)x(t_2)]$

depends on $t_2 - t_1$ only, then the process is said to be wide-sense stationary. In that case, the auto-correlation is often expressed simply as $R_{xx}(\tau)$, where $\tau = t_2 - t_1$.

The auto-correlation provides a means of describing the interdependence of two random variables obtained by observing a random process at times t_1 and t_2 (or $\tau = t_2 - t_1$ seconds apart in the case of a wide-sense stationary process). As $x(t_1)$ and $x(t_2)$ become less correlated, $R_{xx}(t_1, t_2)$ decreases in magnitude. It is therefore apparent that the more rapidly the random process changes with time, the more rapidly will the auto-correlation function decrease as τ increases. This decrease can be characterised by a de-correlation time, τ_0, such that for $\tau > \tau_0$, the magnitude of the auto-correlation function remains below some prescribed value. The de-correlation time of a wide-sense stationary process of zero mean can be defined as the time taken for the magnitude of the auto-correlation to decrease to 1 % of its maximum value (the choice of 1 % is arbitrary).

A quantity that is related to the auto-correlation function is the power spectral density [PSD, $S_{xx}(f)$]. The PSD and the auto-correlation function form a Fourier transform pair:

$$S_{xx}(f) = \int_{-\infty}^{\infty} R_{xx}(\tau) \exp(-2\pi j f \tau)\, d\tau \tag{3.21}$$

$$R_{xx}(\tau) = \int_{-\infty}^{\infty} S_{xx}(f) \exp(2\pi j f \tau)\, df \tag{3.22}$$

This pair of equations constitutes the Einstein-Wiener-Khintchine relations for wide-sense stationary processes.

$S_{xx}(f)$ depicts how the random processes' power is distributed as a function of frequency. The relation between the mean-square value, the PSD, and the auto-correlation of a wide-sense stationary process is given by

$$\mathrm{E}\left[x^2(t)\right] = R_{xx}(0) = 2\int_0^{\infty} S_{xx}(f) df \tag{3.23}$$

Similar to the de-correlation time, the bandwidth of a signal can be defined as the range of frequencies, f_{min} to f_{max}, where

$$R_{xx} \approx 2\int_{f_{min}}^{f_{max}} S_{xx}(f) df. \tag{3.24}$$

For example, if 95 % of the signal power is located between f_{min} and f_{max}, then $f_{max} - f_{min}$ is said to be the 95 % effective bandwidth.

The estimation of $S_{xx}(f)$ from a sample of the ensemble is an involved topic. Good discussion of Welch's averaged periodogram method and the maximum entropy method [115] of PSD estimation is given by Kay and Marple [116], Shanmugan and Breipohl [107], and Press [117].

3.3 Linear Convolutional Filters

This section is an introduction to the relevant key concepts of linear filter theory. For a more comprehensive treatment of filters, filter design and linear systems, see Van Valkenburg [118], Tomlinson [119] and Oppenheim [120].

Section 3.3.1 provides the general theory of linear convolutional filters, otherwise known as Auto-Regressive Moving Average (ARMA) filters. Section 3.3.2 describes the basic high-, low- and band-pass filters. Section 3.3.3 describes a specialised type of filter: the whitening filter.

3.3.1 General Theory and Definitions

One of the central operations in the study of linear systems and signal processing is *linear convolution*. It can be mathematically described by

$$y(t) = \int_{-\infty}^{\infty} h(\tau)x(t-\tau)\mathrm{d}\tau \tag{3.25}$$

where $y(t)$ is the output, $x(t)$ is the input and $h(\tau)$ defines the filter. $h(\tau)$ is called the impulse response of the filter after the observation that if $x(t)$ is an impulse [*ie* $x(0)$ is infinitely large, but $x(t) = 0$ for all $t \neq 0$], then $y(t) = h(t)$.

For a causal filter (one which does not depend of future inputs), $h(\tau)$ is zero for all $\tau < 0$. The output signal of a causal filter at each t is a weighted sum of the input signal prior to t. The precise shape of $h(\tau)$ determines what those weights are and how far into the past the input continues to influence the output.

The causal, discrete time (*ie* sampled) form of (3.25) is given by

$$y_n = \sum_{k=0}^{\infty} h_k x_{n-k} \tag{3.26}$$

where h_k are the filter coefficients and x_n and y_n are the n^{th} samples of $x(t)$ and $y(t)$ respectively. The form of (3.26) is referred to as a *finite impulse response* (FIR) filter because it is most suited to implementations where there are a finite number of non-zero h_k coefficients.

A simple example of a linear convolutional filter is the moving average, where the output is equal to the average of the input T seconds prior to and successive to t. Note that dependency on future input values makes this definition non-causal. The impulse response for such a moving average filter is given by

$$h(t) = \begin{cases} \frac{1}{2T} & |t| \leq T \\ 0 & |t| > T \end{cases} . \tag{3.27}$$

Thus the filter described by (3.27) gives an equal weight of $\frac{1}{2T}$ to all input values T seconds either side of the present input.

An alternate, and often more useful, representation of linear convolution is in the frequency domain:

$$Y(f) = X(f)H(f) \tag{3.28}$$

where $Y(f)$, $X(f)$ and $H(f)$ are the respective Fourier transforms of $y(t)$, $x(t)$ and $h(t)$. $H(f)$ is referred to as the transfer function of the filter.

Equation (3.28) shows how linear convolution can be used to filter a signal on a frequency selective basis. For example, if the filter is designed such that $H(f) = 0$ for all $|f| > f_{\max}$, then the filter effectively eliminates all components of the input located at a frequency above $f_{\max}$.

There is no reason why a linear convolutional filter cannot be applied to a random process. When doing so, it is of interest to find how the statistical properties of the random process are affected.

By inspection of (3.25), it can be seen that $y(t)$ is a sum of random variables, $x(t)$, and by the central limit theorem, it can be expected to tend to a Gaussian distribution. The PSD of a Gaussian process is instrumental to determining the statistics of the process. If a filter with a transfer function of $H(f)$ is applied to a stationary random process having a PSD of $S_{\mathrm{xx}}(f)$, then the PSD of the output is given by

$$S_{\mathrm{yy}}(f) = |H(f)|^2 S_{\mathrm{xx}}(f) \tag{3.29}$$

3.3.2 Low- High- and Band-Pass Filters

A low-pass filter is one that tends to suppress high frequencies (the stop-band) while the low frequencies (the pass-band) are left largely unchanged. In that sense, the ideal low pass filter is one with a transfer function conforming to

$$|H_{\mathrm{lp}}(f)| = \begin{cases} 1 & |f| \leq f_{\mathrm{c}} \\ 0 & |f| > f_{\mathrm{c}} \end{cases} . \tag{3.30}$$

Such a filter is called a brick-wall filter because of its sharp transition from 1 to 0 at $f = f_{\mathrm{c}}$.

A high-pass filter is the opposite of a low-pass filter. It is the low frequencies that are suppressed while the high frequencies are passed. The brick-wall high-pass filter conforms to

$$|H_{\mathrm{hp}}| = \begin{cases} 1 & |f| \geq f_{\mathrm{c}} \\ 0 & |f| < f_{\mathrm{c}} \end{cases} . \tag{3.31}$$

If only a certain band of frequencies is passed by the filter, then it is a band-pass filter:

$$|H_{\mathrm{bp}}| = \begin{cases} 1 & f_1 < |f| \leq f_2 \\ 0 & \text{otherwise} \end{cases} . \tag{3.32}$$

In practice, the sharp transitions in frequency imposed by the brick wall filters

given by (3.30) to (3.32) make them difficult to implement in real time systems. In addition, the impulse responses associated with (3.30) to (3.32) are relatively oscillatory. For these reasons a more gentle transition from the pass band to the stop band is often employed.

Butterworth filters are designed on a "maximally flat" basis, where $|H(f)|$ is as flat as possible in the pass band for a given rate of transition between pass- and stop-band. *Chebychev* filters allow some ripple in the pass-band to achieve a sharper transition.

3.3.3 Whitening Filters

A random process, $x(t)$, is said to be white when it has a constant PSD for all practical frequencies. Such a process has the unique property that $x(t_1)$ is completely independent of $x(t_2)$ for all $t_1 \neq t_2$, *ie* knowledge of $x(t_1)$ reveals absolutely nothing about $x(t_2)$ and its de-correlation time is infinitesimally small.

In many cases dependence between neighbouring samples of a random process can be an impediment to analysis and a special filter might be applied in order to de-correlate the signal. Such a filter is called a *whitening filter* after the fact that a non self-correlated signal has signal power that is equally distributed over all frequencies. Thus a whitening filter is one that is carefully matched to the signal (or the expected characteristics of the signal) so that the output becomes white.

Examples where whitening filters have been of use include: digital tape recording [121], spread spectrum communications [122], spectrum analysis [123], rejection in multiple access computer network media [124], pattern recognition [125], modelling of echo paths in telephony networks [126], and detection of buried objects [127]. A treatment of the evolution and application of whitening filters is given by Sosulin and Kostrov [23].

The basic approaches to implementation of a whitening filter is to estimate the signal PSD (or to assume a reference PSD if adaptive signal processing is not possible) and then construct a filter that has a transfer function equal to the inverse of that PSD:

$$|H(f)| = \sqrt{\frac{1}{S_{xx}(f)}} \tag{3.33}$$

so that when the signal is applied to the input of the filter, the output has a PSD of

$$S_{yy} = |H(f)|^2 S_{xx}(f) = 1. \tag{3.34}$$

A practical implementation of such a filter can be obtained from the coefficients of an all-pole *linear prediction filter* [128] tuned to the signal so that its transfer function matches the inverse of the signal PSD. The all-pole linear prediction filter coefficients are the same coefficients as used by the maximum entropy method [115]

[116] [117] of PSD estimation. They have the property that

$$\hat{S}_{xx}(f) = \frac{1}{\left|\sum_{k=0}^{M} c_k \exp(2\pi \mathrm{j} f \Delta k)\right|^2} \tag{3.35}$$

where $\hat{S}_{xx}(f)$ is the maximum entropy PSD estimate of a signal, $x(t)$, that has been sampled at a rate of Δ samples per second. $c_0, c_1, \ldots, c_M$ are the linear prediction filter coefficients of $x(t)$. Press [117] gives a C program listing for computing the linear prediction filter coefficients. The *pyulear* Matlab function can also be used.

The FIR digital filter described by

$$y_n = \sum_{k=0}^{M} c_k x_{n-k} \tag{3.36}$$

has a transfer function conforming to

$$|H(f)| = \sqrt{\frac{1}{\hat{S}_{xx}(f)}} \tag{3.37}$$

and is thus a whitening filter.

3.4 Conclusion

This chapter has reviewed the present state of EN analysis as it relates to impedance measurement. The outstanding problems with the technique have been described and the mathematical background related to analysis has been explained.

The remainder of the thesis will further develop the theory and application of EN analysis.

Chapter 4

Estimation of Electrochemical Impedance

As discussed in Chapter 3, while analysis of EN in the time domain (by the noise resistance) allows dynamic systems to be monitored, there are some problems with its practical application. Because of its implicit frequency dependency (See Section 3.1) any generalisation that the noise resistance is equal to the polarisation is bound to be false. By the random nature of EN, estimation of the noise resistance involves some uncertainty and the effects of EN bandwidth and duration on the quality of the estimate are not widely known.

This chapter presents the results of new theoretical approach to estimation of electrochemical impedance magnitude using the EPN/ECN measurement. It is based on estimation of the noise resistance using signal pre-processing to control its frequency dependency and to improve its precision.

Once the impedance magnitude has been estimated, its relationship to the physical phenomena can be exploited as per conventional EIS, described in Section 2.2.

In Section 4.1, estimation of impedance magnitude is examined for certain ideal conditions. The objective is to find the maximum likelihood estimator (MLE, See Section 3.2.3) of impedance magnitude for an electrode pair with certain ideal characteristics. It is found to be given by the MLE of the noise resistance. The MLE of the noise resistance is given for Gaussian, white and stationary EN.

In Section 4.2 the effect of a finite EN bandwidth and measurement length on the noise resistance estimate is derived. The estimate is shown to improve as the EN bandwidth and measurement length increase. Equations are given to quantitively describe the relation. Such knowledge can be used to find how short a measurement or how narrow a bandwidth can be used for any required level of precision.

In Section 4.3 signal pre-processing prior to estimation of noise resistance is examined. It is shown how the EN can be conditioned to validate the assumptions of ideal characteristics used for obtaining the MLE in Section 4.1 and to optimise

the shape of the EN power spectral density. It is shown how the frequency dependent nature of the noise resistance can be controlled and even exploited to allow frequency dependent impedances to be investigated. A scheme for estimation of the noise resistance is proposed that incorporates the described signal conditioning (referred to as *matched* conditioning) and allows the noise resistance to be estimated continuously so that it can be applied to time varying systems. The moving average removal (MAR, see Section 3.1.3) technique of signal conditioning is analysed to determine its effect on the noise resistance estimate. The selection of suitable parameters for signal conditioning and estimation (bandwidth, observation time and level of precision) are discussed.

In Section 4.4, experimental tests are conducted to compare practical results with the theory. Comparison is made between polarisation resistance measurements using linear polarisation (LP, see Section 2.1.3) and the noise resistance obtained after signal conditioning that consists of

- linear trend removal only (LTR, see Section 3.1.3);
- LTR followed by MAR; and
- LTR followed by the proposed "matched" signal conditioning.

It is found that the matched signal conditioning has a slight performance gain over MAR. Both techniques are found to produce values that agree well with the LP measurement. LTR by itself is found to yield results that significantly deviate from the LP measurements and have significantly less precision than values obtained using MAR and the matched signal conditioning.

The work described in this chapter has been presented at the IMTC/2000 conference [129] and published in IEEE Transactions on Instrumentation and Measurement [130].

4.1 Impedance Estimation under Ideal Conditions

In this section, the invariance property of the MLE is used to derive the MLE of impedance magnitude under ideal conditions. The derivation starts out with a minimum number of assumptions — assuming only that the equivalent impedance of the electrodes are resistive within the bandwidth of the EN — and then successively adds more assumptions to arrive at an ideal case. The ideal assumptions are:

- The equivalent impedances of the electrodes are purely resistive within the bandwidth of the EN;
- The EN is zero-mean;
- Electrode resistances are equal;

- EPN sources are uncorrelated;
- The EN is white (*ie* it has a constant power spectral density);
- The EN is Gaussian distributed
- The system is stationary over the observation times;

Subsequent sections investigate the performance of the estimate as a function of signal bandwidth and observation time and how signal conditioning can be applied to approximate the ideal conditions and otherwise control the performance of the estimate.

4.1.1 Resistive Electrodes with Zero-Mean EN

Figure 3.2 (page 42) shows the Thevenin equivalent circuit for the EPN/ECN measurement. When the electrodes impedances are purely resistive, $Z_1(f) = R_1$ and $Z_2(f) = R_2$ are the equivalent resistances of each electrode. $v_1(t)$ and $v_2(t)$ are the Thevenin equivalent potential sources, and $v(t)$ and $i(t)$ are the observed EPN and ECN signals respectively.

From Figure 3.2, the $v(t)$ and $i(t)$ are related to $v_1(t)$ and $v_2(t)$ by

$$v_1(t) = v(t) + i(t)R_1 \tag{4.1}$$
$$v_2(t) = v(t) - i(t)R_2 \tag{4.2}$$

In the foregoing, the (t) functional operator will be dropped to simplify notation.

From (4.1) and (4.2), the first order statistics of v_1 and v_2 are given by

$$\mathrm{E}[v_1] = \mathrm{E}[v] + R_1\mathrm{E}[i] \tag{4.3}$$
$$\mathrm{E}[v_2] = \mathrm{E}[v] + R_2\mathrm{E}[i] \tag{4.4}$$

and the second order statistics are given by

$$\mathrm{E}\left[v_1^2\right] = \mathrm{E}\left[v^2\right] + 2R_1\mathrm{E}[vi] + R_1^2\mathrm{E}\left[i^2\right] \tag{4.5}$$
$$\mathrm{E}\left[v_2^2\right] = \mathrm{E}\left[v^2\right] - 2R_2\mathrm{E}[vi] + R_2^2\mathrm{E}\left[i^2\right] \tag{4.6}$$
$$\mathrm{E}[v_1v_2] = \mathrm{E}\left[v^2\right] + (R_1 - R_2)\mathrm{E}[vi] - R_1R_2\mathrm{E}\left[i^2\right] \tag{4.7}$$

where "E" denotes statistical expectation.

The first order statistics are usually made equal to zero by trend removal and signal conditioning, effectively eliminating (4.3) and (4.4) from the system of equations.

If $\hat{\sigma}_{\mathrm{v}}^2$, $\hat{\sigma}_{\mathrm{i}}^2$ and $\hat{\sigma}_{\mathrm{iv}}$ are the MLEs of $\mathrm{E}[v_2^2]$, $\mathrm{E}[i_2^2]$ and $\mathrm{E}[iv]$, then by invoking the

invariance property of the MLE,

$$\hat{\sigma}_1^2 = \hat{\sigma}_v^2 + 2\hat{R}_1\hat{\sigma}_{iv} + \hat{R}_1^2\hat{\sigma}_i^2 \tag{4.8}$$

$$\hat{\sigma}_2^2 = \hat{\sigma}_v^2 - 2\hat{R}_2\hat{\sigma}_{iv} + \hat{R}_2^2\hat{\sigma}_i^2 \tag{4.9}$$

$$\mathrm{E}[v_1 v_2] = \hat{\sigma}_v^2 + \left(\hat{R}_2 - \hat{R}_1\right)\hat{\sigma}_{iv} - \hat{R}_1\hat{R}_2\hat{\sigma}_i^2 \tag{4.10}$$

where $\hat{\sigma}_1^2$, $\hat{\sigma}_2^2$, $\hat{R}_1$ and $\hat{R}_2$ are the MLEs of $\mathrm{E}[v_1^2]$, $\mathrm{E}[v_2^2]$, R_1 and R_2 respectively.

Equations (4.8) and (4.9) give the MLEs of $\mathrm{E}[v_1^2]$ and $\mathrm{E}[v_2^2]$ as a function of the observed EN (v and i) and the electrodes' resistances. Equation (4.10) implicitly gives the MLE of R_1 and R_2 as a function of v, i and $\mathrm{E}[v_1 v_2]$.

4.1.2 Identical Electrodes

In (4.8) to (4.10), with 4 unknowns ($\hat{\sigma}_1^2$, $\hat{\sigma}_2^2$, $\hat{R}_1$ and $\hat{R}_2$) and only three equations, it is clear that R_1 and R_2 cannot be estimated independently without further information. Although any information regarding the resistance of the electrode impedance or source variance will yield the 4^{th} equation, the common assumption is that the electrodes are identical [13] [18] [100] [98] so that $R_1 = R_2 = R$. Then (4.10) reduces to

$$\hat{R} = \sqrt{\frac{\hat{\sigma}_v^2 - \mathrm{E}[v_1 v_2]}{\hat{\sigma}_i^2}} \tag{4.11}$$

Note that $\rho = \mathrm{E}[v_1 v_2]$ is taken to be a random variable. If it is known to have a probability density function of $p_\rho(\rho)$ with the most likely value [*ie*, the maximum value of $p_\rho(\rho)$] being $\rho = \rho_{\max}$, then by the fundamental theorem of expectation

$$\mathrm{E}\left[R^2\right] = \int_{-\infty}^{\infty} \left(\frac{\mathrm{E}[v^2] - \rho}{\mathrm{E}[i^2]}\right) p_\rho(\rho)\mathrm{d}\rho = \frac{\mathrm{E}[v^2] - \mathrm{E}[\rho]}{\mathrm{E}[i^2]} \tag{4.12}$$

and by the invariance property, the MLE becomes

$$\hat{R} = \sqrt{\frac{\hat{\sigma}_v^2 - \rho_{\max}}{\hat{\sigma}_i^2}} \tag{4.13}$$

In the absence of any information regarding ρ, all that can be said is that ρ is symmetrically distributed between $-\mathrm{E}[v_1]\,\mathrm{E}[v_2]$ and $\mathrm{E}[v_1]\,\mathrm{E}[v_2]$. It is symmetrically distributed because if it was known not to be, then that qualifies as information about the v_1 and v_2 correlation which can be put to use. With symmetry, $\mathrm{E}[\rho] = 0$ and the MLE becomes that of the case where $\mathrm{E}[\rho]$ is known to be zero, *ie* the MLE for uncorrelated sources.

4.1.3 Uncorrelated Sources

In the case where the EN sources are known to be uncorrelated,

$$\mathrm{E}[v_1 v_2] = \mathrm{E}[v_1]\,\mathrm{E}[v_2] = 0 \tag{4.14}$$

and (4.7) reduces to

$$R = \sqrt{\frac{\mathrm{E}[v^2]}{\mathrm{E}[i^2]}} = \frac{\sigma_\mathrm{v}}{\sigma_\mathrm{i}} = R_\mathrm{n} \tag{4.15}$$

where σ_v^2 and σ_i^2 are the variances of v and i respectively and R_n is recognised as the noise resistance. Equation (4.11) becomes

$$\hat{R} = \frac{\hat{\sigma}_\mathrm{v}}{\hat{\sigma}_\mathrm{i}}. \tag{4.16}$$

Equation (4.15) gives the electrode resistance as a function of the EN statistics under the conditions of identical, resistive electrodes and uncorrelated sources. Equation (4.16) gives the MLE of the electrode resistance given the MLE of the observed EN variances under the same conditions.

4.1.4 Gaussian, White and Stationary EN

Finally, if the observed EPN and ECN are assumed to be stationary, white, zero mean and Gaussian distributed, then the MLE of the observed EN characteristics are given by

$$\hat{\sigma}_\mathrm{v}^2 = \frac{1}{M}\sum_{m=1}^{M} v_m^2 \tag{4.17}$$

$$\hat{\sigma}_\mathrm{i}^2 = \frac{1}{M}\sum_{m=1}^{M} i_m^2 \tag{4.18}$$

$$\hat{\sigma}_\mathrm{iv} = \frac{1}{M}\sum_{m=1}^{M} i_m v_m \tag{4.19}$$

where v_m and i_m are samples of v and i, and M is the total number of samples.

If the observed EN is found to conform to some other distribution, the MLE estimates of (4.17) to (4.19) can be replaced with the MLE estimates corresponding to the observed distribution. However, two factors make (4.17) to (4.19) the preferred choice in general:

1. The EN can be made to approach the assumed conditions by use of appropriate signal conditioning as investigated in Section 4.3.

2. Equations (4.17) to (4.19) are robust, *ie*, if the actual distribution deviates from the assumed distribution, they still provide reasonable estimates of vari-

ance and correlation.

The process of estimation by (4.17) to (4.19) will be referred to as estimation by the mean-square.

For the case of uncorrelated EN sources and identical, resistive electrodes,

$$\hat{R} = \sqrt{\frac{\sum v_n^2}{\sum i_m^2}} \tag{4.20}$$

As the sample rate becomes infinitely fast, (4.20) tends to

$$\hat{R} = \sqrt{\frac{\int_{-T}^{T} v^2(t)\mathrm{d}t}{\int_{-T}^{T} i^2(t)\mathrm{d}t}} = \frac{P_\mathrm{v}}{P_\mathrm{i}} \tag{4.21}$$

where

$$P_\mathrm{x} = \frac{1}{2T}\int_{-T}^{T} x^2(t)\mathrm{d}t \tag{4.22}$$

is the average power of the signal, $x(t)$, over the time interval $[-T, T]$. Equation (4.21) is the continuous version of (4.20).

4.2 Band-Limited EN over a Finite Time Interval

Estimation by the mean-square as derived in Section 4.1.4 assumes that the EN is white so that its samples are independent. This cannot generally be the case because any practical signal is band-limited. Depending on the sample rate, it is therefore possible that neighbouring samples are correlated and in the limit approaching the continuous case of (4.21), correlation between samples is a certainty.

This section investigates the estimation of noise resistance by the mean-square when the EN signals are taken to be band-limited to a fixed range of frequencies, but otherwise conform to the assumptions listed in Section 4.1.

The analysis is divided into two parts. In Section 4.2.1, the signal power, (4.22), is examined. In Section 4.2.2, the results from Section 4.2.1 are used to derive the statistics of the noise resistance estimate as a function of observation time and signal bandwidth.

4.2.1 Signal Power

The EN signal (either potential or current) is denoted by $x(t)$. $x(t)$ is assumed to be Gaussian distributed and band-limited to $[W_1, W_2]$ (radians/second) with a constant PSD within that bandwidth. It is the task of the signal conditioning (see Section 4.3) to approximate these characteristics and thus the bandwidth and conformance to the assumed PSD shape will vary to some degree depending on the quality of the approximation.

Papoulis [111] gives the expectation and variance of P_x (denoted respectively by η_P and σ_P^2) as

$$\eta_P = \eta_y \tag{4.23}$$

$$\sigma_P^2 = \frac{1}{T}\int_0^{2T}\left(1-\frac{\tau}{2T}\right)\left[R_{yy}(\tau)-\eta_y^2\right]\mathrm{d}\tau \tag{4.24}$$

where $R_{yy}(\tau)$ is the auto-correlation of $y(t) = x^2(t)$ and η_y is the expectation of $y(t) = x^2(t)$.

Equation (4.23) shows that the expectation of P_x is equal to the expectation of $y(t) = x^2(t)$ and thus P_x is seen to be an unbiased estimator of the signal variance.

If $x(t)$ has an auto-correlation of $R_{xx}(t)$ then, for any Gaussian distributed, zero mean $x(t)$, $R_{yy}(t)$ is given as [111]

$$R_{yy} = R_{xx}^2(0) + 2R_{xx}^2(t) \tag{4.25}$$

The power spectral density of $x(t)$ is taken to be a constant, S_{xx}, over $\pm[W_1, W_2]$ radians per second so that

$$\eta_y = \frac{S_{xx}\,(W_2 - W_1)}{\pi} \tag{4.26}$$

$$R_{yy}(t) - \eta_y^2 = \frac{2S_{xx}^2}{\pi^2 t^2}\left[\sin(W_2 t) - \sin(W_1 t)\right]^2. \tag{4.27}$$

Substituting (4.26) and (4.27) into (4.25) and using algebraic manipulation software to evaluate, it is found that

$$\frac{\sigma_P^2}{\eta_P^2} = \frac{4f(TW_1, TW_2) + g(TW_1, TW_2) + h(TW_1, TW_2) - 2}{2(TW_2 - TW_1)^2} \tag{4.28}$$

where

$$f(x,y) = x\mathrm{Si}(4x) - (x+y)\mathrm{Si}(2x+2y) + y\mathrm{Si}(4y) + (y-x)\mathrm{Si}(2y-2x) \tag{4.29}$$

$$g(x,y) = \mathrm{Ci}(4x) + \mathrm{Ci}(4y) - 2\mathrm{Ci}(2x+2y) + 2\mathrm{Ci}(2y-2x) \tag{4.30}$$

$$h(x,y) = \cos(4x) + \cos(4y) - 2\cos(2x+2y) + 2\cos(2y-2x) \tag{4.31}$$

and

$$\mathrm{Si}(x) = \int_0^x \frac{\sin(x)}{x}\mathrm{d}x \tag{4.32}$$

$$\mathrm{Ci}(x) = \int_0^x \frac{\cos(x)-1}{x}\mathrm{d}x \tag{4.33}$$

Note that the cosine integral given above, $\mathrm{Ci}(x)$, is a non-standard definition. The standard definition includes a logarithm term. However, after substitution into (4.28), the logarithm terms are found to cancel.

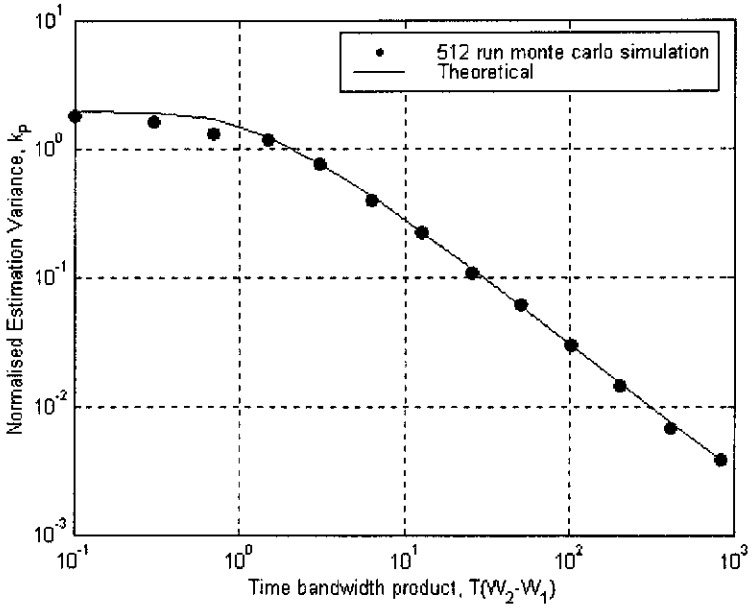

Figure 4.1: k_P versus time-bandwidth product, $TW_1 = 0.1$ radians/sec

The dimensionless quantity

$$k_P = \frac{\sigma_P^2}{\eta_P^2} \tag{4.34}$$

is defined for convenience. A calculation of P_x with very little variance between separate observations compared to its mean has a small k_P and a calculation with a large degree of scatter compared to its mean will have a large k_P. Given zero mean, stationary $x(t)$ and given that P_x is an unbiased estimator of $\mathrm{E}\left[x^2(t)\right]$, the variance of P_x is then the mean square error of the estimate. If this error is thought of as noise while $\mathrm{E}\left[x^2(t)\right]$ is thought of as a signal then the signal to noise ratio, $\mathrm{SNR_P}$, is given in decibels by

$$\mathrm{SNR_P} = 20\log_{10}\left(\frac{\eta_P}{\sigma_P}\right) = -10\log_{10}(k_P) \tag{4.35}$$

Thus, in the following, k_P quantifies the signal to noise ratio, or the *relative precision* of the calculation.

Figures 4.1 and 4.2 plot k_P as a function of the time-bandwidth product, $T(W_2 - W_1)$, along with the results of a simulation to confirm the theory.[1]

In Figure 4.1, W_1 is held constant, while in Figure 4.2, $W_2 = 2W_1$. From Figures 4.1 and 4.2, it can be seen that the value of k_P decreases in magnitude as the time-bandwidth product increases, indicating less scatter when longer observations are made or when signals with wider bandwidths are analysed. There is little differ-

[1]Simulation is performed using the *normSVarianceSim* (see Section A.4, page 146) and the theoretical curve is obtained using *normSVariance* (Section A.3, page 144).

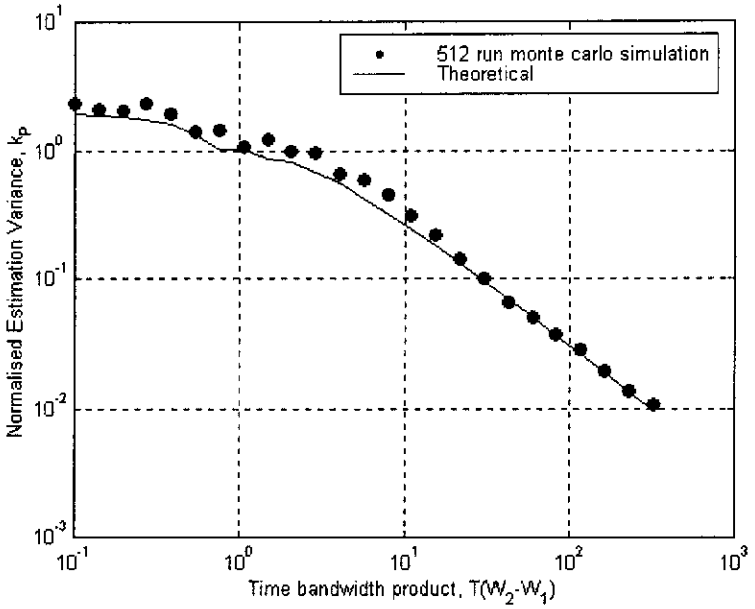

Figure 4.2: k_P versus time-bandwidth product, $\frac{W_2}{W_1} = 2$

ence between Figures 4.1 and 4.2, except for only slight deviation for larger values of k_P. This suggests that the location of the signal in the frequency domain is of only slight significance in comparison to the bandwidth of the signal.

If the $T(W_2 - W_1)$ product is large, it is found that (4.28) reduces to

$$k_P \approx \frac{\pi}{T(W_2 - W_1)} = \frac{1}{T_{res}(f_2 - f_1)} \tag{4.36}$$

where $T_{res} = 2T$ is the time resolution and $f_n = \frac{W_n}{2\pi}$ defines the signal bandwidth in Hertz.

Equation (4.36) shows, by inverse proportionality, that any increase in the signal bandwidth or increase in the measurement time will decrease k_P (*ie* the relative precision of P_x). It can be seen that the three quantities (time resolution, frequency resolution and relative precision) can be traded between one another, with the product of the three remaining approximately unity.

4.2.2 Noise Resistance

Let P_v and P_i be the EPN and ECN power estimate respectively, as computed by (4.22). The mean-square estimate of noise resistance is then given by (4.21) so that

$$E\left[\hat{R}_n^2\right] = E\left[\frac{P_v}{P_i}\right] = E\left[P_v E\left[\frac{1}{P_i}\middle| P_v\right]\right] \approx E[P_v]\, E\left[\frac{1}{P_i}\right] \tag{4.37}$$

$$E\left[\hat{R}_n\right] \approx E\left[\sqrt{P_v}\right] E\left[\frac{1}{\sqrt{P_i}}\right]. \tag{4.38}$$

In (4.37) and (4.38), the approximations are accurate when P_v and P_i have small variances relative to the means, which is signified by a small k_P. The approximation also becomes equality for all k_P if P_v and P_i are statistically independent.

To evaluate (4.37) and (4.38), the fundamental theorem of expectation, (3.15, page 51) is applied, but first the probability density function of P_v and P_i must be found.

P_v and P_i are the result of squaring and integrating a stationary Gaussian distributed random variable. P_v and P_i are therefore chi-squared distributed [111]. (see Section 3.2.1.) The probability density function is given by

$$p_P(\alpha) = \frac{n(n\alpha)^{\frac{n}{2}-1}\exp\left[\frac{-n\alpha}{2\sigma_x^2}\right]}{2^{\frac{n}{2}}\sigma_x^n\Gamma\left(\frac{n}{2}\right)}U(\alpha) \tag{4.39}$$

where n is the number of degrees of freedom, σ_x^2 is the variance of the respective signal (potential or current), $U(\alpha)$ is the unit step function and $\Gamma(z)$ is Euler's Gamma function, the continuous version of the factorial operator.

A general expression for $\mathrm{E}\left[P_x^M\right]$ can be derived, allowing $\mathrm{E}\left[P_x^{-1}\right]$, $\mathrm{E}\left[P_x^{-0.5}\right]$, $\mathrm{E}\left[P_x^{0.5}\right]$ and $\mathrm{E}\left[P_x\right]$ to be easily evaluated.

By the fundamental theorem of expectation it follows that

$$\mathrm{E}\left[P_x^M\right] = \int_{-\infty}^{\infty}\alpha^M p_P(\alpha)\mathrm{d}\alpha = \frac{1}{\Gamma\frac{n}{2}}\left(\frac{n}{2\sigma_x^2}\right)^{\frac{n}{2}}\int_0^{\infty}\alpha^{\frac{n}{2}-1+M}\exp\left(\frac{-n\alpha}{2\sigma_x^2}\right)\mathrm{d}\alpha \tag{4.40}$$

The integral (which happens to be the Laplace transform of $\alpha^{\frac{n}{2}-1+M}$ with respect to α, evaluated at $s = \frac{n}{2\sigma_x^2}$) is listed in tables of the Laplace transform. It follows that

$$\mathrm{E}\left[P_x^M\right] = \frac{\Gamma\left(\frac{n}{2}+M\right)}{\Gamma\left(\frac{n}{2}\right)}\left(\frac{2\sigma_x^2}{n}\right)^M \tag{4.41}$$

By (4.41), $\mathrm{E}\left[P_x^M\right]$ is easily evaluated for $M \in \{-1, -0.5, 0.5, 1, 2\}$ and is substituted into (4.37) and (4.38) to give

$$k_P = \frac{\sigma_P^2}{\eta_P^2} = \frac{\mathrm{E}\left[P_x^2\right]}{\mathrm{E}^2\left[P_x\right]} - 1 = \frac{2}{n} \tag{4.42}$$

$$\mathrm{E}\left[\hat{R}_n\right] \approx D_n R_n \tag{4.43}$$

$$\mathrm{E}\left[\hat{R}_n^2\right] - \mathrm{E}^2\left[\hat{R}_n\right] \approx \left(\frac{n}{n-2} - D_n^2\right)R_n^2 \tag{4.44}$$

$$k_R = \frac{\mathrm{E}\left[\hat{R}_n^2\right]}{\mathrm{E}^2\left[\hat{R}_n\right]} - 1 \approx \frac{n}{(n-2)D_n^2} - 1 \tag{4.45}$$

where

$$D_n = \frac{\Gamma\left(\frac{n+1}{2}\right)\Gamma\left(\frac{n-1}{2}\right)}{\Gamma^2\left(\frac{n}{2}\right)} \tag{4.46}$$

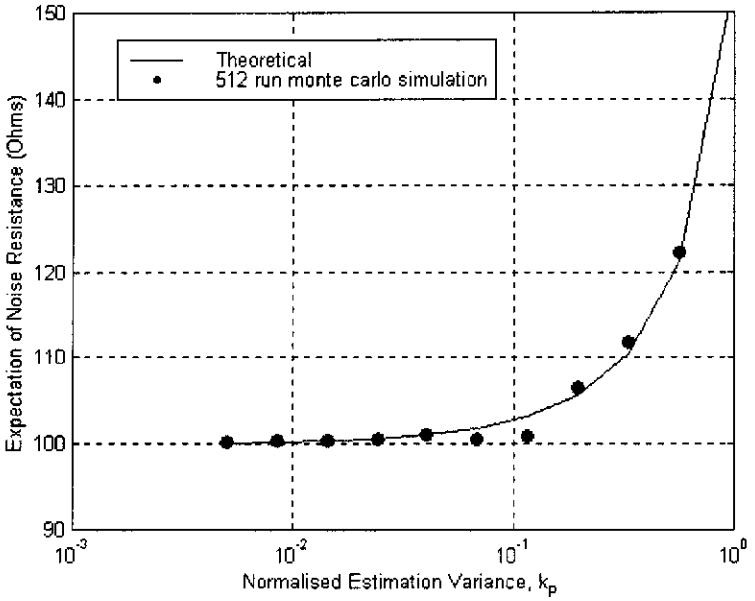

Figure 4.3: Expectation of noise resistance estimate for ideal resistance of 100 Ω

Equation (4.42) links the effective number of degrees of freedom, n, in P_x to the relative precision of P_x (*ie* k_P). It cannot simply be said that n is equal to the number of samples in the time interval because a chi-squared distribution is the sum of the square of *independent* Gaussian variables. The signal is band-limited, so neighbouring samples may be correlated, depending on the sample rate.

The expectation of the noise resistance estimate is given by (4.43). The variance is given by (4.44). Both these quantities are governed by the D_n coefficient, (4.46). Closer inspection of (4.46) shows that D_n approaches unity from above as the number of degrees of freedom, n becomes large (*ie* small k_P), but rapidly rises above unity as n becomes small (*ie* large kP). From (4.43) then, the mean-square estimate of noise resistance is seen to be unbiased for large n and the noise resistance is overestimated for small n. Figure 4.3 shows the results of a computer simulation to confirm this point.[2]

Using (4.42) and (4.46) to eliminate n and D_n from (4.45), it is found that for small k_P

$$k_R \approx \frac{k_P}{2} \tag{4.47}$$

so that the noise resistance estimate is approximately twice as precise as the individual potential and current variance estimates. Figure 4.4 shows the results of a computer simulation to confirm (4.47).[2]

[2]Simulation is performed using the *RnVarianceSim* routine (see Section A.8, page 156) and the theoretical curve is obtained using *RnVariance* (Section A.7, page 155).

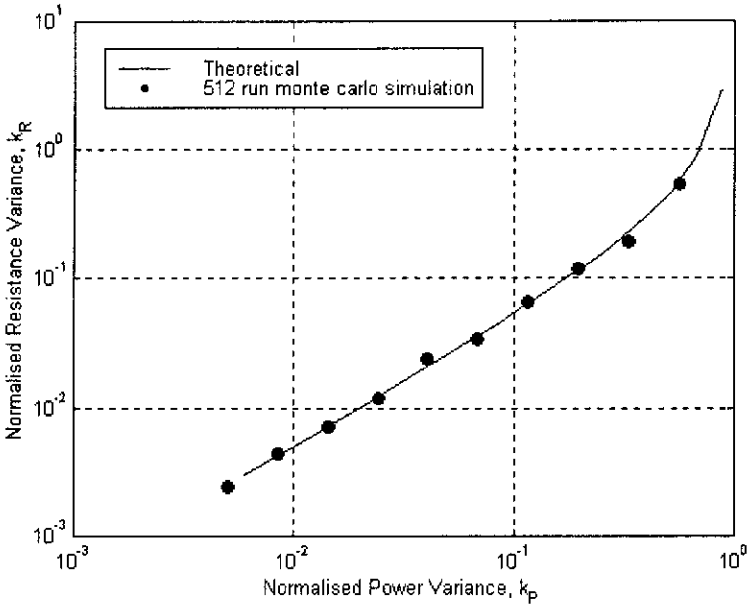

Figure 4.4: k_{R} versus k_{P}

4.3 Signal Conditioning

The assumptions in Section 4.1 regarding the EN characteristics cannot generally be applied to raw EN. It is the purpose of this section to show how the raw EN can be conditioned to approximate the various assumed characteristics and to provide additional control over the estimation of noise resistance.

A raw EN measurement will deviate from the ideal characteristics in the following ways:

1. The equivalent impedances are not necessarily frequency independent;
2. Raw EN is not zero-mean;
3. The electrode impedances might not be identical;
4. EN sources are not necessarily uncorrelated;
5. Raw EN rarely has constant PSD and is always band-limited;
6. Raw EN is not necessarily Gaussian distributed;
7. The system is not necessarily stationary over any arbitrary time interval.

Points 3 and 4 require knowledge of electrode asymmetry and the degree to which the sources are correlated. This information can then be applied to the system of equations (4.8) to (4.10) and a solution thus obtained. The work of Bautista and Huet [109] and Mansfeld *et al* [22] investigated the noise resistance and spectral noise impedance under conditions of asymmetric electrodes.

Point 7 can be addressed by reducing the observation time until it is reasonable to assume that the signal is stationary over that time period. In doing so, however, one must be aware of the trade-offs implied by (4.36). If a suitable combination of relative precision, signal bandwidth and observation time cannot be achieved, then the analysis must be abandoned.

Points 1, 2, 5 and 6 can be addressed by pre-processing the EN signals and is the subject of this section.

As is described in Section 4.3.1, a bandpass filter in combination with a whitening filter can be used to flatten the signal PSD and focus the calculation onto a specific range of frequencies and thus enable frequency dependent impedances to be studied. The filtration also results in zero mean EN, as discussed in Section 4.3.2 and, by the central limit theorem, a signal that additionally tends to Gaussian. Section 4.3.3 explains how a flattened PSD leads to an optimum precision for a given restricted bandwidth.

A *matched* signal conditioning scheme that implements the above mentioned approaches is described in Section 4.3.4. Analysis of the MAR technique of signal conditioning as it relates to the theory developed in this chapter is given in Section 4.3.5. The selection of the various parameters affecting signal pre-processing is discussed in Section 4.3.6.

4.3.1 Frequency Selectivity

Suppose a linear convolutional filter with a transfer function of $H(f)$ is applied to the raw EPN and ECN, $v_{\mathrm{R}}(t)$ and $i_{\mathrm{R}}(t)$ to obtain $v(t)$ and $i(t)$. Then the noise resistance of $v(t)$ and $i(t)$ is given by

$$R_{\mathrm{n}}^2 = \frac{\sigma_{\mathrm{v}}^2}{\sigma_{\mathrm{i}}^2} = \frac{\int_0^\infty S_{\mathrm{v}}(f)\mathrm{d}f}{\int_0^\infty S_{\mathrm{i}}(f)\mathrm{d}f} = \frac{\int_0^\infty |H(f)|^2 S_{\mathrm{v_R}}(f)\mathrm{d}f}{\int_0^\infty |H(f)|^2 S_{\mathrm{i_R}}(f)\mathrm{d}f} \tag{4.48}$$

where $S_{\mathrm{v}}(f)$ and $S_{\mathrm{i}}(f)$ are respectively the PSDs of $v(t)$ and $i(t)$ and $S_{\mathrm{v_R}}(f)$ and $S_{\mathrm{i_R}}(f)$ are respectively the PSDs of $v_{\mathrm{R}}(t)$ and $i_{\mathrm{R}}(t)$.

The spectral noise impedance is given by

$$R_{\mathrm{sn}}^2(f) = \frac{S_{\mathrm{v}}(f)}{S_{\mathrm{i}}(f)} = \frac{|H(f)|^2 S_{\mathrm{v_R}}(f)}{|H(f)|^2 S_{\mathrm{i_R}}(f)} = \frac{S_{\mathrm{v_R}}(f)}{S_{\mathrm{i_R}}(f)} \tag{4.49}$$

Equation (4.48) shows the noise resistance to be affected by the filter process, but (4.49) shows that the spectral noise impedance remains unaltered.

Suppose the filter is a band-pass filter limiting the signals to a range of $[f_1, f_2]$ and further that the filter is a whitening filter matched to the ECN signal within

that bandwidth so that

$$|H(f)| = \begin{cases} \sqrt{\frac{1}{S_{i_R}(f)}} & \text{for } f_1 < |f| < f_2 \\ 0 & \text{elsewhere} \end{cases} \tag{4.50}$$

Then (4.48) becomes

$$R_n^2 = \frac{\int_{f_1}^{f_2} \frac{S_{v_R}(f)}{S_{i_R}(f)} df}{\int_{f_1}^{f_2} \frac{S_{i_R}(f)}{S_{i_R}(f)} df} = \frac{1}{f_2 - f_1} \int_{f_1}^{f_2} R_{sn}^2(f) df \tag{4.51}$$

Equation (4.51) shows that after filtering the EN by (4.50) the square of the noise resistance is equal to the mean of the square of the spectral noise impedance over the bandwidth of the filtered signal. This demonstrates the frequency selectivity of a noise resistance calculation. If the EN signals are restricted to a specific bandwidth, the noise resistance estimate is effectively focused onto that part of the impedance. By examining a different range of EN frequencies, the estimate is focused to a different part of the electrode impedance. That range of frequencies can be controlled by design of the filter, $H(f)$. By decreasing the bandwidth, greater frequency resolution will be achieved but, by (4.36), only at the expense of precision and/or time resolution. Frequency selectivity can also be used to control the effects of measurement noise if it is known that instrumentation effects dominate in a particular range of frequencies.

If the filter is matched to the EPN instead of the ECN, then

$$|H(f)| = \begin{cases} \sqrt{\frac{1}{S_{v_R}(f)}} & \text{for } f_1 < |f| < f_2 \\ 0 & \text{elsewhere} \end{cases} \tag{4.52}$$

and by (4.48)

$$\frac{1}{R_n^2} = \frac{1}{f_2 - f_1} \int_{f_1}^{f_2} \frac{1}{R_{sn}^2(f)} df. \tag{4.53}$$

If $R_{sn}(f)$ is independent of frequency for $f_1 < |f| < f_2$ with a value of R_{sn0}, then both (4.51) and (4.53) give $R_n = R_{sn0}$.

4.3.2 Zero Mean EN

The traditional approach of conditioning EN prior to computation of noise resistance involves trend removal, as discussed in Section 3.1.3, where a DC trend is estimated and then subtracted to determine the residuals. The noise resistance is then calculated on these residuals. Since the residuals are, by definition, raw EN minus the DC estimate, the residuals are zero mean.

In general, any highpass/bandpass filter in the steady state, by virtue of the fact that it restricts the signal to a band of frequencies that does not include zero, results

in a zero mean output. A highpass/bandpass filter is thus a frequency selective method of trend removal. MAR is an example of a frequency selective trend removal technique, but it can also be used, to some degree, to focus the calculation bandwidth in a similar manner as described in Section 4.3.1. If there is basis to believe that a DC trend is described by a certain deterministic model, there is no reason why an appropriate model based trend removal scheme (*eg* spline fitting, LTR, higher order polynomial regression) cannot be applied prior to further signal conditioning. Alternatively, a correction factor can be applied subsequent to the estimate, as is described by Mansfeld *et al* [15]. The frequency selective trend removal might then be used to provide additional protection against DC trend by removal of any low frequency residual trend left by deviations from the assumed model, *eg* if LTR were used to remove an exponential or oscillatory or otherwise non-linear trend.

4.3.3 Minimising Variance of Signal Power by Whitening

The major point of deviation from the ideal EN characteristics is the band limitation. The effect on the noise resistance calculation of varying the bandwidth of band-limited, but otherwise white, EN has been investigated in Section 4.2. This section addresses the question: constrained to a fixed, finite bandwidth, what shaped PSD within that bandwidth results in minimum relative precision, k_{P}, associated with (4.22)?

The approximate answer, as will be shown, is a signal with a flat PSD within its bandwidth. This can be achieved by the band-limited whitening filter given by (4.50) to whiten the ECN signal, or by (4.52) to whiten the EPN signal. Given that the raw potential and current measurements are sure to have different PSDs, it is not generally possible to whiten both by application of the same filter sequence to each signal. Rather, if the ECN signal is selected to take the ideal white PSD, then the noise resistance is given by (4.51). If the EPN signal is to take the ideal white PSD, then the noise resistance is given by (4.53).

Picking up from (4.22) and (4.24) and substituting for $R_{\mathrm{yy}}(t)$ using (4.25), the relative precision is given for an arbitrary $x(t)$ as

$$k_{\mathrm{P}} = \frac{\sigma_{\mathrm{P}}^2}{\eta_{\mathrm{P}}^2} = \frac{1}{T}\int_0^{2T}\left(1-\frac{\tau}{2T}\right)\frac{R_{\mathrm{xx}}^2(\tau)}{R_{\mathrm{xx}}^2(0)}\mathrm{d}\tau \tag{4.54}$$

Because the products inside the integral are both positive quantities for all τ, for a fixed $R_{\mathrm{xx}}(0)$, the integral can be minimised with respect to $R_{\mathrm{xx}}(\tau)$ by letting $R_{\mathrm{xx}}(\tau)$ equal to zero for all $\tau \neq 0$. This corresponds to an $x(t)$ that has an infinite bandwidth and a constant PSD. That is to say, k_{P} for a Gaussian distributed $x(t)$ is minimised if $x(t)$ is white.

However, such an $R_{\mathrm{xx}}(t)$ violates the constraint that the signal is band-limited to some fixed range of frequencies. $x(t)$ must be band-limited to some finite region

either by necessity due to instrumentation limitations, or by intent so as to focus the calculation to a particular range of frequencies, *eg* a range where the equivalent impedance of the electrodes is believed to be equal to the polarisation resistance or solution resistance. The foregoing derives a pair of criteria against which the auto-correlation function of a signal can be tested. If the criteria hold, then the signal possesses a PSD shape that yields a local minimum of k_{P}, given the fixed bandwidth and measurement length. The band-limited white signal will then be tested against these criteria.

Let $S_{\mathrm{xx}}(f)$ be the PSD of $x(t)$ and let $x(t)$ be band-limited to the range f_1 to f_2. Then $S_{\mathrm{xx}}(f) = 0$ for all $|f| \notin [f_1, f_2]$. Since $R_{\mathrm{xx}}(t)$ is the inverse Fourier transform of $S_{\mathrm{xx}}(f)$, from (4.54) it follows that

$$k_{\mathrm{P}} = \frac{\sigma_{\mathrm{P}}^2}{\eta_{\mathrm{P}}^2} = \frac{2}{T}\int_0^{2T}\left(1-\frac{\tau}{2T}\right)\left[\frac{\int_{f_1}^{f_2} S_{\mathrm{xx}}(f)\cos(2\pi f\tau)\mathrm{d}f}{\int_{f_1}^{f_2} S_{\mathrm{xx}}(f)\mathrm{d}f}\right]^2 \mathrm{d}\tau. \tag{4.55}$$

The optimum PSD is derived by setting to zero the first derivative of (4.55) with respect to $S_{\mathrm{xx}}(f_{\mathrm{m}})$, where f_{m} is an arbitrary frequency in $[f_1, f_2]$. This yields an infinite number of simultaneous equations (one for each f_{m}) that jointly describe the optimum PSD.

In order to facilitate calculation of the derivative, (4.55) is rewritten as a Riemann sum:

$$k_{\mathrm{P}} = \lim_{\Delta f\to 0}\frac{2}{T}\int_0^{2T}\left(1-\frac{\tau}{2T}\right)\cdot \left[\frac{\sum_{n\neq m}[S_{\mathrm{xx}}(f_{\mathrm{n}})\cos(2\pi f_{\mathrm{n}}\tau)\Delta f]+S_{\mathrm{xx}}(f_{\mathrm{m}})\cos(2\pi f_{\mathrm{m}}\tau)\Delta f}{\sum_{n\neq m} S_{\mathrm{xx}}(f_{\mathrm{n}})\Delta f+S_{\mathrm{xx}}(f_{\mathrm{m}})\Delta f}\right]^2 \mathrm{d}\tau \tag{4.56}$$

In (4.56), the infinitesimal element corresponding to the particular $S_{\mathrm{xx}}(f)$ that the derivative is taken with respect to, $S_{\mathrm{xx}}(f_{\mathrm{m}})$, is separated out from the summations. It is now possible to take the 1st derivative of (4.56) with respect to $S_{\mathrm{xx}}(f_{\mathrm{m}})$, which results in

$$\frac{\mathrm{d}k_{\mathrm{P}}}{\mathrm{d}S_{\mathrm{xx}}(f_{\mathrm{m}})} = \lim_{\Delta f\to 0}\frac{4}{T}\int_0^{2T}\left(1-\frac{\tau}{2T}\right)\frac{R_{\mathrm{xx}}(\tau)\left[R_{\mathrm{xx}}(0)\cos(2\pi f_{\mathrm{m}}\tau)-R_{\mathrm{xx}}(\tau)\right]}{R_{\mathrm{xx}}^3(0)}\mathrm{d}\tau\Delta f \tag{4.57}$$

Even though (4.57) approaches zero in the limit regardless of $R_{\mathrm{xx}}(t)$ (indicating that a change in $S_{\mathrm{xx}}(f_{\mathrm{m}})$ for an infinitesimally small Δf has an infinitesimally small effect on k_{P}), it can still be made identically equal to zero over the range of frequencies taken by f_{m} (the bandwidth of the signal) by proper selection of $R_{\mathrm{xx}}(t)$. Such a selection ensures an optimum value for k_{P}, subject to the limited signal bandwidth. Assuming that $R_{\mathrm{xx}}(0) \neq 0$, the first criterion for an optimum k_{P} can then be stated as

$$\int_0^{2T}\left(1-\frac{\tau}{2T}\right)R_{\mathrm{xx}}(\tau)\left[R_{\mathrm{xx}}(0)\cos(2\pi f_{\mathrm{m}}\tau)-R_{\mathrm{xx}}(\tau)\right]\mathrm{d}\tau = 0 \tag{4.58}$$

An expression for the 2nd derivative of k_P with respect to $S_{xx}(f_m)$ is derived and used to test whether the optimum k_P is a local minimum or a local maximum. Following a similar methodology as for the 1st derivate results in

$$\int_0^{2T} \left(1 - \frac{\tau}{2T}\right) R_{xx}(\tau)[R_{xx}(0)\cos(2\pi f_m \tau) - R_{xx}(\tau)] \cdot [R_{xx}(0)\cos(2\pi f_m \tau) - 3R_{xx}(\tau)]\, d\tau > 0 \tag{4.59}$$

which is the criterion for k_P to be a local minimum.

If a signal with an auto-correlation function of $R_{xx}(t)$ is band-limited to the range $[f_1, f_2]$ and (4.58) and (4.59) hold true for all $f_m \in [f_1, f_2]$, then $R_{xx}(t)$ (or equivalently, the PSD of the signal) is of a shape that yields a local minimum of k_P, subject to the fixed bandwidth of the signal. It is noted here that for a stationary signal, the auto-correlation, $R_{xx}(t)$, of a signal is merely the inverse Fourier transform of the PSD, $S_{xx}(f)$. They both carry identical information and if one is known, the other is inferred implicitly.

In the absence of a general solution for (4.58), it is hypothesised that a signal with a constant PSD, S_{xx}, within its limited bandwidth of f_1 to f_2 has an optimum $R_{xx}(t)$ as T becomes large. By taking the inverse Fourier transform of the described PSD, the auto-correlation is found to be given by

$$R_{xx}(\tau) = \frac{S_{xx}}{\pi\tau}\left[\sin(2\pi f_2 \tau - \sin(2\pi f_1 \tau)\right]. \tag{4.60}$$

By use of symbolic manipulation software, substitution of (4.60) into (4.58) confirms that (4.60) is an optimal solution for large T.

Figure 4.5 shows a plot of the 1st derivate for a large, but still finite, T for a signal with flat PSD, band-limited to the range [235 mHz, 777 mHz].[3] In Figure 4.5, the 1st derivative can be seen to be approximately zero over the signal bandwidth, indicating that the PSD is nearly optimal within that bandwidth. Some adjustment may be possible to improve the PSD slightly so that the derivative is identically equal to zero for finite measurement times. The flat PSD is taken as being near optimal for most practical applications.

A numerical analysis of (4.59) shows the 2nd derivative to be always positive for the test case of $f_1 = 235$ mHz and $f_2 = 777$ mHz, which confirms that the PSD yields a local minimum and not a local maximum of k_P.

4.3.4 Matched Signal Conditioning

A signal conditioning scheme, depicted in Figure 4.6 for estimation of the noise resistance is proposed that makes use of the concepts of Sections 4.3.1 to 4.3.3 to approximate the ideal EN characteristics. The scheme will be referred to in this work

[3]The *optimumRxx* routine (See Section A.6, page 154) is used to compute the 1st and 2nd derivatives of k_P.

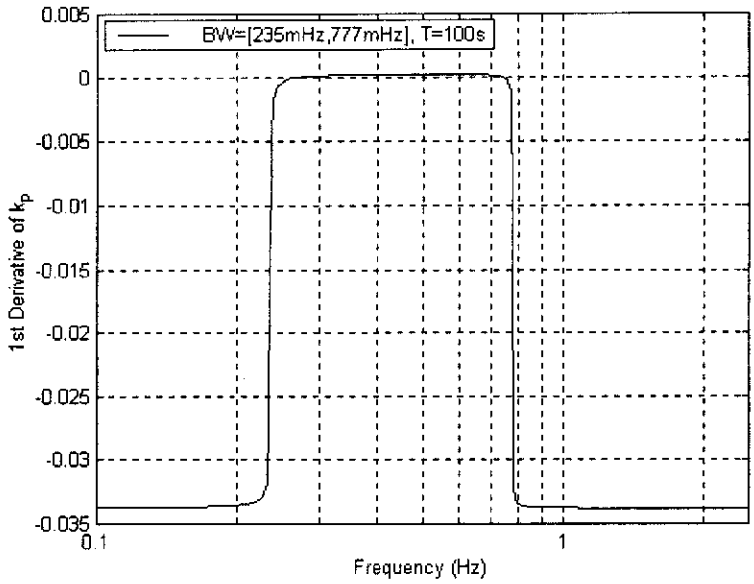

Figure 4.5: 1st derivative of k_P for a white, band-limited signal

as *matched* signal conditioning because the filters are constructed such that they match the raw EN to the assumed ideal characteristics. It could also be described as near optimal because it attempts to produce a signal PSD that is nearly-optimum, as described in Section 4.3.3. The scheme is implemented by the *nSigmaImpedance* routine. (see Section A.5, page 148.)

In Figure 4.6 there are two parallel paths for estimating the variance of the EPN and ECN signals separately. Each path consists of signal conditioning and variance estimation. The signal conditioning consists of two stages. The first is a whitening filter [implemented using the linear prediction filter coefficients], which flattens the PSD to match the near-optimal shape as derived in Section 4.3.3. The second is a band-pass filter to limit the signal to the given range of frequencies that the noise resistance is to be calculated over. In this way a pair of zero mean band-limited signals with approximately constant PSDs within their bandwidth are obtained. By the central limit theorem, the signals also tend to Gaussian distributed. The remainder of each path constitutes the estimation of signal variance by the mean-square, which, with the given signal characteristics, is seen to be the MLE of the noise resistance. Finally, the two variance estimates are divided to obtain the square of the noise resistance estimate within the bandwidth of the conditioning filters.

In Figure 4.6, the whitening filter is matched to the ECN so that the noise resistance is given by (4.51).

The two main features of the scheme depicted in Figure 4.6 that differentiate it from MAR (see Section 4.3.5) is the flat PSD and the independent control over bandwidth and frequency location. Such independent control allows the calculation to be focused to any range of frequencies independently of the bandwidth, *ie* f_1 and

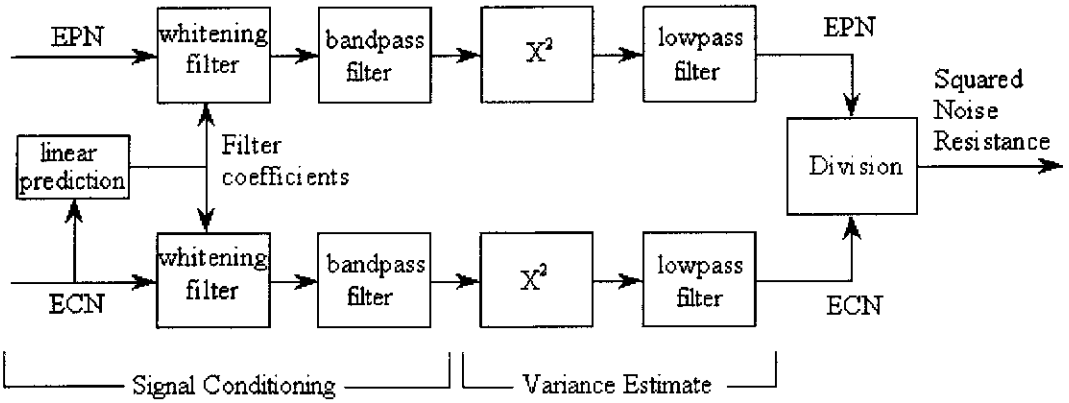

Figure 4.6: Noise Resistance calculation using the proposed matched signal conditioning

f_2 in (4.51) are independent.

Although it is not shown in Figure 4.6, it may be desirable to apply LTR (or any other appropriate model based trend removal) prior to the signal conditioning stage.

To illustrate the effects of the various parameters controlling the noise resistance calculation depicted in Figure 4.6, a computer simulation has been generated with a step in resistance from 1 kΩ to 500 Ω so that the response to a step change in electrode resistance can be seen.[4]

The noise resistance has been then computed[5] over the data using

- a whitening filter and then again with no whitening filter;
- different bandpass filter bandwidths; and
- different low pass filter bandwidths.

Figure 4.7 compares the continuous noise resistance computed with and without the whitening filter stage. From the figure, it is clear that the whitening filter has resulted in an estimate with a significantly improved variance.

Figure 4.8 shows the effect of varying the bandwidth of the bandpass filter stage. The figure shows that the estimate with the larger bandwidth has less variance. The trade-off is that the use of a wider bandwidth means that the estimate has impaired frequency resolution.

Figure 4.9 shows the effect of varying the cut-off frequency (and thus the averaging time) of the final low-pass filter stage. It shows that using a lower frequency

[4]A pair of Gaussian and white signals with unity variance are generated using the Matlab function *normrnd*. The signals are scaled so that the ratio of their standard deviations is 1000 for the first half and 500 for the second half. The result is then cumulatively summed with Matlab's *cumsum* function to produce a $\frac{1}{f}$ type PSD

[5]Using *shape* (See Section A.10, page 158) to perform the signal whitening and the Matlab functions *butter* and *filter* to design and implement the bandpass and low pass filters.

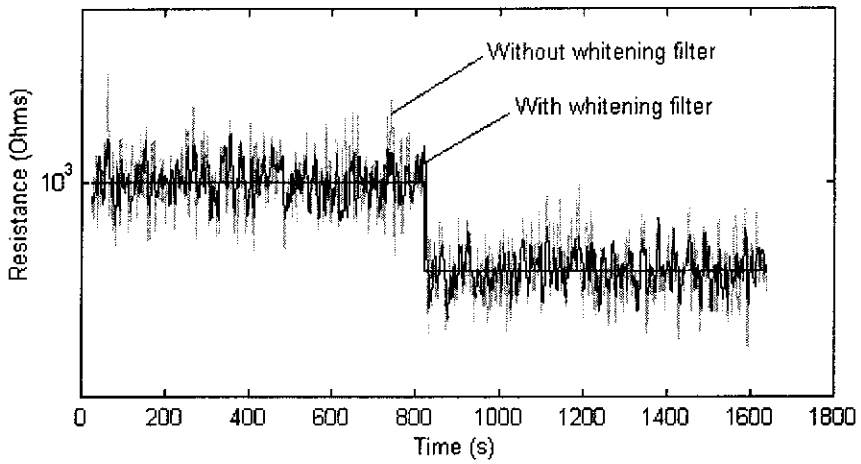

Figure 4.7: Noise resistance with and without a whitening filter

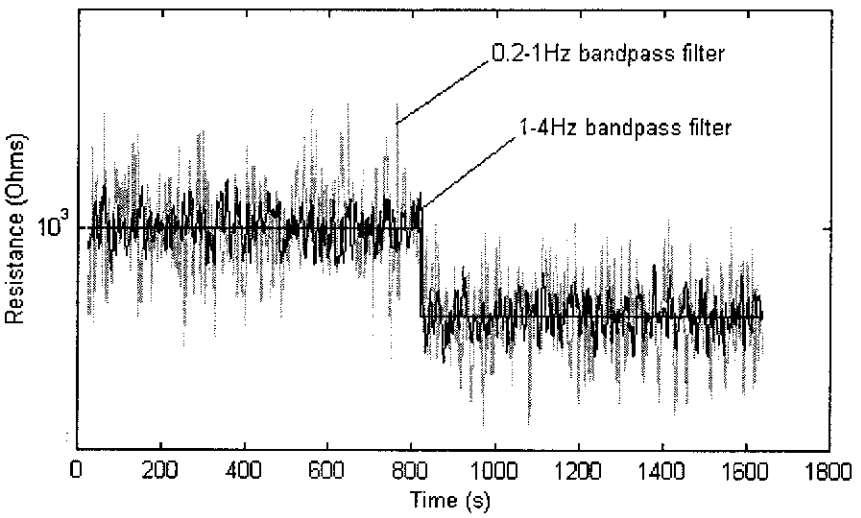

Figure 4.8: Noise resistance calculated over two different bandwidths

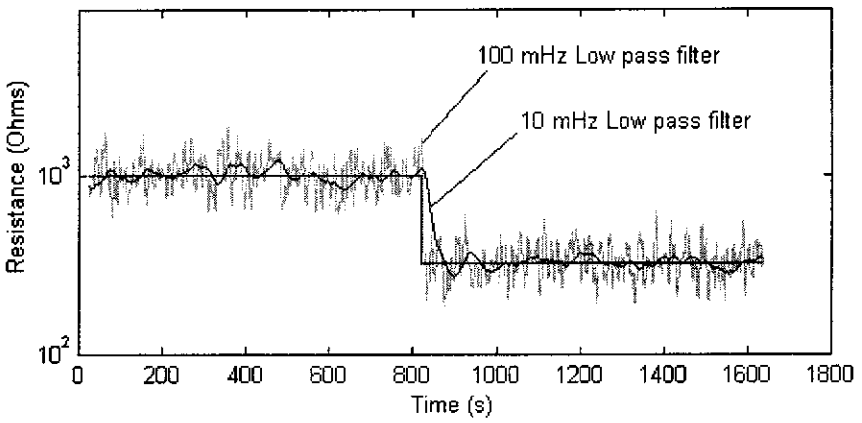

Figure 4.9: Noise resistance calculated using two different low pass filter cut-off frequencies

(longer averaging time) results in improved variance. However, as can be seen by the slower response to the step in resistance, this improvement is only achieved at the expense of time resolution.

4.3.5 An Analysis Moving Average Removal

Another useful form of signal conditioning is the moving average removal (MAR) method proposed by Tan *et al* [50] [16]. A moving average low pass filter is applied to the signal to obtain a waveform that is taken to be the DC trend. Trend removal is then accomplished by subtracting the DC trend from the original signal. This section provides analysis of the method to determine the effective bandwidth and the centre frequency of the resulting signal. Once the effective bandwidth is known, (4.36) can be used to predict the approximate performance of the MAR technique. The PSD of the trend-removed signal is also tested against the two criteria for an optimal PSD, (4.58) and (4.59).

The first task is to determine the PSD of the output of the moving average filter. Unlike the whitening filter, the moving average does not adapt to the signal. The output PSD is very much dependent on the input PSD. EN is often observed to conform to a $\frac{1}{f^n}$ type model, where its PSD takes a $\frac{1}{f^n}$ shape. [21] [63] [89] [54]

A moving average of length T_m can be described by a linear convolutional filter with the impulse response as given in (3.27, page 56). The transfer function of the MAR filter is then given by the Fourier transform of (3.27), subtracted from unity:

$$H_{\mathrm{MAR}}(f) = 1 - \frac{\sin(\pi T_\mathrm{m} f)}{\pi T_\mathrm{m} f} \tag{4.61}$$

Applying this filter to a signal having a PSD of $\frac{1}{f^n}$ then results in a signal, $x(t)$,

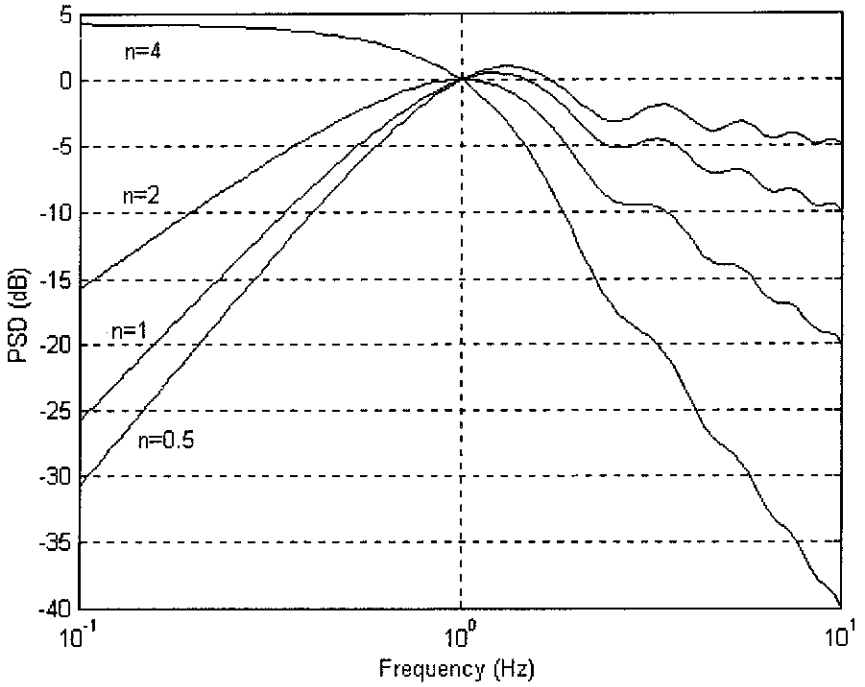

Figure 4.10: PSD of a $\frac{1}{f^n}$ signal after processing by MAR

with a PSD of $S_{xx}(f)$ as given by

$$S_{xx}(f) = \frac{1}{f^n}|H_{MAR}(f)|^2 = \frac{1}{f^n}\left[1 - \frac{\sin(\pi T_m f)}{\pi T_m f}\right]^2 \tag{4.62}$$

Figure 4.10 shows a plot of $S_{xx}(f)$ for an averaging time of $T_m = 1$ s with $n = 0.5$, $n = 1$, $n = 2$ and $n = 4$. As can be seen from Figure 4.10, $S_{xx}(f)$ depends significantly on n. For the different values of n, the $S_{xx}(f)$ has a different bandwidth and centre frequency.

The foregoing will numerically examine $S_{xx}(f)$ for $n = 2$, *ie* for a PSD with a -20 dB/decade rate of roll-off.

By numerical analysis, it is found that $S_{xx}(f)$ takes its maximum value for $T_m f$ approaching 1.000.

Also, by numerical analysis, 99 % of the signal power is located between $T_m f = 0.294$ and $T_m f = 3.40$, giving a 99 % effective bandwidth of $\frac{3.1}{T_m}$. Similarly, 95 % of the signal power is found to be located between $T_m f = 0.312$ and $T_m f = 3.20$ for a 95 % effective bandwidth of $\frac{2.9}{T_m}$. The differences between the 99 % and 95 % bandwidths are only slight, so the effective bandwidth of the signal is taken to lie approximately between $T_m f = 0.3$ and $T_m f = 3.3$, covering a total bandwidth of $\frac{3}{T_m}$.

These results are summarised for a $\frac{1}{f^2}$ input as

$$f_{\text{centre}} \approx \frac{1}{T_{\text{m}}} \tag{4.63}$$

$$f_1 \approx \frac{0.3}{T_{\text{m}}} \tag{4.64}$$

$$f_2 \approx \frac{1}{0.3T_{\text{m}}} \tag{4.65}$$

$$f_2 - f_1 \approx \frac{3}{T_{\text{m}}} \tag{4.66}$$

where f_{centre} is the frequency at which the maximum signal power occurs and f_1 and f_2 are the upper and lower cut-off frequencies of the signal's effective bandwidth.

Having obtained the effective bandwidth of the filtered signal, it is now possible to make use of (4.36, page 68) to predict the approximate performance of the signal variance estimate. It is noted that the PSD does not identically match the PSD assumed in the derivations and hence the predictions are only approximate.

Figure 4.11 plots the 1st derivative of the relative precision for the PSD of a $\frac{1}{f^2}$ signal after application of MAR of length $T_{\text{m}} = 1$ s.[6] With $T_{\text{m}} = 1$ s, the signal bandwidth occupies approximately 0.3 Hz to 3.3 Hz. As can be seen from Figure 4.11, the 1st derivative is non-zero over this bandwidth and the first criterion for an optimum PSD, (4.58), fails, indicating that MAR does not produce an optimum PSD for a $\frac{1}{f^2}$ input.

The moving average removal has some advantages and disadvantages in comparison with the matched signal conditioning. One advantage is its relative simplicity — there is only one filter stage and no need to compute LPR coefficients. Also, the length of the filter's impulse response can typically be quite long, which results in an output that tends more strongly to a Gaussian distribution (by the central limit theorem). Its disadvantages are its non-optimal PSD shape, its dependence on input PSD shape and, as can be seen from (4.63) and (4.66), the centre frequency and bandwidth are not independently controllable because T_{m}, the only controllable parameter, determines both.

4.3.6 Selection of Conditioning Parameters

The time, bandwidth and precision of the estimate are all controllable to a degree. The observation time, T_{res}, defines the time interval over which the noise resistance calculation is to be estimated. The bandwidth of the signal is defined by two cut-off frequencies, f_1 and f_2, and can be controlled by the signal conditioning parameters.

[6] The *optimumRxx* routine (see Section A.6, page 154) is used to compute the 1st and 2nd derivatives of k_{P}. The auto-correlation function is given by the inverse Fourier transform of (4.62) with $n = 2$.

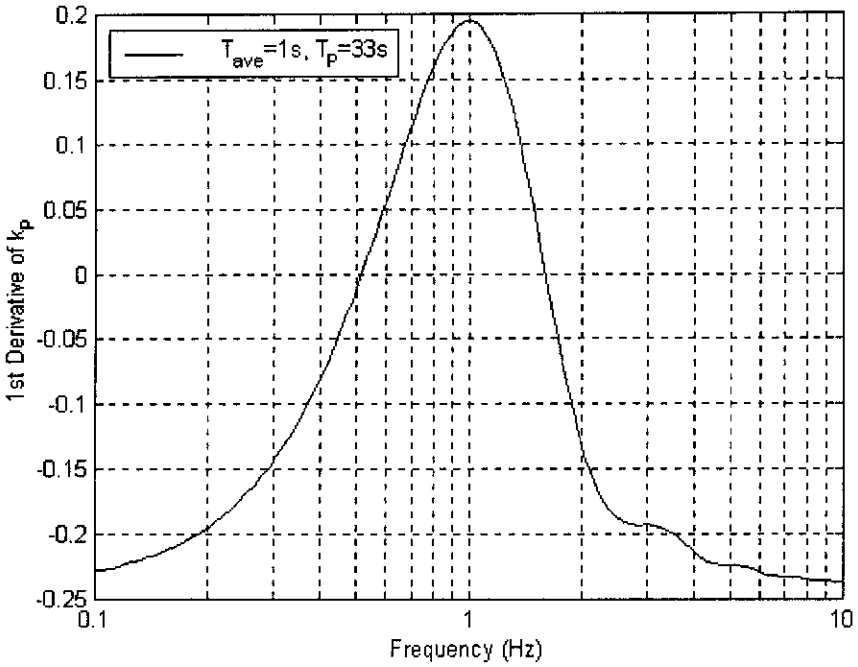

Figure 4.11: 1st derivative of k_{P} for a $\frac{1}{f^2}$ signal processed by MAR

The relative estimation variance, k_{P} is a desired precision and is approximately related to T_{res}, f_1 and f_2 by (4.36, page 68).

It is desirable to have a measurement with as much precision as possible (*ie* small k_{P}). Due to the relationship given by (4.36), excessive precision can result in unacceptably long measurement times (*ie* large T_{res}) or unacceptably wide bandwidths (*ie* large $f_2 - f_1$). The foregoing describes how to make a compromising selection of the various parameters.

Precision: k_{P}

Suppose that a calculation is required that will allow a difference in noise resistance between the arbitrary values of R_{n1} and R_{n2} to be detected. The relative precision of the variance estimate, k_{P}, is given by (4.36). The final precision of the noise resistance is similarly defined as k_{R} and is related to k_{P} by (4.47) for small k_{P}.

A value for k_{P} must be selected such that an estimate of R_{n1} can be adequately resolved from an estimate of R_{n2}. That is to say, the probability density functions of the two estimates must be sufficiently separated (say by a distance of N times their standard deviations) in order to resolve the two:

$$R_{\mathrm{n2}} - R_{\mathrm{n1}} = N(\sigma_{\mathrm{rn1}} + \sigma_{\mathrm{rn2}}) \tag{4.67}$$

where σ^2_{rn1} and σ^2_{rn2} are the respective variances of the R_{n1} and R_{n2} estimates,

N defines the desired level of confidence and it is assumed that $R_{n2} > R_{n1}$. If $R_{n1} > R_{n2}$, the roles are reversed.

With $k_R = \frac{k_P}{2} = \left(\frac{\sigma_{rn1}}{R_{n1}}\right)^2 = \left(\frac{\sigma_{rn2}}{R_{n2}}\right)^2$, the solution for k_P results as

$$k_P = \frac{2}{N^2}\left(\frac{R_{n2} - R_{n1}}{R_{n2} + R_{n1}}\right)^2 \tag{4.68}$$

For equally likely R_{n1} and R_{n2}, from the Gaussian cumulative probability distribution, $N = 2$ yields a 4.5 % probability of an estimate being closer to the incorrect resistance than the correct one, while $N = 3$ yields a 0.27 % probability.

From (4.68) the value of k_P that resolves a change in noise resistance from R_{n1} to R_{n2} with any given degree of certainty can be determined. Once a suitable value for k_P has been determined it remains to find an acceptable combination of T_{res}, f_1 and f_2 that yields that k_P.

Bandwidth: f_1 and f_2

Equation (4.36) shows that the precision can be improved by using a large signal bandwidth. Naturally, the largest possible bandwidth would normally be selected. But as discussed previously in Sections 4.3.1 and 4.3.2, there is some advantage to restricting the bandwidth to achieve a frequency selective calculation. The selection of the range of frequencies for the calculation is therefore an important facet of a successful noise resistance calculation.

A number of tools are available for making a judgement as to an appropriate band of frequencies to focus the calculation on to. Simple PSD diagrams such as the one in Figure 4.16 (page 89) can be used to locate measurement noise. As can be seen by the reference measurement noise PSD in Figure 4.16, the lower frequencies have a signal to noise ratio of about 40 dB, while the higher frequencies are dominated by measurement noise. A noise resistance estimate utilising this signal might thus be restricted to below 1 Hz in order to control the effect of measurement noise.

A spectral noise impedance calculation can be used to assess the shape of the electrode impedance and help identify frequency bands of interest. For example if the equivalent impedance is believed to approximate to a parallel resistor/capacitor combination, the low frequency resistive plateau can be located. Figure 4.20 (page 91) shows an example spectral noise impedance calculation derived from the EPN of Figure 4.16. In Figure 4.20, the effect of measurement noise in the potential measurement can be seen to have significant effect from about 1 Hz and up. Below 1 Hz, the spectral noise impedance is approximately flat and might be taken to correspond to the low frequency plateau of a parallel RC impedance. Based on this diagram, a noise resistance calculation might be carried out over a range extending up to the frequency of $f_2 = 1$ Hz.

In Figure 4.16 the PSD has a roll-off rate of approximately -20 dB/dec up to

1 Hz. If MAR is to be applied to the data set of Figure 4.16 to cover a frequency range extending up to $f_2 = 1$ Hz, then T_m can be set to 3.3 s by (4.65). This fixes f_1 at 90 mHz by (4.64) for a bandwidth of 910 mHz by (4.66).

For the matched conditioning, there is no restriction on the selection of f_1 so the bandwidth can be set to anything from above 0 Hz (with f_1 approaching f_2) up to f_2 (with $f_1 = 0$). Since, from (4.36), there is little to be gained in terms of precision by decreasing f_1 much below 10 % of f_2, f_1 might be set to $\frac{f_2}{10}$ to exclude any possible DC trend (or residuals thereof), located below 100 mHz in this example. It is possible to use a narrower bandwidth in order to focus the calculation onto a narrower band of the electrode's impedance if required.

Observation Time: T_{res}

By use of the signal power, (4.22, page 65), as an estimate of the signal variance, the noise resistance estimate uses a time average as an estimate of an ensemble average. This assumes that there is no significant change in the noise resistance during the measurement and thus a limitation is placed on the acceptable observation time. Once the required precision and signal bandwidth has been set, the observation time is fixed by (4.36). It may become evident that the observation time is unpractically large with the given level of precision and bandwidth for a given task. In that case, some compromise on the precision and/or bandwidth needs to be made in order to decrease the required observation time and improve the estimate's ability to resolve rapid changes in the noise resistance.

4.4 Experimental Comparison of Signal Conditioning Methods

Although it is shown that MAR is not an optimal means of conditioning the EN signals, there is still some advantage due to its relative simplicity. There is no need for calculation of prediction filter coefficients, as with the matched conditioning and there is only one filter stage compared to the two stages used by the matched conditioning. The advantages of the MAR are then a reduction in the processing complexity and the ease of use.

The advantages of the matched conditioning are that the precise location and width of the range of frequencies used for the noise resistance calculation are easily controlled and that the conditioned EN signals take on a near-optimum PSD. It can almost be guaranteed that the PSD of the conditioned signals is negligible outside the desired bandwidth, whereas with MAR, there is some degree of reliance on the raw EN taking an appropriate shape.

The following example compares the operation of the proposed matched signal conditioning with the LTR and the MAR methods. The measurements were all

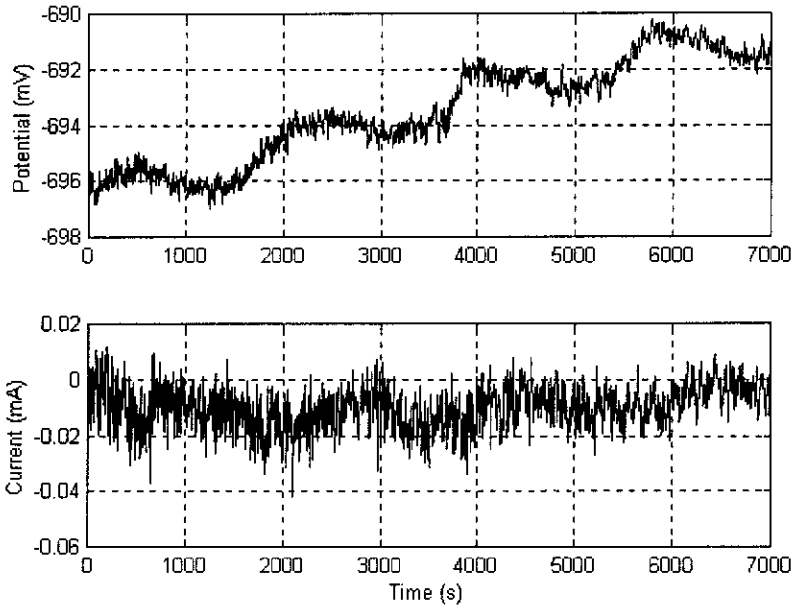

Figure 4.12: Raw EPN and ECN

taken from a CO_2 corrosion system using a pair of mild steel electrodes mounted on a dual cylinder electrode and immersed in 2 % NaCl at 60 °C. The experiment was repeated a number of times. For each repetition, the polarisation resistance of each electrode was measured by linear polarisation (LP) for comparison with the noise resistance. Figures 4.12 to 4.24 present data from the first measurement while Table 4.1 summarises the data.

Figure 4.12 shows the raw EPN and ECN measurements. There is significant DC trend in the potential measurement that needs to be removed before the variance of the signals can be reliably estimated using a mean square calculation.

Figure 4.13 shows the EPN and ECN after applying LTR.[7] These are the residuals from applying linear regression to the raw signals. The EPN plot demonstrates a typical problem with LTR. If the DC trend takes a non-linear form, such as the oscillatory behaviour in this case, it is not removed by a linear model.

Figure 4.14 shows the EPN and ECN after trend removal by MAR (subsequent to application of LTR).[8] A moving average of length 14.7 s is used in this case. The oscillatory trend that remains after LTR is seen to be removed by the MAR.

Figure 4.15 shows the EPN and ECN after whitening and band-pass filtering, *ie* after applying the matched signal conditioning.[9]. As with MAR, the oscillatory trend has been removed. The specific differences in character between the two methods are not clear in the time domain. Figures 4.16 to 4.19 examine LTR, MAR and the

[7]The Matlab functions *polyfit* and *polyval* are used to perform linear regression on the EN signals.
[8]The *MAVFilt* routine (see Section A.1, page 142) is used for moving average removal.

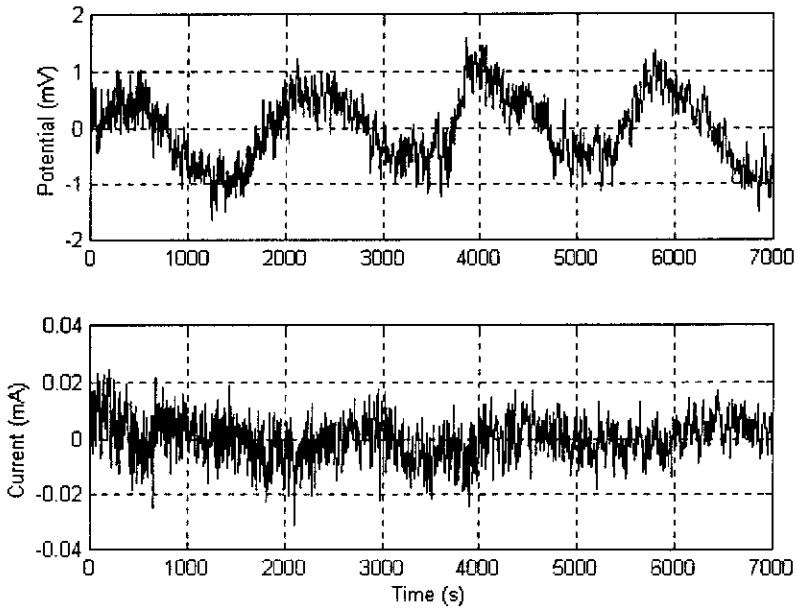

Figure 4.13: EPN and ECN after trend removal by LTR

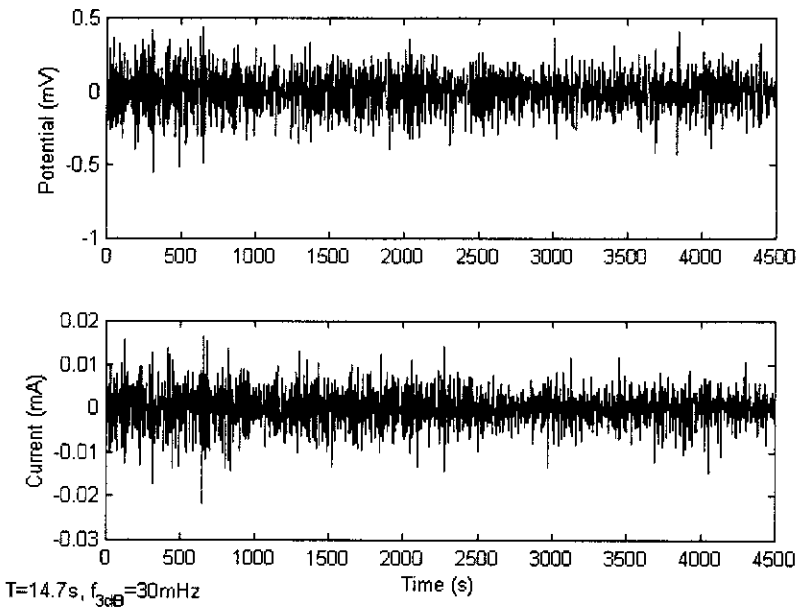

Figure 4.14: EPN and ECN after trend removal by MAR.

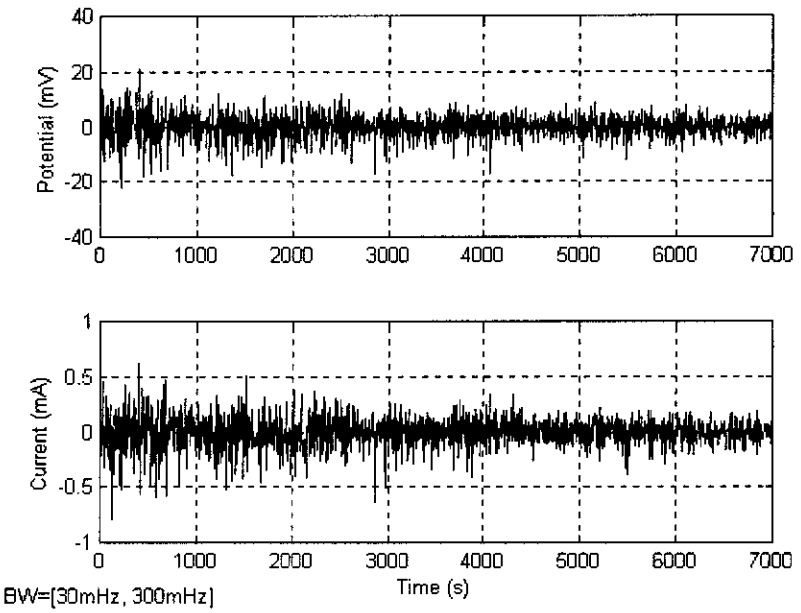

Figure 4.15: EPN and ECN after matched conditioning.

matched signal conditioning procedures in the frequency domain.

Figure 4.16 shows the PSD of the raw EPN. The lower plot shows the level of measurement noise. It can be seen that the frequencies above 1 Hz are dominated by measurement noise (see Appendix C) and contain very little EN. Below 1 Hz, the measurement takes a more $\frac{1}{f^n}$ type shape. With a roll-off rate of approximately -20 dB/decade, the order of the $\frac{1}{f^n}$ noise is approximately 2. This plot demonstrates how some form of signal conditioning can improve the performance of a variance estimate: The signal, by its $\frac{1}{f}$ nature, has a very narrow bandwidth. By (4.36), the mean of the square performs very poorly as an estimate of signal variance in this case, but can be improved by widening of the signal bandwidth.

Figure 4.17 shows the PSD of the EPN after LTR. There is very little change in the signal's PSD in this case. The LTR has removed the linear trend, as can be seen from the time domain plot, but it has done little to widen the signal's bandwidth or make it any more an approximation to an optimal shape than the original signal. The ensuing noise resistance calculation is still effectively restricted to the narrow band of frequencies extending up to approximately 5 mHz to 10 mHz.

Figure 4.18 shows the PSD of the EPN after MAR. The lower frequencies have been significantly attenuated while the higher frequencies remain untouched. The result is a signal that is very much tuned to a relatively narrow range of frequencies. The PSD shape is not optimal in the sense described in Section 4.3.3 and the location and width of the signal in the frequency domain are not independently controllable.

[9]The *shape* function (see Section A.10, page 158) implements this signal conditioning. Band pass filtering is achieved by the Matlab function *filter*, with filter coefficients obtained from *butter*.

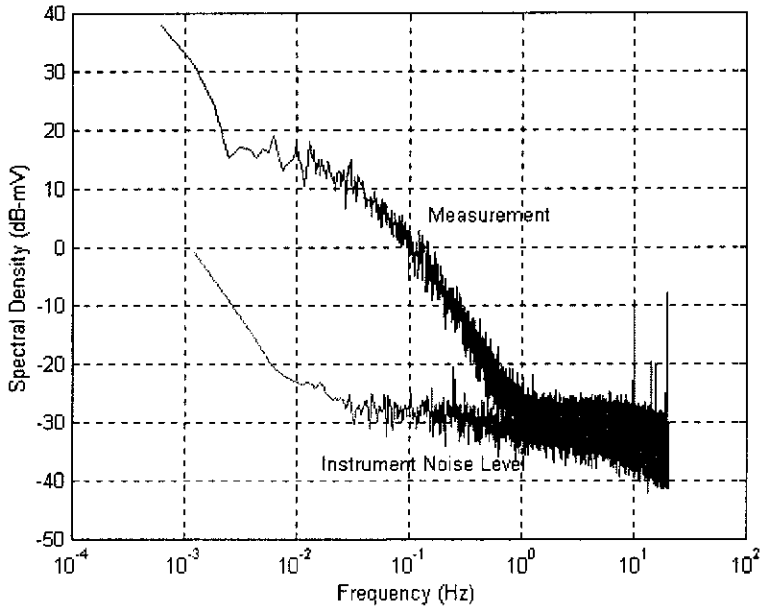

Figure 4.16: Power spectral density of the raw EPN measurement.

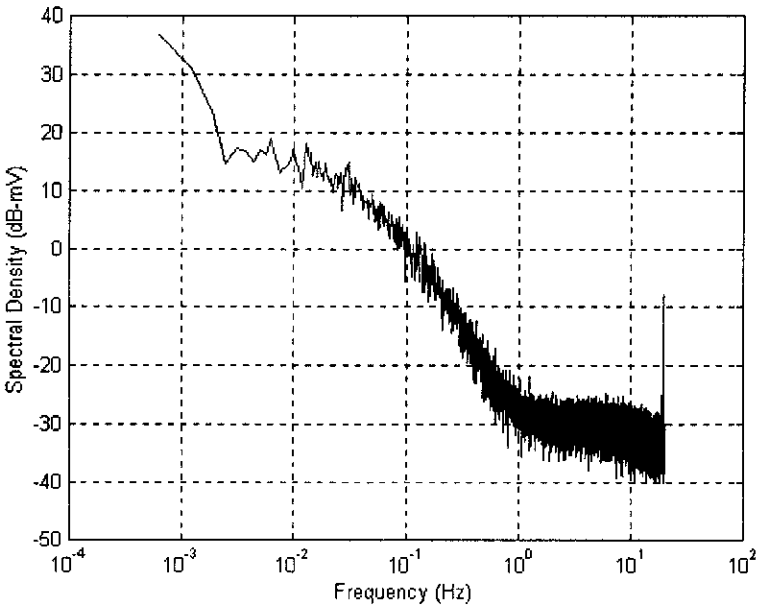

Figure 4.17: Power spectral density of the EPN after LTR.

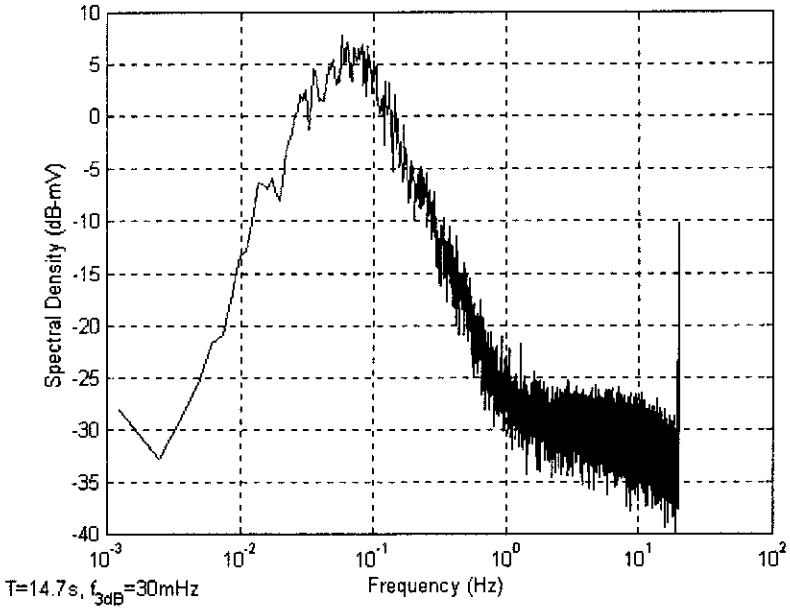

Figure 4.18: Power spectral density of the EPN after MAR.

Measurement noise (located above 1 Hz), although small in magnitude compared to the dominant frequencies located at 70 mHz, is still observable and may have some small influence. However, the signal, with an effective bandwidth of approximately 200 mHz, is more suitable for variance estimation than the LTR signal.

Figure 4.19 shows the PSD of EPN after matched filtering. This PSD conforms well to the near-optimal shape described in Section 4.3.3. The matched filtering allows independent control over the upper and lower frequencies defining the signal bandwidth. All signs of measurement noise have been removed. This signal is better suited to variance estimation by the mean-square than the raw, LTR, or MAR signals because of its flat PSD and wider bandwidth of 270 mHz.

The spectral noise impedance from the measurement is given in Figure 4.20. The rise in impedance above 1 Hz is likely due to the instrumentation noise that can be seen in the potential measurements in Figure 4.16 above 1 Hz. Either diffusion effects (*ie* a Warburg impedance) or non-stationarity might explain the slight rise in impedance towards lower frequencies.

Figures 4.21 to 4.23 show distribution plots of the EPN and ECN signals after conditioning by LTR, MAR and the matched filter.[10] Reference Gaussian probability density functions are overlayed for comparison.

As can be seen from Figure 4.21, for LTR, the EPN is a very poor approximation to a Gaussian distribution. The ECN appears more Gaussian distributed but there is a relatively large degree of scatter in the distribution. The distributions in Figure 4.22, for the MAR conditioned signal, both correlate well with the overlayed

[10]The Matlab function *hist* is used for estimation of the probability distributions.

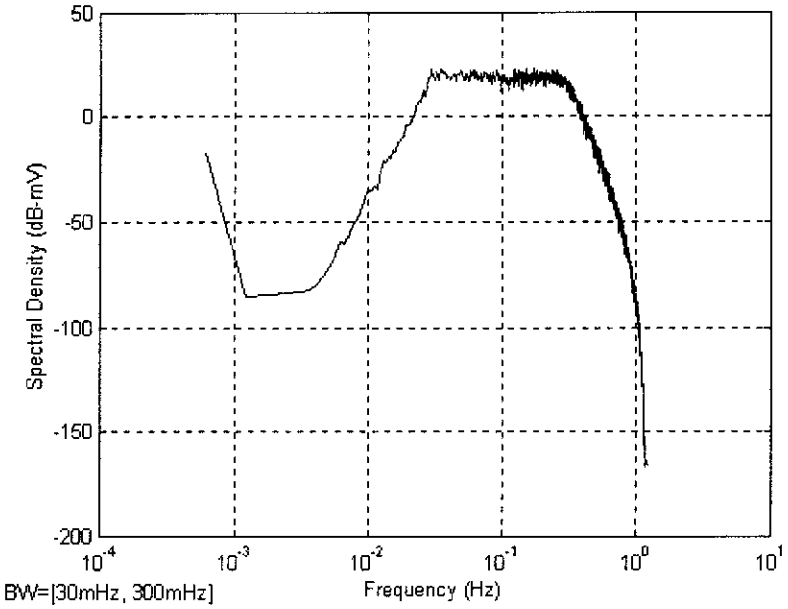

Figure 4.19: Power spectral density of the EPN after matched conditioning.

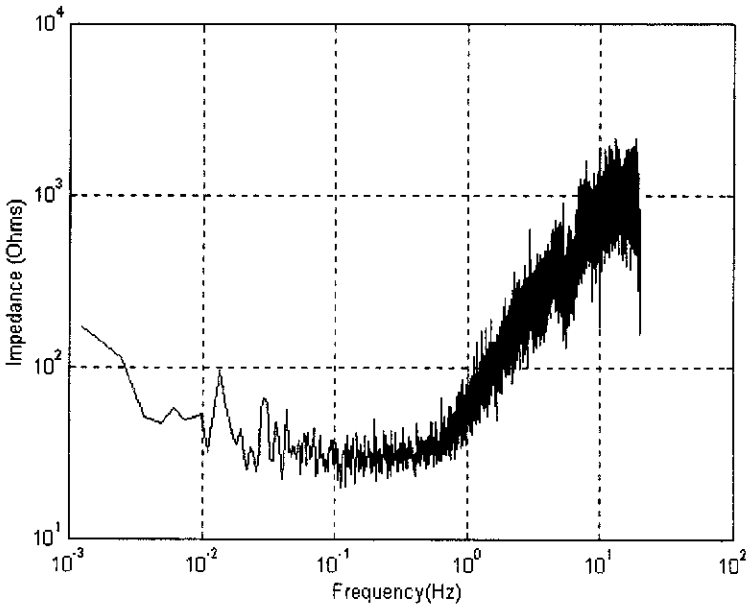

Figure 4.20: Spectral noise impedance of the EN.

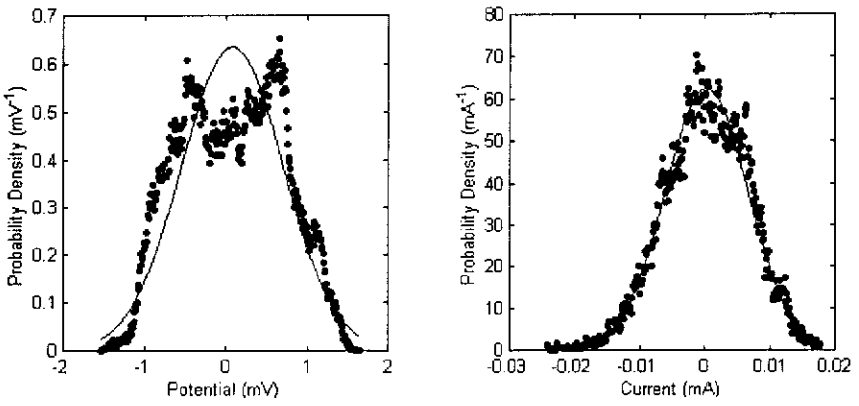

Figure 4.21: Distribution of EPN and ECN after application of LTR.

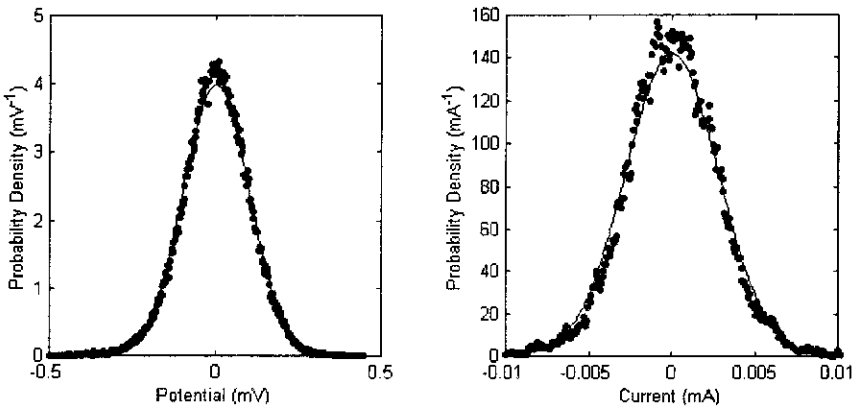

Figure 4.22: Distribution of EPN and ECN after application of MAR.

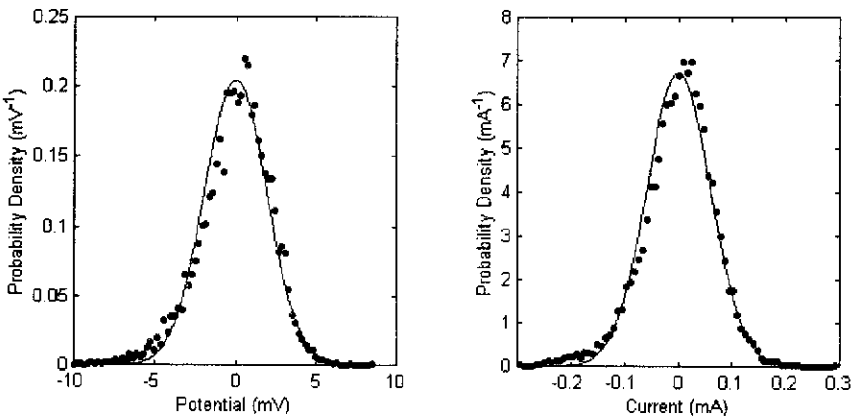

Figure 4.23: Distribution of EPN and ECN after matched signal conditioning.

Gaussian distributions. For the matched signal conditioning, Figure 4.23, the signals appear reasonably Gaussian in distribution except for some degree of skew. Thus it can be seen that the MAR has produced a signal pair that more closely resembles a Gaussian distribution than has the matched filter. Both techniques have produced signals that are more convincingly Gaussian than LTR by itself.

Table 4.1 summarises the results of noise resistance calculations using LTR, MAR and the matched conditioning for the investigated system.[11] Assuming Tafel constants of $\beta_A = \beta_B = 230$ mV/decade, the resistances listed in the table are translated into a corrosion current (*ie* corrosion rate) by the Stern-Geary equation (2.22) according to $I_0 \approx \frac{50.0\text{mV}}{R}$, where I_0 is the corrosion current and R is the resistance. For example, the LP measurements in the 1st repetition give corrosion currents of 1.06 mA and 1.14 mA. Because of the additional uncertainty involved with assuming values for the Tafel constants, the remaining discussion will focus on the resistances estimated from the EN instead.

For each repetition, the measurement was divided into 750 s time intervals, overlapped by 50 %. For each interval, the noise resistance is calculated by (4.21, page 65) after signal conditioning first by LTR, then MAR and finally by whitening and band-pass filtering. The "Measured R_n" lists the result of these three calculations averaged over the different intervals. The "Measured σ_{R_n}" lists the standard deviation. The "Measured k_R" is the square of the ratio of the two previous quantities, and the "Predicted k_R" is the value of this ratio as predicted by (4.36, page 68) and (4.47, page 70). The "LP" column lists the result of the linear polarisation measurements that followed the EN measurements — one for each of the two electrodes — and provides estimates of the polarisation resistance by an independent technique.

It is noted that the standard deviation calculations in Table 4.1 are the standard deviation of the residuals after linear regression on the set of R_n calculations, which can account for the significantly lower than predicted observed k_P in the first two measurements. This was necessary because of some possible non-stationarity in some of the repetitions. Figure 4.24 shows the set of noise resistance values (and the linear trend line) obtained from the 1st repetition using matched signal conditioning. As can be seen, there is a significant increasing trend in the noise resistance for the 1st repetition. The 2nd and 7th repetition have no significant trend, while the 5th has an increasing trend and the 6th is decreasing.

From Table 4.1, it is seen that the results from LTR are significantly larger than the LP measurements and have a significantly larger k_R than those obtained from the other two noise resistance calculations. This suggests that the LTR is over estimating the noise resistance and is less precise than the MAR and matched

[11] The *RnCalc* function [29] is used to compute the noise resistance after the EN signals have been conditioned

	LTR	MAR	Matched	LP
1st Repetition		28 to 300 mHz	30 to 300 mHz	
Measured R_n	83.7 Ω	32.9 Ω	31.3 Ω	47 Ω, 44 Ω
Measured σ_{R_n}	20 Ω	0.8 Ω	0.97 Ω	
Measured k_R	5.5×10^{-2}	5.9×10^{-4}	9.6×10^{-4}	
Predicted k_R		2.5×10^{-3}	2.5×10^{-3}	
2nd Repetition		46 to 500 mHz	50 to 500 mHz	
Measured R_n	67.2 Ω	26.8 Ω	25.4 Ω	35 Ω, 30 Ω
Measured σ_{R_n}	16 Ω	0.7 Ω	0.5 Ω	
Measured k_R	5.6×10^{-2}	7.0×10^{-4}	4.4×10^{-4}	
Predicted k_R		1.5×10^{-3}	1.5×10^{-3}	
3rd Repetition		23 to 250 mHz	10 to 250 mHz	
Measured R_n	64.4 Ω	32.6 Ω	32.1 Ω	40 Ω, 36 Ω
Measured σ_{R_n}	19 Ω	2.2 Ω	1.6 Ω	
Measured k_R	8.8×10^{-2}	4.6×10^{-3}	2.4×10^{-3}	
Predicted k_R		2.9×10^{-3}	2.8×10^{-3}	
4th Repetition		46 to 500 mHz	10 to 500 mHz	
Measured R_n	67.4 Ω	33.3 Ω	33.1 Ω	33 Ω, 30 Ω
Measured σ_{R_n}	17 Ω	1.4 Ω	1.2 Ω	
Measured k_R	6.2×10^{-2}	1.8×10^{-3}	1.4×10^{-3}	
Predicted k_R		1.5×10^{-3}	1.4×10^{-3}	
5th Repetition		46 to 500 mHz	25 to 500 mHz	
Measured R_n	70.0 Ω	27.8 Ω	26.6 Ω	27 Ω, 26 Ω
Measured σ_{R_n}	13 Ω	1.4 Ω	0.9 Ω	
Measured k_R	3.4×10^{-2}	2.5×10^{-3}	1.2×10^{-3}	
Predicted k_R		1.5×10^{-3}	1.4×10^{-3}	

Table 4.1: Comparison of noise resistance calculations using LTR, MAR and matched signal conditioning

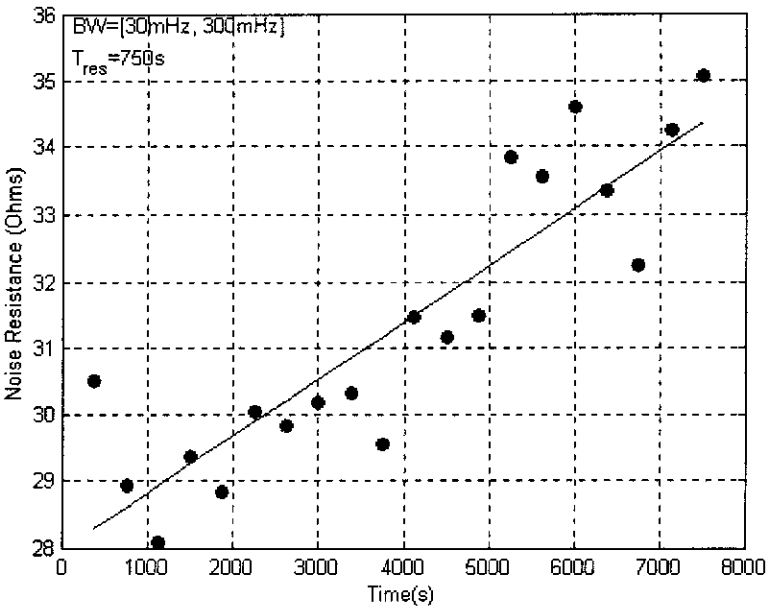

Figure 4.24: Noise resistance of the 1st repetition calculated over 750 s overlapping time intervals using matched signal conditioning.

methods.

The results from the MAR and the matched methods are in better agreement with the LP measurements than the results from LTR. Except for the 1st repetition, the k_R for MAR is larger than or approximately equal to that for matched despite the calculation bandwidth being similar. This suggests that the MAR and matched methods can produce a more accurate result but that the matched method can be have better precision.

Except for the 1st and 2nd repetition, where the measured k_R is significantly less than the predicted k_R, there is good agreement between the measured and predicated relative estimation variance.

4.5 Summary and Conclusions

1. The maximum likelihood estimator (MLE) of electrode impedance magnitude has been derived for resistive electrodes within the bandwidth of the EN:

   The estimation requires additional information regarding the resistance of the two electrodes — *eg* the relationship between the resistances of the two electrodes.

   The MLE of electrode resistance is a function of the MLEs of the variance of the EN signals and source EN cross correlation. If the source EN cross correlation is unknown, then the expectation of the estimate is equal to the estimate given independent sources.

For independent sources and identical resistive electrodes, the MLE of equivalent impedance magnitude has been found to be equal to the MLE of noise resistance.

For Gaussian, white and stationary EN the MLE of variance of the EN signals are given by the mean of the square of the respective signals. Thus the MLE of impedance magnitude is a function of the mean of the square of the EN signals and the source EN cross correlation.

2. The performance of the mean-square estimate of noise resistance for Gaussian, stationary, band-band-limited EN has been investigated:

   When the mean of the square is applied to band-limited, but otherwise white EN, there is a trade off between precision, bandwidth and observation time. The estimate is unbiased for large bandwidths and observation times but overestimates for narrow bandwidths and short observation times.

3. The application of signal conditioning to validate and control noise resistance estimation by the mean of the square has been explored:

   Much can be achieved by the use of linear convolutional filters for signal conditioning:

   - By the central limit theorem, it has been demonstrated how the application of linear convolutional filters tends to validate an assumption that the signals are Gaussian distributed, thus allowing the use of the mean of the square as the MLE of signal variance.
   - A bandpass filter can be used to focus the estimate onto a given range of frequencies in order to investigate the electrode equivalent impedance when it is not a frequency independent quantity. It can also be used for residual trend removal.
   - A whitening filter has been proposed to validate the assumption of a white PSD when the mean of the square is used as the MLE of signal variance. It has been shown that the mean of the square of a signal that is white within its bandwidth results in near optimum precision, subject to its fixed bandwidth.

   A method of *matched* signal conditioning has been proposed. By producing signals that have a white PSD within a fixed, easily controllable bandwidth, it allows the mean of the square to be used as the MLE for resistance estimation and allows independent control over the centre frequency and the bandwidth of the estimate.

   The moving average removal (MAR) as a signal conditioning method has been investigated. It has been shown to yield a PSD shape that is dependent on

the input signal and that does not generally optimise the precision of the mean-square estimate. It does not allow independent control over centre frequency and bandwidth of the estimate, but does offer some advantage over the proposed matched signal conditioning in reduced computational complexity.

The factors affecting the selection of signal conditioning parameters have been discussed.

4. Results from experimental data have been presented to compare linear trend removal (LTR), MAR and matched signal conditioning.

   There has been found to be generally good agreement between the observed performance of the resistance estimate and the performance as predicted by the theory. The MAR and the matched signal conditioning methods agree better with the linear polarisation measurements than does analysis by LTR.

Chapter 5

Further Analysis of Electrochemical Noise Data

This chapter proposes three new analysis techniques based on three distinct kernels: (i) time varying noise impedance for examining electrode impedance continuously; (ii) complex noise impedance, for generation of Nyquist impedance diagrams of asymmetric electrodes; and (iii) cross correlation between the EPN and ECN signals for detection of asymmetric electrodes. The addition of these techniques increases the utility of the data obtained from a noise resistance measurement.

Time varying noise impedance. The noise resistance is computed as a function of both time and frequency. The result is a three dimensional surface that shows how the noise impedance changes during the course of a measurement. It provides the same information that a conventional spectral noise impedance diagram does but can be applied to systems that exhibit some degree of variation during the course of measurement. Such information can prove useful for selection of an appropriate bandwidth for the basic noise resistance estimate described in Chapter 4 at different points in the measurement when a dynamic system is being investigated. This work has been presented at the IEEE Instrumentation and Measurement Conference 2000 [129] and published in IEEE Transactions on Instrumentation and Measurement [130].

Complex noise impedance. Given an asymmetric electrode pair, a quantity that can be thought of as the phase of the spectral noise impedance can be extracted from the EN measurement and a Nyquist impedance diagram can be constructed. Although Gabrielli *et al* [14] demonstrate impedance measurements using EN with phase information intact, their approach relates to the EN obtained from a single electrode under potentiostatic/galvanostatic control. Constructing Nyquist impedance diagrams from the dual electrode setup of Eden *et al* [13], Figure 3.1 (page 40), using simultaneous EPN/ECN mea-

surements was not previously done because the conventional spectral noise impedance provides no phase information about the impedance of the electrode pair. Half of the impedance information is missing from a spectral noise impedance calculation. The complex noise impedance technique allows the other half to be extracted as long as the electrode pair demonstrates some asymmetry. Generally speaking, the addition of phase information allows the precise topology of the impedance under investigation, and thus the physical characteristics associated with the impedance, to be more confidently inferred. This work has been submitted for publication in the Journal of the Electrochemical Society [131].

Cross correlation. The correlation between the EPN and ECN signals is proposed to assess the symmetry of an electrode pair, *ie*, to detect an electrode pair with different impedances or noise power spectral densities. This is important because much of the theory linking the spectral noise impedance to the impedance of the electrodes assumes the electrode pair to be nominally identical [13] [19]. In addition, computation of complex noise impedance requires that the electrodes exhibit some asymmetry in EN and impedance. By examining correlation between EPN and ECN signals, the presence of an asymmetric electrode pair can be detected. This work has been presented at the IEEE region 10 conference 2001 [132] and has been submitted for publication in Corrosion Science [133].

5.1 Time Varying Noise Impedance

The kernel for this technique is the noise resistance as given by (3.1, page 41) and the estimation of which is discussed in Chapter 4.

The time varying noise resistance, as introduced by Tan *et al* [50] uses of a sliding window to estimate the noise resistance as a function of time. Using the signal power (time average of the square) over a given time interval ($2T$) as an estimator of signal variance, the time varying noise resistance estimate can mathematically be expressed by (3.3, page 41).

For each t, (3.3) gives an estimate of the noise resistance during the T seconds before and after t. Plotted against t, it gives the time varying noise resistance with a time resolution of $2T$. Figure 5.1 shows an example.[1]

With the appropriate signal conditioning (see Chapter 4), the EPN and ECN signals are band-limited to the range $[f_1, f_2]$ and the ECN signal is whitened within that bandwidth. Then the noise resistance is as given by (4.51, page 73). The time

[1] Generated using the *nSigmaImpedance* routine (see Section A.5, page 148) over different bandwidths at different points in the measurement.

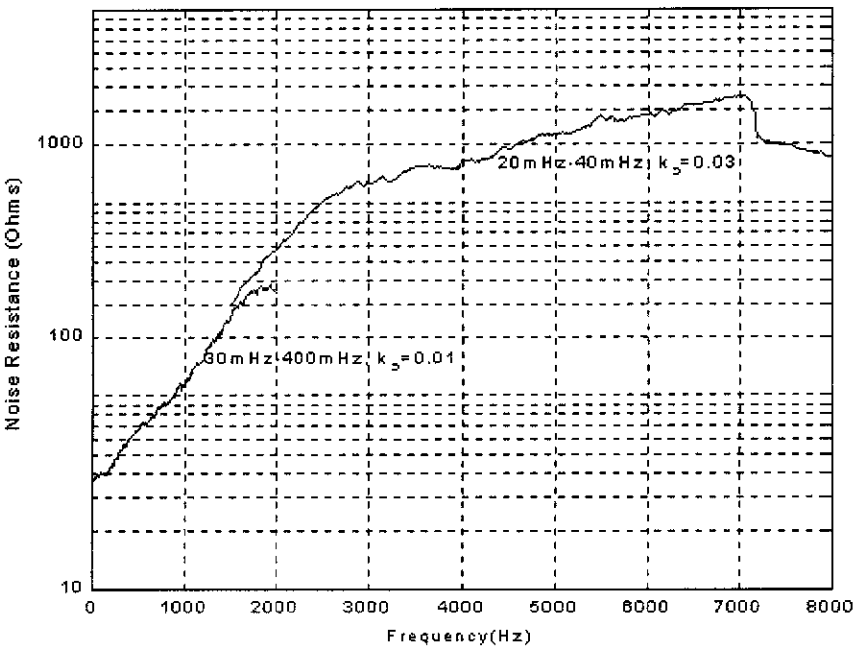

Figure 5.1: Example time varying noise resistance.

varying noise *impedance*, the technique proposed in this section, results when the noise resistance given by (4.51) is computed over a series of consecutive sub-bands.

To express it mathematically, let $v(t)|_{f_1,f_2}$ and $i(t)|_{f_1,f_2}$ denote the band-limited, whitened EN signals. Then the time varying noise impedance estimate is given by

$$\hat{R}_{\mathrm{n}}(t, f_1, f_2) = \sqrt{\frac{\int_{t-T}^{t+T} v^2(\tau)|_{f_1,f_2} \mathrm{d}\tau}{\int_{t-T}^{t+T} i^2(\tau)|_{f_1,f_2} \mathrm{d}\tau}} \tag{5.1}$$

The two major parameters of the estimate are the time resolution, controlled by the width of the sliding window, T, and the frequency resolution, determined by the EN bandwidth, $f_2 - f_1$. Improved frequency resolution can be obtained using a greater number of narrower sub-bands and improved time resolution is achieved by use of smaller time intervals. However, as discussed in Chapter 4, there is a trade off between the level of precision, the time resolution and the frequency resolution.

Figure 5.2 shows an example time varying noise impedance calculated over double-octave ($\frac{f_2}{f_1} = 2^2$) consecutive sub-bands, while Figure 5.3 shows the result calculated over narrower, half-octave ($\frac{f_2}{f_1} = 2^{0.5}$) sub-bands using the same level of precision.[2]

The data used for analysis in Figures 5.1 to 5.3 were collected from a mild-steel / NaCl system initially saturated with CO_2 to create a corrosive environment. During the course of the experiment, N_2, an inert gas, was bubbled into the solution

[2]The *nSigmaImpedance* function (see Section A.5, page 148) with multiple bandwidths is used to perform the calculation. Plotting is done with the Matlab routines *contourf* and *surf*.

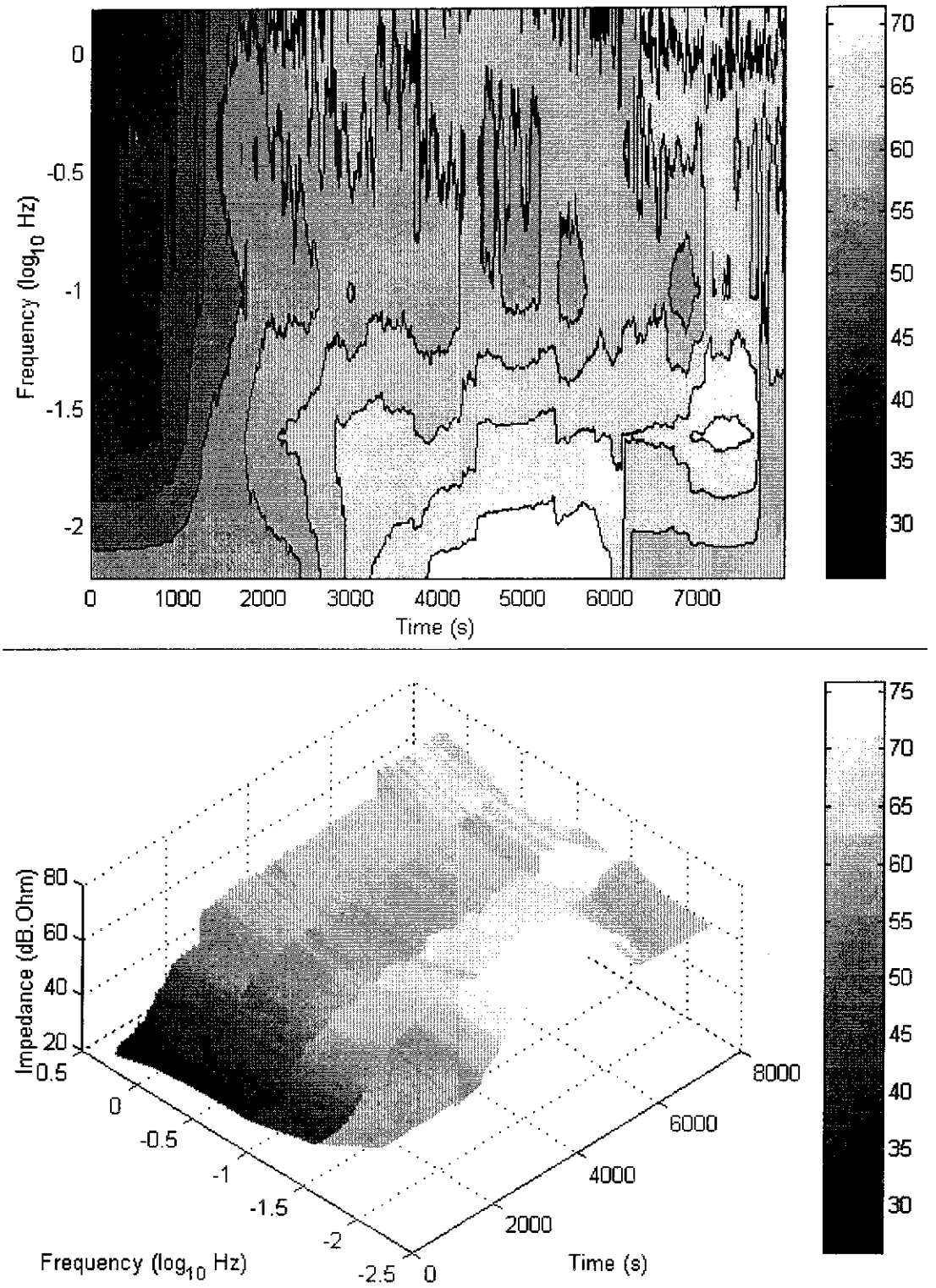

Figure 5.2: Time varying spectral noise impedance — double-octave sub-bands.

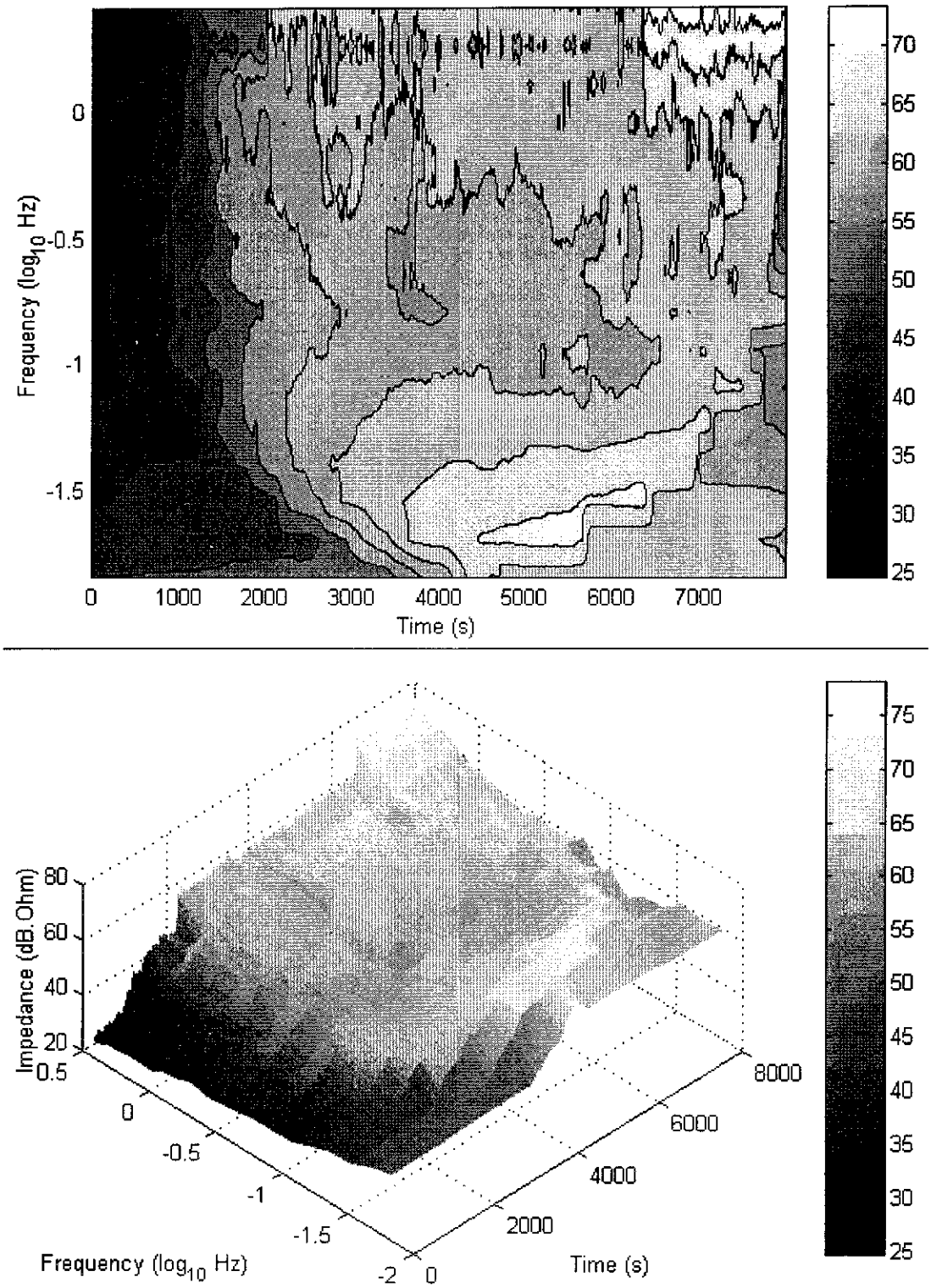

Figure 5.3: Time varying spectral noise impedance — half-octave sub-bands.

to slow the corrosion process by gradually displacing the dissolved CO_2. According to EIS theory (see Section 2.2), due to an increase in polarisation resistance, a decrease of corrosion rate should be reflected by a general increase in the observed electrochemical impedance.

Figures 5.2 and 5.3 show contour and surface plots of a time varying impedance. On the contour plots, the time axis is shown horizontally and the frequency axis is shown vertically. The magnitude of the impedance is colour coded and the contour lines show lines of constant magnitude. Consequently, vertical contour lines indicate impedance that is independent of frequency, but is time variable. Horizontal contour lines indicate constant, but frequency dependent impedance. The lighter colours indicate areas of high impedance, while the darker colours indicate areas of low impedance. The corresponding surface plots are given to assist the reader with visualisation of the impedance.

Therefore Figures 5.2 and 5.3 can be seen to start out with low impedance, but to steadily increase in magnitude. Additionally, from 3000 s onwards, the magnitude can be seen to significantly increase when moving from mid-frequency towards lower frequencies. This is typical of a parallel RC impedance. Moving from mid-frequency towards higher frequencies, the impedance can also be seen to increase in magnitude. This can be explained by measurement noise in the EPN measurement: In the authors' instrumentation set up, the EPN contains far greater measurement noise than does the ECN and is mainly visible at the higher frequencies (see C).

By comparison of Figures 5.2 and 5.3, in the area around $f = 10^{-1.5}$ Hz and $t = 2000$ s to $t = 3000$ s, the effect of the improved frequency resolution in Figure 5.3 can be seen to provide more information regarding the shape of the impedance in this frequency range. In Figure 5.2, the contour lines are almost vertical, indicating no resolved frequency dependence, whereas in Figure 5.3, the improved frequency resolution has resulted in roughly diagonal contours, which suggest time and frequency dependence. In addition, at the higher frequencies, *eg* at $f = 10^{-0.5}$ Hz, in Figure 5.2, the contour lines are very fuzzy with poorly resolved frequency. In Figure 5.3, they are clearly defined.

In contrast, the time resolution can be seen to have degraded with the improvement in frequency resolution. For example, towards the end of the measurement at $t = 7700$ s and $f = 10^{-1.5}$ Hz, a decrease in impedance magnitude is seen. In Figure 5.2, where the frequency resolution is poor, the sudden decrease is clearer than in Figure 5.3, indicating superior time resolution.

Figures 5.2 and 5.3 also demonstrate the multi-resolution ability of the technique. In (5.1), T can be varied for each f_1, f_2 combination to suit the signal bandwidth. Because the sub-bands located at higher frequencies tend to possess wider bandwidths, a finer time resolution can be achieved while the same level of precision is maintained. This allows the higher frequency sub-bands to better resolve discrete

events while still enabling the lower frequency sub-bands to compensate for a low bandwidth by using a course time resolution. For example, in Figures 5.2 and 5.3, the precise location where the instrument switches dynamic ranges, thus increasing the effect of measurement noise, can be clearly pinpointed from the sudden increase in high frequency impedance (at approximately $t = 6200$ s, $f = 100$ Hz).

In order to assess the increase in electrode impedance quantitatively, a time varying noise resistance [equation (3.3), page 41] can be employed, but first an appropriate bandwidth must be selected for the calculation. The spectral noise impedance, $R_{\mathrm{sn}}(f)$, may be an undesirable choice in this case because of the non-stationary behaviour of the system. The time varying noise impedance [equation (5.1)], such as depicted in Figures 5.2 and 5.3, might be used instead.

Figure 5.1 (page 100) shows a time varying noise resistance calculation over two separate sub-bands for two different periods of time. From $t = 0$ to 2000 s, the noise resistance is computed over a bandwidth of $[10^{-1.5}, 10^{-0.4}]$ Hz, while from $t = 1500$ s to 8000 s, a bandwidth of $[10^{-1.7}, 10^{-1.4}]$ Hz is used. These bands are selected based on information obtained from Figure 5.3: Up to $t = 2000$ s, with the near vertical contour lines, very little frequency dependence can be seen and the frequency range between $[10^{-1.5}, 10^{-0.4}]$ Hz might be thought to cover a low frequency plateau of the impedance. From approximately $t = 2000$ s, a significant frequency dependence emerges. The general trend is an increase in magnitude at lower frequencies with the low-frequency plateau becoming confined to a lower band of frequencies as time progresses. A sub-band of $f = [10^{-1.7}, 10^{-1.4}]$ Hz is selected to cover what vaguely resembles a low frequency plateau for $t > 2000$ s. It is noted, from Figure 5.3, that around $t = 3000$ s the impedance is seen to decrease in magnitude again below $10^{-1.5}$ Hz, which cannot be explained by a simple Randle's cell model (see Section 2.2.4) and the results of a noise resistance calculation after $t = 3000$ s should be treated with caution.

5.2 Complex Noise Impedance

A complex function has two components: a magnitude and a phase. Any impedance is a complex function of frequency and the equivalent impedance of an electrode is no different. Unfortunately the spectral noise impedance is an entirely real valued function. Half the information (the phase component) is missing. Without the phase information, the precise topology of the equivalent electrode impedance cannot be inferred with as much confidence. However, given some degree of asymmetry in the electrode pair, it is possible to recover the phase information from the EPN/ECN measurement as the following demonstrates.

5.2.1 Analysis

The kernel for the complex noise impedance is defined as

$$Z_{\mathrm{sn}}(f) = \mathrm{E}\left[\frac{V(f)}{I(f)}\right] \tag{5.2}$$

and its phase is given by

$$\Theta_{\mathrm{sn}}(f) = \arg\{Z_{\mathrm{sn}}(f)\} \tag{5.3}$$

where $\Theta_{\mathrm{sn}}(f)$ is the phase of $Z_{\mathrm{sn}}(f)$ and $V(f)$ and $I(f)$ are the Fourier transforms of the EPN and ECN signals respectively. The "E" operator denotes statistical expectation and the "arg" operator (argument) denotes the phase of its complex operand.

The measurement circuit is modelled as in Figure 3.2 (page 42), which is similar to the model of Bertocci *et al* [19] with the solution resistance incorporated into the electrodes' equivalent impedance. In Figure 3.2, $v_1(t)$ and $v_2(t)$ are the Thevenin equivalent EPN sources, $v(t)$ and $i(t)$ are respectively the measured EPN and ECN signals and $Z_1(f)$ and $Z_2(f)$ are the electrodes' equivalent impedances.

The spectral noise impedance gives an impedance magnitude relating to the individual electrode impedances as described by (3.7, page 43). The phase information is recovered by (5.3). The following derives the relation between $\Theta_{\mathrm{sn}}(f)$ and the equivalent impedances of the electrodes.

From Figure 3.2,

$$I(f) = \frac{V_1(f) - V_2(f)}{Z_1(f) + Z_2(f)} \tag{5.4}$$

and

$$V(f) = V_1(f) - I(f)Z_1(f) = \frac{V_1(f)Z_2(f) + V_2(f)Z_1(f)}{Z_1(f) + Z_2(f)} \tag{5.5}$$

where $V(f)$, $I(f)$, $V_1(f)$ and $V_2(f)$ are the respective Fourier transforms of $v(t)$, $i(t)$, $v_1(t)$ and $v_2(t)$.

Substituting (5.4) and (5.5) into (5.2) gives

$$\begin{aligned} Z_{\mathrm{sn}} &= \mathrm{E}\left[\tfrac{V_2(f)}{V_1(f)-V_2(f)}\right] Z_1(f) + \mathrm{E}\left[\tfrac{V_1(f)}{V_1(f)-V_2(f)}\right] Z_2(f) \\ &= \alpha(f)Z_1(f) + \beta(f)Z_2(f) \end{aligned} \tag{5.6}$$

where $\alpha(f)$ and $\beta(f)$ are statistical properties relating to the EPN sources, $V_1(f)$ and $V_2(f)$, and are defined as implied by (5.6). It is usual to assume that the two EPN sources, $v_1(t)$ and $v_2(t)$, are statistically independent. [19] [109] [100]

After further analysis and assuming statistical independence of the sources, it is possible to prove (see Appendix D) that the $\alpha(f)$ and $\beta(f)$ terms are entirely real valued. Thus the phase of the complex noise impedance, $\Theta_{\mathrm{sn}}(f)$, depends entirely on the phase of a weighted sum of the two electrodes' impedances.

If the sources cannot be assumed independent, then the $\alpha(f)$ and $\beta(f)$ coefficients cannot generally be said to be entirely real valued and $\Theta_{\mathrm{sn}}(f)$ becomes distorted by the phase of $\alpha(f)$ and $\beta(f)$. Any further use of $\Theta_{\mathrm{sn}}(f)$ requires information on the correlation between the sources so that the distortion can be taken into account. The remaining work assumes independence of the sources.

5.2.2 Equal Impedances

It is instructive to investigate the behaviour of (5.6) when the two electrode impedances are identical. Setting $Z_1(f) = Z_2(f) = Z(f)$, (5.6) reduces to (see Appendix E)

$$Z_{\mathrm{sn}}(f) = \left\{ \mathrm{E}\left[\left| \frac{V_1(f)}{V_1(f) - V_2(f)} \right|^2 \right] - \mathrm{E}\left[\left| \frac{V_2(f)}{V_1(f) - V_2(f)} \right|^2 \right] \right\} \cdot Z(f). \tag{5.7}$$

In this case, $Z_{\mathrm{sn}}(f)$ is proportional to $Z(f)$. The constant of proportionality is entirely real valued with either a zero, positive or negative value. As long as the constant of proportionality is non-zero, the phase of $Z_{\mathrm{sn}}(f)$, $\Theta_{\mathrm{sb}}(f)$, is therefore equal to the phase of the two identical electrode impedances with possibly 180 ° (π radians) inversion depending on the sign of the constant of proportionality. That is to say

$$\Theta_{\mathrm{sn}}(f) = \arg Z(f) = n\pi \tag{5.8}$$

where n is an integer.

5.2.3 Identical Electrodes

In (5.7), an anomaly occurs when the two EPN sources have identical properties. The constant of proportionality becomes equal to zero. In that case, no phase information can be extracted as the phase of zero is undefined. This enforces an important restriction on the method because it means that asymmetry is required for the phase to be recovered.

5.2.4 Disparate EN Sources

Another illustrative case is when there is a large disparity in the EPN originating from each electrode. The limiting cases are when $v_1(t)$ is negligible compared to $v_2(t)$ and *vice versa*.

In the case where $v_1(t)$ is negligible, (5.6) becomes

$$Z_{\mathrm{sn}}(f) = -Z_2(f) \tag{5.9}$$

If $v_2(t)$ is negligible, then

$$Z_{\mathrm{sn}}(f) = Z_1(f) \tag{5.10}$$

Thus, when the EPN originating from electrode 1 is dominant over the EPN from electrode 2, the phase, $\Theta_{sn}(f)$, tends to represent the phase of $Z_2(f)$ (with 180 ° inversion). If the EPN from electrode 2 dominates, then $\Theta_{sn}(f)$ represents $Z_1(f)$ (without the 180 ° inversion).

5.2.5 Construction of a Nyquist Diagram

It is common to visualise a complex function with a polar plot of magnitude versus phase, known as a Nyquist plot. See references [134], [135], [136] and [137] for examples making use of Nyquist diagrams for visualisation of electrode impedances obtained from AC polarisation measurements.

Bertocci *et al* [19] showed that when the electrode impedances are identical, the spectral noise impedance, $R_{sn}(f)$, is theoretically equal to the impedance magnitude. Hence, when the electrode impedances are identical but the noise sources differ, a polar plot of $R_{sn}(f)$ versus $\Theta_{sn}(f)$ is equivalent to a Nyquist diagram of the electrodes' impedance.

5.2.6 Estimation

The theory thus far has dealt with properties involving abstract statistical expectations. The magnitude and phase [as described by $R_{sn}(f)$ and $\Theta_{Xsn}(f)$] need to be estimated from random data. If the system is known to be stable over a given period of time, the obvious approach is to replace the expectation in (5.2) with an average over separate measurements or time segments. This is similar to Welch's averaged periodogram method of PSD estimation (see Press [117] for a discussion on PSD estimation). The following describes the process.

- The EPN and ECN measurements are split into a number of (possibly overlapping) segments. These segments are used for averaging purposes. A greater number of segments yields a more precise result. The disadvantages are a loss of frequency resolution and/or longer measurements are required.
- The EPN and ECN Fourier transforms are calculated for each segment. This is the operation that moves the data from the time domain into the frequency domain.
- Each EPN transform is divided by the corresponding ECN transform as in (5.2), giving the dimensions of an impedance.
- The result of the division is averaged across all segments.

This yields a frequency dependent and complex valued quantity. As long as the two electrodes under examination are not identical, the phase of this average

converges to what can be thought of as the phase of the spectral noise impedance [or more strictly the phase of (5.6)] as the number of segments increase.

The more similar the two electrodes become, the more difficult it is to extract the phase because a larger number of segments are required to reach an acceptable level of precision. The limiting case is when the electrodes are perfectly symmetrical and it becomes impossible to extract the phase information.

This restricts the technique to either slightly asymmetric, but very stable systems where it is possible to take very long measurements to increase the number of segments used in the average, or to systems that are asymmetric by design, *eg* the electrochemical emission spectroscopy technique [110] [68].

5.2.7 Examples

Results from two computer simulations are given to illustrate the Nyquist impedance diagrams obtained for a symmetrical electrode pair and an asymmetric electrode pair.[3]

Figures 5.4 and 5.5 show the effect of electrode symmetry. In Figure 5.4, the simulated electrode pair has identical impedance and source EPN characteristics, while in Figure 5.5, the EPN power from one electrode is one quarter that of the other. As can be seen, the phase in Figure 5.4 appears quite randomly distributed and the resulting Nyquist diagram does not have any discernible shape. In Figure 5.5, there is less random scatter and the Nyquist diagram matches well with the theoretical curve [derived from (5.6)].

Figure 5.6 shows results obtained from a physical system. A pair of 3.0 cm^2 cylindrical mild steel electrodes was polished to 1200 grit. It was immersed into 1000 ppm $NaNO_2$ and left to stabilise for four hours before NaCl was added to give 4000 ppm NaCl. The EPN/ECN measurement was conducted continuously after immersion of the electrodes at a sample rate of 0.195 seconds/sample for a total of 170 hours. The measurements used an ACM AutoZRA (described in Appendix C) and a double junction $Ag^+/AgCl$ reference electrode as depicted in Figure 3.1, (page 40). The system has been observed to exhibit significant crevice corrosion between one electrode and its Teflon separator, while the other remained relatively free of visible corrosion. Because corrosion has been found to be localised to only one of the two electrodes, the electrodes can be said to be highly asymmetric. $Z_{sn}(f)$ and $R_{sn}(f)$ are computed over the last 11 hours of data and used to construct the Nyquist impedance diagram depicted in Figure 5.6.[4] The phase in Figure 5.6 is taken from $Z_{sn}(f)$ and the magnitude from $R_{sn}(f)$. As can be seen by the approximately circular Nyquist diagram, the phase information has been readily recovered.

[3]The simulations are generated using the *viSynth2* function (see Section A.12, page 163) and the complex noise impedance is computed by *VIZEstimate* (Section A.13, page 170)

[4]Using the *VIZEstimate* function (See Section A.13, page 170).

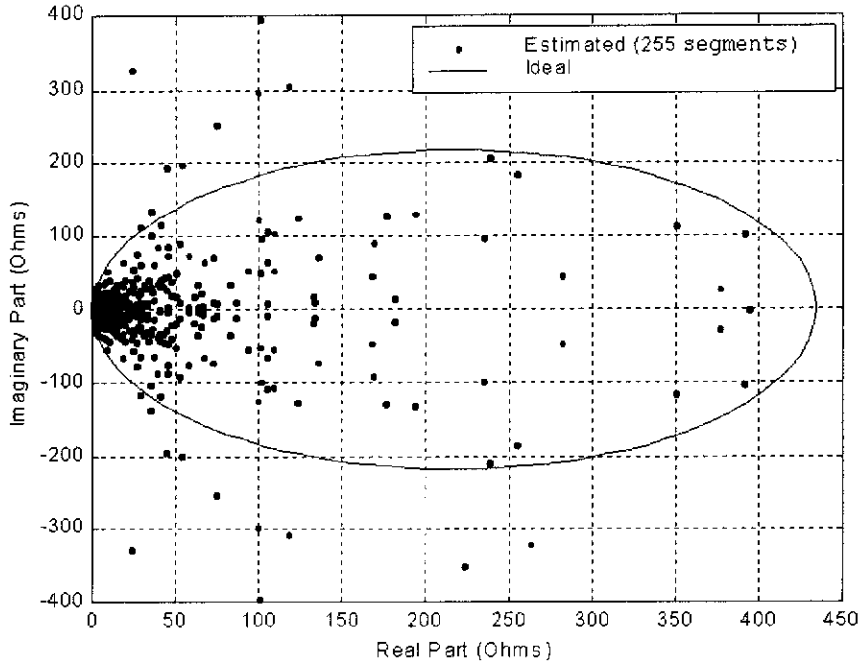

Figure 5.4: Nyquist plot from a simulated symmetrical system.

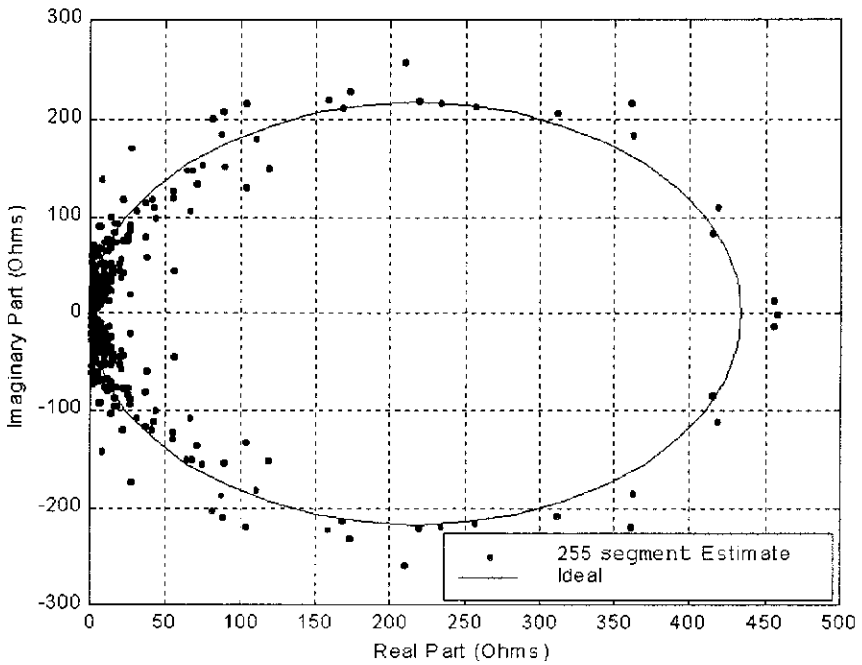

Figure 5.5: Nyquist plot from a simulated system with asymmetric EPN sources.

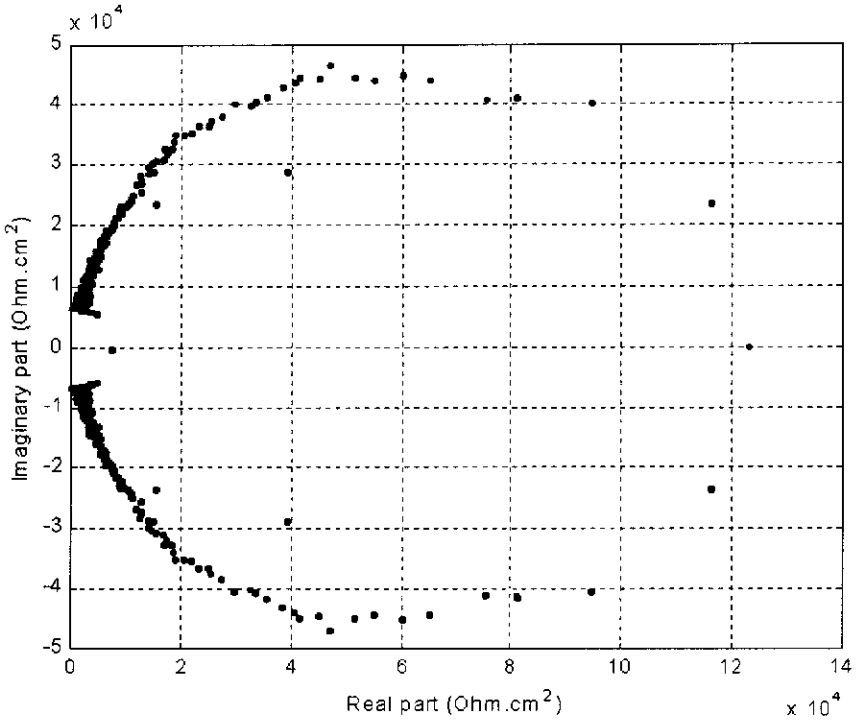

Figure 5.6: Nyquist plot from a physical system.

Based on the circular shape, the impedance of the dominating electrode might be modelled as a parallel resistor/capacitor combination with a resistance of approximately 100 $k\Omega.cm^2$.

5.3 EN Correlation and Electrode Symmetry

The work of Bertocci *et al* [19] and Bautista and Huet [109] provides analysis of how the noise resistance and spectral noise impedance are related to the impedance and EN associated with each electrode. The theory shows the spectral noise impedance to be a weighted sum of two components [equation (3.7), page 43]. When the impedances of the two electrodes are identical, then the spectral noise impedance is equal to the magnitude of the electrode impedances [equation (3.8), page 43]. Therefore, before attempting to interpret the spectral noise impedance, it is important to know whether or not the two electrodes have similar impedances.

Similarly, phase recovery using the method described in Section 5.2 requires an asymmetric electrode pair, otherwise the phase cannot be extracted. Again, it is important to know whether or not the electrode pair is symmetric.

For this work, an electrode pair is considered symmetrical if they possess equal impedances and the of the EPN signals originating from each of the electrodes are statistically equal.

In order to ensure identical impedances, the impedance of each electrode can be directly measured using non-EN techniques, such as LP and EIS. However, this negates the need for a spectral noise impedance measurement as the impedances will already be known. Also, the LP and EIS techniques involve the application of external signals to the electrodes, which may be undesirable and they require the use of a potentiostat and other relatively expensive hardware.

In this work, the correlation between the measured EPN and ECN signals [$v(t)$ and $i(t)$] is proposed to detect electrode pairs with dissimilar impedances and EPN characteristics. This allows the symmetry of the electrode pair to be assessed entirely from the EN data obtained from a simultaneous EPN/ECN measurement (Figure 3.1, page 40). No additional measurements are required.

Section 5.3.1 derives the correlation coefficient and coherence function as a function of the equivalent circuit parameters [$S_{v1}(f)$, $S_{v2}(f)$, $Z_1(f)$ and $Z_2(f)$, Figure 3.2, page 42] relating to the EPN/ECN measurement and discusses how they can be used to detect asymmetry on a quantitative basis. A qualitative graphical representation is also discussed.

It is noted that $Z_1(f)$ and $Z_2(f)$ in Figure 3.2 are the frequency dependent gradients of the potential/current curves associated with each electrode about the mixed potential [the average value of $v(t)$]. These gradients may or may not be equal to the gradients about each individual electrode's free corrosion potential, depending on the degree of polarisation and non-linearity of the electrodes.

Section 5.3.2 describes an experiment devised to test the theory. The cross-correlation between an observed EPN/ECN measurement is compared with the cross-correlation as predicted by the theory using data obtained by independent methods [linear polarisation (LP) and EPN measurements on each electrode separately]. Section 5.3.3 presents the results.

5.3.1 Potential/Current Correlation

The coefficient of correlation between $v(t)$ and $i(t)$ obtained from an EPN/ECN measurement is defined as

$$r_{vi} = \frac{\mathrm{E}\left[v(t)i(t)\right] - \mathrm{E}\left[v(t)\right]\mathrm{E}\left[i(t)\right]}{\sigma_v \sigma_i} \tag{5.11}$$

where "E" denotes statistical expectation, and σ_v^2 and σ_i^2 are the variances of $v(t)$ and $i(t)$ respectively.

For stationary $v(t)$ and $i(t)$, the coherence function is defined as

$$P_{vi}(f) = \frac{|S_{vi}(f)|}{\sqrt{S_v(f) S_i(f)}} \tag{5.12}$$

where $S_v(f)$ and $S_i(f)$ are the PSDs of $v(t)$ and $i(t)$ respectively.

$S_{vi}(f)$ is the cross spectral density of $v(t)$ and $i(t)$, defined for a stationary process as the Fourier transform of the auto-correlation function, $R_{vi}(t) = \mathrm{E}[v(t)i(t+\tau)]$:

$$\int_{-\infty}^{\infty} R_{vi}(\tau) \exp(-2\pi \mathrm{j} f \tau) \mathrm{d}\tau = \mathrm{E}[V(f)I^*(f)] \tag{5.13}$$

where $V(f)$ and $I(f)$ are the Fourier transforms of $v(t)$ and $i(t)$ respectively and * denotes complex conjugation.

In deriving r_{vi} and $P_{vi}(f)$ in terms of the equivalent circuit parameters, two assumptions are made:

1. The EN is zero mean. If some form of trend removal is applied prior to analysis, as is common practice in EN analysis [15] (see Section 4.3), then the EN is by definition zero mean.

2. The EPN sources, $v_1(t)$ and $v_2(t)$, are taken to be statistically independent. (This is a common assumption [19] [100] [109].) If they are not statistically independent, the degree of correlation between $v_1(t)$ and $v_2(t)$ needs to be known before analysis can proceed. Possible reasons why $v_1(t)$ and $v_2(t)$ might be correlated include mains pick-up on both electrodes and, at very low frequencies, cell temperature fluctuations.

By circuit analysis of Figure 3.2,

$$I(f) = \frac{V_1(f) - V_2(f)}{Z_1(f) + Z_2(f)} \tag{5.14}$$

$$V(f) = \frac{Z_2(f)V_1(f) + Z_1(f)V_2(f)}{Z_1(f) + Z_2(f)} \tag{5.15}$$

where $V_1(f)$ and $V_2(f)$ are the respective Fourier transforms of $v_1(t)$ and $v_2(t)$ in Figure 3.2.

Realising that

- $XX^* = |X|^2$ for any complex X;
- the PSD of any stationary $x(t)$ is given by $\mathrm{E}[|X(f)|^2]$ where $X(f)$ is the Fourier transform of $x(t)$; and
- for statistically independent and zero mean $v_1(t)$ and $v_2(t)$, $\mathrm{E}[V_1(f)V_2(f)] = 0$,

then substituting (5.14) and (5.15) into (5.13) gives

$$S_{vi}(f) = \frac{Z_2(f)S_{v1}(f) - Z_1(f)S_{v2}(f)}{|Z_1(f) + Z_2(f)|^2} \tag{5.16}$$

where $S_{v1}(f)$ and $S_{v2}(f)$ are the respective PSDs of $v_1(t)$ and $v_2(t)$.

Since $R_{\mathrm{vi}}(t)$ and $S_{\mathrm{vi}}(f)$ form a Fourier transform pair for stationary $v(t)$ and $i(t)$, it follows that

$$\int_{-\infty}^{\infty} S_{\mathrm{vi}}(f)\mathrm{d}f = R_{\mathrm{vi}}(0) = \mathrm{E}\left[v(t)i(t)\right]. \tag{5.17}$$

If the EN is band-limited to a range of frequencies from f_1 to f_2 so that $V(f)$ and $I(f)$ are zero for all frequencies outside the range $[f_1, f_2]$, then

$$\mathrm{E}\left[v(t)i(t)\right] = \int_{-f_2}^{-f_1} S_{\mathrm{vi}}(f)\mathrm{d}f + \int_{f_1}^{f_2} S_{\mathrm{vi}}(f)\mathrm{d}f = 2\int_{f_1}^{f_2} \mathrm{Re}\left\{S_{\mathrm{vi}}(f)\right\}\mathrm{d}f \tag{5.18}$$

where $\mathrm{Re}\{z\}$ denotes the real part of z.

Observing that for zero mean $v(t)$ and $i(t)$, $\mathrm{E}[v] = \mathrm{E}[i] = 0$ and by substitution into (5.11), r_{vi} can be expressed as:

$$r_{\mathrm{vi}} = \frac{2}{\sigma_{\mathrm{v}}\sigma_{\mathrm{i}}} \int_{f_1}^{f_2} \mathrm{Re}\left\{S_{\mathrm{vi}}(f)\right\}\mathrm{d}f \tag{5.19}$$

Substituting (5.16) into (5.19) gives the coefficient of correlation:

$$r_{\mathrm{vi}} = \frac{2}{\sigma_{\mathrm{v}}\sigma_{\mathrm{i}}} \int_{f_1}^{f_2} \frac{\mathrm{Re}\left\{Z_2\right\} S_{\mathrm{v1}} - \mathrm{Re}\left\{Z_1\right\} S_{\mathrm{v2}}}{|Z_1 + Z_2|^2}\mathrm{d}f. \tag{5.20}$$

Equation (5.20) will be discussed shortly. But first, substituting (5.16) into (5.12) gives the coherence function:

$$P_{\mathrm{vi}}(f) = \frac{1}{\sqrt{S_{\mathrm{v}}S_{\mathrm{i}}}} \frac{Z_2 S_{\mathrm{v1}} - Z_1 S_{\mathrm{v2}}}{|Z_1 + Z_2|^2} \tag{5.21}$$

where the (f) functional operators have been dropped from (5.20) and (5.21) for ease of notation.

By inspection of (5.21), for statistically independent $v_1(t)$ and $v_2(t)$, when $Z_1 = Z_2$ and $S_{\mathrm{v1}} = S_{\mathrm{v2}}$, then $P_{\mathrm{vi}}(f)$ is zero. Also, when $P_{\mathrm{vi}}(f) \neq 0$ then it can be stated that $Z_1 \neq Z_2$ and/or $S_{\mathrm{v1}} \neq S_{\mathrm{v2}}$. That is to say, if the electrodes are symmetric, then $P_{\mathrm{vi}}(f)$ is zero and if $P_{\mathrm{vi}}(f)$ is non-zero, then the electrodes are asymmetric. Note that zero $P_{\mathrm{vi}}(f)$ does not necessarily indicate symmetric electrodes, however. For zero $P_{\mathrm{vi}}(f)$, all that can be stated is that $Z_2 S_{\mathrm{v1}} = Z_1 S_{\mathrm{v2}}$. A zero $P_{\mathrm{vi}}(f)$ must be interpreted as no *detected* asymmetry.

Furthermore, if $P_{\mathrm{vi}}(f)$ is zero, then by (5.12) $S_{\mathrm{vi}}(f)$ is zero and by (5.19), so too is r_{vi}. Note that the converse is not necessarily true: an r_{vi} of zero does not imply that $P_{\mathrm{vi}}(f)$ is zero. $P_{\mathrm{vi}}(f)$ provides a more general (and frequency dependent), test for asymmetry than r_{vi}. From (5.20), it can be seen that only the real parts of Z_1 and Z_2 over the bandwidth of the EN play any role in determining whether or not r_{vi} is zero. If use of only the real parts of the impedances when testing for asymmetry

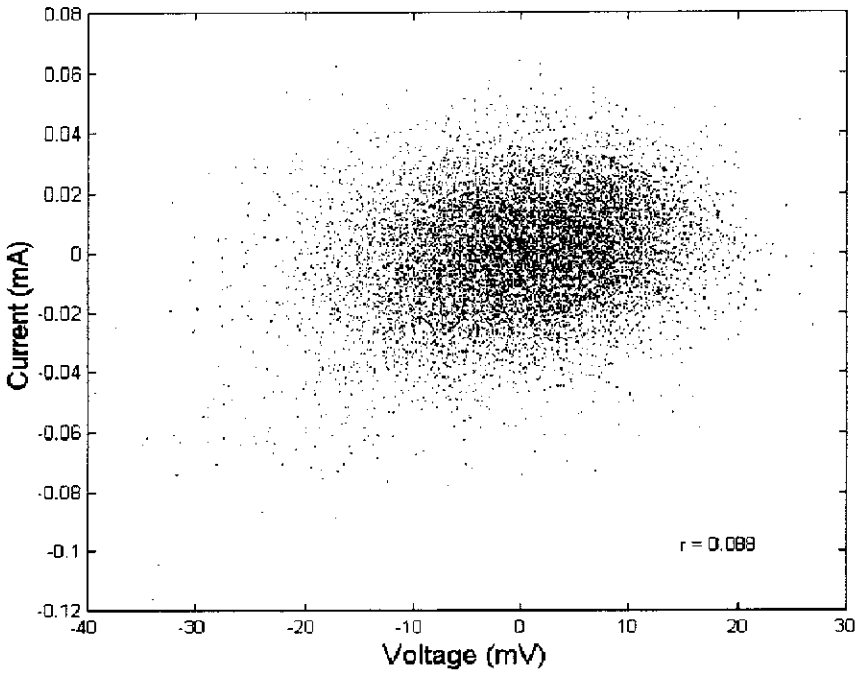

Figure 5.7: EPN/ECN density plot for a symmetrical electrode pair.

can be deemed sufficient, then the simplicity offered by the time domain analysis with r_{vi} can be justified over frequency domain analysis using $P_{\mathrm{vi}}(f)$.

If the impedances are known to be purely resistive over the bandwidth of the EN with $Z_1(f) = R_1$ and $Z_2(f) = R_2$ for all $f_1 < |f| < f_2$, then (5.20) becomes

$$r_{\mathrm{vi}} = \frac{1}{\sigma_{\mathrm{v}}\sigma_{\mathrm{i}}} \frac{\sigma_{\mathrm{v}1}^2 R_2 - \sigma_{\mathrm{v}2}^2 R_1}{(R_1 + R_2)^2} \tag{5.22}$$

Equation (5.22) shows that, in a similar manner to $P_{\mathrm{vi}}(f)$ in (5.21), when the electrode impedances behave resistively within the bandwidth of the EN, a non-zero r_{vi} indicates asymmetric electrodes and that symmetric electrodes have an r_{vi} of zero.

The electrode symmetry can be assessed graphically by density plots as in Figures 5.7 and 5.8, where the EPN and ECN are plotted on separate axes after application of the appropriate signal processing (see Section 4.3). Figure 5.7 is from a system that has been found to exhibit only a low degree of asymmetry, while Figure 5.8 comes from an asymmetric system. The density plot in Figure 5.7 shows very little correlation between EPN and ECN signals with good symmetry about the horizontal and vertical axes. This is indicative of a low correlation. In Figure 5.8, definite positive correlation can be seen between the EPN and ECN signals with the only axes of symmetry being diagonals. This is indicative of a positive correlation.

As is demonstrated in Section 5.1, the noise resistance can be computed as a

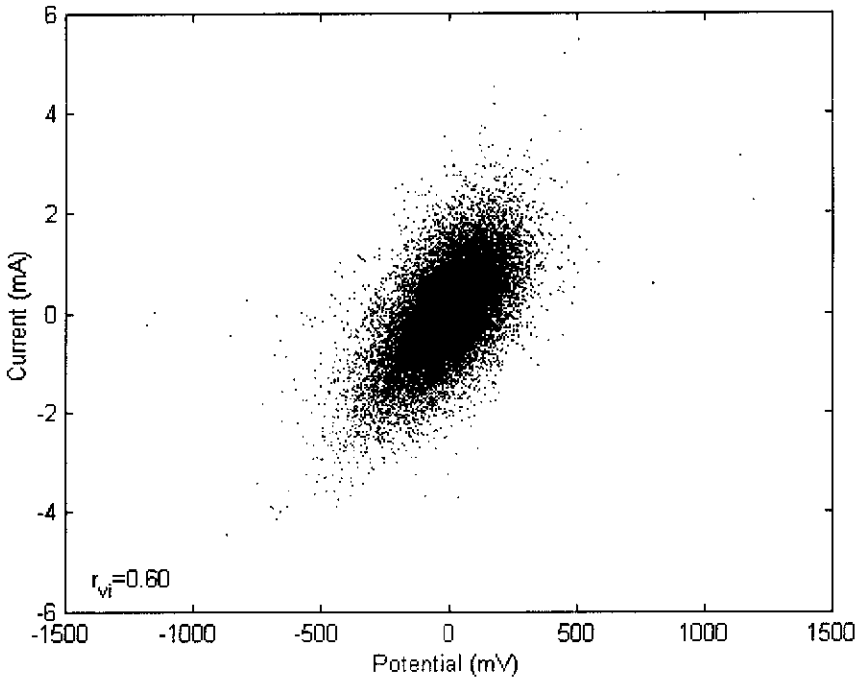

Figure 5.8: EPN/ECN plot for an asymmetric electrode pair.

function of time and frequency to depict how it varies across a range of frequencies as the measurement progresses. Although it is not explored here, it may be possible to similarly place the correlation coefficient onto a time-frequency plane by the same methods and use it to show how symmetry within certain bandwidths varies during the course of an experiment. This could further aid the selection of an appropriate bandwidth for a noise resistance calculation by showing the regions where the assumption of symmetric electrodes fails.

5.3.2 Experimental Procedure

A series of experimental tests have been performed to verify the relationship suggested by (5.22). A system with nominally symmetric electrodes has been obtained by placing two electrodes of equal surface area in solution together. Asymmetry was obtained in two ways: (i) an electrode pair of differing exposed surface area was used; and (ii) electrodes with equal exposed surface area were placed in separate solution of differing concentrations with a salt bridge providing conductance between the two cells.

Four mild steel electrodes were prepared. Two were 3.0 cm^2 cylindrical electrodes that were mounted onto a dual cylinder electrode identical to the one used by Tan *et al* [138] [16]. The third and fourth were cylindrical rods that were immersed directly into solution. The ends were rounded and their shafts were sealed with adhesive heat shrink. The exposed surface areas were found to be 8.8 cm^2 and

1.0 cm^2 respectively. All electrodes were polished with 800 grit sandpaper and cleaned with ethanol prior to immersion.

The selected pair of electrodes was immersed in 600 mL of 1 % NaCl solution with 33 mg/L of sodium bicarbonate buffer. The solution was held at 50 °C by a hot plate and aerated with CO_2. After five minutes of immersion, CO_2 aeration was stopped so that a consistent level of turbulence could be achieved. After a further five minutes, electrochemical measurements were commenced:

1. A linear polarisation (LP) measurement was taken on each of the electrodes to give R_{p1} and R_{p2}, which are taken to represent R_1 and R_2 in (5.22).

2. The Thevenin equivalent EPN originating from each electrode was measured separately to obtain σ_{v1}^2 and σ_{v2}^2 in (5.22). The free corrosion potential of each electrode was also noted.

3. A simultaneous EPN/ECN measurement was taken as depicted by Figure 3.1 (page 40) so that the cross correlation, r_{vi}, can be computed and compared with that obtained by (5.22) using the data from steps 1 and 2.

Measurements were repeated in order to assess the degree of stability of the system and dissolved CO_2 levels were replenished between measurements by reintroduction of CO_2 aeration.

The process was repeated using the 3.0 cm^2 electrode pair (designated as experiments A1 and A2), with fresh solution and repolished electrodes before each experiment. A further set of measurements was obtained using the 8.8 cm^2 and 1.0 cm^2 electrode pair (designated A3).

A 3 % NaCl, 100 mg/L sodium bicarbonate solution (cell 1) was coupled to a 0.3 % NaCl, 10 mg/L sodium bicarbonate solution (cell 2) by a nitrate salt bridge. Both solutions were continuously aerated with CO_2 and held at 60 °C by a pair of hot plates. One 3.0 cm^2 electrode was immersed in each solution and a further set of LP, EPN and EPN/ECN measurements was obtained. The EPN/ECN measurement was repeated: the first time with the reference electrode in cell 1 and the second time in cell 2.

For the EPN/ECN measurement with the reference in cell 1, the resistance of the salt bridge appears as a solution resistance in series with the impedance of the working electrode in cell 2 and similarly when the reference is in cell 2 [19]. With knowledge of R_{p1}, R_{p2}, σ_{v1}^2, and σ_{v2}^2 obtained from the LP and EPN measurements, the noise resistance is used to infer the resistance of the salt bridge, R_s (by Equation 27 in reference [19]). With the reference in cell 1, $R_1 = R_{p1}$ and $R_2 = R_{p2} + R_s$ is substituted into (5.22) to predict r_{vi}. And similarly for the reference in cell 2, $R_1 = R_{p1} + R_s$ and $R_2 = R_{p2}$ is substituted.

The measurements are designated B1 for the reference in cell 1 and B2 for the reference in cell 2.

Experiment	LP		EPN		EPN/ECN
	R_{p1}	R_{p2}	σ^2_{v1}	σ^2_{v2}	r_{vi}
A1	60 Ω	60 Ω	0.31	0.69	0.34
A2	70 Ω	90 Ω	0.50	0.50	-0.21
					-0.16
A3	30 Ω	120 Ω	0.07	0.93	-0.47
	30 Ω	130 Ω	0.04	0.96	
B1	30 Ω	40 Ω[7]	0.86	0.14	0.93
B2	30 Ω[7]	40 Ω	0.86	0.14	-0.27

Table 5.1: LP and EN data collected from different symmetric and asymmetric systems.

LP and EN measurements were performed in a similar manner. to that described by Tan *et al* [138] [16] The LP measurements used an EG&G Princeton Applied Research Model 273A potentiostat with M398A software. A platinum counter electrode and a double junction $Ag^+/AgCl$, 3M KCl reference electrode were used. The EN measurements employed an ACM AutoZRA (see Appendix C) zero resistance ammeter, also using a double junction $Ag^+/AgCl$, 3M KCl reference electrode for potential sensing purposes.

The EN is pre-processed by the techniques described in Section 4.3.[5] The bandwidth of the EN analysis is selected to cover a low frequency range where the spectral noise impedance[6] is found to be approximately flat and where the EN measurements do not appear to exhibit any significant signs of instrumentation noise. σ^2_{v1}, σ^2_{v2} and r_{vi} are computed from the EN data over this bandwidth.

5.3.3 Experimental Results

Table 5.1 summarises the results of the LP and EN measurements. The signal variances listed under the EPN column are normalised such that $\sigma^2_{v1} + \sigma^2_{v2} = 1$. The r_{vi} under the EPN/ECN column are computed over a bandwidth of [0.02,0.2] Hz for experiments A1 to A3, and over [0.1,1] Hz for B1 and B2.

Table 5.2 lists the observed corrosion potentials of each electrode individually, and for when the two electrodes are coupled. The table shows that, in all cases, the two electrodes were never observed to have free corrosion potentials differing by more than 4 mV. The polarisation curves obtained from the LP measurements on each electrode individually are found to be approximately linear over a range 5 mV either side of the free corrosion potential in all cases. Thus it is expected that the gradient of the polarisation curves remained approximately equal to the polarisation resistance (plus solution resistance) for the low levels of polarisation

[5]Using the *shape* routine (Section A.10, page 158).
[6]As determined by the *zMansfeld* routine (Section A.14, page 172).
[7]Add 1.8 kΩ salt bridge resistance.

Experiment	Electrode 1	Electrode 2	Coupled
A1	-697 mV	-607 mV	-698 mV
A2	-700 mV	-700 mV	-701 mV
	-701 mV	-697 mV	-698 mV
	-700 mV	-698 mV	-700 mV
A3	-696 mV	-695 mV	-696 mV
	-695 mV	-693 mV	-695 mV
B1	-714 mV	-710 mV	-718 mV
B2	-714 mV	-710 mV	-714 mV

Table 5.2: Observed corrosion potentials for coupled and uncoupled electrodes.

Experiment	Observed r_{vi}	Predicted r_{vi}
A1	0.34	0.39
A2	-0.21	-0.12
	-0.16	
A3	-0.47	-0.44
		-0.59
B1	0.93	0.93[8]
B2	-0.27	-0.32[8]

Table 5.3: Predicted and observed correlation coefficients, r_{vi}.

experienced when the two electrodes were coupled for an EPN/ECN measurement.

Table 5.3 compares r_{vi} as observed from the EPN/ECN measurements with the r_{vi} as computed by (5.22) using the data obtained from the LP and potential EN measurements. The table generally shows good agreement between the observed and predicted values. The r_{vi} of 0.93 for experiment B1 indicates the system to be highly asymmetric. Similarly the r_{vi} for experiment A3 indicates a significant degree of asymmetry.

Notice that for B2, r_{vi} is significantly smaller than for B1 despite the measurements being taken from the same asymmetric system. This is an example of a case where no significant asymmetry is *detected* despite significant asymmetry being present.

Figures 5.9 and 5.10 show the EPN/ECN density plots from experiments A2 and B1 respectively.

In figure 5.9, there is reasonable symmetry about the horizontal and vertical, which indicates low correlation between EPN and ECN signals and hence a small r_{vi}. In figure 5.10, the only line of symmetry is a diagonal, which indicates strong positive correlation between EPN and ECN and hence a positive r_{vi} that approaches

[8]Noise resistance from the EPN/ECN measurements are used to estimate salt bridge resistance (1.8 kΩ), which is added in series to the appropriate polarisation resistance prior to substitution into (5.22).

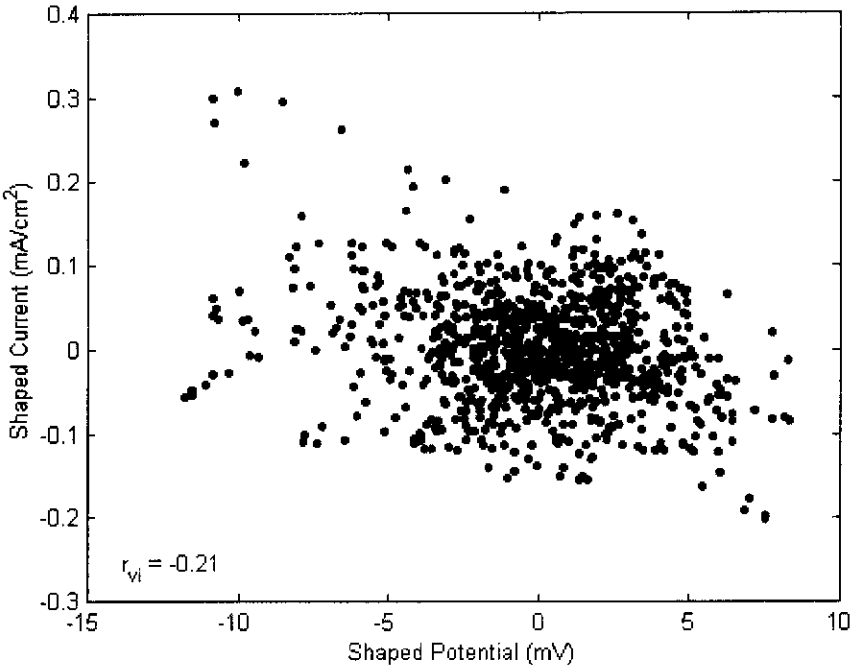

Figure 5.9: EPN/ECN density plot for experiment A2.

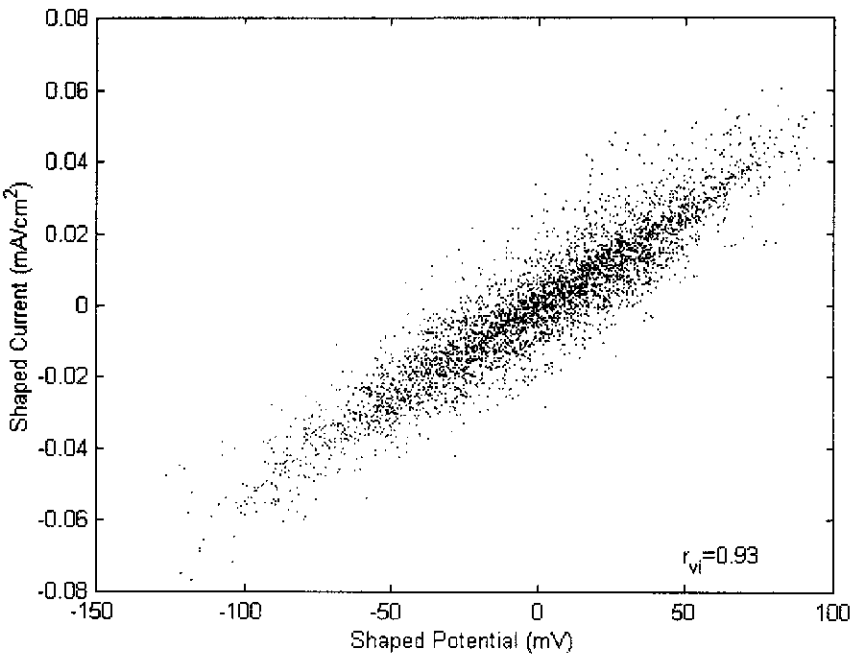

Figure 5.10: EPN/ECN density plot for experiment B1.

unity.

5.4 Summary and Conclusions

Three new electrochemical noise (EN) analysis techniques for time varying noise impedance, complex noise impedance phase recovery and asymmetric electrode detection have been proposed that can be applied to the EN data from a noise resistance measurement.

The time varying spectral noise impedance enhances the understanding of a dynamic system by depicting noise resistance as a function of both time and frequency. In doing so, it is possible to examine how the spectral noise impedance varies during the course of an experiment. An example has been presented to demonstrate the trade-off between time and frequency resolution and to show how the technique can be used to select an appropriate bandwidth for a noise resistance calculation.

A new method to extract the phase of an electrode pair's impedance has been presented. Using this information, a Nyquist impedance diagram can be constructed entirely from simultaneous EPN/ECN data, which can provide further insight into the nature of the electrode impedance. It has been shown, with supporting simulations, that the technique requires some asymmetry of the electrode pair. Its use has been demonstrated by an example application to a physical system.

The cross correlation between the EPN and ECN signals has been proposed as a means of assessing the symmetry of an electrode pair. It has been shown that when the EPN originating from each electrode is statistically independent, non-zero correlation indicates an asymmetric electrode pair and that symmetric electrode pairs yield zero correlation. Good agreement between theory and practice has been observed from experimental tests using mild steel electrodes in NaCl solution saturated with CO_2.

Chapter 6

Hardware and Software for Multi-Sampling a Wire Beam Electrode

The wire beam electrode (WBE) technique (see Section 2.3.3) requires the acquisition of electrochemical data from a large number of mini-electrodes. In this chapter, an individual mini-electrode will be referred to as a "wire". Because typical electrochemical instrumentation is only capable of taking measurements off two working electrodes [*eg* the ACM AutoZRA, used for simultaneous electrochemical potential noise (EPN) and electrochemical current noise (ECN) measurement], some form of multiplexing hardware is required to automate the measurement process.

Three types of measurements are typically required from a WBE:

1. Simultaneous EPN/ECN associated with any pair of wires for a noise resistance measurement;
2. The ECN between an isolated wire and the remaining WBE;
3. The EPN of any wire with respect to a reference electrode.

These measurements respectively enable the construction of

1. a noise resistance distribution map;
2. a galvanic current distribution map; and
3. a corrosion potential distribution map.

See Eren *et al* [88] and Tan *et al* [28] for examples of such corrosion related distribution maps.

The usual form of a multiplexer (selecting, as an output, exactly one of many inputs) is insufficient for this task because that would allow only the EPN from each

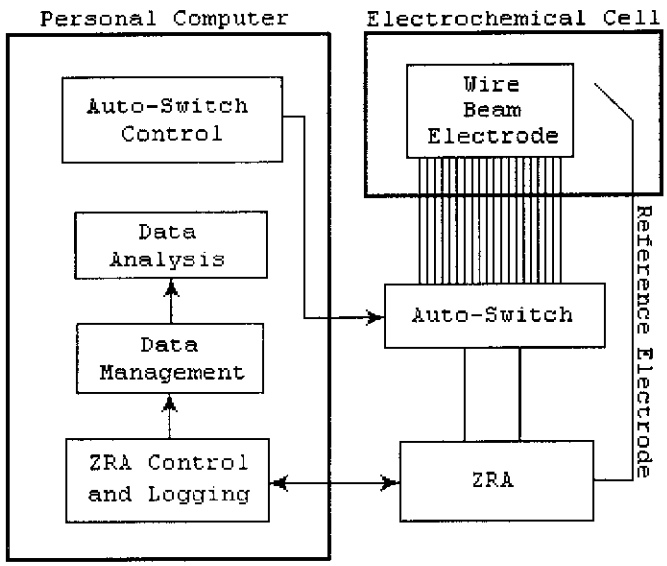

Figure 6.1: WBE Measurement System.

individual wire to be measured. It would be impossible to measure noise resistance or ECN across the WBE surface with an ordinary multiplexer. Instead, a system where the 100 inputs can be connected to either of two outputs in arbitrary combinations is required.

This chapter describes the design, construction and operation of an "auto-switch" that has been built specifically for multiplexing measurements off a WBE. The work described in this chapter has been presented at the Instrumentation and Measurement Technology Conference 1998 [139] and published in the IEEE Transactions on Instrumentation and Measurement [88].

Section 6.1 provides an overview of the components involved in a WBE measurement system. In 6.2, the construction and design of the auto-switch is discussed. Data from tests on the auto-switch are presented in Section 6.3 to illustrate its effect on the measured EN. The controlling software is described in Section 6.4. Before the logged data can be properly analysed, the data needs to be broken up into segments relating to each individual wire and measurement type. Section 6.5 describes the software used for this data management process. In Section 6.6, an example of corrosion mapping over the WBE surface is presented. Section 6.7 discusses some possible modifications to the auto-switch to improve its utility and reliability.

6.1 Overview of a WBE Measurement System

Figure 6.1 shows an overview of the measurement system that incorporates the WBE and the auto-switch.

The WBE, consisting of a 10×10 matrix of wires, is immersed in the electrochemical cell together with a reference electrode for potential sensing purposes.

The 100 wires are multiplexed to a zero resistance ammeter (ZRA) via the auto-switch, which is able to rapidly connect/disconnect any selected combination of wires. Prior to the development of the auto-switch, multiplexing to the ZRA had to be done manually, which severely limited the practical use of the WBE measurement system.

The ZRA takes continuous EPN and ECN measurements off the auto-switch, which is logged on a personal computer. The ZRA and its control/logging software are commercially available products.

Data management, discussed in Section 6.5, involves defining the structure of the logged data and identifying which portions of the measurement correspond to which wires and measurement type.

Data analysis involves inference of corrosion information from the data logged. The WBE is a developing corrosion monitoring technique. Its data analysis depends on the type of corrosion system being investigated and is an extensive subject. Chapters 4 and 5 discuss data analysis of noise resistance/impedance measurements, although the WBE technique is not conceptually limited to these techniques.

The auto-switch control software is responsible for reconfiguring the auto-switch at regular intervals to select different combinations of wires for measurement.

This chapter is concerned with the auto-switch, its control software and the data management.

6.2 Auto-Switch Construction

Figure 6.2 shows the conceptual diagram of the auto-switch. It consists of two banks of switches connecting each of the 100 wires to two separate lines, termed the left and right lines. The left and right lines are then connected to the ZRA's working electrode connections for current and potential sensing purposes.

The switches can be programmed in an arbitrary fashion to select any combination of wires for any desired measurement configuration. For example, the galvanic current between wire 1 and the remaining WBE can be measured by opening all but switch 1 on the left bank and closing all but switch 1 on the right (or vice versa).

Section 6.2.1 discusses the modular design of the auto-switch. Section 6.2.2 shows how modules can be interconnected in series and parallel. Section 6.2.3 examines the simplified circuit diagram of a module.

6.2.1 Modular Design

The auto-switch is required to handle a 10×10 WBE, *ie* 100 wire connections. For practical reasons, it is divided into modules. Figure 6.3 shows the block diagram

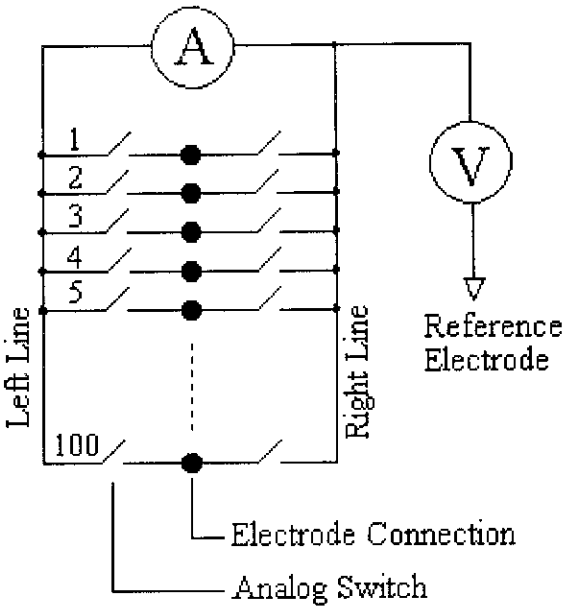

Figure 6.2: Conceptual diagram of the autoswitch.

of a single module capable of handling up to 24 wires. Setting or clearing the corresponding bit of a shift register sets each analogue switch either open or closed and thus either connects or disconnects the corresponding wire to the ZRA (via the left or right line).

Programming is achieved by serially clocking bits B0 and B1 into the shift registers. To completely re-program the module, 24 pairs of bits need to be clocked into the module.

6.2.2 Interconnection of Modules

The modular design allows an arbitrary sized WBE to be utilised without requiring redesign of the auto-switch. More wires can be facilitated by fitting additional modules either in series or parallel.

B0′ and B1′ are used for interconnecting modules serially. Figure 6.4 shows a combination of five serial and parallel module connections resulting in a total wire handling capacity of 120. The three stage parallel connection means that 6 data bits and 1 clock bit are required in total for programming the auto-switch. The two stage serial connection means that a total of 48 of these 6 data bits must be clocked in before the system has been fully reprogrammed. In the configuration shown in Figure 6.4, the first 24 sets of B1 and B0 are redundant because there are no serially connected stages to accept them. As many modules as required can be connected in serial and parallel combinations to handle any given WBE size. The more parallel stages, however, the more data bits are required for reprogramming and the more serial stages, the longer it will take to completely reprogram the entire auto-switch.

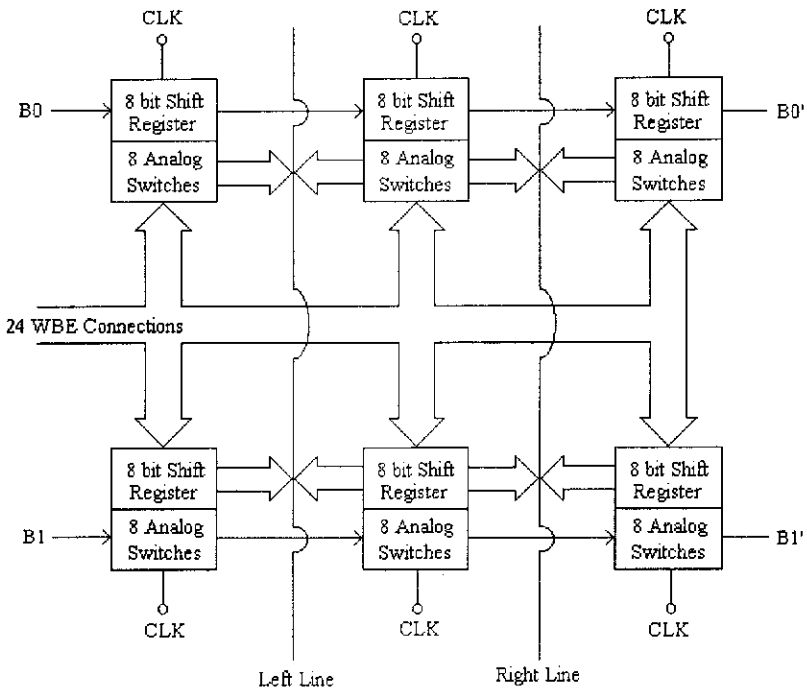

Figure 6.3: Auto switch module block diagram.

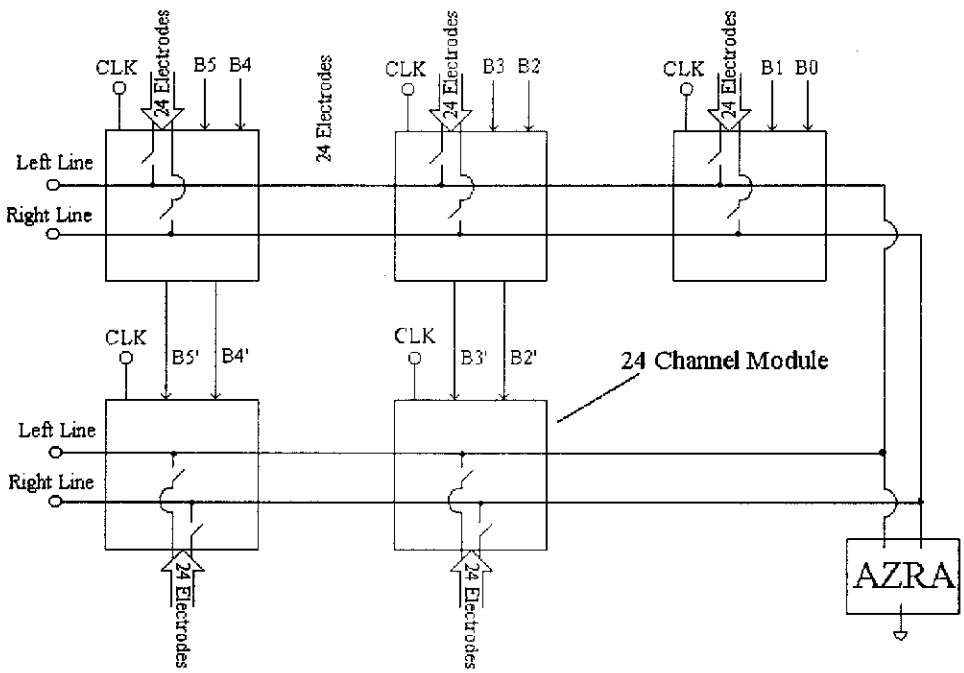

Figure 6.4: Interconnection of autoswitch modules.

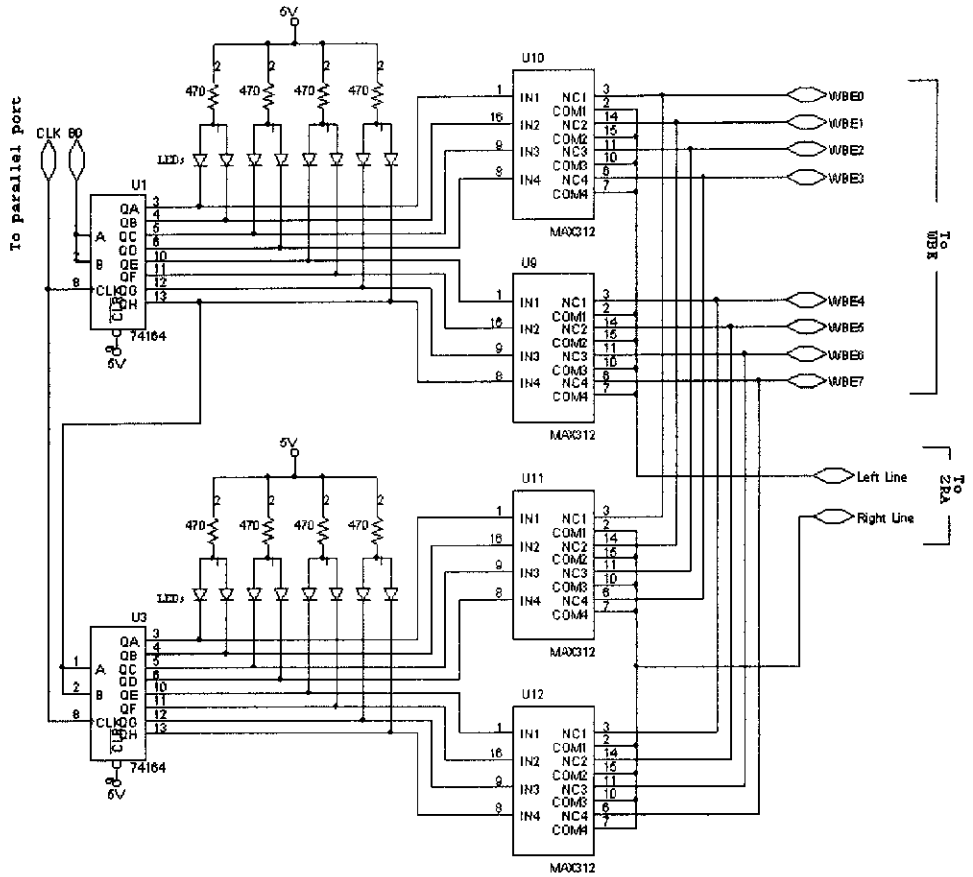

Figure 6.5: Simplified circuit diagram of the autoswitch module

6.2.3 Simplified Circuit Diagram

Figure 6.5 shows a simplified circuit diagram of a module. The module shown in Figure 6.5 uses two 8-bit shift registers and four quad analogue switches and is capable of handling 8 wires. The practical module uses six 8-bit shift registers and twelve quad analogue switches in a similar configuration to Figure 6.5 to handle 24 wires.

In Figure 6.5, the clock signal, CLK, and the programming bits, B0, are obtained from the parallel port of a personal computer. 16 bits are serially clocked into shift registers U1 and U3 to reprogram the module. In the practical module there are two parallel stages of shift registers requiring an additional input, B1, from the parallel port.

Connected to each output of each shift register is an LED and the input of an analogue switch. If, for example, QA of shift register U1 is high, then the normally closed analogue switch in U10 is set open by the signal on IN1 so that WBE0 is isolated from the left line. When QA becomes low, IN1 closes the switch and WBE0 becomes connected to the left line. In addition, the LED attached to QA lights up

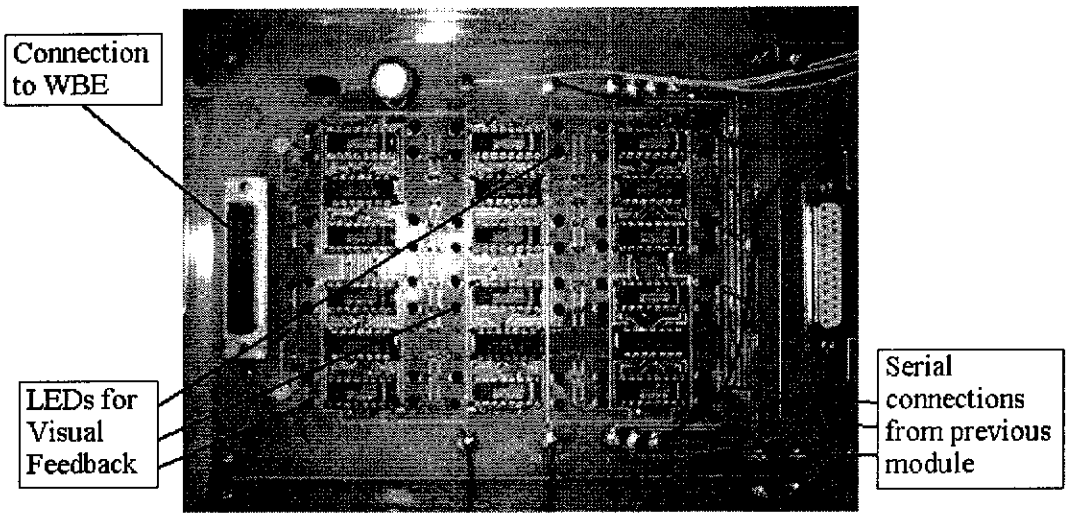

Figure 6.6: Photograph of a single autoswitch module.

to provide visual confirmation of the state of the module. WBE0 can be connected to the right line by lowering QA of shift register U3 instead.

The two major components comprising the auto-switch are the shift registers and the analogue switches. The 74LS164 8-bit shift register has been selected for its size, its serial in, parallel out capability and its ready availability. Speed of operation is not a design issue. However, the 45 MHz clock frequency limit of the 74LS family is considered to be more than adequate.

In order to minimise the resistance between wires connected by the auto-switch, the MAX312CPE is selected for its very low on resistance, given by data sheets to be nominally 6.5 Ω and guaranteed less than 10 Ω. Cross-talk at 20 kHz is guaranteed better than 96 dB.

Connection to the WBE is achieved by DB25 plugs and flat ribbon cable. Programming (*ie* B0 and CLK in Figure 6.5) are facilitated also by DB25 plugs so that the parallel port of a personal computer can be used. Connection of the left and right lines to the ZRA is achieved by BNC connectors for coaxial cable.

Figure 6.6 shows a photograph of a single module. The WBE connection and the layout of the LEDs are illustrated. The serial connection to the previous module can be seen too. Figure 6.7 shows the complete auto-switch, consisting of a total of five modules. The power supply and the connections to the computer's parallel port and to the ZRA are illustrated.

6.3 Testing and Results

The auto-switch is used to perform 3 main tasks: noise resistance measurements between pairs of wires; potential measurements between any wire and the reference

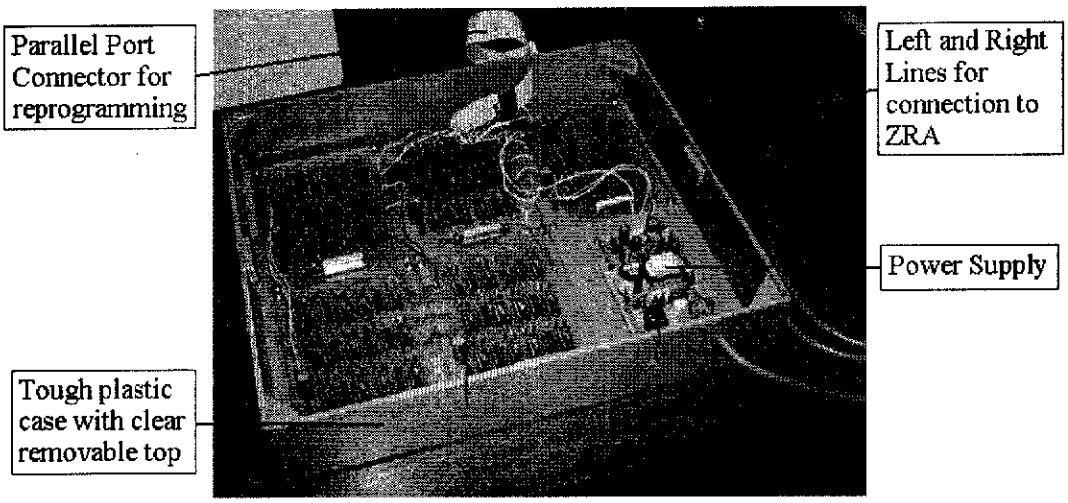

Figure 6.7: Photograph of a the autoswitch.

electrode; and current measurements between any wire and the remaining WBE. Data from tests to verify the auto-switches ability to perform these tasks are given in Sections 6.3.1 to 6.3.3. In Section 6.3.4 the EPN and ECN waveforms obtained from a noise resistance measurement are compared with and without the auto-switch.

6.3.1 Noise Resistance Measurements

The noise resistance (R_n) measurement has been conducted between neighbouring pairs of wires. Figure 6.8 depicts the state of the auto-switch for a noise resistance measurement between wires 2 and 3.

By taking a series of R_n measurements between successive wire pairs, R_n can be mapped over the WBE surface. The measurement has worked well in 3 % NaCl solution with CO_2 aeration: similar R_n values have been obtained with and without the auto-switch (*eg* 400 $\Omega.cm^2$ versus 412 $\Omega.cm^2$). When inhibitor (Champion Cortron IRN-100) is added, similar R_n are also obtained (*eg* 2372 $\Omega.cm^2$ versus 2484 $\Omega.cm^2$). These results were repeated. In general, the auto-switch has not been found to significantly affect the R_n measurements.

6.3.2 Corrosion Potential Measurements

A corrosion potential measurement has been taken between an individual wire and the reference electrode. Figure 6.9 depicts the state of the auto-switch for a corrosion potential measurement at wire 3.

Successive potential measurements allow the measurement/mapping of corrosion potential over the WBE surface. Figure 6.10 shows an example potential waveform obtained through the auto-switch. There appears to be significant transient behaviour in this potential waveform. It is found that unearthing the reference

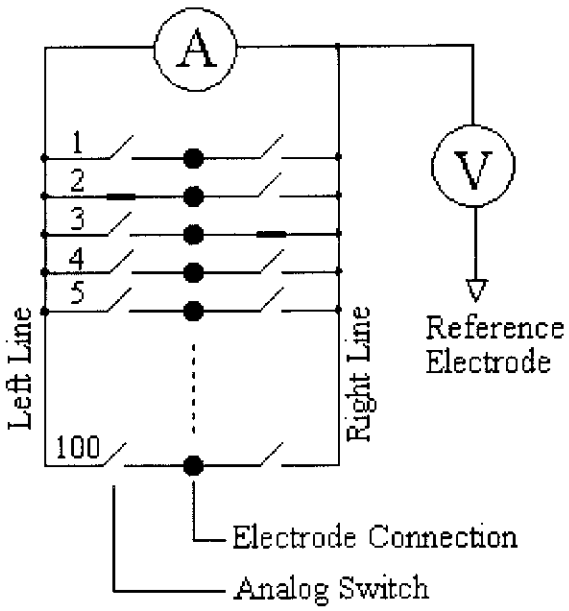

Figure 6.8: Autoswitch configuration for a noise resistance measurement.

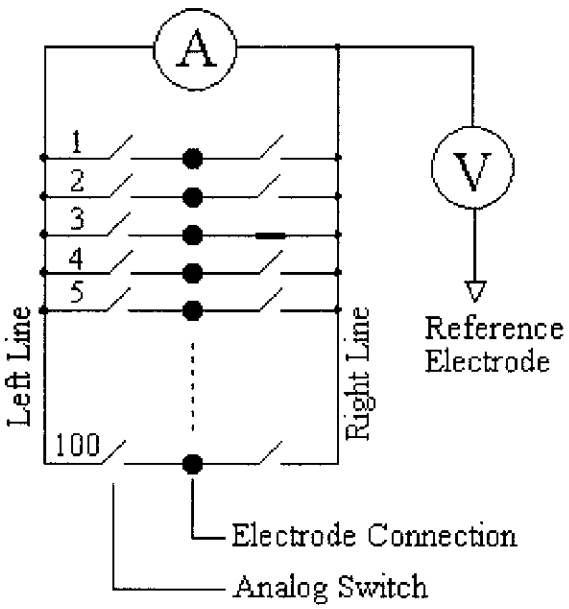

Figure 6.9: Autoswitch configuration for a potential measurement.

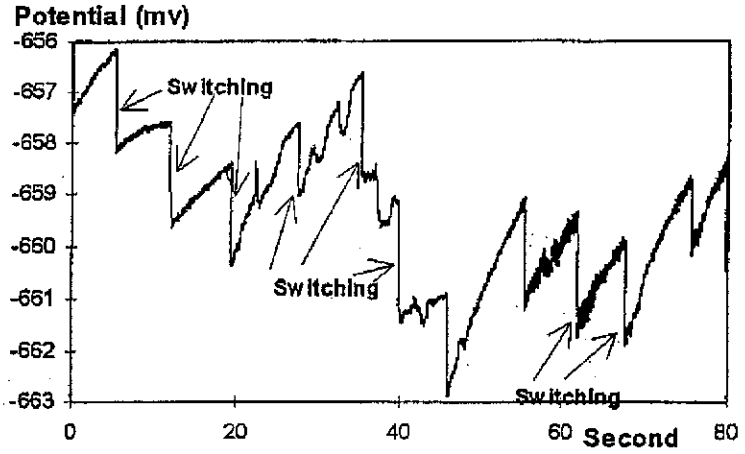

Figure 6.10: Measurements of potential from each wire using the auto-switch.

electrode dramatically reduces the transients' settling times.

6.3.3 Galvanic Current Measurements

A galvanic current measurement is taken between a single wire and the remaining WBE. Figure 6.11 depicts the state of the auto-switch for a galvanic current measurement between the third and the remaining wires.

Successive galvanic current measurements allow a galvanic current distribution map over the WBE to be obtained. As shown in Figure 6.12, the auto-switch performs the switching action between wires quite adequately. It is clearly shown that some of the wires are cathodic (negative current) while others are anodic (positive current).

6.3.4 Effect of Auto-Switch on EPN and ECN measurements

The test has also been run with an oxygen-aerated system. Figure 6.13 shows the EPN waveforms obtained. The first waveform, section A, is the measurement without the use of the auto-switch, followed by a brief period, in section B, of about 20 seconds of no measurement while the auto-switch is attached to the system and then the measurement, in section C, through the auto-switch. The DC difference between the two waveforms is only very slight — about 1 %. It is most likely the result of DC drift between the time the two measurements were taken.

Figure 6.14 shows the ECN waveform obtained in the oxygen aerated system. Again, section A depicts the measurement without the auto-switch, section B, the brief period where the auto-switch is connected and section C, the plot resulting from the measurement with the auto-switch.

Both Figures 6.13 and 6.14 show that the auto-switch does not appreciably affect the measurements made on the system. The noise resistance was calculated for both

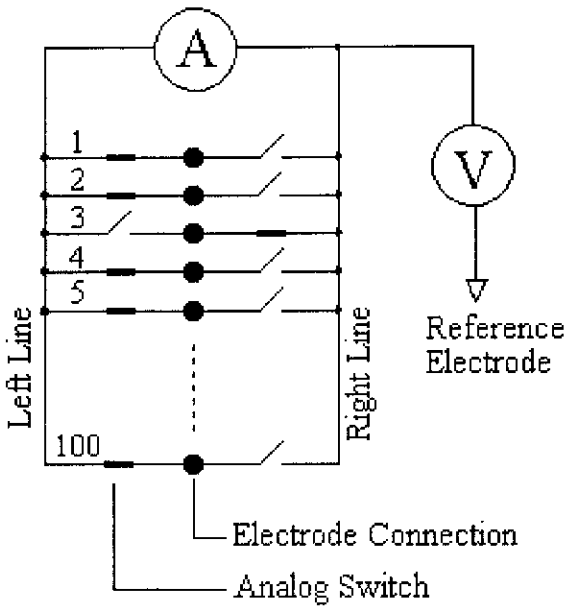

Figure 6.11: Autoswitch configuration for a galvanic current measurement.

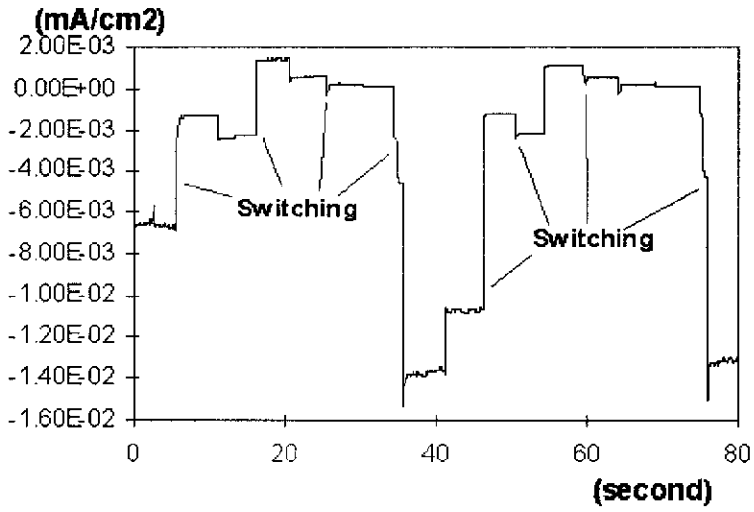

Figure 6.12: Galvanic current between a single wire and the remaining electrodes.

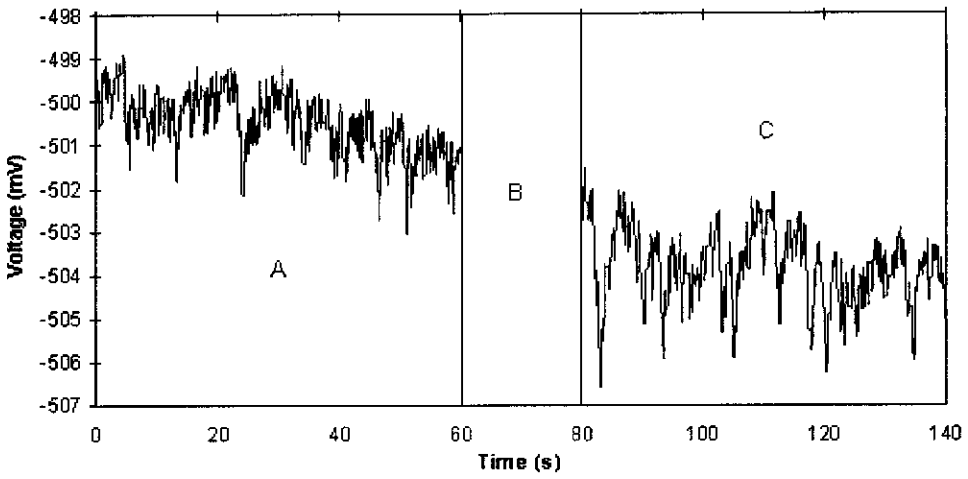

Figure 6.13: Comparison of EPN waveforms with and without the auto-switch.

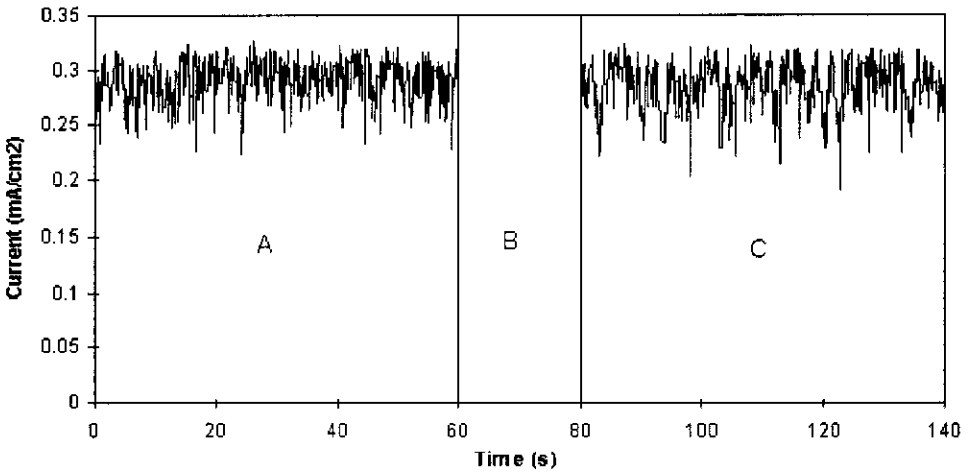

Figure 6.14: Comparison of ECN waveforms with and without the auto-switch.

cases and found to be 10.8 $\Omega.cm^2$ without the auto-switch and 10.3 $\Omega.cm^2$ with the auto-switch.

6.4 Control of the Auto-Switch

The auto-switch is programmed via the parallel port of a personal computer. Bits B0 to B5 and the clock signal (CLK) in Figure 6.4 are taken directly off the data output pins of a parallel port. No special interface hardware is required on the auto-switch. The CLK signal is generated by explicitly raising and lowering the relevant data bit of the parallel port. For every set of bits to be sent to the auto-switch, two writes to the parallel port are made. *eg* suppose [B0,B1,B2,B3,B4,B5] = [0,0,0,0,0,0] is to be written to the auto-switch, first [B0,B1,B2,B3,B4,B5,CLK] = [0,0,0,0,0,0,0]

and then [B0,B1,B2,B3,B4,B5,CLK] = [0,0,0,0,0,0,1] are output to the parallel port. The first output places B0 and B5 on the auto-switch inputs, the second raises CLK so that B0 and B5 are shifted into the auto-switch's shift registers.

There is one central data structure and one central output routine in the controlling software. The central data structure depicts the state of auto-switch and is referred to as the switch-state array. It is an array of boolean values that describe the on/off state of each individual switch in auto-switch. The central output routine accepts a switch-state array as a parameter and outputs the correct sequence of bytes to the parallel port in order to place the auto-switch into the specified state. The software consults an easily modified text file that describes the wire-number assignments on the auto-switch in order to determine the correct output sequence.

The task of the user interface to the control software is to construct a switch-state array based on user input, which can then be passed to the central output routine. There are two ways in which the user can enter information:

1. A specific type of measurement is specified (potential measurement, galvanic current measurement or noise resistance measurement) and then the relevant electrode number or pair of electrode numbers are specified (*eg* noise resistance, wires 51 and 52). The controlling software then converts this information into a switch-state array.

2. In order to cater for unforeseen configurations, a switch-state array can be specified directly. This is achieved by specifying a pair of 30 digit hexi-decimal numbers that bit-wise describe the state of the left and right banks of switches. For example, the pair of numbers fffff fffff fffff fffff fffff fffff and 00000 00000 00000 00000 00000 00000 specify that all switches connecting electrodes to the left line are to be closed while all switches connecting electrodes to the right line are to be opened.

In addition, the controlling software is capable of placing the auto-switch into a series of predetermined configurations with set delays in between. This allows a series of measurements to be taken off the WBE without any need for the apparatus to be supervised. For example, a sequence of interleaved potential and galvanic current measurements of duration, say, 10 seconds each can be taken on each electrode. These pre-programmed sequences are specified in easily modified text files. The operator selects any one of these pre-programmed sequences for the controlling software to execute.

6.5 Data Management

The EN data is logged as a pair of continuous waveforms by the ZRA. Both potential and current are always logged in all cases, even if it is only the potential or the

current one is interested in. The results are EN waveforms similar to those of Figures 6.10 and 6.12. Sudden steps or spikes are often observed whenever the switch is reprogrammed, referred to as switching events. The measured waveform needs to be broken up into sections corresponding to each switch state. Once this is done, the measurement from each switch-state can be analysed accordingly. However, as no synchronising information is communicated between the auto-switch and ZRA control software, the approximate points of each switching event must be estimated from the measured waveform. Locating and specifying each of these points, referred to here as calibration, can prove cumbersome if done manually. Software has been developed for automatic calibration (autocalibration) of a measurement.

The autocalibration is based on two methods: *rate-of-change* thresholding and *zero-crossing*. The analyst specifies an approximate time where the first switching event occurs, T_0, and an approximate time interval between successive events, T. The autocalibration routines then use this information to locate the approximate times of all the switching events, $T_1, \ldots, T_n$, by the rate-of-change and zero-crossing methods. The analyst specifies whether autocalibration is to be performed using the potential or the current waveform.

Given that a previous switching event occurs at time T_i, the time of the next event, T_j, is nominally located at $T_{\text{nom}} = T_i + T$. The autocalibration routines examine a segment, x, of the waveform $\frac{T}{2}$ seconds before and after T_{nom} with the rate-of-change and zero-crossing analysis.

The rate-of-change thresholding method determines T_j as the point closest to T_{nom} where the rate of change of x first exceeds a pre-determined threshold. It fails if the first such point is outside a pre-determined tolerance or if no such point is found.

The *zero-crossing* method determines T_j as the point closest to T_{nom} where x first crosses its mean value. It fails if the first such located point is outside a pre-determined tolerance.

If the *rate-of-change* method does not fail, then T_j is taken as given by the rate-of-change method. Otherwise the zero-crossing method is used. If they both fail, then T_j is taken to be the nominal, T_{nom}. The process is then repeated to locate the next switching event.

Once the data has been calibrated, the analyst requires a function that will extract a particular type of measurement from a specified wire coordinate [*eg* the potential waveform from the noise resistance measurement on the wire at coordinate (3, 6) on the WBE]. In order to define concepts such as "the noise resistance measurement" and to enable specific wires to be referenced, the analyst defines a measurement profile.

The need for a measurement profile arises because the pre-programmed sequences run by the auto-switch control software can take many varied forms. For example,

in scenario A, a measurement might consist of 100 successive corrosion potential measurements across the surface of the WBE, followed by 100 galvanic current measurements, followed by 100 noise resistance measurements. Alternatively, scenario B, the measurement might consist of 100 interleaved corrosion potential, galvanic current and noise resistance measurements. The measurement profile specifies to the data management software how each segment of the waveform is to be interpreted (either as a corrosion potential, a galvanic current or a noise resistance) and to which wire/wires that segment corresponds.

The measurement profile consists of an array of numbers. The data management software examines each number in turn to decide what type of data segments to expect. When it runs out of numbers, it goes back to the beginning of the array.

Three constants are predefined: `POTENTIAL`, `CURRENT`, `RESISTANCE`. Although it is transparent to the analyst, they are given values of 1, 1 000 and 1 000 000 respectively so that, for example, consecutive potential measurements can be specified as n`*POTENTIAL`, where n is the number of consecutive potential measurements (1 to 999). Scenario A can then be specified by

```
[100*POTENTIAL, 100*CURRENT, 100*RESISTANCE]
```

whereas scenario B can be specified by

```
[1*POTENTIAL, 1*CURRENT, 1*RESISTANCE].
```

Wire coordinates are handled by providing two layers of access. On the lower layer, wires are simply referred to by number (1 to 100), as with the auto-switch. Data segments are extracted after consulting the measurement profile. Above that layer, wire coordinates (x, y) are mapped to a wire number before control is passed through to the lower layer.

In order to cope with switching transients and random error in the autocalibration, a pre-determined margin is clipped from the beginning and end of each segment before the data is returned to the analyst.

6.6 Examples of Corrosion Mapping

Localised corrosion has been detected by an electrochemical testing system utilising the auto-switch. When a mild steel WBE is partially immersed in a 0.017 mole NaCl + 0.008 M Na_2CO_3 solution, localised corrosion has observed.

The data management and analysis software is implemented using Mathsoft's Mathcad. The software produces surface distribution maps such as depicted in Figures 6.15 to 6.17.

Figure 6.15 shows the galvanic current distribution found after the WBE has been exposed for 1 hour. The areas of relatively high current (the lighter areas)

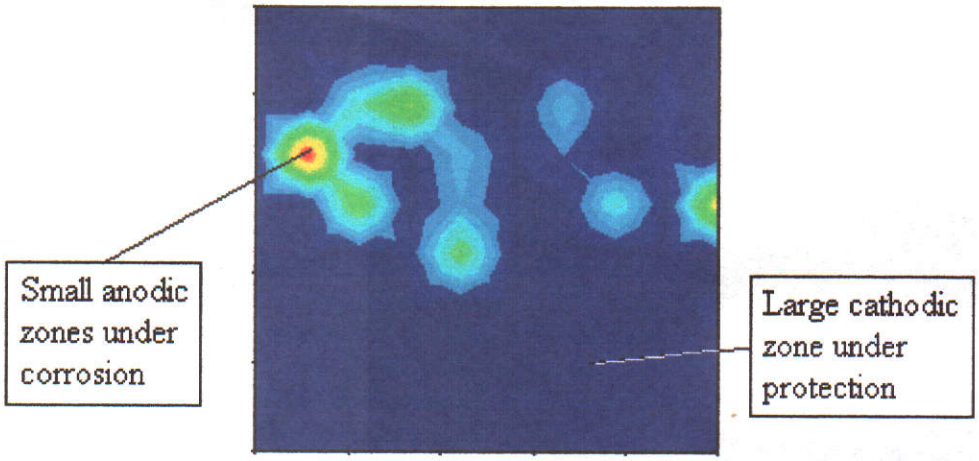

Figure 6.15: Galvanic current distribution on the WBE after exposure for 1 hr.

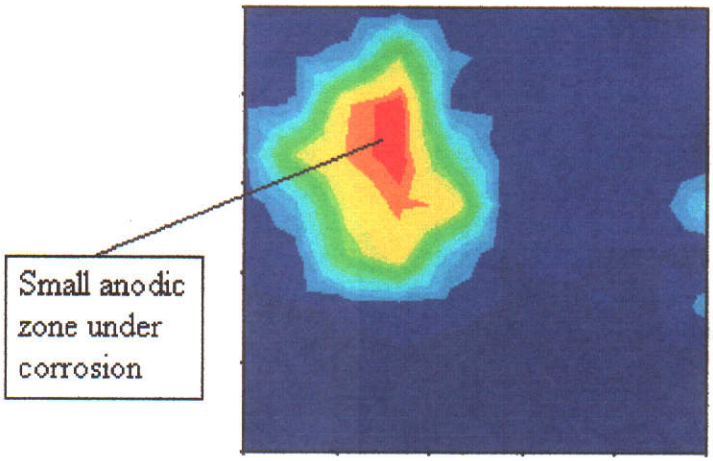

Figure 6.16: Galvanic current distribution on the WBE after exposure for 4 days.

represent anodic areas and the darker areas are cathodic. Electron charge moves from the anode to the cathode during a redox reaction, resulting in corrosion of the anode. The anodic regions are observed to be relatively small and scattered. This is because the corrosion patterns are still unestablished.

Figure 6.16 shows the galvanic current distribution found after the sensor has been exposed for four days. In comparison with the results of Figure 6.15, the anodic region here has matured to become better established and more clearly defined.

Figure 6.17 shows the corrosion potential distribution measured at the same time as the current distribution of Figure 6.16. Electron current flows from the lower potential regions to the higher potential regions. The shapes of the two distributions corroborate with one another.

In addition, the corrosion patterns of Figures 6.16 and 6.17 have been found to be in a good agreement with visual observations of the WBE surface.

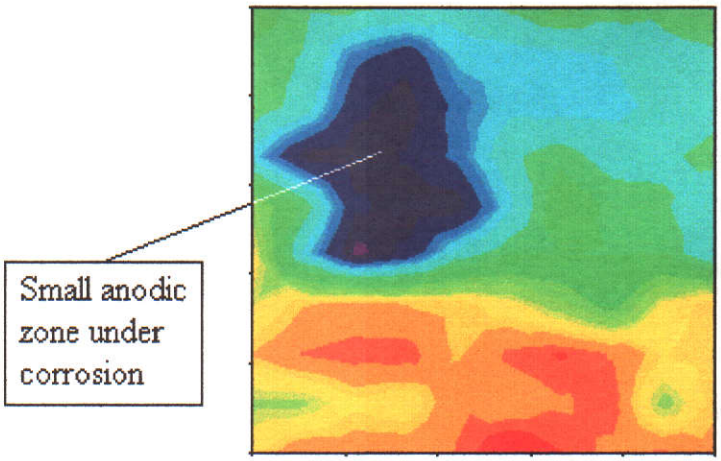

Figure 6.17: Corrosion potential distribution on the WBE after exposure for 4 days.

6.7 Possible Improvements

6.7.1 Integrated Auto-Switch and ZRA

It is expected that the integration of a ZRA into the construction of the auto-switch will decrease the overall hardware cost. From a technical point of view, control will be simplified as both the ZRA and auto-switch can be controlled from a single communication port by a single piece of software and calibration information can be recorded alongside the EN data. In order to maintain the flexibility provided by a separate auto-switch and ZRA, external access to the left and right lines of the auto-switch can still be provided, thus allowing the auto-switch to be used with a third party ZRA or any other device.

6.7.2 TCP/IP or IEEE 488.2 Interface

In the present implementation, the ZRA requires a serial communication port and the auto-switch requires a parallel port. Since communication ports can be a premium on general purpose computers, it is preferable to rationalise their use. In addition, the use of a physical communication port necessitates a dedicated machine. With the proliferation of intranets and the Internet in general, ethernet adaptors are becoming increasingly common on personal computers. If the auto-switch is given an ethernet adaptor and is assigned an Internet Protocol address, it can be controlled without requiring a dedicated communications port, or even a dedicated machine. Control can be affected by any machine on the computer network (throughput, latency and security permitting.)

Alternatively an IEEE 488.2 General Purpose Interface Bus can be utilised without consuming valuable input/output ports on the computer. This has the advantage of improved reliability compared to a TCP/IP interface.

6.7.3 Monolithic Integrated Circuit

At present, assembly of auto-switch is a time consuming and it is difficult to obtain a reliable product. A single integrated circuit can be designed to incorporate the analogue switches and shift registers of a single module. This will greatly simplify construction and improve reliability in general.

Since the present auto-switch has been completed, a new semiconductor switch (ADG714BRU) has been manufactured by Analogue Devices. The ADG714BRU incorporates a shift register and analogue switches into a single integrated circuit. This will reduce the number of discrete components required to build an auto-switch and greatly improve its production costs and reliability. The draw back is that the shift register outputs will no longer be available for connection to LEDs. An alternate method of visual feedback will have to be devised.

6.8 Summary and Conclusions

A system for multiplexing electrochemical noise measurements on a wire beam electrodes has been developed. The hardware consists of an array of analogue switches that are controlled by a series of shift registers. The analogue switches are able to rapidly connect and disconnect any combination of 100 wires to either of two lines, which are then connected to standard electrochemical noise instrumentation. Data management software has been developed in the Mathcad environment that enables the data associated with a specific wire coordinate and measurement type to be easily extracted from the measured waveform and analysed.

Chapter 7

Summary and Conclusions

In Chapter 4, the use of electrochemical noise (EN) for estimation of electrochemical impedance has been examined. In agreement with previous literature, it has been found that the noise resistance (R_n) is theoretically equal to the impedance magnitude within the bandwidth of the EN under various ideal circumstances. In order to allow more confident estimation of the noise resistance, the factors affecting the estimate have been examined. It is found that the duration of the measurement and the bandwidth of the EN are both important factors that significantly affect precision. There is a trade-off between the length of a measurement; the bandwidth of the EN; and the relative precision of the estimate. The product of the three quantities remains always approximately equal to unity.

A signal conditioning scheme is proposed that forms EN signals with certain ideal characteristics that aid in estimation of R_n (EN with a flat power spectral density within its bandwidth, zero mean, and approaching a Gaussian distribution). It also allows the bandwidth of the EN to be easily controlled so that the implicit frequency dependence of R_n can be exploited to focus the estimate onto any desired range of frequencies — for example, a range where the cell impedance is suspected to be equal to the polarisation resistance or solution resistance. This is advantageous over a system where no signal conditioning is attempted because

- the analyst is no longer required to assume that the EN covers an appropriate bandwidth;
- the bandwidth of the EN can be maximised to yield a more precise estimate; and
- the signals take on characteristics that are more conducive to estimation of R_n than raw EN.

The moving average removal technique for trend removal has been analysed with respect to its effect on the performance of the noise resistance estimate. It is found to be a useful technique that can be used to focus the noise resistance estimate onto

a specific range of frequencies, as with the proposed signal conditioning. However, independent control over the bandwidth and location of that range of frequencies is not possible.

Experimental tests have been carried out to compare the performance of linear trend removal, moving average trend removal, and the proposed signal conditioning. The results show that R_n compares well with linear polarisation measurements when moving average removal or the proposed signal conditioning are used (with careful selection of the EN bandwidth), but that linear trend removal by itself performs poorly with the test data. The proposed signal condition is seen to yield slightly improved precision in relation to the moving average removal. The precision yielded by these two methods is found to be in reasonable agreement with the theory.

As a result of this work, the implicit frequency dependency of R_n can be controlled (and exploited) and the estimation of R_n can be optimised so that the R_n technique can be applied with greater confidence. This allows fairer comparison between information obtained from R_n and information obtained by non-EN techniques (*eg* linear polarisation and AC polarisation). It also makes time domain analysis with R_n an acceptable alternative to the frequency domain analysis offered by $R_{sn}(f)$. $R_{sn}(f)$ is difficult to apply to dynamic systems, where impedance changes with time, but by continuously calculation of R_n over a sliding window [16], dynamic systems can be monitored.

In Chapter 5, three novel EN analysis techniques are proposed that make use of the data obtained from a simultaneous potential/current measurement (*ie* an R_n measurement): the time varying spectral noise impedance; the complex noise impedance; and the EN power factor.

The time varying spectral noise impedance is a computation of R_n as a function of time and frequency so that the frequency dependent nature of a dynamic system can be examined. An example for a system where the corrosion rate gradually decreases is presented and the results used to demonstrate how to select an appropriate bandwidth for R_n calculations at various points in the measurement for the purpose of estimating polarisation resistance.

The complex noise impedance is a method of retrieving information regarding the phase of the cell impedance so that a Nyquist impedance diagram can be constructed entirely from a simultaneous potential/current EN measurement. Previously, only the magnitude of the cell impedance was available, making it impossible to construct a Nyquist diagram. It is found that the method requires some asymmetry between the two working electrodes. An example from a localised corrosion system, where one electrode is found to have no visible corrosion while the other exhibits significant crevice corrosion, is presented as an example.

The EN power factor is defined and, based on an equivalent circuit model, it is shown to have some ability for detecting an asymmetric electrode pair. It allows the symmetry of a system to be assessed entirely from the simultaneous potential/current data without any need for additional measurements. Once a system is known to be symmetric, the R_n can be estimated more confidently, or once a system is known to exhibit some asymmetry, the complex noise impedance can be computed.

The addition of these three techniques to the set of EN analysis tools improves the general utility of the EN technique.

In Chapter 6, the details of an auto-switch are presented. The auto-switch is used for rapid, automatic configuration of a wire beam electrode. It is able to arbitrarily connect 100 mini-electrodes to two connectors for use with conventional, dual working-electrode electrochemical instrumentation and hardware and electrochemical noise instrumentation in particular. The auto-switch eliminates the need for the connections to be made manually, which enables researchers to utilise the wire beam electrode technique of monitoring localised corrosion with greater ease and rapidity.

Appendix A

Source and Documentation for Selected Matlab Functions

This appendix contains the source code and documentation for selected Matlab functions that have been developed for EN analysis and used in this thesis. The following is only a subset of the full set of routines, which can be obtained from the world wide web at http://chemistry.curtin.edu.au/staff/alowe/en [29].

A.1 MAVFilt

name :

MAVFilt - apply a moving average low pass filter to a signal.

Synopsis :

```
y = MAVFilt (x, N)
```

Description :

A Moving average filter of length `N` samples is applied to the signal, `x`, with the result returned as `y`.

Example :

```
x=flickergenerate(1,0.1,1024,1);
y=x-MAVFilt(x,80);
plot(y)
```

Generates some random data with a $\frac{1}{f}$ PSD and then uses a moving average filter of length 8 seconds to remove the trend.

See also :

shape, Matlab Native Function: polyfit.

Source :

```
function [y, sx, nn] = MAVFilt (x, N, ovrlap)

N=round(N);
h = ones(N,1)/N;
y = conv(x,h);
idx1 = round(N/2);
idx2 = idx1 + length(x)-1;
y = y(idx1:idx2);
```

A.2 NoiseNyquist

Name :

`NoiseNyquist`

Synopsis :

`[x, y] = noiseNyquist(pV, pI, Z, N)`

Description :

Returns `x` and `y` for a nyquist impedance plot with `r=sqrt(pV./pI)` and `theta=angle(Z)` as returned by the `vizEstimate` function. `N` band-limits the plot to use only the first `N` frequency points in `pV`, `pI` and `Z`.

Example :

```
[v,i,dvdt,is] = visynth5(8192,[100e-6 100e-6],[-680,-690],
   [0.1 0.1 0.01 0.01],[200 -200 150 -130],0.025,[0 0 0 0],
   ones(2048,1)/512);
[pv,pi,z]=vizestimate(v,i,512,0.025);
[x,y]=noisenyquist(pv,pi,z,512);
plot(abs(x),y, '.')
```

Synthesises some EN data for an asymmetric system and generates a Nyquist impedance diagram from it.

See also :

vizEstimate.

Source :

```
function [x, y] = noiseNyquist(pV, pI, Z, N)

NN=length(pV);
idx=[1:N (NN-N+1):NN];
```

```
r=sqrt(pV(idx)./pI(idx));
theta=angle(Z(idx));

x=r.*cos(theta);
y=r.*sin(theta);
```

A.3 normSVariance

Name :

`normSVariance` - Computes the normalised variance of a signal's power.

Synopsis :

`sigma = normSVariance (W1, W2, T)`

Description :

If the power of a zero mean, normally distributed signal, $x(t)$, with a white PSD, is band-limited to `W1` to `W2` radians per second and is computed over a time interval of `2T` by $P = \frac{1}{2T}\int_{-T}^{T} x^2(t)\mathrm{d}t$, then P will have a certain expected value, η_P, and variance, σ_P^2. The function `normSVariance` computes the normalised variance of P, as defined by $k_P = \frac{\sigma_P^2}{\eta_P^2}$.

If `length(W1)`$= i$, `length(W2)`$= j$ and `length(T)`$= k$ then `sigma` is an $i \times j \times k$ three dimensional matrix.

`T` defaults to 1.

Example :

```
w2=logspace(-1,2,20);
kP=normsvariance(0.01, w2, 1);
loglog((w2-0.01)/2/pi,kP)
```

Plots the normalised variance of P as a function of signal bandwidth in Hertz for `T`$= 1$ s and `W1`$= 0.01$ radians per second.

See also :

optimumRxx, RnVariance, RnVarianceSim, SVariance, SExpected, normSVarianceSim, normSVarianceSolveW2, normSVarianceSolveW1, normSVarianceSolveT, nSigmaImpedance.

Source :

```
function sigma = normSVariance (W1, W2, T)
```

```
if nargin == 2
   T=1;
end

sigma = zeros(length(W1),length(W2),length(T));

for k=1:length(T)
%   disp (['T = ' num2str(T(k))]);
   sigma(:,:,k) = calculate (W1, W2, T(k));
end

function sigma = calculate (W1, W2, T)
% W1(n), W2(m) are vectors, sigma is nxm matrix.  T is scalar.

W1 = tocolumnvector(W1);
W2 = tocolumnvector(W2)';

n=length(W1);
m=length(W2);

W1 = W1*ones(1,m);
W2 = ones(n,1)*W2;

% Make sure we don't have any W1=W2 anomalies.
eqMask = (W1==W2);
W2=1.0001*(eqMask.*W1) + (1-eqMask).*W2;


W1=W1*T;
W2=W2*T;
SM=W1+W2;
DF=abs(W1-W2);

a = -2;

a = a + 4*W1.*sineint(4*W1);
a = a + 4*W2.*sineint(4*W2);
a = a - 4*SM.*sineint(2*SM);
a = a + 4*DF.*sineint(2*DF);
```

```
a = a + cosint(4*W1);
a = a + cosint(4*W2);
a = a - 2*cosint(2*SM);
a = a + 2*cosint(2*DF);

a = a + cos(4*W1);
a = a + cos(4*W2);
a = a - 2*cos(2*SM);
a = a + 2*cos(2*DF);

sigma = a./DF./DF/2;
```

A.4 normSVarianceSim

Name :

`normSVarianceSim` - Estimates the mean and variance of a signal's power by monte-carlo simulation.

Synopsis :

`[variance, mean] = normSVarianceSim (W1, W2, T, N)`

Description :

Estimates the mean and variance of $P = \frac{1}{2T}\int_{-T}^{T} x^2(t)\mathrm{d}t$, where $x(t)$ is a zero mean, normally distributed signal that is white, but band-limited to `W1` to `W2` radians per second by use of an `N` run monte-carlo simulation.

Example :

```
w2=logspace(-1,2,20);
kP=normsvariance(0.01, w2, 2);
kpSim=zeros(size(kP));3
for n=1:length(kpSim);
  [v,m]=normSVarianceSim(0.01,w2(n),2,256);
  kpSim(n)=v/m/m;
end
loglog((w2-0.01)/2/pi,kP,'-', (w2-0.01)/2/pi,kpSim,'.')
```

Plots the normalised variance of P as a function of signal bandwidth in Hertz for `T`= 2 s using the theoretical equation (`normSVariance`) and the monte-carlo simulation (`normSVarianceSim`).

See also :

optimumRxx, RnVariance, RnVarianceSim, SVariance, SExpected, normSVari-

ance, normSVarianceSolveW2, normSVarianceSolveW1, normSVarianceSolveT, nSigmaImpedance

Source :

```
function [variance, mean] = normSVarianceSim (W1, W2, T, N)

fs=2*10*max(W1, W2)/2/pi;

sumS = 0;
sumS2 = 0;

for i=1:N
   x = GenerateSignal (W1, W2, 2*T, fs);
   s = sum(x.*x)/2/T/fs;
   sumS = sumS + s;
   sumS2 = sumS2 + s.*s;
end

ES = sumS/N;
ES2 = sumS2/N;

mean = ES;
variance = ES2 - ES*ES;
%nsigma = ES2/ES/ES - 1;

function x = GenerateSignal (W1, W2, T, fs)

f1=min(W1,W2)/2/pi;
f2=max(W1,W2)/2/pi;

Nx = T*fs;
if (Nx-floor(Nx) < unifrnd(0,1))
Nx = ceil(Nx);
else
Nx = floor(Nx);
end

NN= max(Nx,64);
x = normrnd(0,1,NN,1);
x = brickBPF(x,f1,f2,fs);
```

```
x = x(1:Nx);
```

A.5 nSigmaImpedance

Name :

`nSigmaImpedance` - Estimates the noise resistance over a given set of frequency bands as a continuous function of time.

Synopsis :

```
[z, r, f, t, downsampled, shaped, bpfed, powers] =
    nSigmaImpedance (v,i,fs,nSigma,fedges,nmem,norm,ovrlap,T)
```

Description :

- `z`, `r`, `f` and `t`:
  The noise resistance, `z`, and potential/current cross correlation, `r`, of the EN signals `v` and `i` is determined over frequency bands determined by the vector `fedges` as a continuous function of time. `t` provides a time axis and, if multiple sub-bands are used, `f` provides a frequency axis. `z` is typically used as a measure of corrosion rate, whereas `r` is used to assess electrode symmetry.
- `downsampled`, `shaped`, `bpfed` and `powers`:
  Prior to estimation of the noise resistance and cross correlation, the signals are whitened and band-pass filtered, as per the "matched" signal conditioning. The outputs `downsampled`, `shaped`, `bpfed` and `powers` are dual column vectors giving the signals at the various stages of the computation with the first column corresponding to the potential and the second to current. `downsampled` is simply a down-sampled copy of `v` and `i` after application of an anti-aliasing filter. `shaped` is the result of applying a whitening filter such that the current EN takes a flat PSD. `bpfed` are the shaped signals after band-pass filtering with a zero-phase, 6^{th} order Butterworth band-pass filter with bandwidth as determined by `fedges`. `powers` are the result of low pass filtering the square of the band-pass filtered signals (*ie* they are a time average of the square, giving the signal power). `z`, the noise resistance, is then the square root of the ratio of the two signal powers.
- `v`, `i` and `fs`:
  These are the raw EN input potential and current measurements from which to estimate the noise resistance and cross-correlation. `fs` is the sample frequency in Hertz.

- `fedges`:
  `fedges` is a vector describing the bandwidths over which the calculation is to be performed. `fedges=[f1 f2]` results in a single estimate over the frequency range of `f1` to `f2`. `fedges=[f1 f2 f3]` results in a pair of estimates, the first over `f1` to `f2`, the second over `f2` to `f3`. This may be extended up to an arbitrary number of sub-bands. The narrower each individual sub-band is, the greater the frequency resolution of the estimate. The output `f` is a vector containing the centre frequency of each sub-band. `length(f)` is equal to `length(fedges)-1`.
- `nSigma` and `T`:
  `T` determines the length of the final low-pass filter stage for the signal power calculation. It sets the time resolution of the estimate. `length(T)` should be equal to `length(fedges)-1`. If `T` is not specified, then for each estimate over the bandwidth determined by `fedges`, a value of `T` is found such that the normalised variance of the estimate is equal to `nSigma`. According to the theory, if the signal bandwidth is W, then there is a trade off between W, `nSigma` and `T` approximating $W\times$ `nSigma` $\times$ `T` $=$ constant.
- `nmem`:
  To save on calculation complexity, the whitening stage of signal conditioning is confined to the frequencies above the cut-off frequency of the band-pass filter. By specifying an `nmem`> 1, the whitening filter whitens down to `nmem` times lower than this cut-off frequency. `nmem` defaults to 1.
- `norm`:
  The noise resistance is usually calculated using the root-mean-square, $\sqrt{\overline{|x|^2}}$, as an estimate of standard deviation. By using a different norm, a different order estimate can be achieved using $\sqrt[n]{\overline{|x|^n}}$, where n=`norm`. *eg* `norm`$= 1$ uses the mean of the absolute value, $\overline{|x|}$, which might be useful if the data contains some intermittent spikes. `norm` defaults to 2.
- `ovrlap`:
  Deprecated for the present implementation of MAVFilt.
- Dimensions of `z` and `r`:
  Each estimate is a continuous time dependent quantity and is therefore a vector of the same length as `v` and `i`. If m =`length(f)` and n =`length(v)`=`length(i)`, then `size(z)`=`size(r)`$= [mn]$ so that `z` is a matrix with time on the horizontal and frequency on the vertical.

Example :

```
% Define a time varying capacitance that starts at 10uF and
```

```
% and finishes at 100uF.
C=11e-9*(1:8192) + 10e-6;
C = C'*[1 1];

% Synthesise some EN using the capacitance.
[v,i,dvdt,is]=visynth5(8192,C,[-680,-690],
[0.1 0.1 0.01 0.01], [200 -200 150 -130],
0.025, [0 0 0 0],ones(2048,1)/512);

% Calculate the noise resistance over 5 sub-bands between
% 10-1Hz and 101Hz with a 0.05 normalised variance.
fedges=logspace(-1,1,6);
[z,r,f,t]=nsigmaimpedance(v,i,40,0.05,fedges);

% Plot the results
idx=1:5:length(z);
surf(t(idx),log10(f),20*log10(z(:,idx)));
shading interp;
view (120,30)
xlabel('Time (s)')
ylabel('Frequency (log_{10} Hz)')
zlabel('Noise Resistance (dB-Ohms)')
```

See also :

optimumRxx, RnVariance, RnVarianceSim, SVariance, SExpected, normSVariance, normSVarianceSolveW1, normSVarianceSolveT, normSVarianceSolveW2, normSVarianceSim

Source :

```
function [z, r, f, t, downsampled, shaped, bpfed, powers] =
   nSigmaImpedance (v, i, fs, nSigma, fedges, nmem, norm,
      ovrlap, T)

% if (nargin < 9) use default T
if (nargin < 8)
   ovrlap = 0;
end
if (nargin < 7)
   norm = 2;
end
if (nargin < 6)
```

```
   nmem = 1;
end

% Make a row vector
szv = size(v);
if (szv(2)>szv(1))
   v=v';
end
szi = size(i);
if (szi(2)>szi(1))
   i=i';
end

Tmax = length(v) / fs;
f1 = fedges(1:(length(fedges)-1));
f2 = fedges(2:length(fedges));
if (nargin < 9)
   disp ('Solving for required time intervals ...')
   % normSVariance returns a T that specifies interval [-T, T]
   T = normSVarianceSolveT (2*pi*f1, 2*pi*f2, nSigma, Tmax/2)
end
T=T*2; % Convert to [0, T]

f=[];
z=[];
r=[];

for n=1:length(f1)

  disp (['Analysing over bandwidth [' num2str(f1(n)) ', '
  num2str(f2(n)) '] Hz'])

  if T(n) < 0.98*Tmax
  % nyquist to at least 4x upper bandwidth
  R = fs/f2(n)/8;
  % But lets not be silly about it
  if (length(v)<1024*R)
    R = length(v)/1024;
    if (R < 1)
      R = 1;
```

```
  end
end
loglen = log(length(v))/log(2);
if ((loglen-floor(loglen)) == 0)
  % for efficient FFT
  R = 2^floor(log(R)/log(2));
else
  R = floor(R);
end
if (R < 1) R = 1; end
  RR = factor(R);
  while (max(RR) > 8)
    R = R-1;
    RR = factor(R-1);
  end
  fsn = fs/R;
  vFilt = v-v(1);
  iFilt = i-i(1);

  disp ('     downsampling ...');
  for j=1:length(RR)
    vFilt = decimate (vFilt, RR(j));
    iFilt = decimate (iFilt, RR(j));
  end
  downsampled = [vFilt iFilt];

  disp ('     shaping ...');
  nnmem = nmem * fsn/f1(n);
  if (nnmem > 0)
    [vFilt, iFilt] = shape( vFilt, iFilt, nnmem);
  end
  shaped = [vFilt iFilt];

  % Consruct a zero phase filter
  disp ('     BPFing ...');
  [a, b, c, d] = butter(6, [f1(n) f2(n)]/(fsn/2));
  coeff=ss2sos(a,b,c,d);
  imp=zeros(length(vFilt),1); imp(1)=1;
  h=sosfilter (coeff, imp);
  H=abs(fft(h));
```

```
    vFilt = BrickBPF (vFilt, f1(n), f2(n), fsn, 0, H);
    iFilt = BrickBPF (iFilt, f1(n), f2(n), fsn, 0, H);
    bpfed = [vFilt iFilt];

    disp ('     Calculating powers ...');
    vFilt = abs(vFilt).^norm;
    iFilt = abs(iFilt).^norm;
    vFilt = MAVFilt(vFilt,fsn*T(n), ovrlap*fsn*T(n));
    iFilt = MAVFilt(iFilt,fsn*T(n), ovrlap*fsn*T(n));
    powers = [vFilt iFilt];

    disp ('     Calculating resistance ...');
    res = (vFilt./iFilt) .^ (1/norm);

    disp ('     Calculating correlation ...');
    cor = MAVFilt(bpfed(:,1).*bpfed(:,2),fsn*T(n),
              ovrlap*fsn*T(n) )
          ./ sqrt( powers(:,1).*powers(:,2) );

    disp ('     Upsampling ...');
    res = interp (res, R);
    cor = interp (cor, R);
    z = [z res(1:length(v))];
    r = [r cor(1:length(v))];
    f = [f sqrt(f1(n)*f2(n))];

  else
    disp (['Warning: At n=' num2str(n) ', T(n)='
          num2str(T(n)) ' is too large']);
  end

end

t = (0:(length(v)-1)) / fs;
z=z';
f=f';
```

A.6 optimumRxx

Name :

`optimumRxx` - Determines whether a signal with the given auto-correlation function yields an optimum variance estimate with respect to its power spectral density.

Synopsis :

```
[D1,D2]=optimumRxx (Rxx,f,T)
```

Description :

$\texttt{D1} = \int_0^{2T} \left(1 - \frac{\tau}{2T}\right) R_{xx}(\tau) \left[R_{xx}(0)\cos(2\pi f_m \tau) - R_{xx}(\tau)\right] \mathrm{d}\tau$

$\texttt{D2} = \int_0^{2T} \left(1 - \frac{\tau}{2T}\right) \left[R_{xx}(0)\cos(2\pi f_m \tau) - R_{xx}(\tau)\right]\left[R_{xx}(0)\cos(2\pi f_m \tau) - 3R_{xx}(\tau)\right] \mathrm{d}\tau.$

A signal that has an auto-correlation function of $R_{xx}(t)$ that satisfies `D1` $= 0$ and `D2` > 0 for all f_m within the signal's bandwidth has a minimum variance of signal power over a fixed time interval of 0 to 2T. Thus a signal possessing such an auto-correlation function is optimally suited (with respect to its PSD) to variance estimation by the mean of the square.

This function returns `D1` and `D2` numerically calculated for the given `Rxx` and `T` at the frequencies contained in `f`.

The `Rxx` is assumed to cover the interval [0, 2T).

Example :

```
t=(0:1599)/40;      % Time interval [0 40)
W2=2*pi;            % Upper cut-off 1Hz
W1=2*pi/10;         % Lower cut-off 0.1Hz

% Compute the auto-correlation of a signal with a flat PSD
% within its limited bandwidth of W1 to W2 radians per second.
Rxx=(sin(W2*t)-sin(W1*t))/pi./t;
Rxx(1)=(W2-W1)/pi;

% Test the auto-correlation function against the criteria for
% an optimal variance estimate over 10-1.5Hz to 100.5Hz
fm=logspace(-1.5,0.5);
[d1,d2]=optimumrxx(Rxx,fm,length(Rxx)/40/2);

% Plot the results
subplot(2,1,1); semilogx(fm,d1); grid
subplot(2,1,2); semilogx(fm,d2); grid
```

The first plot shows the D1 function to be approximately zero over 0.1 Hz to 1 Hz and the second plot shows the D2 function to be positive over the interval. The signal power over a 40 second interval is therefore a near-optimal estimator (but still sub-optimal as D1 is not identically zero) of signal variance with respect to its PSD.

See also :

shape, MAVFilt, nSigmaImpedance, normSVariance

Source :

```
function [D1,D2]=optimumRxx (Rxx,f,T)

N=length(Rxx);
Rxx=tocolumnvector(Rxx);

% work out the time subdivisions for numerical
% approximation to the integral
dt = 2*T/N;
t=((0:(N-1))*dt)';
%t=0:dt:(2*T-dt);

D1=[];
D2=[];

for n=1:length(f)
  u = cos(2*pi*f(n)*t);

  d1 = 8*(1-t/2/T).*Rxx.*(Rxx(1)*u-Rxx)/(Rxx(1)^3)/T;
  d2 = 4*(1-t/2/T).*(Rxx(1)*u - Rxx).*(Rxx(1)*u -
       3*Rxx)/(Rxx(1)^4)/T;

  D1 = [D1 sum(d1)*dt];
  D2 = [D2 sum(d2)*dt];
end
```

A.7 RnVariance

Name :

RnVariance - Calculates the expectation and variance of a noise resistance calculation.

Synopsis :

`[meanR, varR] = RnVariance (k, R)`

Description :

Determines, by calculation, the expectation and variance of a noise resistance calculation, using an ideal resistance of `R` constrained to relative estimation variance of `k`.

Example :

`[m,v]=rnvariance(0.1,1000)` Gives `m`=1026.7 and `v`=5.7095×10^4.

See also :

RnVarianceSim, SVariance, SExpected, normSVariance.

Source :

```
function [meanR, varR] = RnVariance (k, R)

szk = size(k);
if (szk(2) > szk(1))
  k = k';
end;

n = 2./k;
Dn = chi2DCoeff (n);

meanR = R * Dn;
varR = (n./(n-2) - Dn.*Dn)*R*R;
```

A.8 RnVarianceSim

Name :

`RnVarianceSim` - Performs a monte-carlo simulation to estimate the expectation and variance of a noise resistance calculation.

Synopsis :

`[meanR, varR] = RnVarianceSim (k, R, N)`

Description :

Determines, by simulation, the expectation and variance of a noise resistance calculation, using an ideal resistance of `R` constrained to relative estimation variance of `k`, with `N` runs in the monte-carlo simulation.

Example :

```
k=logspace(-2, -1,10);
[m,v]=rnvariance(k,1000);
[msim,vsim]=rnvariancesim(k,1000,64);
loglog(k,v./m./m,'-', k,vsim./msim./msim,'.')
```

See also :

RnVariance, SVariance, SExpected, normSVariance.

Source :

```
function [meanR, varR] = RnVarianceSim (k, R, N)

% Use a two second interval
W1 = 1;
W2max = normSVarianceSolveW2 (min(k), 1);
fs = 2 * W2max/2/pi * 10;
Nx = round (2.1*fs); % 2.1 seconds
Nx = 2^ceil(log(Nx)/log(2)); % help the FFT

meanR = zeros(length(k), 1);
varR = zeros(length(k), 1);

for kk = 1:length(k)

   sumR = 0;
      sumR2 = 0;
   f1 = W1/2/pi;
   f2 = normSVarianceSolveW2 (k(kk), 1) /2/pi;

   for nn=1:N
      v = R*generatesignal(2*pi*f1, 2*pi*f2, Nx/fs, fs);
      i = generatesignal(2*pi*f1, 2*pi*f2, Nx/fs, fs);
      NCalc = 2*fs; % 2 seconds (ie T=1s)
      NCalc = round( NCalc+unifrnd(-0.5,0.5,1,1) );
      estR = RnCalc(v(1:NCalc),i(1:NCalc),NCalc);
      sumR = sumR + estR;
      sumR2 = sumR2 + estR*estR;

   end

   meanR(kk) = sumR/N
   varR(kk) = sumR2/N - meanR(kk)*meanR(kk)
```

```
end
```

A.9 SExpected

Name :

`SExpected` - Calculates the expected power of a white, band-limited signal.

Synopsis :

```
ex = SExpected (W1, W2)
```

Description :

Calculates `ex` = `(W2-W1)`/π. If `length(W1)` = m and `length(W2)` = n, then `size(ex)` = $[m, n]$.

Example :

`sexpected(2*pi/10,2*pi)` gives `ex`=1.8000.

See also :

SVariance, normSVariance.

Source :

```
function ex = SExpected (W1, W2)

ex = zeros(length(W1), length(W2));
for m=1:length(W1)
   for n=1:length(W2)
      ex(m,n)=(abs(W2(n)-W1(m)))/pi;
   end
end
```

A.10 shape

Name :

`shape`

Synopsis :

```
[vs, is] = shape (v, i, nmem, Nwidth, Nadv, T)
```

Description :

Shapes `i` such that it is white over time scales of `Nwidth` samples. Applies the same filter to `v`. Theoretically then, `psd(vs)` is equal to `psd(v)/psd(i)`. `Nwidth` defaults to the length of `v`. The first `Nadv` points of each filtration are

used and the next window is advanced by the same amount. It defaults to `Nwidth`. Scaling is done so that the PSD of the output at $f = 1$ equals the PSD of the input at $f = 1$. `T` is the sample rate, which is used for scaling purposes only. `T` defaults to 1.

`nmem` gives the order of the MEM PSD estimate model for construction of the whitening filter. If nmem is zero, all that is done is to remove the mean from `v` and `i`.

Example :

```
raw=flickergenerate(1,1,8192,2);
[vs,is]=shape(raw(:,1),raw(:,2), 40);
subplot(2,2,1); plot(raw(:,1)); title('Raw Potential');
subplot(2,2,2); plot(raw(:,2)); title('Raw Current');
subplot(2,2,3); plot(vs); title('Shaped Potential');
subplot(2,2,4); plot(is); title('Shaped Current');
```

See also :

nSigmaImpedance, MAVFilt.

Source :

```
function [vs, is, amem] = shape (v, i, nmem, Nwidth, Nadv, T)

v = ToColumnVector (v);
i = ToColumnVector (i);


if nargin < 6
   T = 1;
end
if nargin < 5
   Nwidth = length(v);
end
if nargin < 4
   Nadv = Nwidth;
end
if (Nadv > Nwidth)
   disp ('Shape: Warning - Nadv > Nwidth.  Clipping it back ...')
   Nadv = Nwidth;
end
```

```
if (nmem == 0)

   v = v-mean(v);
   i = i-mean(i);

else

   nmem = round(nmem);
   v = v-v(1);
   i = i-i(1);
   idx1 = 1;
   idx2 = round(idx1+Nwidth-1);
   vzf = zeros(nmem,1);
   izf = zeros(nmem,1);
   vs = zeros(length(v),1);
   is = zeros(length(i),1);

   while (idx1 <= length(v))
      if (idx2 <= length(v))
         vsn = v(idx1:idx2);
         isn = i(idx1:idx2);
      else
         vsn = [v(idx1:length(v)); zeros(idx2-length(v),1)];
         isn = [i(idx1:length(i)); zeros(idx2-length(i),1)];
      end

      [pyy,f,amem] = pyulear (isn, nmem, length(isn));
      % bii = amem / sum(amem); % Original scaling

      % Scaling so that PSD at f=1 remains unchanged
      n=0:(length(amem)-1);
      bii = amem / abs(sum(amem.*exp(-2*pi*sqrt(-1)*T*n')));

      % aii = zeros(1,length(bii)); aii(1) = 1;
      aii = 1;

      if (idx1 == 1)
 % filter the first set in the reverse direction
         [dummy, vzf] = filter (bii, aii, v(nmem:-1:1));
         [dummy, izf] = filter (bii, aii, i(nmem:-1:1));
```

```
        end

        idx2 = round(idx1 + Nadv - 1);
        vsn = vsn(1:idx2-idx1+1);
        isn = isn(1:idx2-idx1+1);
        [vsn, vzf] = filter (bii, aii, vsn, vzf);
        [isn, izf] = filter (bii, aii, isn, izf);
        vs(idx1:idx2) = vsn;
        is(idx1:idx2) = isn;
        idx1 = idx2+1;
        idx2 = round(idx1+Nwidth-1);

    end

    vs=vs(1:length(v));
    is=is(1:length(i));

end
```

A.11 SVariance

Name :

`SVariance` - Computes the variance of a signal's power over a set bandwidth and time interval.

Synopsis :

```
sigma = SVariance (W1, W2, T)
```

Description :

Calculates the variance, `sigma`, of $\frac{1}{2T}\int_{-T}^{T} x^2(t)\mathrm{d}t$ when x is normal and white, but band-limited to between `W1` and `W2` (radians per second).

If `length(W1)` $= i$, `length(W2)` $= j$ and `length(T)` $= k$ then `sigma` is an $i \times j \times k$ three dimensional matrix.

Note that `sigma` is theoretically dependent on `W1` $\times$ `T` and `W2` $\times$ `T`. `T` therefore defaults to 1, but it may take an array of values.

Example :

```
W1=0.01;
W2=logspace(-1, 1);
T=20;
sigma=svariance(W1,W2,T);
```

```
loglog((W2-W1)*T,sigma)
```

See also :

normSVariance, SExpected.

Source :

```
function sigma = SVariance (W1, W2, T)

if nargin == 2
   T=1;
end

sigma = zeros(length(W1),length(W2),length(T));

for k=1:length(T)
   sigma(:,:,k) = calculate (W1, W2, T(k));
end


function sigma = calculate (W1, W2, T)
% W1(n), W2(m) are vectors, sigma is nxm matrix.
% T is scalar.

W1 = tocolumnvector(W1);
W2 = tocolumnvector(W2)';

n=length(W1);
m=length(W2);

W1 = W1*ones(1,m);
W2 = ones(n,1)*W2;

W1=2*W1*T;        % Depends only on W1*T and W2*T !!
W2=2*W2*T;
SM = W1+W2;
DF = abs(W1-W2); % Interchanges W1/W2 roles if W1 > W2

a = 0;

a = a + DF.*sineint(DF);
a = a + W1.*sineint(2*W1);
```

```
a = a + W2.*sineint(2*W2);
a = a - SM.*sineint(SM);
a = 2*a;

a = a +   cosint(2*W1);
a = a +   cosint(2*W2);
a = a + 2*cosint(DF);
a = a - 2*cosint(SM);

a = a +   cos(2*W2);
a = a +   cos(2*W1);
a = a + 2*cos(DF);
a = a - 2*cos(SM);

a = a - 2;

sigma = a/2/T/T/pi/pi;
```

A.12 viSynth2

Name :

`viSynth2` - Simulates an EPN/ECN measurement using a potential source model.

Synopsis :

```
[v, i] = viSynth2 (v1, v2, r1, r2, C1, C2, T)
```

Description :

Synthesises a potential/current EN measurement of a coupled pair of electrodes. The electrodes are assumed to have Thevenin equivalent potential EN sources as given by `v1` and `v2` and Thevenin equivalent impedances consisting of the parallel combination of the polarisation resistance and double layer capacitance of `r1/C1` and `r2/C2`. `r1` and `r2` can be vectors of the same length as `v1` and `v2` to allow a time varying polarisation resistance. `C1` and `C2` are constants.

The sample rate is `T` seconds per sample.

Example :

```
T=0.025;
% Synthesise the EN sources
source=flickergenerate(3,T,8192,2);
```

```
% Simulate EPN/ECN measurement
[v,i] = visynth2(source(:,1)-normrnd(-700,5),
source(:,2)-normrnd(-700,5), 2000,
500, 100e-6, 100e-6, T);
% Compute and plot the spectral noise impedance
[z,f]=zmansfeld(v,i,T,4);
loglog(f,z)
```

See also :

viSynth3, viSynth5, flickerGenerate, MakeECN, Matlab Native Function: normrnd.

Source :

```
function [v, i, p1, p2] = viSynth2 (v1, v2, r1, r2, C1, C2, T)

if (length(r1) == 1)
  r1 = r1*ones(size(v1));
end
if (length(r2) == 1)
  r2 = r2*ones(size(v2));
end

N = length (v1);
e = v1-v2;
dg1 = derivative (1./r1, T);
dg2 = derivative (1./r2, T);

i = zeros (N, 1);
va = zeros (N, 1);
vb = zeros (N, 1);
p1 = zeros(N,1);
p2 = zeros(N,1);

rC1 = C1/(C1+C2);
rC2 = C2/(C1+C2);

% Fill in initial values with a rough guess
for n=1:4
   va(n) = r2(n)*v1(n) / (r1(n) + r2(n));
   vb(n) = r1(n)*v2(n) / (r1(n) + r2(n));
   i(n) = e(n) / (r1(n) + r2(n));
```

```
end

lastG1 = 0;
lastG2 = 0;
lastDG1 = 0;
lastDG2 = 0;

for n=5:N

   if (mod(n, 100) == 0)
      disp(n)
   end

   G1=1/r1(n);
   G2=1/r2(n);
   dG1=dg1(n);
   dG2=dg2(n);

   dif = rC1*G2 - rC2*G1;
   summ = rC1*G2 + rC2*G1;
   trans = rC2*dG1 - rC1*dG2;

   smallDif = ( 200*abs(dif) <= summ );
   smallC = ( C1+C2 <= summ*T/pi );

   hasChanged = (n == 5);
   hasChanged = hasChanged + (G1-lastG1)/G1 > 0.01;
   hasChanged = hasChanged + (G2-lastG2)/G2 > 0.01;
   hasChanged = hasChanged + (dG1 < 0.99*lastDG1) +
                    (dG1 > 1.01*lastDG1);
   hasChanged = hasChanged + (dG2 < 0.99*lastDG2) +
                    (dG2 > 1.01*lastDG2);

   if hasChanged
      lastG1 = G1;
      lastG2 = G2;
      lastDG1 = dG1;
      lastDG2 = dG2;
      % Design the current Filter
      if smallDif
```

```
        a0 = rC1+rC2;
        b0 = rC1*G2; % = rC2*G1 since dif=0
        b1 = (C1+C2)*rC1*rC2;

        b = [b1 b0];
        a = [a0];

        wc = max(pi/T, b0/b1);
bLPF = wc;
aLPF = [1 wc];

pin=1;

     else
        if smallC
   a0 = (G1+G2)*dif + (C1+C2)*trans;
           b0 = G1*G2*dif + (C1+C2)*rC1*rC2*(G2*dG1-G1*dG2);
           b1 = (C1+C2)*summ*dif +
                (C1+C2)*(C1+C2)*rC1*rC2*trans;
           b2 = (C1+C2)*(C1+C2)*rC1*rC2*dif;

           b = [b2 b1 b0];
           a = [a0];

           wc = max(sqrt(b0/b2), pi/T);
           bLPF = wc^2;
           aLPF = [1 1.414*wc wc^2];

           pin=2;

        else
           a0 = (G1+G2)*dif + (C1+C2)*trans;
           a1 = (C1+C2)*dif;
           b0 = G1*G2*dif + (C1+C2)*rC1*rC2*(G2*dG1-G1*dG2);
           b1 = (C1+C2)*summ*dif +
                (C1+C2)*(C1+C2)*rC1*rC2*trans;
           b2 = (C1+C2)*(C1+C2)*rC1*rC2*dif;

           b = [b2 b1 b0];
           a = [a1 a0];
```

```
            wc = max([sqrt(b0/b2) a0/a1 pi/T]);
            bLPF = wc;
            aLPF = [1 wc];

            p1n=3;

         end % smallC

      end % smallDif

      % Digitise the current filter
      bL = length(b);
      aL = length(a);
      if (bL + aL > 1)
         fprecious = ( b(bL)/b(1) * a(aL)/a(1) )^(1/(aL+bL-2))
            / 2 / pi;
      else
         fprecious = wc/2/pi;
      end
      b = conv(b, bLPF);
      a = conv(a, aLPF);
      [bzi, azi] = bilinear (b, a, 1/T,
            min(fprecious, sqrt(1/T/2)));

   end % hasChanged

   % Execute the current filter
   k = 0;
   for nn = 1:length(bzi);
      k = k + bzi(nn)*e(n-nn+1);
   end
   for nn = 2:length(azi);
      k = k - azi(nn)*i(n-nn+1);
   end
   i(n) = k/azi(1);
   p1(n) = p1n;

   if hasChanged
      % Design the voltage filter
```

```
if smallC
   a0 = G1+G2;
   b0 = G1;
   b1 = (C1+C2)*rC1;
   c0 = G2;
   c1 = (C1+C2)*rC2;

   c = [c1 c0];
   b = [b1 b0];
   a = [a0];

   wc = max ([c0/c1 b0/b0 pi/T]);
   bLPF = wc;
   aLPF = [1 wc];

   p2n=1;

else
   a0 = G1+G2;
   a1 = C1+C2;
   b0 = G1;
   b1 = (C1+C2)*rC1;
   c0 = G2;
   c1 = (C1+C2)*rC2;

   c = [c1 c0];
   b = [b1 b0];
   a = [a1 a0];

   wc = max ([c0/c1 b0/b1 a0/a1 pi/T]);
   bLPF = wc;
   aLPF = [1 wc];

   p2n=2;

end % smallC

% Digitise the voltage filter
cL = length(c);
bL = length(b);
```

```
   aL = length(a);
   if (bL + aL > 1)
      fpreciousB =
         (b(bL)/b(1)*a(aL)/a(1))^(1/(aL+bL-2))
         / 2 / pi;
   else
      fpreciousB = wc/2/pi;
   end

   if (cL + aL > 1)
      fpreciousC=
         (b(bL)/b(1)*a(aL)/a(1))^(1/(aL+bL-2))
         /2/pi;
   else
      fpreciousC = wc/2/pi;
   end

   c = conv(c, bLPF);
   b = conv(b, bLPF);
   a = conv(a, aLPF);
   [bzv, azvb] = bilinear (b, a, 1/T,
           min(fpreciousB, sqrt(1/T/2)));
   [czv, azvc] = bilinear (c, a, 1/T,
           min(fpreciousC, sqrt(1/T/2)));

end % hasChanged

% Execute the Voltage Filter
k = 0;
for nn = 1:length(bzv)
   k = k + bzv(nn)*v1(n-nn+1);
end
for nn = 2:length(azvb)
   k = k - azvb(nn)*va(n-nn+1);
end
va(n) = k/azvb(1);
k = 0;
for nn = 1:length(czv)
   k = k + czv(nn)*v2(n-nn+1);
end
```

```
    for nn = 2:length(azvc)
       k = k - azvc(nn)*vb(n-nn+1);
    end
    vb(n) = k/azvc(1);
    p2(n) = p2n;

end % for n=5:N

v = va+vb;
```

A.13 VIZEstimate

Name :

`VIZEstimate` - Estimates some frequency domain characteristics of a potential/current EN pair.

Synopsis :

`[pV, pI, Z, f, EV, EI] = VIZEstimate (v,i,N,T,window)`

Description :

Estimates the potential PSD, `pV`, the current PSD, `pI`, the expectation of the potential and current Fourier transforms, `EV` and `EI` and the expectation of the ratio of the potential and current Fourier transforms, `Z`.

$$\begin{aligned} \texttt{pV} &= \mathrm{E}\left[|V(f)|^2\right], \\ \texttt{pI} &= \mathrm{E}\left[|I(f)|^2\right], \\ \texttt{EV} &= \mathrm{E}\left[V(f)\right], \\ \texttt{EI} &= \mathrm{E}\left[I(f)\right], \\ \texttt{Z} &= \mathrm{E}\left[\frac{V(f)}{I(f)}\right]. \end{aligned}$$

These quantities are useful for the spectral noise impedance calculation and for construction of a noise impedance Nyquist diagram.

`v` and `i` are the input potential and current EN waveforms. The expectations are estimated by dividing `v` and `i` into 50 % overlapped segments each of length `N`. The mean is subtracted from each segment and then multiplied by the `window` function. `window` defaults to `hanning(N)`. The corresponding operation is then performed on each segment (*eg* Fourier transform then absolute value then square for `pV`) and the result averaged over all the segments.

`f` gives the frequency vector over which the outputs are estimated.

Example :

```
[v,i,dvdt,is]=visynth5(8192,[100e-6 100e-6],[-680,-690],
                [0.1 0.1 0.01 0.01], [200 -200 150 -130],
                0.025, [0 0 0 0], ones(2048,1)/512);
[pv,pi,z]=vizestimate(v,i,512,0.025);
[x,y]=noisenyquist(pv,pi,z,512);
plot(abs(x),y, '.')
```

Synthesises some EN data for an asymmetric system and generates a Nyquist impedance diagram from it.

See also :

ZMansfeld, NoiseNyquist, nSigmaImpedance, RnCalc.

Source :

```
function [pV, pI, Z, f, EV, EI] = VIZEstimate (v,i,N,T,window)

if nargin < 5
   window = hanning(N);
end

if nargin < 4
   T=1;
end

NN = length(v);
pV = zeros(N,1);
pI = zeros(N,1);
EV = zeros(N,1);
EI = zeros(N,1);
Z = zeros(N,1);
n = 0;
idx = 1;

while (idx+N < NN)
   vfft = v(idx:(idx+N-1));
   vfft = vfft - mean(vfft);
   vfft = fft(vfft.*window);

   ifft = i(idx:(idx+N-1));
   ifft = ifft - mean(ifft);
   ifft = fft(ifft.*window);
```

```
    pV = pV + abs(vfft.*vfft);
    pI = pI + abs(ifft.*ifft);
    EV = EV + vfft;
    EI = EI + ifft;
    Z = Z + vfft./ifft;
    n = n+1;
    idx = round(idx+N/2);
  en

  pV = pV/n;
  pI = pI/n;
  EV = EV/n;
  EI = EI/n;
  Z = Z/n;

  f=fftshift( ( (-N/2):(N/2-1) ) /N/T );
```

A.14 ZMansfeld

Name :

ZMansfeld - Computes the spectral noise impedance of a potential/current EN pair.

Synopsis :

`[z, f, sv, si] = ZMansfeld (v, i, T, RF)`

Description :

Computes the spectral noise impedance, **z**, as determined by $\sqrt{\frac{S_v(f)}{S_i(f)}}$, where $S_v(f)$=**sv** and $S_i(f)$=**si** are the power spectral densities of the input waveforms, **v** and **i**. **f** is the frequency vector over which **z** is estimated.

T gives the sample rate, which is used for appropriate scaling. **RF** determines the size of each overlapping segment, **nfft** = verb—length(v)/RF—. **RF** defaults to 4, which results in 7 overlapping segments.

Example :

```
[v,i,dvdt,is]=visynth5(8192,[100e-6 100e-6],[-680,-690],
              [0.1 0.1 0.01 0.01], [200 -200 150 -130],
              0.025, [0 0 0 0], ones(2048,1)/512);
[z,f,sv,si] = zmansfeld(v,i,0.025,4);
loglog(f,z)
```

Synthesises some EN then calculates and plots its spectral noise impedance.

See also :

VIZEstimate, nSigmaImpedance, noiseresistance, Matlab Native Function: psd.

Source :

```
function [z, f, sv, si] = ZMansfeld (v, i, T, RF)

if nargin < 4
   RF = 4;
end

NFFT = length(v);
NFFT = log(NFFT)/log(2);
NFFT = 2^floor(NFFT);
NFFT = NFFT/RF;

[sv, f] = psd (v, NFFT, 1/T, hanning (NFFT), NFFT/2, 'mean');
 si     = psd (i, NFFT, 1/T, hanning (NFFT), NFFT/2, 'mean');
 z = sqrt (sv./si);
```

Appendix B

Publications

The work described in the thesis has been presented at four conferences, [139], [140], [129], [132] and published in three refereed journal articles [88], [130], [28]. It is expected that two additional refereed journal articles will be published in the Journal of the Electrochemical Society [131] and Corrosion Science [133].

Appendix C

The Author's Electrochemical Noise Instrumentation

Eden [40] asserts that an important part of EN measurements is "a knowledge of the intrinsic noise of the instrumentation itself ... as is the immunity to adventitious noise arising from external sources." To that end, this appendix provides some technical background on the instrument used for EN measurements in this work. The data presented helps distinguish between EN and measurement noise. Apart from measurement noise, other instrumentation side effects that might be taken into account in the analysis are examined.

Section C.1 lists the documented specifications of the instrument. Section C.2 gives the results of a frequency response test. Section C.3 discusses the issue of sample rate and Section C.4 investigates the level of measurement noise introduced by the instrument and the reference electrode ($Ag^+/AgCl$).

C.1 Instrument Specifications

The instrument under investigation is the AutoZRA (superseded by the Gill AC), from ACM instruments, UK. The unit provides connectors for two working electrodes (WE1 and WE2) and one reference electrode (RE). Internally the two working electrodes are connected via a zero resistance ammeter with potential logging capabilities of 10^{13} Ω input impedance. Using a 24 bit analogue to digital converter, it is capable of simultaneously logging potential and current EN to a microcomputer via a serial connection with a maximum sample rate of 50 samples/sec. The zero resistance ammeter is equipped with a range selector by means of a counter resistance.

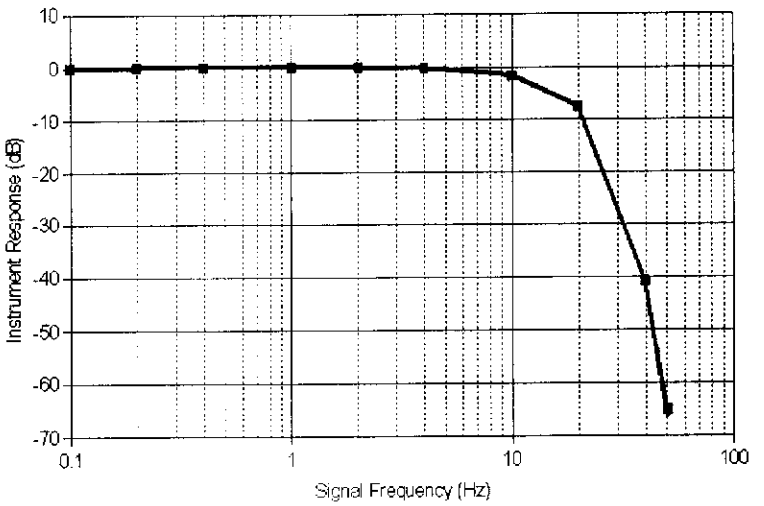

Figure C.1: Frequency Response of ACM AutoZRA

C.2 Frequency Response

A sine wave voltage generator was connected between a working electrode and reference electrode connection. The signal was logged via the AutoZRA for input frequencies from 0.1 Hz up to 50 Hz and for sample periods from 25 ms (40 samples/sec) up to 325 ms (3.1 samples/sec). The input amplitude and frequency was simultaneously monitored by an analogue cathode ray oscilloscope (CRO).

Figure C.1 shows the frequency response of the AutoZRA as determined by correlating the reading on the CRO with the data logged by the AutoZRA. The plot represents how much a signal is attenuated by the AutoZRA as a function of signal frequency. The response is found to be completely independent of sample rate. It has a 3 dB pass band from 0 Hz up to approximately 13 Hz and a 40 dB stop band from about 40 Hz upward. The high frequency roll-off is estimated to be -80 dB/dec.

These parameters are consistent with a 4^{th} order Butterworth low pass filter, with a cut-off frequency of 13 Hz.

C.3 Sample Rate

The instrument is limited to a sample rate of 50 samples/sec. Because much of the work reported in this thesis is concerned with more than just the of mean-square of the sampled EN, digital aliasing introduced by the sample process might be of some concern. As can be seen from the frequency response tests summarised in Figure C.1, the instrument does contain an anti-aliasing filter, but not one that adapts to the sample rate. With the half power pass band of the anti-aliasing filter extending up to 13 Hz, a sample rate in excess of 30 samples/sec should be adequate to avoid the majority of digital aliasing effects.

Another concern is mains interference, located at 50 Hz. While the anti-aliasing filter significantly attenuates such interference, it is found that significant residue still exists in the sampled signal. In order to ensure the aliased mains interference does not appear at random frequencies within the measurement, all sample periods in the thesis are of the form $10n + 5$ milliseconds, where n is any integer (*eg*, samples rates of 25 ms, 35 ms, 145 ms.) Such a sample rate conveniently places all aliased odd harmonics of a 50 Hz signal at half the Nyquist frequency while placing the even harmonics alternately at the Nyquist frequency and at DC. Since the even harmonics of mains interference are usually relatively small in magnitude, the majority of the mains interference therefore manifests itself at half the Nyquist frequency, where it can be easily identified and filtered off if necessary.

C.4 Measurement Noise

Being a real world device, the AutoZRA necessarily introduces noise of its own into every measurement. In addition, a reference electrode is used to facilitate potential measurements. The reference electrode ideally does not fluctuate in potential at all as it is required to provide a stable reference. However, this cannot be assumed to be the case with a practical reference. In this context, measurement noise is taken to encompass noise introduced by the AutoZRA and by the reference electrode.

C.4.1 Measurement Potential Noise

Two $Ag^+/AgCl$ reference electrodes were prepared and placed into approximately 2 % NaCl solution at room temperature. The configuration of the standard double junction reference electrodes used throughout this thesis places the actual electrode outside the cell. In that respect, the effect of cell temperature on the characteristics of the reference electrode are greatly diminished. The instrument was connected between the two reference electrodes in order to log the potential difference between them. Figure C.2 depicts the measurement setup.

Figure C.3 shows the PSD of the combined noise from two references and the instrument, as measured by the set up in Figure C.2. A useful measurement usually only consists of noise from one reference and the instrument.

Figure C.5 shows the PSD of the potential noise originating from the instrument, as determined by the set up of Figure C.4.

By comparing Figures C.3 and C.5, it can be concluded that the potential noise from the instrument is approximately white, with a magnitude of -30 dB.mV and that the potential noise originating from the pair of reference electrodes is mainly confined to below 100 mHz with a $\frac{1}{f}$ type shape, approaching a magnitude of approximately 0 dB.mV at 1 mHz. If the noise from the two references are taken to be statistically independent, it might be assumed that a single reference electrode

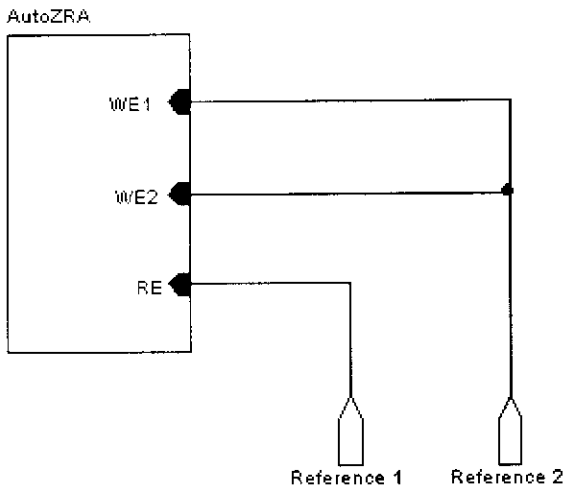

Figure C.2: Measurement of potential noise between two working electrodes

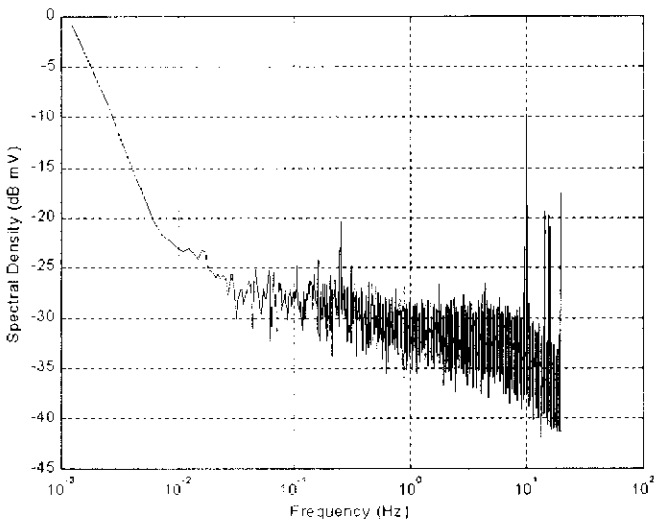

Figure C.3: PSD of measurement noise between two reference electrodes

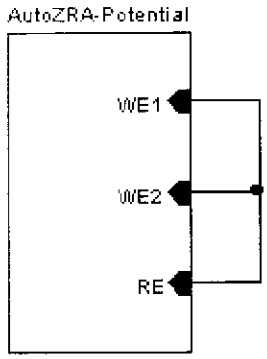

Figure C.4: Measurement of potential noise originating from the AutoZRA

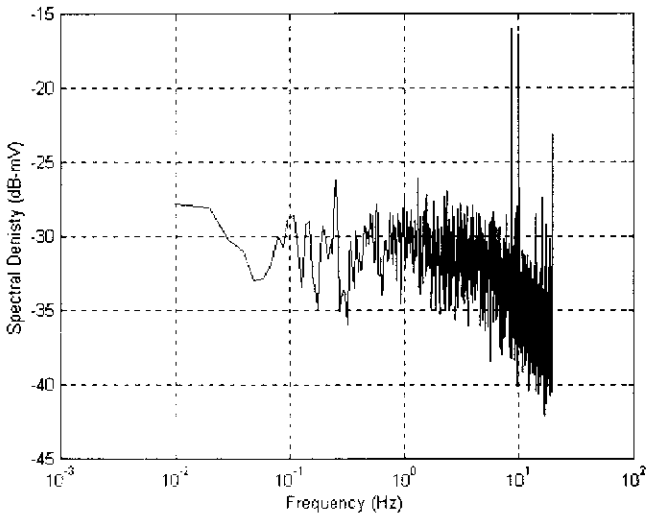

Figure C.5: PSD of measurement potential noise originating from the AutoZRA

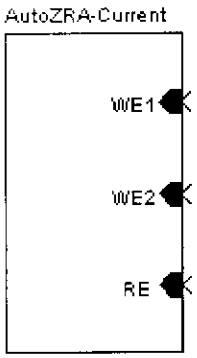

Figure C.6: Measurement of current noise originating from the AutoZRA

Counter Resistance	Maximum Range		Noise Level	Dynamic Range
	Magnitude	dB.mA	dB.mA	dB.mA
100 Ω	5 mA	11		
1 kΩ	500 μA	−9	−90	81
10 kΩ	50 μA	−29	−110	81
100 kΩ	5 μA	−49	−130	81
1 MΩ	500 nA	−69	−150	81
10 MΩ	50 nA	−89		

Table C.1: Noise level and dynamic range of a current measurement with the AutoZRA

therefore approaches approximately −3 dB.mV at 1 mHz.

C.4.2 Measurement Current Noise

The current noise originating from the instrument was measured by the set up of Figure C.6, where the ammeter is left open circuit and would ideally measure zero.

The measurement was repeated for each of the instrument's dynamic ranges. The PSDs of four of them are plotted in Figure C.7. The sample rate is 40 samples/sec, which places the odd harmonics of mains interference, after aliasing, at 10 Hz. In Figure C.7, the mains interference is clearly visible at this frequency.

The results are summarised in Table C.1.

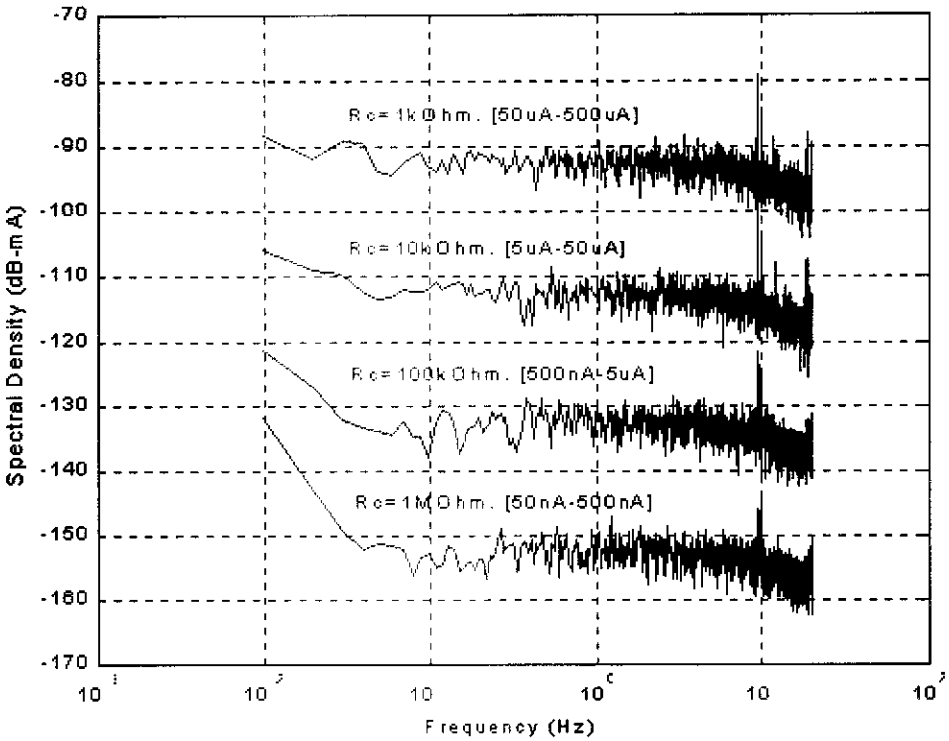

Figure C.7: Current Measurement noise of ACM AutoZRA

Appendix D

Real α and β coefficients

The problem is to prove that the $\alpha(f)$ and $\beta(f)$ coefficients in (5.6, page 105) are entirely real valued. In order to facilitate analysis, the relevant quantities are split into real and imaginary components. Let

$$V_1(f) = x_1 + \mathrm{j}y_1 \tag{D.1}$$

and

$$V_2(f) = x_2 + \mathrm{j}y_2 \tag{D.2}$$

where x_1, x_2, y_1 and y_2 are real and $\mathrm{j}^2 = -1$ and $V_\mathrm{n}(f)$ is the Fourier transform of $v_\mathrm{n}(t)$:

$$V_\mathrm{n}(f) = \int_{-\infty}^{\infty} v_\mathrm{n}(t)\cos(2\pi ft)\mathrm{d}t - \mathrm{j}\int_{-\infty}^{\infty} v_\mathrm{n}(t)\sin(2\pi ft)\mathrm{d}t \tag{D.3}$$

x_1, x_2, y_1 and y_2 are, in general, frequency dependent quantities. The (f) functional operator is omitted to simplify notation.

Let

$$\begin{aligned} x_\mathrm{A} + \mathrm{j}y_\mathrm{A} &= \frac{V_2(f)}{V_1(f) - V_2(f)} \\ &= \frac{x_2 + \mathrm{j}y_2}{(x_1 - x_2) + \mathrm{j}(y_1 - y_2)} \\ &= \frac{[x_2(x_1 - x_2) + y_2(y_1 - y_2)] + \mathrm{j}[x_1y_2 - x_2y_1]}{(x_1 - x_2)^2 + (y_1 - y_2)^2} \end{aligned} \tag{D.4}$$

where x_A and y_A are real.

Then

$$\alpha(f) = \mathrm{E}[x_\mathrm{A}] + \mathrm{j}\mathrm{E}[y_\mathrm{A}] \tag{D.5}$$

where

$$\mathrm{E}[x_\mathrm{A}] = \mathrm{E}\left[\frac{x_2(x_1 - x_2) + y_2(y_1 - y_2)}{(x_1 - x_2)^2 + (y_1 - y_2)^2}\right] \tag{D.6}$$

$$\mathrm{E}[y_\mathrm{A}] = \mathrm{E}\left[\frac{x_1y_1 - x_2y_1}{(x_1 - x_2)^2 + (y_1 - y_2)^2}\right]. \tag{D.7}$$

Let

$$\begin{aligned} x_{\mathrm{B}} + \mathrm{j}y_{\mathrm{B}} &= \frac{V_1(f)}{V_1(f) - V_2(f)} \\ &= \frac{x_1 + \mathrm{j}y_1}{(x_1 - x_2) + \mathrm{j}(y_1 - y_2)} \\ &= \frac{[x_2(x_1 - x_2) + y_1(y_1 - y_2)] + \mathrm{j}[x_1 y_2 - x_2 y_1]}{(x_1 - x_2)^2 + (y_1 - y_2)^2} \end{aligned} \tag{D.8}$$

where x_{B} and y_{B} are real.

Then

$$\beta(f) = \mathrm{E}[x_{\mathrm{B}}] + \mathrm{j}\mathrm{E}[y_{\mathrm{B}}] \tag{D.9}$$

where

$$\mathrm{E}[x_{\mathrm{B}}] = \mathrm{E}\left[\frac{x_1(x_1 - x_2) + y_1(y_1 - y_2)}{(x_1 - x_2)^2 + (y_1 - y_2)^2}\right] \tag{D.10}$$

$$\mathrm{E}[y_{\mathrm{B}}] = \mathrm{E}\left[\frac{x_1 y_1 - x_2 y_1}{(x_1 - x_2)^2 + (y_1 - y_2)^2}\right] = \mathrm{E}[y_{\mathrm{A}}]. \tag{D.11}$$

If $\mathrm{E}[y_{\mathrm{A}}]$ and $\mathrm{E}[y_{\mathrm{B}}]$ [the imaginary components of $\alpha(f)$ and $\beta(f)$] can be shown to be zero, then it follows that $\alpha(f)$ and $\beta(f)$ are entirely real valued.

By the fundamental theorem of expectation,

$$\mathrm{E}\left[\frac{x_1 y_2 - x_2 y_1}{(x_1 - x_2)^2 + (y_1 - y_2)^2}\right] = \int_{V_4} \frac{x_1 y_2 - x_2 y_1}{(x_1 - x_2)^2 + (y_1 - y_2)^2} p_{\mathrm{x_1 x_2 y_1 y_2}}(x_1, x_2, y_1, y_2)\mathrm{d}V_4 \tag{D.12}$$

where $\mathrm{d}V_4 = \mathrm{d}x_1\mathrm{d}x_2\mathrm{d}y_1\mathrm{d}y_2$ is an elemental piece of the four dimensional space, V_4 and $p_{\mathrm{x_1 x_2 y_1 y_2}}(x_1, x_2, y_1, y_2)$ is the joint probability density function of x_1, x_2, y_1, and y_2. Since $v_1(t)$ is taken to be independent of $v_2(t)$, it follows that x_1 and y_1 are independent of x_2 and y_2 so that

$$p_{\mathrm{x_1 x_2 y_1 y_2}}(x_1, x_2, y_1, y_2) = p_{\mathrm{x1y1}}(x_1, y_1) p_{\mathrm{x_2 y_2}}(x_2, y_2). \tag{D.13}$$

Due to the central limit theorem, the Fourier transform of a stationary random process has a distribution that tends to Gaussian [141] so that $p_{\mathrm{x_1 y_1}}(x_1, y_1)$ and $p_{\mathrm{x_2 y_2}}(x_2, y_2)$ both tend to bi-variate Gaussian distributions. In order to completely specify a Gaussian $p_{\mathrm{xy}}(x, y)$, the first order statistics ($\mathrm{E}[x]$ and $\mathrm{E}[y]$) and the second order statistics ($\mathrm{E}[x^2]$, $\mathrm{E}[y^2]$ and $\mathrm{E}[xy]$) or equivalently, the variances and the cross correlation) are required.

By inspection of (D.3), the expectation of the imaginary parts, $\mathrm{E}[y_1]$ and $\mathrm{E}[y_2]$, are seen to be zero for all f and the expectation of the real parts, $\mathrm{E}[x_1]$ and $\mathrm{E}[x_2]$, are seen to be zero for all non-zero f. Because of orthogonality between the real and imaginary parts in (D.3), $\mathrm{E}[x_1 y_1]$ and $\mathrm{E}[x_2 y_2]$ are both zero for stationary $v_1(t)$ and $v_2(t)$. If the variances of the real and imaginary parts of $V_{\mathrm{n}}(f)$ are respectively given by $\sigma^2_{\mathrm{x_n}}$ and $\sigma^2_{\mathrm{y_n}}$ (with $n = 1, 2$) and the mean of the real parts given by $\mu_{\mathrm{x_n}}$, then

the joint Gaussian probability density function of $V_n(f)$ is completely specified:

$$p_{x_1x_2y_1y_2}(x_1,x_2,y_1,y_2) = \frac{\exp\left[-\frac{(x_1-\mu_{x_1})^2}{2\sigma_{x_1}^2} - \frac{y_1^2}{2\sigma_{y_1}^2}\right]}{2\pi\sigma_{x_1}\sigma_{y_1}} \cdot \frac{\exp\left[-\frac{(x_2-\mu_{x_2})^2}{2\sigma_{x_2}^2} - \frac{y_2^2}{2\sigma_{y_2}^2}\right]}{2\pi\sigma_{x_2}\sigma_{y_2}} \quad \text{(D.14)}$$

where $\sigma_{x_n}^2$ and $\sigma_{y_n}^2$ are related to the PSD of $v_n(t)$ and μ_{x_n} is zero for all non-zero frequencies.

Substituting (D.14) into (D.12) by use of symbolic manipulation software (Mathcad Pro v7), it is found that the integral in (D.12) reduces to zero due to odd symmetry over the four dimensional space.

Consequently, $\mathrm{E}[y_A] = \mathrm{E}[y_B] = 0$ and it can be stated that

$$\alpha(f) = \mathrm{E}[x_A] = \mathrm{E}\left[\frac{x_2(x_1-x_2)+y_2(y_1-y_2)}{(x_1-x_2)^2+(y_1-y_2)^2}\right] \quad \text{(D.15)}$$

$$\beta(f) = \mathrm{E}[x_B] = \mathrm{E}\left[\frac{x_1(x_1-x_2)+y_1(y_1-y_2)}{(x_1-x_2)^2+(y_1-y_2)^2}\right] \quad \text{(D.16)}$$

which are both real valued quantities.

It is noted that if the two signals cannot be assumed independent, then equation (D.12) does not reduce to zero and the $\alpha(f)$ and $\beta(f)$ coefficients cannot be assumed entirely real valued. This has been confirmed by a numerical test case.

Appendix E

Complex Noise Impedance for Identical Impedances

From (5.6, page 105), (D.15) and (D.16, page 184), when the electrode impedances are identical with $Z_1(f) = Z_2(f) = Z(f)$, it follows that

$$\begin{aligned} Z_{\mathrm{sn}}(f) &= [\alpha(f) + \beta(f)]Z(f) \\ &= (\mathrm{E}[x_{\mathrm{A}}] + \mathrm{E}[x_{\mathrm{B}}])\, Z(f) \\ &= \mathrm{E}\left[\frac{x_2(x_1 - x_2) + y_2(y_1 - y_2) + x_1(x_1 - x_2) + y_1(y_1 - y_2)}{(x_1 - x_2)^2 + (y_1 - y_2)^2}\right] \cdot Z(f) \\ &= \mathrm{E}\left[\frac{x_1^2 + y_1^2 + x_2^2 + y_2^2}{(x_1 - x_2)^2 + (y_1 - y_2)^2}\right] \cdot Z(f) \\ &= \left\{\mathrm{E}\left[\left|\frac{V_1(f)}{V_1(f) - V_2(f)}\right|^2\right] - \mathrm{E}\left[\left|\frac{V_2(f)}{V_2(f) - V_2(f)}\right|^2\right]\right\} \cdot Z(f) \end{aligned} \tag{E.1}$$

Appendix F

Table of Abbreviations

AC	Alternating Current
AE	Auxiliary Electrode
ASTM	American Society for Testing and Materials
BPF	Band Pass Filter
DC	Direct Current
ECN	Electrochemical Current Noise
EES	Electrochemical Emission Spectroscopy
EIS	Electrochemical Impedance Spectroscopy
EN	Electrochemical Noise
EPN	Electrochemical Potential Noise
FIR	Finite Impulse Response filter
HPF	High Pass Filter
LED	Light Emitting Diode
LTR	Linear Trend Removal
LP	Linear Polarisation
LPF	Low Pass Filter
LPR	Linear Polarisation Resistance; Also, Linear PRediction filter
MAR	Moving Average Removal
MLE	Maximum Likelihood Estimate
PSD	Power Spectral Density
RE	Reference Electrode
WBE	Wire Beam Electrode
WE	Working Electrode
ZRA	Zero Resistance Ammeter

Table F.1: Table of Abbreviations

Bibliography

[1] ISO, *Corrosion of metals and alloys. Basic terms and definitions (ISO 8044:1999)*, 1999.

[2] G. Schmitt and S. Feinen, "Effect of anions and cations on the pit initiation in co_2 corrosion of iron and steel," in *Proceedings of Corrosion 2000*, National Association of Corrosion Engineers, 2000.

[3] National Bureau of Standards, *Economic Effects of Metallic Corrosion in the United States*, 1978. A report to the Congress.

[4] J. D. Anderton, P. J. Garnett, W. R. Liddelow, R. K. Lowe, and I. J. Manno, *Foundations of Chemistry*. Melbourne, Australia: Longman Cheshire, 1984.

[5] R. D. Kane, "Corrosion monitoring for industrial and process applications," *Corrosion Engineering*, vol. 1, no. 4, 2001. http://www.clihouston.com /news5.htm (2001-07-18).

[6] Gamry Instruments, United Kingdom, *EIS Theory*. http://www.gamry.com /g2/ftp/download/Literature/1999/EIS300.zip.

[7] F. Mansfeld, "Electrochemical impedance spectrscopy (eis) as a new tool for investigation methods of corrosion protection," *Electrochmica Acta*, vol. 35, no. 10, pp. 1533–1544, 1990.

[8] A. J. Bard and L. R. Faulkner, *Electrochemical Methods: Fundamentals and Applications*. USA: John Wiley and Sons, 1980.

[9] M. Stern and A. L. Geary *J. Electrochem. Soc.*, vol. 104, p. 56, 1957.

[10] M. Stern and E. D. Weisert *Proc. AM. Soc. Test. Mater.*, vol. 59, p. 1280, 1959.

[11] J. A. González, A. Molina, M. L. Escudero, and C. Anrade, "Errors in the electrochemical evaluation of very small corrosion rates - i. polarization resistance method applied to corrosion of steel in concrete," *Corrosion Science*, vol. 25, no. 10, pp. 917–930, 1985.

[12] J. L. Dawson, "Electrochemical noise measurement: The definitive in-situ technique for corrosion applications?," in *Electrochemical Noise Measurement for Corrosion Applications* (J. R. Kearns, J. R. Scully, P. R. Roberge, D. L. Reichert, and J. L. Dawson, eds.), ASTM STP 1277, p. 3, American Society for Testing and Materials, 1996.

[13] D. A. Eden, K. Hladky, D. G. John, and J. L. Dawson, "Electrochemical noise — simultaneous monitoring of potential and current noise signals from corroding electrodes," in *Proceedings of Corrosion 86*, National Association of Corrosion Engineers, 1986.

[14] C. Gabrielli, F. Huet, and M. Keddam, "Flucatuations in electrochemical systems. ii. application to a diffusion limited redox process," *J. Chem. Phys.*, vol. 99, no. 9, 1993.

[15] F. Mansfeld, Z. Sun, C. H. Hsu, and A. Nagiub, "Concerning trend removal in electrochemical noise measurements," *Corrosion Science*, vol. 43, no. 2, pp. 341–352, 2001.

[16] Y. J. Tan and S. I. Bailey, "The monitoring of the formation and destruction of corrosion inhibitor films using electrochemical noise analysis (ena)," *Corrosion Science*, vol. 38, no. 10, p. 1681, 1996.

[17] F. Mansfeld and C. C. Lee, "Discussion of 'the monitoring of the formation and destruction ...'," *Corrosion Science*, vol. 39, no. 6, pp. 1141–1143, 1997.

[18] J. F. Chen and W. F. Bogaerts, "The physcial meaning of noise resistance," *Corrosion Science*, vol. 37, no. 11, pp. 1839–1842, 1995.

[19] U. Bertocci, F. Huet, and M. Keddam, "Noise resistance applied to corrosion measurements i. theoretical analysis," *Journal of the Electrochemical Society*, vol. 144, no. 1, pp. 31–37, 1997.

[20] F. Mansfeld and C. C. Lee, "Frequency dependence of the noise resistance for polymer-coated metals," *J. Electrochem. Soc.*, vol. 144, no. 6, pp. 2068–2071, 1997.

[21] H. Xiao and F. Mansfeld, "Evaluation of coating degradation with electrochemical impedance spectroscopy and electrochemical noise analysis," *J. Electrochem. Soc.*, vol. 141, no. 9, p. 2332, 1994.

[22] F. Mansfeld, C. Chen, C. C. Lee, and H. Xiao, "The effect of asymmetric electrodes on the analysis of electrochemical impedance and noise data," *Corrosion Science*, vol. 38, no. 3, p. 497, 1996.

[23] Y. G. Sosulin and V. V. Kostrov, "Whitening filter: Evolution and application," *Radiotekhnika i Elektronika*, vol. 43, no. 9, pp. 1030–1043, 1998.

[24] F. Mansfeld, C. C. Lee, and G. Zhang, "Comparison of electrochemical impedance and noise data in the frequency domain," *Electrochmica Acta*, vol. 43, no. 3–4, pp. 435–438, 1998.

[25] C. C. Lee and F. Mansfeld, "Analysis of electrochemical noise data for a poassive system in the frequency domain," *Corrosion Science*, vol. 40, no. 6, pp. 959–962, 1998.

[26] Y. J. Tan, "The effect of inhomogeneity in organic coatings on electrochemical measurements using a wire beam electrode," *Progress in Organic Coatings*, vol. 19, p. 89, 1991.

[27] Y. J. Tan, "A new method for crevice corrosion studies and its use in the investigation of oil-stain," *Corrosion*, vol. 50, no. 4, p. 266, 1994.

[28] Y. J. Tan, S. Bailey, B. Kinsella, and A. Lowe, "Mapping corrosion kinetics using the wire beam electrode in conjunction with electrochemical noise resistance measurements," *J. Electrochem. Soc.*, vol. 147, no. 2, pp. 530–539, 2000.

[29] A. M. Lowe, "Electrochemical noise analysis with matlab." http://chemistry.curtin.edu.au /staff/alowe/en, 2001.

[30] Intercorr, "Classic corrosion photographs from intercorr international inc.." http://www.clihouston.com /failures.html, 2001.

[31] P. J. Gellings, *Introduction to Corrosion Prevention and Control*. The Netherlands: Delft University Press, 1985.

[32] American Society for Testing and Materials, West Conshohocken, PA, *Standard Practice for Measurement of Time-of-Wetness on Surfaces Exposed to Wetting Conditions as in Atmospheric Corrosion Testing*, 1999.

[33] American Society for Testing and Materials, West Conshohocken, PA, *Standard Practice for Perparing, Cleaning, and Evaluating Corrosion Test Specimens*, 1999.

[34] American Society for Testing and Materials, West Conshohocken, PA, *Standard Guide for Examination and Evaluation of Pitting Corrosion*, 1999.

[35] American Society for Testing and Materials, West Conshohocken, PA, *Standard Guide for On-Line Monitoring of Corrosion in Plant Equipment (Electrical and Electrochemical Methods)*, 1996.

[36] American Society for Testing and Materials, West Conshohocken, PA, *Standard Practice for Conducting Potentiodynamic Polarization Resistance Measurements*, 1997.

[37] Y. J. Tan, "Monitoring localized corrosion processes and estimating localized corrosion rates using a wire-beam electrode," *Corrosion*, vol. 54, no. 5, p. 403, 1998.

[38] G. W. Walter, "A review of impedance plot methods used for corrosion performance analysis of painted metals," *Corrosion Science*, vol. 26, no. 9, pp. 681–703, 1986.

[39] W. P. Iverson, "Transient voltage changes produced in corroding metals and alloys," *J. Electrochem. Soc.: Electrochemical Sciences*, vol. 115, p. 617, 1968.

[40] D. A. Eden, "Electrochemical noise — the first two octaves," in *Proceedings of Corrosion 98*, National Association of Corrosion Engineers, 1998.

[41] C. Gabrielli, F. Huet, M. Keddam, and R. Oltra, "A review of the probabilistic aspects of localized corrosion," *Corrosion*, vol. 46, no. 4, p. 226, 1990.

[42] C. Gabrielli, F. Huet, and M. Keddam, "Investigation of metallic corrosion by electrochemical noise techniques," in *Electrochemical and Optical Tehcniques for the Study and Monitoring of Metallic Corrosion* (M. G. S. Ferreira and C. A. Melendres, eds.), vol. 203 of *NATO ASI Series E: Applied sciences*, pp. 135–190, Dordrecht: Kluwer Academic Publishers, 1991.

[43] C. Gabrielli and M. Keddam, "Reivew of applications of impedance and noise analysis to uniform and localized corrosion," *Corrosion*, vol. 48, no. 10, pp. 794–811, 1992.

[44] Y. J. Tan, B. Kinsella, and S. I. Bailey, "Unsolved problems and new developments in electrchemical noise analysis," in *Corrosion 97*, National Association of Corrosion Engineers, 1997.

[45] A. Legat and C. Zevnik, "The electrochemical noise of mild and stainless steel in various water solutions," *Corrosion Science*, vol. 35, no. 5, p. 1661, 1993.

[46] D. D. MacDonald, C. Liu, and M. P. Manahan, "Electrochemical noise measurements on carbon and stainless steels in high subcritical and supercritical aqueous environments," in *Electrochemical Noise Measurement for Corrosion Applications* (J. R. Kearns, J. R. Scully, P. R. Roberge, D. L. Reichert, and J. L. Dawson, eds.), ASTM STP 1277, pp. 247–265, American Society for Testing and Materials, 1996.

[47] U. Bertocci, F. Huet, B. Jaoul, and P. Rousseau, "Noise resistance applied to corrosion measurements ii. experimental tests," *Journal of the Electrochemical Society*, vol. 144, no. 1, pp. 37–43, 1997.

[48] A. Legat and V. Dolecek, "Chaotic analysis of electrochemical noise measured on stainless steel," *J. Electrochem. Soc.*, vol. 142, no. 6, p. 1851, 1995.

[49] R. G. Hardon, P. Lambert, and C. L. Page, "Relationship between electrochemical noise and corrosion rate of steel in salt contaminated concrete," *British Corrosion Journal*, vol. 23, no. 4, pp. 2–25, 1988.

[50] Y. J. Tan, B. Kinsella, and S. I. Bailey, "The evaluation of corrosion inhibitor film persistency using electrochemical impedance spectrscopy and electrochemical noise analysis." in *Proceedings of Corrosion 96*, National Association of Corrosion Engineers, 1996. paper 352.

[51] Y. J. Tan, B. Kinsella, and S. I. Bailey, "Monitoring batch treatment inhibitor performance continuously using electrochemical noise analysis," *British Corrosion Journal*, vol. 32, no. 3, p. 212, 1997.

[52] C. T. Chen and B. S. Skerry, "Assessing the corrosion resistance of painted steel by ac impedance and electrochemical noise techniques," *Corrosion*, vol. 47, no. 8, p. 598, 1991.

[53] M. Hashimoto, S. Miyajima, and T. Murata, "An experimental study of potential fluctuation during passive film brekdown and repair on iron," *Corrosion Science*, vol. 33, no. 6, pp. 917–925, 1992.

[54] J. Goellner, A. Burkert, A. Heyn, and J. Hickling, "Using electrochemical noise to detect corrosion: Evaluation of a round-robin experiment," *Corrosion*, vol. 55, no. 5, p. 476, 1999.

[55] M. Keddam, M. Krarti, and C. Pallotta, "Some aspects of the fluctuations of the passive current on stainless steel in presence of chlorides — their relation to the probabilistic approach of pitting corrosion," *Corrosion*, vol. 43, no. 8, 1987.

[56] P. C. Pistorius, "The effect of some fundamental aspects of the pitting corrosion of stainless steel on electrochemical noise measurements," in *Electrochemical Noise Measurement for Corrosion Applications* (J. R. Kearns, J. R. Scully, P. R. Roberge, D. L. Reichert, and J. L. Dawson, eds.), ASTM STP 1277, pp. 343–358, 1996.

[57] D. E. Williams, C. Wstcott, and M. Fleischmann, "Studies of the initiation of pitting corrosion on stainless steels," *J. Electroanal. Chem.*, vol. 180, pp. 549–564, 1984.

[58] D. E. Williams, C. Westcott, and M. Fleischmann, "Stochastic models of pitting corrosion of stainless steels." *J. Electrochem. Soc.: Electrochemical Science and Technology*, vol. 132, no. 8, pp. 1796–1811, 1985.

[59] R. G. Kelly, M. E. Inman, and J. L. Hudson, "Analysis of electrochemical noise for type 410 stainless steel in chloride solutions," in *Electrochemical Noise Measurement for Corrosion Applications* (J. R. Kearns, J. R. Scully, P. R. Roberge, D. L. Reichert, and J. L. Dawson, eds.), ASTM STP 1277, pp. 101–113, American Society for Testing and Materials, 1996.

[60] T. F. Barton, D. L. Tuck, and D. B. Wells, "The identification of pitting and crevice corrosion spectra in electrochemical noise using an artifical neural network," in *Electrochemical Noise Measurement for Corrosion Applications* (J. R. Kearns, J. R. Scully, P. R. Roberge, D. L. Reichert, and J. L. Dawson, eds.), ASTM STP 1277, pp. 157–169, American Society for Testing and Materials, 1996.

[61] L. Beaunier, J. Frydman, C. Gabrielli, F. Huet, and M. Keddam, "Comparison of spectral analysis with fast fourier transform and maximum entropy method. application to the role of molybdenum implantation on localized corrosion of type 304 stainless steel," in *Electrochemical Noise Measurement for Corrosion Applications* (J. R. Kearns, J. R. Scully, P. R. Roberge, D. L. Reichert, and J. L. Dawson, eds.), ASTM STP 1277, pp. 114–128, American Society for Testing and Materials, 1996.

[62] A. M. P. Simoes and M. G. S. Ferreira, "Crevice corrosion studies on stainless steel using electochemical noise measurements," *British Corrosion Journal*, vol. 22, no. 1, p. 21, 1987.

[63] P. R. Roberge, "Analysis of electrochemical noise by the stochastic process detector method," *Corrosion*, vol. 50, no. 7, p. 502, 1994.

[64] P. R. Roberge, "Quantifying the stochastic behaviour of electrochemical noise measurment during the corrosion of aluminum," in *Electrochemical Noise Measurement for Corrosion Applications* (J. R. Kearns, J. R. Scully, P. R. Roberge, D. L. Reichert, and J. L. Dawson, eds.), ASTM STP 1277, pp. 142–156, American Society for Testing and Materials, 1996.

[65] J. R. Scully, S. T. Pride, H. S. Scully, and J. L. Hudson, "Some correlations between metastable pitting and pit stabilization in metals," *Electrochemical Society Proceedings*, vol. 95-15, p. 15, 1995.

[66] S. T. Pride, J. R. Scully, and J. L. Hudson, "Analysis of electrochemical noise from metastable pitting in aluminum ages al-2*Electrochemical Noise Measurement for Corrosion Applications* (J. R. Kearns, J. R. Scully, P. R. Roberge,

D. L. Reichert, and J. L. Dawson, eds.), ASTM STP 1277, pp. 307–331, American Society for Testing and Materials, 1996.

[67] M. Schneider, K. Nocke, and H. Pohl, "In-situ investigation of crevice corrosion by electrochemical noise analysis," *Materials Science Forum*, vol. 217–222, p. 1547, 1996.

[68] K. Habib, "Modified electrochemical emission spectrscopy (mees) as technique of ndt for detection localized corrosion of corrper alloys in seawater," *Optics and Lasers in Engineering*, vol. 33, pp. 1–13, 2000.

[69] S. Smith and R. Francis, "Use of electrochemical current noise to detect initiation of pitting conditions on copper tubes," *British Corrosion Journal*, vol. 25, no. 4, p. 285, 1990.

[70] R. A. Cottis and C. A. Loto, "Electrochemical noise generation during scc of a high strength carbon steel," *Corrosion*, vol. 46, no. 1, p. 12, 1990.

[71] H. J. DeBruyn, K. Lawson, and E. E. Heaver, "On-line monitoring using electrochemical noise measurement in co-co_2-h_2o systems," in *Electrochemical Noise Measurement for Corrosion Applications* (J. R. Kearns, J. R. Scully, P. R. Roberge, D. L. Reichert, and J. L. Dawson, eds.), ASTM STP 1277, pp. 214–229, American Society for Testing and Materials, 1996.

[72] Y. Watanabe and T. Kondo, "Current and potential fluctuation characteristics in igscc processess of stainless steels," in *Proceedings of Corrosion 98*, National Association of Corrosion Engineers, 1998. paper 376.

[73] Y. Watanabe and T. S. du T. Kondo, "Electrochemical noise characteristics of igscc in stainless steels in pressurized high-temperature water," in *Proceedings of Corrosion 98*, National Association of Corrosion Engineers, 1998. paper 129.

[74] R. Oltra, B. Chapey, F. Huet, and L. Renaud, "Coupling of acoustic emission and electrochemical noise measurement techniques in slurry erosion-corrosion studies," in *Electrochemical Noise Measurement for Corrosion Applications* (J. R. Kearns, J. R. Scully, P. R. Roberge, D. L. Reichert, and J. L. Dawson, eds.), ASTM STP 1277, pp. 361–374, American Society for Testing and Materials, 1996.

[75] K. Hladky and J. L. Dawson, "Corrosion monitoring using low frequency electrochemical noise." http://www.khdesign.demon.co.uk /noiseindex.htm, 1982.

[76] A. Legat, "Influence of electrolute movement on measured electrochemical noise," *Corrosion*, vol. 56, no. 11, pp. 1086–1092, 2000.

[77] G. Blanc, I. Epelboin, C. Gabrielli, and M. Keddam, "Electrochemical noise generated by anodic dissolution or diffusion processes," *Journal of the Electrochemical Society*, vol. 75, p. 97, 1977.

[78] M. Seralathan and S. K. Rangarajan, "Fluctuation phenomena in electrochemistry part 1. the formalism," *J. Electroanal. Chem.*, vol. 208, pp. 13–28, 1986.

[79] M. Seralathan and S. K. Rangarajan, "Fluctuation pehnomena in electrochemistry part 2. modelling the noise sources," *J. Electroanal. Chem.*, vol. 208, pp. 29–56, 1986.

[80] C. Gabrielli, F. Huet, and M. Keddam, "Fluctuations in electrochemical systems. i. general theory on diffusion limited electrochemical reactions," *J. Chem. Phys.*, vol. 99, no. 3, p. 7232, 1993.

[81] R. A. Cottis, "Modelling of electrochemical noise due to the activation-controlled dissolution of metals," in *Modelling Aqueous Corrosion* (K. R. Trethewey and P. R. Roberge, eds.), pp. 369–379, Kluwer Academic Publishers, 1994.

[82] F. Huet, M. Jerome, P. Manolatos, and F. Wenger, "Influence of hydrogen absorption on the electrochemical potential noise of an iron electrode under corrosion with gas evolution," in *Electrochemical Noise Measurement for Corrosion Applications* (J. R. Kearns, J. R. Scully, P. R. Roberge, D. L. Reichert, and J. L. Dawson, eds.), ASTM STP 1277, pp. 375–386, American Society for Testing and Materials, 1996.

[83] U. Bertocci, F. Huet, B. Jaoul, and P. Rousseau, "Frequency analysis of transients in electrochemical noise: Mathematical relationships and computer simulations," *Corrosion*, vol. 56, no. 7, pp. 675–683, 2000.

[84] Q. D. Zhong, "Potential variation of a temporarily protective oil coating before its degradation," *Corrosion Science*, vol. 43, no. 2, pp. 317–324, 2001.

[85] G. Huang, C. Wu, J. Jin, and G. Li, "Study on localized corrosion of metal under oil film," *Corrosion Science and Protection Technology*, vol. 12, no. 1, pp. 30–31, 2000.

[86] Q. D. Zhong, "Study on crevice corrosion of copper using wire beam electrode," *Journal of Chinese Society for Corrosion and Protection*, vol. 19, no. 3, pp. 189–192, 1999.

[87] Y. J. Tan and S. Yu, "Study and evaluation of organic coating by use fo wire beam electrode," *Materials Protection (China)*, vol. 25, no. 6, pp. 4–9, 1992.

[88] H. Eren, A. M. Lowe, Y. J. Tan, S. I. Bailey, and B. Kinsella, "An autoswitch for multisampling of a wire beam electrode corrosion monitoring system," *IEEE Transactions on Instrumentation and Measurement*, vol. 47, no. 5, pp. 1096–1100, 1998.

[89] K. Hladky and J. L. Dawson, "The measurement of corrosion using electrochemical 1/f noise," *Corrosion Science*, vol. 22, no. 3, p. 231, 1982.

[90] P. C. Searson and J. L. Dawson, "analysis of electrochemical noise generated by corroding electrodes under open-circuit coditions," *J. Electrochemical Soc.: Electrochemical Science and Technology*, vol. 135, no. 8, p. 1908, 1988.

[91] F. Mansfeld and H. Xiao, "Electrochemical noise analysis of iron exposed to nacl solution of different corrosivity," *J. Electrochem. Soc.*, vol. 140, no. 8, pp. 2205–2209, 1993.

[92] G. Gusmano, G. Montesperelli, and E. Traversa in *Proceedings of Corrosion 93*, National Association of Corrosion Engineers, 1993. paper 355.

[93] A. Legat and E. Govekar, "A comparison of spectral and chaotic analysis of electrochemical noise," in *Electrochemical Noise Measurement for Corrosion Applications* (J. R. Kearns, J. R. Scully, P. R. Roberge, D. L. Reichert, and J. L. Dawson, eds.), ASTM STP 1277, pp. 129–141, American Society for Testing and Materials, 1996.

[94] X. D. Dai, *Wavelet Applications in Process Sensor Data Analysis*. PhD thesis, Washington University Sever Institute of Technology, 1996.

[95] A. A. Alawadhi and R. A. Cottis, "Electrochemical noise signature analysis using power and cross-spectral densities," in *Proceedings of Corrosion '99*, National Association of Corrosion Engineers, 1999.

[96] M. Hashimoto, S. Miyajima, and T. Murata, "A sotchastic analysis of potential fluctuation during passive film breakdown and repair on iron," *Corrosion Science*, vol. 33, no. 6, pp. 885–903, 1992.

[97] M. Hashimoto, S. Miyajima, and T. Murata, "A spectrum analysis of potential fluctuation during passive film breakdown and repair on iron," *Corrosion Science*, vol. 33, no. 6, pp. 905–915, 1992.

[98] R. A. Cottis, S. Turgoose, and J. Mendoza-Flores, "The effects of solution resistance on electrochemical noise resistance measurments: A theroetical analysis," in *Electrochemical Noise Measurement for Corrosion Applications* (J. R. Kearns, J. R. Scully, P. R. Roberge, D. L. Reichert, and J. L. Dawson, eds.), ASTM STP 1277, pp. 93–100, American Society for Testing and Materials, 1996.

[99] Y. J. Tan, *Electrochemical Studies on Carbon Dioxide Corrosion and its Inhibition.* PhD thesis, Curtin University of Technology, Perth, Western Australia, 1996.

[100] Y. J. Tan, "Interpreting electrochemical noise resistance as a statistical linear polarisation resistance," *Journal of Corrosion Science and Engineering*, vol. 1, 1999. paper 11.

[101] D. A. Eden and A. N. Rothewell in *Proceedings of Corrosion 92*, National Association of Corrosion Engineers, 1992.

[102] G. P. Bierwagen, "Calculation of noise resistance from simultaneous electrochemical voltange and current noise data," *Journal of the Electrochemical Society*, vol. 141, no. 11, pp. 1155–1157, 1994.

[103] F. Mansfeld, L. T. Hans, C. C. Lee, and G. Zhang, "Evaluation of corrosion protection by polymer coatings using electrochemical impedance spectrscopy and noise analysis," *Electrochemica Acta*, vol. 43, pp. 2933–2945, 1998.

[104] U. Bertocci, J. Frydman, C. Gabrielli, F. Huet, and M. Keddam, "Analysis of electrochemical noise by power spectral density appled to corrosion studies. maximum entropy method or fast fourier transform?," *Journal of the Electrochemical Society*, vol. 145, no. 8, pp. 2780–2786, 1998.

[105] F. Huet, U. Bertocci, C. Gabrielli, and M. Keddam, "Part i - advanced monitoring and analytical techniques," in *Proceedings of Corrosion 97*, p. 11, National Association of Corrosion Engineers, 1997.

[106] F. Huet, U. Bertocci, C. Gabrielli, and M. Keddam, "Part ii - corrosion-resistance coatings," in *Proceedings of Corrosion 97*, p. 20, National Association of Corrosion Engineers, 1997.

[107] K. S. Shanmugan and A. M. Breipohl, *Random Signals: Detection, Estimation and Data analysis.* John Wiley and Sons, 1988.

[108] J. S. Bendat, *Random Data Analysis and Measurement Procedures.* New York: John Wiley and Sons, 2nd edition ed., 1986.

[109] A. Bautista and F. Huet, "Noise resistance applied to corrosion measurement iv. asymmetric coated electrodes," *Journal of the Electrochemcal Society*, vol. 146, no. 5, pp. 1730–1736, 1999.

[110] J. F. Chen and W. F. Bogaerts, "Electrochemical emission spectroscopy for monitoring uniform and localized corrosion," *Corrosion*, vol. 52, no. 10, pp. 753–758, 1996.

[111] A. Papoulis, *Probability, Random Variables and Stochastic Processes.* New York: McGraw-Hill, 1965.

[112] J. Honerkamp, *Stochastic Dynamical Systems: Concepts, Numerical Methods, Data Analysis.* VCH Publishers, 1994.

[113] H. Cramer, "A contribution to the theory of statistical estimation," *Skandinavisk Aktuarietidskrift*, vol. 29, pp. 85–94, 1946.

[114] C. R. Rao, "Information and the accuracy attainable in the estimation of statistical parameters," *Null. Calcutta Math. Soc.*, vol. 37, pp. 81–91, 1945.

[115] J. P. Burg, "Maximum entropy spectral analysis," in *Proceedings of the 37th Meeting of the Society of Exploration Geophysics*, (Oklahoma City), 1967.

[116] S. M. Kay and S. L. M. Jr., "Spectrum analysis - a modern perspective," *Proceedings of the IEEE*, vol. 69, no. 11, pp. 1380–1419, 1981.

[117] W. H. Press, *Numerical Recipes in C: the art of scientific computing.* Cambridge, England: Cambridge University Press, 1992.

[118] M. E. V. Valenburg, *Analog Filter Design.* London, England: Hold Rinehart and Winston, 1987.

[119] G. H. Tomlinson, *Electrical Networks and Filters: Theory and Design.* Prentice Hall, 1991.

[120] A. V. Oppenheim, A. S. Willsky, and I. T. Young, *Signals and Systems.* Prentice-Hall, 1983.

[121] E. Wong and J. C. Mallinson, "Noise-whitening filters for digital recording," in *Proceedings of INTERMAG Conference*, (Washington, DC), 1970. paper 12.6.

[122] F. M. Hsu, "Digital whitening techniques for improving spread spectrum communications performance in the presence of narrowband jamming and interference," *IEEE Transactions on Communications*, vol. 26, no. 2, pp. 209–216, 1978.

[123] R. Kumaresan, B. P. Agrawal, and M. R. Sridhar, "Optimum whitening filter for spectrum analysis," 1983. ASSP Spectrum Estimation Workshop 2 (IEEE Acoustics, Speech, and Signal Processing Society).

[124] A. M. Monk, M. Davis, L. B. Milstein, and C. W. Helstrom, "Noise-whitening approach to multiple-access noise rejection in a cdma system," in *Proceedings fo the 1994 IEEE National Telesystems Conference*, (San Diego, CA, USA), IEEE, 1994.

[125] I. S. Moreno, V. Kober, V. Lashin, J. Campos, L. P. Yaroslavsky, and M. J. Yzuel, "Whitening preprocessing of colour components for patter recognition," in *Proceedings of SPIE — The international Society for Optical Engineering, Second Iberoamerican Meeting on Optics*, (Guanajuato, Mexico), 1995.

[126] W. P. Ng, J. M. H. Elmirhgani, R. A. Cryan, and S. Broom, "Non-instrusive whitening of speech using least mean square and divergence detection technique," in *Proceedings of IEEE Global Telecommunications Conference*, IEEE, 1999.

[127] A. Trucco, S. D. Serio, and V. Murino, "Buried object detection by autoregeressive pre-whitening," in *Oceans Conference Record*, vol. 1, (Poscataway, NJ, USA), pp. 126–132. IEEE, 1999.

[128] J. Makhoul, "Whitening filters: A tutorial review," *Proceedings of the IEEE*, vol. 63, no. 4, pp. 562–80, 1975.

[129] A. M. Lowe, H. Eren, Y. J. Tan, S. I. Bailey, and B. J. Kinsella, "Continuous corrosion rate estimation by noise resistance calculation," in *Proceedings of IEEE Instrumentation and Measurement Technology Conference 2000*, pp. 1286–1291, 2000.

[130] A. M. Lowe, H. Eren, Y. J. Tan, S. I. Bailey, and B. J. Kinsella, "Continuous corrosion rate measurement by noise resistance calculation," *IEEE Transactions on Instrumentation and Measurement*, vol. 50, no. 5, pp. 1059–1065, 2001.

[131] A. M. Lowe, H. Eren, and S. I. Bailey, "Electrochemical noise analysis: Nyquist impedance diagrams," *Journal of the Electrochemical Society*, 2002. To be published.

[132] A. M. Lowe, H. Eren, and C. C. Fung, "Detection of electrode asymmetry in electrochemical noise analysis," in *Proceedings of TENCON 2001*, pp. 309–312, IEEE Region 10, 2001.

[133] A. M. Lowe, H. Eren, and S. I. Bailey, "Electrochemical noise analysis: Detection of electrode asymmetry," *Corrosion Science*, 2002. To be published.

[134] J. M. Bastidas, J. L. Polo, C. L. Torres, and E. Cano, "A study of the stability of aisi 315l stainless steel pitting corrosion through its transfer function," *Corrosion Science*, vol. 43, no. 2, pp. 269–281, 2001.

[135] G. Rocchini, "The corrosion-trend monitoring with the impedance technique," *Materials and Corrosion*, vol. 49, no. 1, pp. 18–26, 1998.

[136] S. Feliu, J. C. Galvan, and M. Morcillo, "The charge transfer reaction in nyquist diagrams of painted steel," *Corrosion Science*, vol. 30, no. 10, pp. 989–998, 1990.

[137] C. Gabrielli, "Corrosion measurement is also a matter of impedance," *Mesures*, vol. 52, no. 12, pp. 80–93, 1987.

[138] Y. J. Tan, S. I. Bailey, and B. Kinsella, "Factors affecting the determination of electrochemical noise resistance," *Corrosion*, vol. 55, no. 5, p. 469, 1999.

[139] H. Eren, Y. J. Tan, S. Bailey, B. Kinsella, and A. Lowe, "An auto-switch for multi-sampling of a wire beam electrode corrosion monitoring system," in *Proceedings of Instrumentation and Measurement Technology Conference 98*, (St. Paul, Minnesota), pp. 197–201, IEEE, 1998.

[140] A. M. Lowe and H. Eren, "Signal analysis and synthesis as applied to electrochemical noise in corrosion," in *Proceedings of TENCON 2000*, pp. 240–245, IEEE region 10, 2000.

[141] E. J. Hannan, *Multiple Time Series*. New York: John Wiley and Sons, 1970.